Biochemical and genetic analysis of Dam1c ring assembly at the budding yeast kinetochore

Dissertation

zur

Erlangung des Doktorgrades

Dr. rer. nat.

der Fakultät für Biologie

an der

Universität Duisburg-Essen

vorgelegt von

Alexander Dudziak

aus Gladbeck

Die der vorliegenden Arbeit zugrundeliegenden Experimente wurden in der Abteilung für Molekulare Genetik I der Universität Duisburg-Essen durchgeführt.

1. Gutachter: Prof. Dr. Stefan Westermann
2. Gutachter: Prof. Dr. Andrea Musacchio
3. Gutachter: Prof. Dr. Thomas U. Mayer

Vorsitzender des Prüfungsausschusses: Prof. Dr. Hemmo Meyer

Tag der mündlichen Prüfung: 17. Dezember 2021

DOI: 10.17185/duepublico/75233
URN: urn:nbn:de:hbz:464-20211222-071631-1

In the context of this doctoral work, the following articles were published:

Phospho-regulated Bim1/EB1 interactions trigger Dam1c ring assembly at the budding yeast outer kinetochore

Alexander Dudziak, Lena Engelhard, Cole Bourque, Björn Udo Klink, Pascaline Rombaut, Nikolay Kornakov, Karolin Jänen, Franz Herzog, Christos Gatsogiannis, Stefan Westermann The EMBO Journal (2021) 40: e108004, DOI: 10.15252/embj.2021108004

Cdc4 phospho-degrons allow differential regulation of Ame1^{CENP-U} protein stability across the cell cycle

Miriam Böhm, Kerstin Killinger, Alexander Dudziak, Pradeep Pant, Karolin Jänen, Simone Hohoff, Karl Mechtler, Mihkel Örd, Mart Loog, Elsa Sanchez-Garcia, Stefan Westermann eLife 2021;10:e67390, DOI: 10.7554/eLife.67390

Summary

During mitotic cell division, chromosomes containing the genetic information of an organism must be equally and accurately distributed to the two new cells. Chromosomes attach to dynamic microtubules of the mitotic spindle and are pulled apart harnessing forces generated by microtubule depolymerization and spindle elongation. Microtubules bind to a well-defined proteinaceous structure, the kinetochore, which is specifically assembled on centromeric chromatin of each chromosome. Besides forming microtubule attachments, kinetochores perform additional functions such as sensing the attachment status of each chromosome and initiating spindle assembly checkpoint signaling. An essential component of the *Saccharomyces cerevisiae* kinetochore is the Dam1 complex (Dam1c). The ten-subunit complex has the propensity to oligomerize into rings with a 16-fold symmetry that encircle microtubules and track their dynamic plus ends. Together with the Ndc80 complex (Ndc80c), which serves as a kinetochore receptor for Dam1c, Dam1c provides the physical link between the kinetochore and spindle microtubules and eventually translates microtubule depolymerization into chromosome movement.

Even though many features of the Dam1 complex have been investigated during the past two decades, employing genetic, cell biological, biochemical, biophysical and structural biological approaches, it is still poorly understood how the complex is specifically recruited to the plus ends of kinetochore microtubules. Furthermore, relatively little is known about interactions of the complex with other proteins such as microtubule-associated proteins (MAPs).

In the present study, the interaction between Dam1c with the autonomous plus end-tracking protein Bim1/EB1 is characterized using a combination of genetics, cell biology and biochemical reconstitution. Furthermore, insights into the structure of the Dam1c-Bim1 complex have been obtained by negative stain electron microscopy and chemical crosslinking. It is demonstrated that Bim1 closely associates with the protrusion domains of the Dam1 complex by binding a conserved SxIP motif located in the C-terminus of the Duo1 subunit. Binding of Bim1 to the complex is required for maximum loading of Dam1c onto kinetochores in metaphase and ensures timely mitotic progression. Phosphorylation by the conserved kinase Mps1 promotes the interaction between Dam1c and Bim1 and overexpression of Mps1 affects the localization of Dam1c during metaphase. In contrast, binding of Bim1 to Dam1c is refractory to phosphorylation by Ipl1/Aurora B. Biochemical and structural analyses reveal that Bim1 induces oligomerization of Dam1c into partially assembled rings with well-defined curvature. Furthermore, Bim1 recruits Bik1/CLIP-170 to Dam1c and by this induces the assembly of Dam1c into complete rings even in the absence of microtubules. Hence, binding of Bim1 and subsequent recruitment of Bik1/CLIP-170 is a novel regulatory mechanism for Dam1c ring assembly. Simultaneous disruption of Bim1-binding to Dam1c and interfering with Cdk1- and Ipl1/Aurora B-regulated Dam1c oligomerization mechanisms is detrimental to

viability of yeast cells and negatively affects growth especially at low temperatures, suggesting that oligomerization of Dam1c is essential for formation of mature kinetochore-microtubule attachments.

Dam1c finally engages with the Ndc80 complex to form load-bearing kinetochore-microtubule attachments. Biochemical reconstitution assays suggest that Dam1c engages either with Bim1-Bik1 or with Ndc80c. This implies that the Dam1c-Bim1-Bik1 and Dam1c-Ndc80c complexes presumably represent two distinct biochemical entities of Dam1c that might exist at different timepoints during the formation of kinetochore-microtubule attachments.

These results demonstrate that binding of Bim1 to Dam1c is an important step in the regulation of outer kinetochore assembly and serves to control oligomerization and kinetochore recruitment of the complex. Kinetochore-localized Mps1 activity promotes binding of Bim1 and ensures specific accumulation of Dam1c in proximity of unattached kinetochores, but not at any other part of the mitotic spindle such as the midzone. Furthermore, Bim1 might serve as temporary placeholder that initially brings Dam1c to the microtubule plus end and is subsequently replaced by the Ndc80 complex to form mature end-on attachments. Previous reports about physical interactions between the metazoan Ska complex, the functional homolog of Dam1c, and the end-binding protein EB1 suggest that the mechanistic principles described in this thesis may be more widely conserved among eukaryotes.

Zusammenfassung

Während der mitotischen Zellteilung müssen Chromosomen, die die genetische Information eines Organismus tragen, gleichmäßig und mit hoher Präzision auf die beiden neu entstehenden Zellen verteilt werden. Hierzu binden Chromosomen an Mikrotubuli der mitotischen Spindel und werden unter Nutzung der Kräfte, die aus der Depolymerisation und Verlängerung der Spindel resultieren, voneinander getrennt. Dabei binden Mikrotubuli an eine bestimmte Proteinstruktur, die Kinetochor genannt wird und spezifisch an den Zentromeren eines jeden Chromosoms gebildet wird. Neben der Bindung an Mikrotubuli erfüllen Kinetochore weitere wichtige Funktionen wie die qualitative Überprüfung der Kinetochor-Mikrotubulus-Interaktion und die Initialisierung der Signalkaskade des mitotischen Checkpoints. Ein essenzieller Bestandteil der Kinetochors der Bäckerhefe *Saccharomyces cerevisiae* ist der Dam1 Komplex (Dam1c). Dieser aus zehn Untereinheiten bestehende Komplex besitzt die Fähigkeit, sich aus 16 einzelnen Komplexen symmetrisch zu einem Ring zusammenzusetzen, der einen Mikrotubulus umschließen und prozessiv an dessen dynamisches Ende binden kann. Zusammen mit dem Ndc80 Komplex (Ndc80c), der am Kinetochor als Rezeptor für den Dam1 Komplex fungiert, stellt der Dam1 Komplex die physische Verbindung zwischen dem Kinetochor und den Mikrotubuli der mitotischen Spindel dar, die letztlich die Mikrotubuli-Depolymerisation in den Transport der Chromosomen umsetzt. Obwohl zahlreiche Eigenschaften des Dam1 Komplexes in den vergangenen zwei Jahrzehnten mittels genetischer, zellbiologischer, biochemischer, biophysikalischer und strukturbiologischer Ansätze erforscht wurden, ist bis heute wenig darüber bekannt, wie der Komplex selektiv an das Plus-Ende der Kinetochor-Mikrotubuli gelangt. Des Weiteren sind physische Interaktionen des Komplexes mit anderen Proteinen, wie Mikrotubuli-assoziierten Proteinen (MAPs), wenig erforscht.

In der vorliegenden Studie wird die Interaktion des Dam1 Komplexes mit dem autonomen Plus-Ende-bindenden Protein Bim1/EB1 mittels einer Kombination aus genetischen, zellbiologischen und biochemischen Methoden untersucht. Zusätzliche liefern elektronenmikroskopische Daten nach Negativkontrastierung und chemisches Crosslinking Einblicke in die Struktur des Dam1c-Bim1 Komplexes. Bim1 lagert sich in der Nähe der sogenannten Protrusion-Domäne an den Dam1 Komplex an, indem es eine konservierte SxIP-Sequenz im C-Terminus der Untereinheit Duo1 bindet. Die Bindung von Bim1 an den Dam1 Komplex wird für eine vollständige Rekrutierung des Komplexes an das Kinetochor während der Metaphase und den korrekten zeitlichen Verlauf der Mitose benötigt. Phosphorylierung durch die konservierte Kinase Mps1 verstärkt die Interaktion zwischen Dam1c und Bim1 und Überexpression von Mps1 beeinträchtigt die Lokalisation des Dam1 Komplexes während der Metaphase. Im Gegensatz dazu ist die Bindung von Bim1 an den Dam1 Komplex resistent gegenüber der Phosphorylierung durch Ipl1/Aurora B. Biochemische und strukturelle Analysen legen offen, dass Bim1 die Oligomerisierung des Dam1 Komplexes in unvollständige Ringe

mit einem einheitlichen Radius auslöst. Zusätzlich rekrutiert Bim1 das Protein Bik1/CLIP-170 zum Dam1 Komplex hinzu und induziert dadurch die Assemblierung vollständiger Ringe sogar in der Abwesenheit von Mikrotubuli. Auf Grundlage dessen ist die Bindung von Bim1 und Bik1/CLIP-170 ein neuartiger Mechanismus, der die Bildung des Dam1c-Rings reguliert. Somit ist Bim1, zusammen mit Phosphorylierung des Dam1 Komplexes durch Cdk1 und Ipl1/Aurora B, einer von nun drei bekannten Mechanismen zur Regulation der Bildung des Dam1c-Rings. *In vivo* Analysen zeigen, dass das Wachstum von Hefezellen, vor allem bei niedrigen Temperaturen, verlangsamt ist, wenn mehrere dieser regulatorischen Mechanismen gleichzeitig beeinträchtigt sind. Dies deutet darauf hin, dass die Oligomerisierung des Dam1 Komplexes für die Bildung vollständiger Kinetochor-Mikrotubulus-Verbindungen entscheidend ist.

Durch Kopplung des Dam1 Komplexes an den Ndc80 Komplex werden letztlich belastbare Kinetochor-Mikrotubulus-Bindungen generiert. Biochemische Rekonstitutionsexperimente zeigen, dass der Dam1 Komplex entweder mit Bim1-Bik1 oder mit dem Ndc80 Komplex interagiert. Diese Beobachtung impliziert, dass der Dam1c-Bim1-Bik1 und Dam1c-Ndc80c Komplex zwei biochemisch unterschiedliche molekulare Varianten des Dam1 Komplexes sind, die möglicherweise zu verschiedenen Zeitpunkten des Aufbaus stabiler Kinetochor-Mikrotubulus-Verbindungen existieren.

Die Ergebnisse dieser Studie zeigen, dass die Bindung von Bim1 an den Dam1 Komplex ein wichtiger Schritt zur Regulierung des Aufbaus des äußeren Kinetochors ist und dazu dient, die Oligomerisierung und Anreicherung des Komplexes am Kinetochor zu kontrollieren. Mps1-Aktivität am Kinetochor fördert die Interaktion mit Bim1 und gewährleistet eine spezifische Anreicherung des Dam1 Komplexes in der Nähe von Kinetochoren, die keine Mikrotubuli gebunden haben. Dadurch wird gleichzeitig eine Anreicherung des Komplexes an anderen Mikrotubuli, zum Beispiel der Mittelzone der Spindel, verhindert. Zusätzlich fungiert Bim1 möglicherweise als Platzhalter, der anfangs den Dam1 Komplex am Plus-Ende eines Mikrotubulus positioniert und anschließend durch den Ndc80 Komplex ersetzt wird, um korrekt konfigurierte Kinetochor-Mikrotubulus-Verbindungen herzustellen. Vorherige Berichte über die physische Interaktion des Ska Komplexes aus Metazoa, des funktionellen Homolog des Dam1 Komplexes, und dem Mikrotubulus Plus-Enden-bindenden Protein EB1 legen die Vermutung nahe, dass die mechanistischen Grundlagen, die in der vorliegenden Dissertation beschrieben werden, unter Eukaryoten weit verbreitet und konserviert sind.

Table of Contents

List of Figures

List of Tables

List of Appendix Figures

List of Appendix Tables

List of Abbreviations

1NM-PP1	4-Amino-1-tert-butyl-3-(1'-naphthylmethyl)pyrazolo[3,4-d]pyrimidine
APC/C	anaphase-promoting complex/cyclosome
APS	ammonium persulfate
ATP	adenosine triphosphate
bp	base pair
Cdc	cell division cycle
CDE	centromere-determining element
Cdk	cyclin-dependent kinase
CH	Calponin homology
CPC	chromosomal passenger complex
DMSO	dimethyl sulfoxide
DTT	dithiothreitol
EBH	end binding protein homology
ECL	enhanced chemiluminescence
EDTA	ethylenediaminetetraacetic acid
FRB	FKBP12-rapamycin-binding
HEPES	4-(2-hydroxyethyl)-1-piperazineethanesulfonic acid
IPTG	isopropyl-β-D-thiogalactopyranosid
kDa	kilodalton
Mat	mating type
MCC	mitotic checkpoint complex
MTBD	microtubule-binding domain
MTOC	microtubule-organizing center
NAA	1-naphthaleneacetic acid
LB	lysogeny broth
OD_{600}	optical density at 600 nm
PBS	phosphate buffered saline
PKA	protein kinase A
PMSF	phenylmethylsulfonyl fluoride
rpm	rotations per minute
SC	synthetic complete
SDS	sodium dodecyl sulfate
SDS-PAGE	sodium dodecyl sulfate polyacrylamide gel electrophoresis

SEC	size exclusion chromatography
SGD	*Saccharomyces* Genome Database
SPB	spindle pole body
TCEP	tris(2-carboxyethyl)phosphine
TEMED	tetramethylethylenediamine
TEV	tobacco etch virus
TIRF	total internal reflection
Tris	tris(hydroxymethyl)aminomethane
v/v	volume percentage
WT	wild type
w/v	weight percentage
YEPD	yeast extract peptone with glucose
YEPRG	yeast extract peptone with raffinose and galactose

1. Introduction

1.1. Principles of the eukaryotic cell cycle

1.1.1. General aspects of eukaryotic cell division

All eukaryotic life depends on mitotic cell division during which the mother cell divides into two identical daughter cells. This process is required for reproduction of unicellular organisms as well as growth, development and self-renewal of multicellular organisms and its key steps are conserved across a broad range of species. The cell cycle follows a strict program of consecutive steps which are defined by oscillating activity of cyclin-dependent kinases (Cdks), the key regulators of the cell cycle. In preparation of cell division, the cell grows and reproduces cellular components such as proteins, RNA and organelles during G1-phase. In the presence of favorable conditions, the cell starts duplicating its genome in the so-called S-phase. Importantly, the genome has to be replicated exactly once during each cell cycle since under- or over-replication leads to aneuploidy. In addition, the centrosome or spindle pole body (SPB), the microtubule-organizing center of metazoan or yeast cells, respectively, are duplicated. S-phase is followed by G2-phase during which the cell further reproduces its cellular content. Afterwards, the genomic DNA of the cell is segregated during mitosis (M-phase). In short, the genomic DNA condenses into chromosomes during prophase with each chromosome composed of two identical sister chromatids which are held together by the cohesin complex. During the following prometaphase, the chromosomes bind to dynamic microtubules of the mitotic spindle via their kinetochores. The architecture of kinetochores and the mitotic spindle will be discussed later. Once attached to the mitotic spindle, the chromosomes are aligned along the equatorial plate during metaphase. Only if every chromosome is correctly attached, i.e. bioriented on the mitotic spindle, the cells progress to anaphase during which the sister chromatids are pulled to opposing poles of the mitotic spindle. Finally, the cell is divided into two cells during cytokinesis (Morgan, 2006).

The exact duplication of the genome and the accurate segregation of chromosomes to the two daughter cells is of ultimate importance to the cell as errors lead to aneuploidy and finally cell death or transformation into malignant cells.

1.1.2. Cyclin-dependent kinases (Cdks) are the major regulators of the eukaryotic cell cycle

The individual events of the cell cycle follow a well-defined program in which each step is initiated after the completion of the previous one. For instance, cells only enter M-phase after complete and correct duplication of the genome during S-phase and chromosome segregation is only initiated if all chromosomes are correctly attached to the microtubules of the mitotic spindle. Transition from metaphase to anaphase is controlled and regulated by the anaphase-promoting complex/cyclosome (APC/C). The APC/C acts as ubiquitin ligase which targets

Securin and Cyclin B for proteosomal degradation and thus induces anaphase onset (Peters, 2006). Another characteristic feature of the cell cycle is its unidirectionality since the progression from one step to the next one is irreversible (Morgan, 2006).

A complex regulatory network of cyclin-dependent kinases (Cdk) is responsible for the exact timing of the individual phases of the eukaryotic cell cycle. Cdks are highly conserved among eukaryotes and their activity depends on binding of different cyclins, as implicated by their name. While there are several different Cdks in metazoans, there is only one Cdk in budding yeast which is called Cdc28 and corresponds to metazoan Cdk1. Different Cdk-cyclin complexes trigger cell cycle-specific processes during the different stages of the cell cycle. For example, the Cdk2-cyclin A complex triggers S-phase-specific events such as DNA replication, while Cdk1-cyclin B is the main regulator during M-phase in human cells. According to their expression and function in the cell cycle, cyclins and Cdks are frequently named G1-, G1/S-, S- or M-cyclin or -Cdk, respectively. In budding yeast, the substrate specificity of the only Cdk, Cdc28, is determined by binding of different cyclins, with Clb5 and Clb6 as S-cyclins and Clb2 and Clb4 as major M-cyclins. Cellular cyclin levels are regulated by multiple mechanism such as transcriptional control, proteasomal degradation, binding of inhibitory proteins or reversible phosphorylation, ensuring that Cdks are only activated at the appropriate cell cycle stage. These different regulatory mechanisms are integrated into feedback loops which allow for the abrupt activation of Cdk during the cell cycle (Morgan, 2006; Örd and Loog, 2019).

In G1-phase, at the beginning of the cell cycle, Cdk activity is low. When the activity of the G1-specific Cdk rises and reaches a certain level, for example as response to an external stimulus, the transcription of G1/S- and S-phase cyclins is initiated. S-Cdk is activated rapidly by degradation of inhibitory proteins such as Sic1 and inactivation of the APC/C. Activity of S-Cdk initiates DNA replication, while activity of G1/S-Cdk is reduced by degradation and transcriptional suppression of the respective cyclin. Transcription of the M-cyclin is initiated towards the end of S-phase and M-Cdk-cyclin complexes accumulate during G2. However, these complexes are kept inactive by inhibitory phosphorylation until their sudden activation. M-Cdk-cyclin activity is responsible for assembly of the mitotic spindle and other mitotic events, finally leading to the alignment of chromosomes at the equatorial plate during metaphase. Transition from metaphase to anaphase is regulated by the APC/C. Activation of the APC/C leads to destruction of S- and M-cyclins and thus inactivation of the respective Cdk. Furthermore, APC/C targets Securin for proteasomal degradation, finally resulting in cleavage of Cohesin by Separase and chromosome segregation in anaphase. As M-Cdk activity declines, its mitotic substrates are dephosphorylated by phosphatases which is essential for spindle disassembly and mitotic exit (Holder et al., 2019; Morgan, 2006).

1.1.3. The spindle assembly checkpoint (SAC) surveils the metaphase-to-anaphase transition

A critical and irreversible step during mitotic progression is the transition from metaphase to anaphase during which chromosomes are equally distributed to the two emerging cells. However, cells must only enter anaphase if all chromosomes are correctly attached to microtubules of the mitotic spindle. Precocious chromosome segregation in the presence of incorrect attachments leads to aneuploidy, which is a common cause of cancer or death during early embryonic development (Gordon et al., 2012; Santaguida and Amon, 2015). Remarkably, a single unattached kinetochore is sufficient to active the SAC and delay anaphase onset (Rieder et al., 1995). Correct attachment of kinetochores is monitored by the spindle assembly checkpoint (SAC), also known as mitotic checkpoint (Musacchio, 2015). The conserved kinase Mps1 is recruited to unattached kinetochores where it phosphorylates MELT repeats of the kinetochore protein Knl1 (Spc105 in budding yeast; Figure 1; London et al., 2012; Shepperd et al., 2012; Yamagishi et al., 2012). The SAC components Bub3 associated with Bub1 binds to phosphorylated MELT repeats and recruits Mad1, Mad2 and BubR1/Mad3 (Primorac et al., 2013). Together with Cdc20, the proteins Bub3, BubR1/Mad3 and Mad2 form the freely diffusible mitotic checkpoint complex (MCC) that binds to and thus inhibits the APC/C (Musacchio, 2015). Interestingly, Cdc20 may play two different roles in the context of APC/C regulation: On the one hand, Cdc20 is an essential activator of the APC/C, on the other hand, Cdc20 is a potent inhibitor of the APC/C as part of the MCC. By formation of the MCC, the cell generates a global signal starting from a single incorrectly attached kinetochore (Musacchio, 2015).

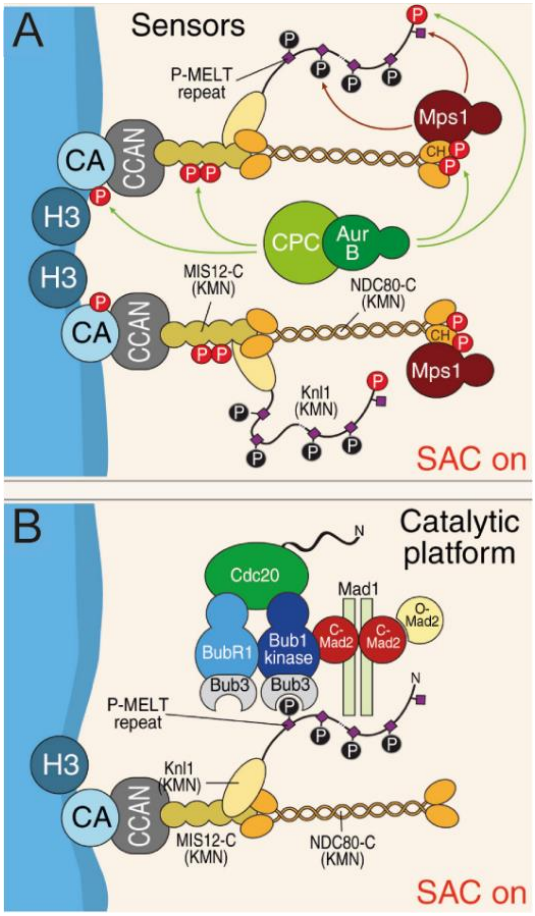

Figure 1: SAC signaling at the kinetochore
A: Aurora B activity promotes release of erroneous kinetochore-microtubule attachments. Mps1 binds to the CH domain of Ndc80 and phosphorylates MELT repeats of Knl1/Spc105.
B: Bub3 recognizes phosphorylated MELT, recruits further SAC components and initiates formation of the diffusible MCC.
Image from Musacchio, 2015

Once all kinetochores are bioriented on the mitotic spindle, the SAC needs to be inactivated in order to allow anaphase onset. However, the mechanisms of SAC silencing are still poorly understood. One model suggests that Mps1 associates with the microtubule-binding CH domains of the Ndc80 complex in a competitive manner (Hiruma et al., 2015; Ji et al., 2015).

Thus, once a kinetochore is attached to a microtubule, Mps1 is displaced from the kinetochore. Alternatively, the kinetochore is stretched upon establishment of biorientation which physically separates Mps1 from its essential substrate Knl1 (Aravamudhan et al., 2015). Another model suggests a crucial role for motor proteins in SAC silencing: Correct kinetochore-microtubule attachments allow the minus-end directed motor protein complex Dynein to strip off SAC components from the kinetochore and transport them away from the kinetochore (Howell et al., 2001; Wojcik et al., 2001).

Finally, biorientation of all kinetochores satisfies the SAC leading to activation of APC/C. As an E3 ubiquitin ligase, APC/C polyubiquitinates Cyclin B and Securin resulting in their rapid proteosomal degradation. As consequence, Separase is activated which cleaves Cohesin that links sister chromatids. In addition, activity of the M-Cdk decreases resulting in the dephosphorylation of mitotic Cdk substrates by phosphatases, eventually initiating mitotic exit (Morgan, 2006; Musacchio, 2015).

1.1.4. The Aurora B kinase releases tension-lacking microtubule-kinetochore attachments

The spindle assembly checkpoint is activated in the presence of erroneous kinetochore-microtubule attachments and delays anaphase onset until all chromosomes are bioriented on the mitotic spindle (1.1.3). However, incorrect attachments need to be released in order to allow reformation of attachments that finally satisfy the SAC. The conserved kinase Aurora B (Ipl1 in *S. cerevisiae*) plays a crucial role in this process by phosphorylating multiple proteins of the outer kinetochore, which disrupts microtubule binding and induces rapid turnover of binding and unbinding (Hauf et al., 2003; Tanaka et al., 2002). Together with INCENP, Survivin and Borealin (Sli15, Nbl1 and Bir1 in *S. cerevisiae*) Aurora B forms the chromosomal passenger complex (CPC) that is recruited to two distinct sites at the centromere in a Haspin- and Bub1-dependent manner. However, experimental data suggest the existence of an Aurora B pool distal form the centromere which is responsible for phosphorylation of outer kinetochore substrates (Broad et al., 2020; Hadders et al., 2020). Using a combination of biochemical reconstitution and genetic approaches it was shown that the CPC binds to the inner kinetochore COMA complex of *S. cerevisiae.* Binding to the COMA complex is crucial for the establishment of bioriented kinetochore-microtubule attachments and faithful chromosome segregation (Fischböck-Halwachs et al., 2019; García-Rodríguez et al., 2019).

Intriguingly, Aurora B activity is closely linked to the SAC. Aurora B indirectly activates the SAC by generating unattached kinetochore. In addition, Aurora B and Mps1, the effector kinase of the SAC, regulate each other's activity and kinetochore localization by an elaborate regulatory network involving counteracting phosphatases (Saurin, 2018). For instance, SAC signaling triggers kinetochore localization of the PP2A-B56 phosphatase, which antagonizes Aurora B activity. As consequence, the PP1 phosphatase is recruited to the kinetochore which in turn

counteracts Mps1 kinase activity (Nijenhuis et al., 2014). This kinase and phosphatase feedback system allows for rapid inactivation of Aurora B and SAC activity once biorientation is achieved (Saurin, 2018).

1.1.5. *Saccharomyces cerevisiae* is a powerful model organism to study the eukaryotic cell cycle

The budding yeast *Saccharomyces cerevisiae* has been used for decades to study the eukaryotic cell cycle and its regulatory factors. Most notably, Leland Hartwell, Nobel Prize laureate in Physiology or Medicine in 2001 for the “discoveries of key regulators of the cell cycle”, used budding yeast for his distinguished research. However, budding yeast proved itself as valuable tool for further Nobel Prize-awarded work on vesicular trafficking, transcription, protection of telomeres and autophagy (Nobel Prize Committee, 2001).

Several characteristics of *S. cerevisiae* make it an ideal organism to study various biological processes. First of all, *S. cerevisiae* is a unicellular eukaryote with a small and completely sequenced genome. Furthermore, budding yeast is amenable to genetic engineering and integrates foreign DNA into its genome by homologous recombination. This allows for efficient and locus-specific genome manipulation such as deletions or insertions of whole genes and integration of point mutations and epitope or fluorescent tags. In addition, a large number of temperature-sensitive alleles have been generated that have normal gene function at the permissive temperature but are compromised at the restrictive temperature. A broad range of auxotrophy or antibiotic resistance markers is available enabling construction of yeast strains with multiple genetic alterations. Budding yeast cells divide approximately every 90 to 120 minutes, depending on the growth conditions. Due to this fast reproduction cycle, it is possible to follow yeast cells during several consecutive cell cycles in a relatively short period of time and to cultivate yeast cells to large quantities. As its name suggests, budding yeast divides by budding. The bud emerges at the end of G1-phase and grows continuously throughout S- and M-phase until it reaches a size slightly smaller than the mother cell. At the end of mitosis, one set of chromosomes is distributed into the bud, which is finally pinched off the mother cell during cytokinesis, forming a new cell. As the bud increases in size during cell cycle progression, the bud size is a great indicator for the current stage of the cell cycle and can be analyzed easily by light microscopy.

S. cerevisiae can be stably maintained as diploid and haploid strains which both proliferate by vegetative cell division (Figure 2). Under conditions of nutrient deficiency, diploid cells sporulate and undergo meiosis. During this process, one diploid cell gives rise to four haploid cells which are encapsulated into an ascus. The four spores within the ascus are called tetrad. If the environmental conditions are favorable, haploid cells proliferate by vegetative cell division. In addition, two haploid cells of opposing mating types (Mat a and Mat α) can fuse to

form a diploid cell again. Haploid yeast cells produce and secrete the mating pheromone a or α factor, which stimulates cells of the opposing mating type to arrest in a G1-like state and to polarize forming a so-called shmoo. Finally, two haploid cells fuse to form a diploid cell. While many naturally occurring yeast strains are able to switch their mating type from a to α and vice versa (homothallism), most laboratory strains are deficient in HO endonuclease activity which is essential for mating type switching. Thus, haploid laboratory strains can be stably propagated without mating type switching and formation of diploid cells (heterothallism). Working with haploid strains brings huge advantages for the analysis of the function of a gene of interest since the phenotype of recessive mutant alleles or the deletion of a gene can be investigated without a wild type copy of the corresponding gene that might compensate for a loss of function. Haploid cells can be arrested in a G1-like status by addition of the respective mating pheromone and synchronously released from this arrest to study cell cycle progression. In laboratory use, haploid strains are derived from sporulated diploid strains. The spores of a tetrad can be separated mechanically using a microneedle and cultivated on rich medium to allow vegetative cell division. Spores can be analyzed for the appropriate genotype and subsequently used for further experiments (Herskowitz, 1988; Morgan, 2006; Schneiter, 2004; Sherman, 2002).

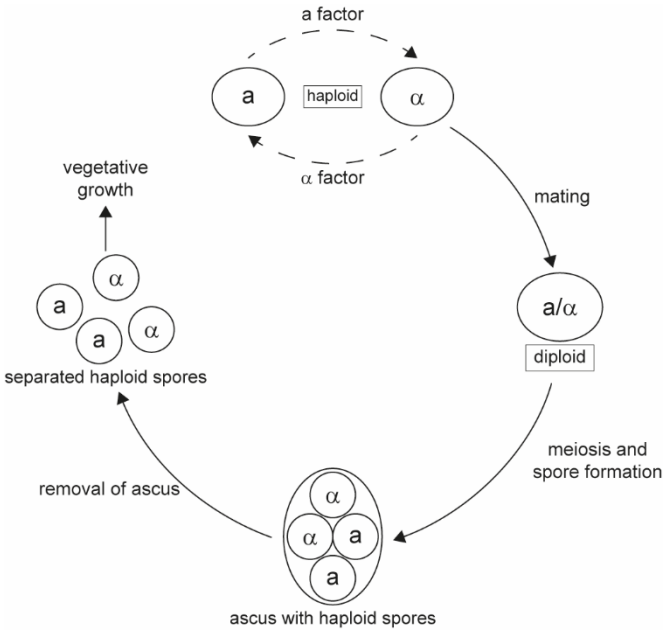

Figure 2: Life cycle of *S. cerevisiae*
Haploid cells of opposing mating types mate to from a diploid cell. Under certain conditions, diploids undergo meiosis. The four resulting spores are packed into an ascus and can be separated after removal of the ascus.

1.1.6. Composition and function of the mitotic spindle

During mitosis, sister chromatids get attached to dynamic microtubules of the mitotic spindle in order to equally segregate chromatids. Spindle microtubules are nucleated from microtubule-organizing centers (MTOCs) which are called centrosomes in higher eukaryotes and spindle poles bodies (SPB) in yeast. In budding yeast, the SPB is embedded into the nuclear envelope so that one site is exposed to the cytoplasm and the other to the nucleoplasm. Microtubules nucleate from an SPB with their minus end anchored at the SPB and their dynamic plus end reaching into the nucleoplasm and cytoplasm, respectively (Winey and Bloom, 2012). Duplication of the SPB is a multi-step process, which is initiated in G1-phase and regulated by Cdk activity. Furthermore, Mps1 (*monopolar spindle 1*) kinase activity is required for multiple events during this process (Winey et al., 1991). The newly assembled SPB is initially positioned next to the mother SPB and subsequently migrates to the opposing site of the nucleus. Positioning of both SPBs on opposing sides of the nucleus is crucial for formation of a bipolar mitotic spindle. SPBs nucleate three different types of microtubules: Astral microtubules are nucleated from the cytoplasmic surface of the SPB and extend into the cytoplasm where they connect with the cell cortex (Figure 3). Their main function is to ensure the correct migration and positioning of the nucleus. Both interpolar and kinetochore microtubules emanate from the nucleoplasmic surface of the SPB. Interpolar microtubules from one SPB interdigitate with interpolar microtubules from the opposing SPB, which significantly contributes to spindle stability. Furthermore, sliding of antiparallel microtubules is essential for spindle elongation during anaphase. Kinetochore microtubules attach to the kinetochore assembled on each chromatid. In budding yeast, a single microtubule binds to one kinetochore, while bundles composed of several microtubules attach to kinetochores of higher eukaryotes (Biggins, 2013; Winey and Bloom, 2012).

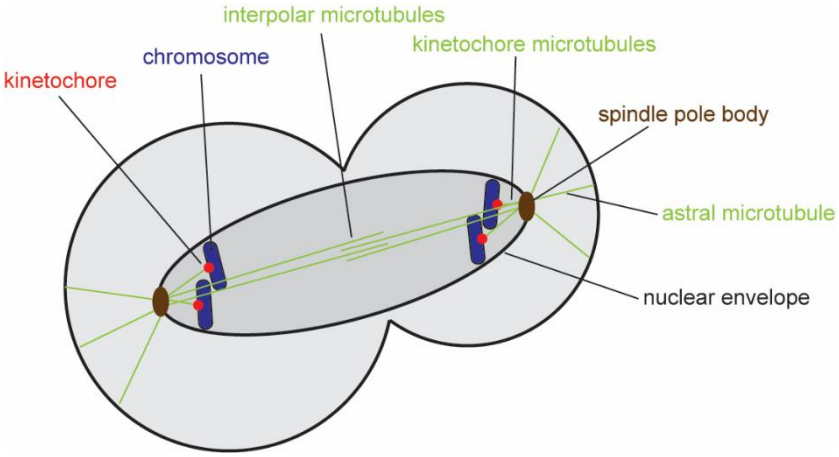

Figure 3: Spindle organization in budding yeast
Schematic illustration of a budding yeast cell in anaphase. Different types of microtubules of the mitotic spindle, SPBs, chromosomes and kinetochores are shown. For reasons of simplicity, a reduced number of microtubules and chromosomes is displayed.

1.2. Architecture and function of the eukaryotic kinetochore

Kinetochores are multi-protein assemblies that are built on centromeric DNA of each chromatid and physically link chromatids to the dynamic plus ends of microtubules of the mitotic spindle.

The kinetochore fulfills various functions in order to ensure faithful and error-free chromosome segregation during mitosis: First, kinetochores stably bind to dynamic microtubules of the mitotic spindle and, intriguingly, even stay attached to the ends of depolymerizing microtubules during establishment of tension across sister kinetochores and chromosome segregation in anaphase. By doing this, kinetochores confer microtubule tip-tracking ability to chromosomes (Musacchio and Desai, 2017). Furthermore, kinetochores are able to sense and monitor their attachment status to spindle microtubules and to activate the spindle assembly checkpoint if required. In this context, kinetochores additionally provide a signaling platform to activate and maintain checkpoint activity (Musacchio, 2015).

Most kinetochore proteins and their functions are largely conserved across various species from unicellular yeasts to humans (Westermann and Schleiffer, 2013). Thus, different model organisms such as *S. cerevisiae*, *Caenorhabditis elegans*, *Drosophila melanogaster* and cultivated human cells are used to study kinetochore proteins. In recent years, however, the kinetochores of several organisms were found to deviate from the canonical architecture. For instance, kinetochores of some lineages of insects, including the silk moth *Bombyx mori*, lack the H3 histone variant CENP-A which is considered crucial for kinetochore assembly in most other eukaryotes (Drinnenberg et al., 2014). Furthermore, kinetoplastids such as *Trypanosoma brucei* completely lack proteins that show any homology to known kinetochore proteins. Instead, these organisms have evolved a set of alternative kinetochore proteins that significantly differ from previously studied organisms (Akiyoshi and Gull, 2014).

1.2.1. Kinetochores assemble specifically on centromeric DNA

Assembly of kinetochores is exclusively restricted to specialized chromatin regions called centromeres. Importantly, there is only one centromere on each chromatid and ectopic kinetochore assembly, resulting in a dicentric chromatid, has fatal consequences for genomic integrity. The complexity of centromeres varies from very short point centromeres in *S. cerevisiae* over regional centromeres present in humans and most other higher eukaryotes to holocentric centromeres spanning the entire length of the chromosome which are found for instance in *C. elegans* and some insect lineages (Musacchio and Desai, 2017).

Centromeric chromatin is characterized by the presence of a specialized histone H3 variant, CENP-A in humans and Cse4 in budding yeast. In contrast to many other eukaryotes, the point centromere of *S. cerevisiae* is defined by its conserved DNA sequence of about 125 bp, which can be subdivided into three different centromere-determining elements (CDE). At least one kinetochore component, the Cbf3 complex, directly binds to one CDE in a sequence-specific manner (Lechner and Carbon, 1991). The histone H3 variant Cse4 is positioned in close proximity to Cbf3 by the chaperone Scm3 (Camahort et al., 2007; Meluh et al., 1998; Stoler et al., 1995, 2007). Importantly, a single Cse4-containing nucleosome is present at budding yeast kinetochores (Furuyama and Biggins, 2007). In contrast, centromere organization is much

more complex in higher eukaryotes where centromeres span over thousands to millions of base pairs containing repetitive α-satellite elements without sequence conservation. Thus, epigenetic marks such as CENP-A appear to play a more prominent role in centromere function and maintenance (Earnshaw and Rothfield, 1985; Musacchio and Desai, 2017; Sullivan et al., 1994). Since centromeres of these organisms are not defined by their DNA sequence, centromeric chromatin containing CENP-A must be maintained over the cell cycle by redistributing CENP-A to the nascent DNA strand during S-phase and its replenishment during the following G1-phase. The histone chaperone HJURP, homolog of Scm3, plays a crucial role in this process (Jansen et al., 2007; Zasadzińska et al., 2018).

1.2.2. The kinetochore is composed of multiple protein complexes which hierarchically assemble at the centromere

The kinetochore consists of several multiprotein complexes which assemble on the centromeric chromatin characterized by CENP-A/Cse4 (Figure 4). Most of the subcomplexes can be purified as recombinant proteins, allowing their detailed analysis *in vitro* (Pesenti et al., 2016). The kinetochore is structurally divided into an inner and outer kinetochore, which make different contributions to kinetochore function (Musacchio and Desai, 2017). The inner kinetochore, composed of the constitutive centromere-associated network (CCAN), is directly recruited to the centromere by interaction of CENP-C with CENP-A (Carroll et al., 2010). Furthermore, CENP-C recruits additional components of the CCAN to the centromere and is thus considered as adaptor connecting the centromere with the CCAN (Hornung et al., 2014; Klare et al., 2015; Screpanti et al., 2011; Weir et al., 2016).

The CCAN recruits subcomplexes of the outer kinetochore, collectively termed as KMN network, which consists of the three complexes Knl1 complex (Knl1 and Zwint in humans, Spc105 and Kre28 in budding yeast), Mtw1 complex (Mtw1, Dsn1, Nsl1 and Nnf1) and the Ndc80 complex (Ndc80, Nuf2, Spc24 and Spc25). Importantly, the KMN network mediates end-on binding of the kinetochore to dynamic microtubules and is responsible for conversion of microtubule depolymerization into chromosome movement in anaphase (Musacchio and Desai, 2017). The Mtw1 complex, a rod-shaped heterotetrameric complex, directly links the KMN network to the CCAN by interaction with Mif2/CENP-C and Ame1/CENP-U (Dimitrova et al., 2016; Hornung et al., 2014; Petrovic et al., 2016; Weir et al., 2016). Furthermore, the Mtw1 complex recruits the Knl1 and Ndc80 complexes and is thus the assembly hub for the KNM network (Dimitrova et al., 2016; Ghodgaonkar-Steger et al., 2020; Petrovic et al., 2016; Weir et al., 2016). Two different mechanisms were described for Knl1 complex recruitment to the Mtw1 complex. In humans, the C-terminal RWD domains of Knl1 appear to interact with the Mtw1 complex, while in budding yeast, Kre28 targets Spc105/Kre28 to the Mtw1 complex (Ghodgaonkar-Steger et al., 2020; Petrovic et al., 2014). MELT repeats of Knl1/Spc105 are phosphorylated by Mps1 and serve as an interaction platform for SAC signaling (London et al.,

2012; Shepperd et al., 2012; Yamagishi et al., 2012).

The Ndc80 complex, composed of Ndc80, Nuf2, Spc24 and Spc25 is the main microtubule-binding component of the kinetochore. All four components of this complex are predominantly composed of coiled-coil domains with globular domains at one end. Ndc80 and Nuf2 each contain one conserved Calponin homology (CH) domain at their N-termini, which are tightly packed in context of the full complex (Ciferri et al., 2008; Wei et al., 2007). Similarly, Spc24 and Spc25 have an elongated coiled-coil structure followed by an RWD domain at their C-terminal ends (Wei et al., 2006). The coiled-coil domains of the four subunits form a four-helix bundle, which is essential for tetramerization of the complex (Valverde et al., 2016). In total, the Ndc80 complex appears as an elongated structure with two globular domains at each end, giving it a dumb-bell shape. By anchoring one end to the kinetochore and extending the other end towards the microtubule, the Ndc80 complex bridges the gap between the kinetochore and microtubules (Musacchio and Desai, 2017).

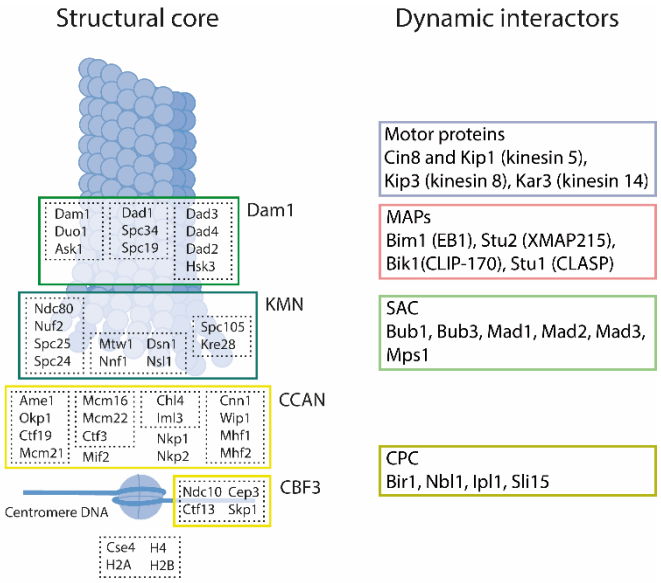

Figure 4: Schematic of the budding yeast kinetochore
Left side: Overview of a kinetochore assembled on a single Cse4 nucleosome. Subcomplexes of the CCAN and KMN and Dam1c assemble in a hierarchical manner. The dynamic plus end of a kinetochore microtubule is shown in the background.
Right side: Compilation of proteins that transiently associate with the kinetochore and contribute to chromosome segregation. Proteins are grouped according to their functional context.

The RWD domains of Spc24 and Spc25 recruit the Ndc80 complex to the kinetochore using two different receptors. The Mtw1 complex directly binds to the RWD domains through its Dsn1 subunit (Dimitrova et al., 2016; Malvezzi et al., 2013; Petrovic et al., 2010, 2016). Alternatively, the Ndc80 complex is recruited by Cnn1/CENP-T (Malvezzi et al., 2013; Nishino et al., 2013; Pekgöz Altunkaya et al., 2016; Schleiffer et al., 2012). The Ndc80 complex binds microtubules though its CH domains by recognizing both the inter- and intradimer interface of tubulin subunits, which makes the complex the major microtubule binding component of the kinetochore (Alushin et al., 2010; Ciferri et al., 2008; Wei et al., 2007; Wilson-Kubalek et al., 2008). In addition, the very N-terminal unstructured tail of Ndc80 is implicated in contacting the microtubule surface. Phosphorylation of the N-terminal tail by Aurora B might regulate microtubule binding by Ndc80c (Wimbish and DeLuca, 2020). However, the tail differently contributes to microtubule binding in different species. While kinetochore function in *S. cerevisiae* is largely unaffected by deletion of the tail (Kemmler et al., 2009; Lampert et al., 2013), kinetochore-microtubule interaction is deficient in human cells expressing the Ndc80

tail deletion mutant (Guimaraes et al., 2008; Miller et al., 2008).

1.2.3. The microtubule-binding Ska and Dam1 complexes support KMN function at the outer kinetochore

In vitro, the single Ndc80c molecules bind to the microtubule lattice but fail in tracking dynamic microtubule ends (Alushin et al., 2010; Lampert et al., 2010; Schmidt et al., 2012; Wilson-Kubalek et al., 2008). In contrast, multimeric Ndc80c assemblies were shown to efficiently track and couple cargoes to depolymerizing microtubule plus ends (Powers et al., 2009; Volkov et al., 2018). These results suggest that Ndc80c alone is not sufficient for faithful chromosome segregation *in vivo*. Instead, further kinetochore subcomplexes, namely the Dam1 complex and Ska complex, confer microtubule end tracking activity to the Ndc80 complex (Lampert et al., 2010, 2013; Schmidt et al., 2012; Tien et al., 2010). Either of the two complexes is present in most eukaryotic species know so far, however, in a mutually exclusive manner. While the Ska complex is predominantly found in higher eukaryotic organisms, the Dam1 complex is restricted to fungal species (van Hooff et al., 2017). In vertebrates, bioriented attachments are additionally stabilized by the Astrin-SKAP complex whose kinetochore localization is negatively regulated by Aurora B (Dunsch et al., 2011; Manning et al., 2010; Schmidt et al., 2010). Based on their shared functions in chromosome segregation and similar microtubule-binding properties, the Ska complex is considered as functional homolog of the Dam1 complex (van Hooff et al., 2017; Welburn et al., 2009). The molecular architecture, biochemical properties and functions in chromosomes segregation of both Ska complex and Dam1 complex will be discussed in the following paragraphs.

1.2.4. The Ska complex crucially contributes to kinetochore-microtubule attachments in metazoans

1.2.4.1. Function of the Ska complex in chromosome segregation

The Ska (*spindle and kinetochore associated*) complex is composed of its three subunits Ska1, Ska2 and Ska3, which was initially also called RAMA1 (Gaitanos et al., 2009; Hanisch et al., 2006; Raaijmakers et al., 2009; Theis et al., 2009; Welburn et al., 2009), and represents the most microtubule-proximal subcomplex of the metazoan kinetochore (Musacchio and Desai, 2017). Localization of the complex to the outer kinetochore depends on both the Ndc80 complex and microtubules as shown by RNAi depletion of Ndc80c or treatment with nocodazole. The Ska complex progressively accumulates at kinetochores during mitosis, reaching its maximum in anaphase (Daum et al., 2009; Gaitanos et al., 2009; Hanisch et al., 2006; Raaijmakers et al., 2009; Theis et al., 2009). Furthermore, Ska complex also localizes to microtubules of the mitotic spindle (Daum et al., 2009; Gaitanos et al., 2009; Theis et al., 2009). While depletion of individual Ska subunits by RNAi still allows normal chromosome alignment at the metaphase plate, cells are frequently delayed in anaphase onset or arrest in

metaphase in a SAC-dependent manner. Furthermore, formation of multipolar spindles and loss of individual chromosomes from the metaphase plate were reported (Gaitanos et al., 2009; Hanisch et al., 2006; Raaijmakers et al., 2009; Theis et al., 2009; Welburn et al., 2009). Depletion of Ska also reduces the cold-stability of kinetochore-microtubules and decreases the inter-kinetochore distance during metaphase, indicative of defects in formation of tension-bearing attachments (Raaijmakers et al., 2009). Recruitment of other core kinetochore complexes is unaffected by Ska depletion, implicating that Ska complex is the most microtubule-proximal kinetochore complex which does not recruit any downstream kinetochore components (Hanisch et al., 2006).

1.2.4.2. Subunit organization of the Ska complex

Structural analysis by X-ray crystallography revealed that two trimeric Ska complexes form a W-shaped dimer (Figure 5A; Jeyaprakash et al., 2012). Each Ska protomer, composed of a single copy of Ska1, Ska2 and Ska3, consists of two bundles of about 40 Å and 90 Å length, respectively, each of them composed of three parallel α helices (Figure 5B). The two bundles are oriented roughly perpendicularly to each other and are connected by short loops, which are assumed to form a rather rigid hinge (Jeyaprakash et al., 2012). Hydrophobic, polar and charged contacts of conserved residues were identified along the entire length of each bundle (Jeyaprakash et al., 2012). Ska1 apparently plays a crucial role in formation of the trimeric Ska complex. While Ska1 binds Ska3 in the absence of Ska2, Ska2 and Ska3 show no physical interaction in the absence of Ska1 (Gaitanos et al., 2009). This notion is supported by the observation that binary interactions within the complex are mainly found between Ska1-Ska3 and Ska1-Ska2, but rarely between Ska2-Ska3 (Jeyaprakash et al., 2012). The N-terminal ends of the short bundle of Ska protomers enable dimerization of the complex, involving conserved hydrophobic interactions and salt bridges (Jeyaprakash et al., 2012).

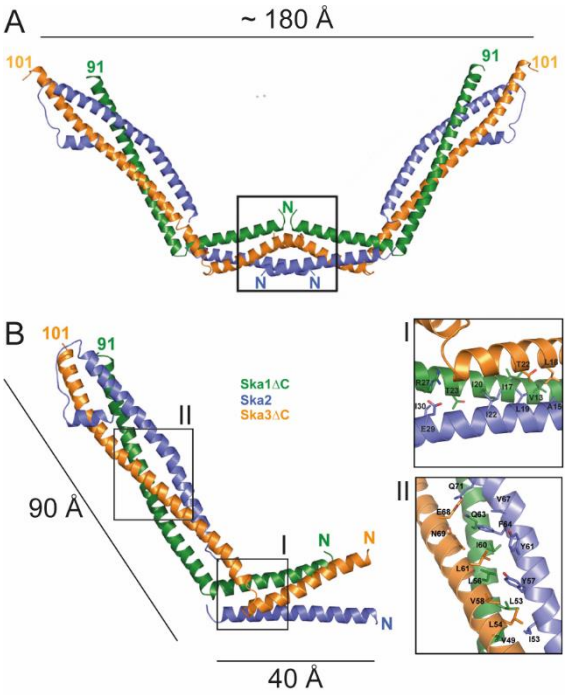

Figure 5: Structure of the Ska complex
Structure of W-shaped dimeric (A) or monomeric (B) Ska complex resolved by X-ray crystallography. The black box in A marks the dimerization interface. Boxed areas in B are shown as magnification on the right side. Amino acids that stabilize the coiled-coil interactions are annotated. Figure modified from Jeyaprakash et al., 2012.

1.2.4.3. The Ska complex directly binds to microtubules

Recombinant Ska complex robustly binds microtubules *in vitro*, not distinguishing straight or curved protofilaments (Abad et al., 2014; Schmidt et al., 2012; Welburn et al., 2009). In addition, Ska itself processively tracks depolymerizing microtubule plus ends and confers plus end tracking activity to the Ndc80 complex (Monda et al., 2017; Schmidt et al., 2012). Two functional domains of the complex were identified as crucial for microtubule binding: the conserved C-terminal half of Ska1 containing a microtubule-binding domain (MTBD) (Abad et al., 2014; Jeyaprakash et al., 2012; Monda et al., 2017) and the intrinsically disordered C-terminus of Ska3, which only marginally contributes to microtubule binding (Abad et al., 2016). While the Ska1 MTBD itself only weakly binds microtubules *in vitro,* artificial dimerization by fusion to GST resulted in more robust microtubule binding (Abad et al., 2014). Structural NMR and X-ray crystallography analysis of the Ska1-MTBD showed that the domain adopts a conformation similar to a winged helix domain (Figure 6, Abad et al., 2014; Schmidt et al., 2012). Conserved basic patches on the surface of the MTBD are essential for microtubule binding and substitution by alanine reduced microtubule binding *in vitro* and delayed mitotic progression *in vivo* (Abad et al., 2014; Monda et al., 2017; Schmidt et al., 2012). Notably, cells harboring mutations of the Ska1-MTBD basic patches almost normally aligned chromosomes at the metaphase plate, suggesting that microtubule binding by Ska complex is rather required for establishing robust kinetochore-microtubule attachments than for formation of initial attachments (Abad et al., 2014). Monda et al. (2017) demonstrated that Ska complex does not only bind to microtubules but also to soluble tubulin dimers and induces oligomerization into larger tubulin assemblies. Again, binding to tubulin depended on multiple positively charged residues in the surface of the Ska1-MTBD. Though several studies identified clusters of basic amino acids on the surface of the MTBD of Ska1 as crucial for microtubule binding, the acidic tails of tubulin subunits appear to be dispensable for binding of the Ska complex. Instead, crosslinking mass spectrometry analysis of Ska complex bound to microtubules suggests that the MTBD of Ska1 rather contacts globular and folded domains of tubulin (Abad et al., 2014).

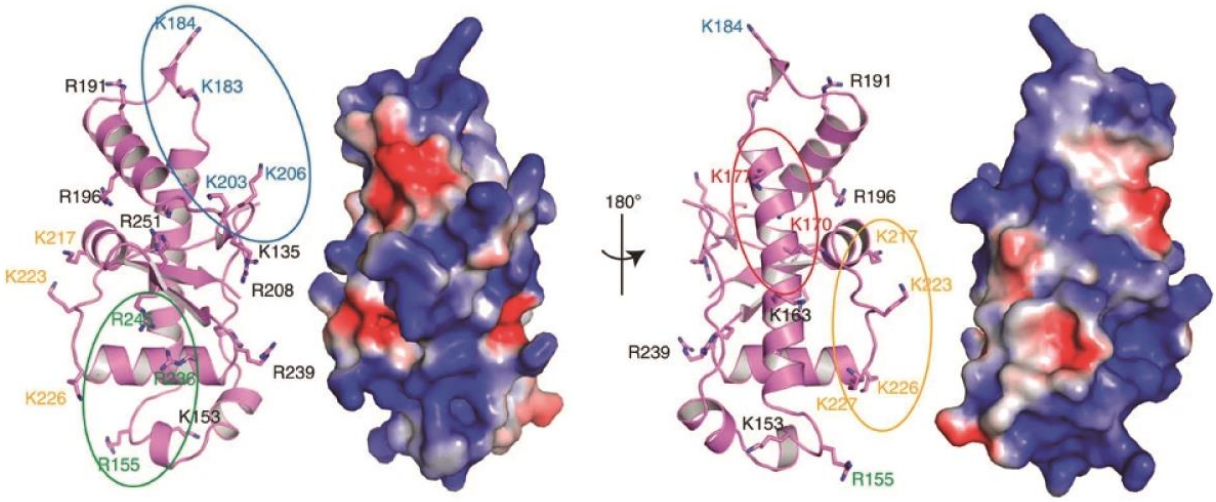

Figure 6: Multiple basic residues are exposed on the surface of the Ska1-MTBD
Cartoon representation and electrostatic surface potential map of Ska1-MTBD shown from two different perspectives. Structural information was obtained by X-ray crystallography. Side chains of surface exposed basic arginine and lysine residues are represented as sticks. Clustered basic residues that were mutated to alanine for microtubule binding studies are labelled in identical colors. Image from Abac et al., 2014.

1.2.4.4. Dynamic phosphorylation and dephosphorylation regulate kinetochore recruitment of the Ska complex

The amount of Ska complex at kinetochores increases during mitosis, culminating in anaphase (Daum et al., 2009; Gaitanos et al., 2009; Hanisch et al., 2006; Raaijmakers et al., 2009; Theis et al., 2009). This raises the possibility that the complex recognizes a distinct conformation of microtubule-attached kinetochores or is subject to dynamic phosphorylation and dephosphorylation during mitosis. Indeed, Ska3 is phosphorylated during mitosis and progressively dephosphorylated as the cell exits from mitosis (Gaitanos et al., 2009; Theis et al., 2009). Chan et al. (2012) identified both Ska1 and Ska3 as substrates of the Aurora B kinase, which negatively regulates Ska's kinetochore association: Inhibition of Aurora B leads to increased accumulation of Ska at kinetochores and promotes binding to the KMN components Mtw1c and Ndc80c (Chan et al., 2012). Expression of Ska1 versions that either prevent or mimic constitutive phosphorylation by Aurora B fail to rescue the Ska1 depletion phenotype indicating that dynamic phosphorylation and dephosphorylation of Ska is essential for chromosome segregation. While the phosphorylation-mimicking version is deficient in kinetochore localization and stabilizing kinetochore-microtubule attachments, the corresponding phosphorylation-preventing mutation normally localizes to kinetochores but prematurely hyper-stabilizes kinetochore microtubule attachments and thus prevents Aurora B-dependent error correction (Chan et al., 2012). Notably, several Aurora B phosphorylation sites reside within the MTBD of Ska1 near conserved basic residues (Chan et al., 2012; Schmidt et al., 2012). This observation allows to speculate that Aurora B negatively affects microtubule binding of the Ska complex by introducing negative charges to

the positively charged surface patches of Ska1-MTBD. However, there are contradictory studies reporting either unaffected or reduced microtubule binding by phosphorylated or phosphorylation-mimicking Ska complex (Chan et al., 2012; Schmidt et al., 2012).

By now, several studies imply that the Ska complex is not only a substrate of Aurora B but is also crucially involved in regulating the kinase-phosphatase balance at kinetochores during mitosis. Aurora B-dependent phosphorylation of Ndc80, Knl1, Dsn1 and histone H3 is reduced after RNAi depletion of Ska1 or Ska3, suggesting that Ska complex stimulates Aurora B activity at the kinetochore (Redli et al., 2016). The latter observation is supported by *in vitro* assays which demonstrate activation of Aurora B by Ska complex even in the absence of INCENP (Redli et al., 2016). Importantly, PP1 phosphatase apparently counteracts Aurora B since specific disruption of PP1 binding to Knl1 prevents kinetochore localization of Ska complex (Redli et al., 2016). Complementing these findings, Sivakumar et al. (2016) demonstrated that Ska1 directly recruits PP1 phosphatase to kinetochores. Notably, this interaction depends on the C-terminal portion of Ska1 harboring the MTBD. Ska1-dependent PP1 recruitment is required for dephosphorylation of Knl1 MELT motifs and thus silencing of Mps1-mediated SAC signaling and progression from metaphase to anaphase (Sivakumar et al., 2016).

1.2.4.5. Interaction between Ska and Ndc80 complexes and its regulation

Though early studies analyzing the physiological function of the Ska complex in cells congruently reported that kinetochore localization of the Ska complex depends on Ndc80c (Gaitanos et al., 2009; Hanisch et al., 2006; Raaijmakers et al., 2009), the mechanistic details of this interaction and its regulation during the cell cycle remain enigmatic to date. Two recent studies using *Caenorhabditis elegans* embryos and mammalian cells, respectively, provided new insights into kinetochore recruitment of the Ska complex. *C. elegans* Ska complex is a trimer composed of two copies of Ska1 and a single copy of Ska3 lacking any protein with homology to Ska2 as known so far (Schmidt et al., 2012). The N-terminal tail of Ndc80 is dispensable for viability in *C. elegans* embryos (Cheerambathur et al., 2013). Preventing phosphorylation of the Ndc80 tail by Aurora B prematurely stabilizes kinetochore-microtubule attachments by recruiting excessive amounts of Ska complex in both *C. elegans* and human cells (Cheerambathur et al., 2017; Wimbish et al., 2020). Besides dephosphorylation of Aurora B target sites within the N-tail of Ndc80, microtubule binding by Ndc80 through a cluster of conserved surface-exposed basic residues of the CH domain is essential for kinetochore localization of Ska complex. The authors suggest that Ska complex recognizes a distinct configuration of Ndc80 which requires dephosphorylation of Aurora B sites in the tail region and microtubule binding by the CH domain. By this, the complex is recruited to kinetochores, supported by the MTBD of Ska1, and stabilizes kinetochore-microtubule attachments prior to anaphase onset (Cheerambathur et al., 2017). These findings were supported by a related study which reported alignment of human Ska complex along microtubule protofilaments

depending on Ndc80c *in vitro* (Janczyk et al., 2017). Electron microscopy revealed that Ska complex forms V-shaped structures along protofilaments. Proximity of Ska complex and the Ndc80 CH domain at kinetochores suggests a functional role of this domain in Ska complex recruitment. Indeed, mimicking constitutive Aurora B phosphorylation of the Ndc80 tail prevents kinetochore association of Ska complex and abolishes Ndc80c-dependent binding to microtubules *in vitro* (Janczyk et al., 2017). However, these findings are challenged by other studies either proposing a requirement of the Ndc80 loop (Wimbish et al., 2020; Zhang et al., 2012, 2017) and coiled-coil region (Huis in 't Veld et al., 2019) or disproving a functional role of the Ndc80 tail and its phosphorylation by Aurora B (Huis in 't Veld et al., 2019).

While binding of Ska complex to Ndc80c was especially investigated focusing on regulation by Aurora B, further studies suggest an additional contribution of Ska3 phosphorylation by Cdk1-Cyclin B (Huis in 't Veld et al., 2019; Zhang et al., 2017). Ska3 is hyperphosphorylated during mitosis (Gaitanos et al., 2009; Zhang et al., 2017) and 14 potential Cdk1-Cyclin B phosphorylation sites matching the minimal consensus site (S/TP) were identified (Zhang et al., 2017). Ska3 phosphorylation by Cdk1-Cyclin B, especially of residues T358 and T360, is essential for kinetochore targeting of Ska complex, presumably by directly stimulating binding to Ndc80c (Huis in 't Veld et al., 2019; Zhang et al., 2017).

1.2.5. Molecular and cellular function of the budding yeast Dam1 complex

1.2.5.1. From classical genetics to high-resolution electron microscopy analysis - a brief history of Dam1c research

Research on the Dam1 complex (Dam1c) started in the late 1990's with the discovery of Duo1 (*death upon overproduction*) and Dam1 (*Duo1 and Mps1 interacting factor*) subunits, which were initially identified as components of the mitotic spindle (Hofmann et al., 1998). In following studies, crucially driven by the Drubin and Barnes lab, Dad1 (Enquist-Newman et al., 2001), Spc19, Spc34, Dad2 and Ask1 (Cheeseman et al., 2001a; Janke et al., 2002), Hsk3 (Li et al., 2002) and Dad3 and Dad4 (Cheeseman et al., 2002; Li et al., 2005) were identified as additional subunits of the heterodecameric complex. While Dam1c, also called DASH or DDD complex, was initially considered as critical for integrity of the mitotic spindle, further studies revealed that Dam1c is actually a component of the outer kinetochore that is capable of microtubule binding (Cheeseman et al., 2001a; Enquist-Newman et al., 2001; Janke et al., 2002; Li et al., 2002).

Identifying all subunits of the complex allowed cloning and purification of recombinant Dam1c from *E. coli* thereby laying the foundation of biochemical analysis of the complex *in vitro*. Key

publications in this context impressively demonstrated that the Dam1 complex is capable of forming microtubule-encircling rings (Figure 7) which processively track depolymerizing microtubule ends (Miranda et al., 2005; Westermann et al., 2005, 2006). These findings are crucial to understand how kinetochores are able to track and stay attached to depolymerizing microtubules and are the basis for biophysical studies investigating how Dam1c binds microtubules and thus contributes to the formation of load bearing attachments. In parallel, cell biological work focused on the physiological function of the complex during mitosis and how it is regulated by mitotic kinases such as Ipl1, Mps1 and Cdk1.

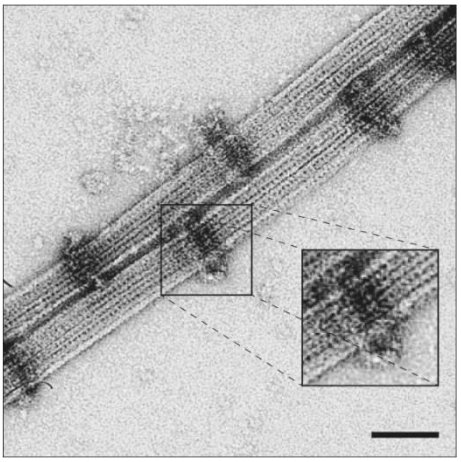

Figure 7: EM micrograph of Dam1c rings on microtubules
Dam1c rings assembled around Taxol-stabilized microtubules are visualized by electron microscopy after negative staining. The area within the black box is shown as enlarged inlay. Scale bar: 50 nm. Image from Westermann et al., 2005.

While low-resolution electron microscopy data of the Dam1 complex were published soon after discovery of the complex, more detailed structural information about the complex was not available for a long time. However, in 2018 Jenni and Harrison published a cryo-EM structure of a truncated Dam1 complex giving valuable insights into the complex' architecture.

1.2.5.2. Genetic and cellular analyses reveal a role of Dam1c in spindle and kinetochore function

Each subunit of the Dam1 complex is essential for viability. Thus, in order to study loss of function mutations of Dam1c subunits, a large number of conditional temperature-sensitive alleles has been developed. Using these genetic tools, it was demonstrated that functional Dam1c is required for integrity of the mitotic spindle. Interfering with Dam1c function results in a SAC-dependent metaphase arrest and cells progressing to anaphase after checkpoint inactivation displayed severe defects such as collapsed or highly bent spindles (Enquist-Newman et al., 2001; Hofmann et al., 1998; Jones et al., 1999, 2001; Li et al., 2005, 2002). Furthermore, chromosome missegregation and biorientation defects are frequently observed in Dam1c mutant strains, consistent with the complex' role in attaching kinetochores to microtubules (Cheeseman et al., 2001b; Jones et al., 2001; Li et al., 2002). Notably, cells overexpressing either Dam1 or Duo1 also arrested as large budded cells with defective spindles (Hofmann et al., 1998). The molecular mechanism for this phenomenon is unclear. However, one can speculate that excessive amounts of Dam1 or Duo1, which are both capable of microtubule binding (Cheeseman et al., 2001a), affect spindle stability or dynamics or that complex assembly is impaired by titrating away other subunits. Additional support for regulation of spindle dynamics by Dam1c comes from the notion that preventing

phosphorylation of Ask1 by Cdk1 reduces microtubule dynamics during mitosis (Higuchi and Uhlmann, 2005). Furthermore, *in vitro* data imply that recombinant Dam1c stabilizes microtubules by promoting their assembly from free tubulin and protecting them from depolymerization (Westermann et al., 2005).

Cellular localization of Dam1c subunits, the ability to bind microtubules *in vitro* and genetic interactions with mutants of outer kinetochore proteins, but not inner kinetochore subunits, congruently led to the conclusion that Dam1c is a component of the outer kinetochore (Cheeseman et al., 2001a, 2001b; Enquist-Newman et al., 2001; Janke et al., 2002). In contrast to other kinetochore proteins, recruitment of Dam1c to kinetochores is reduced after drug-induced depolymerization of microtubules. However, the strength of this effect depends on the applied experimental technique (Akiyoshi et al., 2010; Janke et al., 2002; Jones et al., 1999; Li et al., 2002).

The functional importance of Dam1c in chromosome segregation was also demonstrated by two independent studies employing an artificial recruitment approach of kinetochore assembly. Ask1 fused to TetR or LacI, respectively, was recruited to TetO or LacO arrays of an acentric plasmid or a yeast chromosome with an inactivated centromere. Recruitment of Dam1c is sufficient to ensure mitotic propagation of the plasmid or chromosome (Kiermaier et al., 2009; Lacefield et al., 2009). Conflicting results are reported whether Dam1c alone is sufficient for faithful chromosome segregation or additional kinetochore subcomplexes are required (Kiermaier et al., 2009; Lacefield et al., 2009).

1.2.5.3. The Dam1 complex tracks dynamic microtubules and efficiently couples microtubule depolymerization to chromosome movement

Recombinant Dam1c binds both Taxol-stabilized and dynamic microtubules. Interestingly, the complex oligomerizes into rings that fully encircle the microtubule (Figure 7, Miranda et al., 2005; Westermann et al., 2005, 2006). The rings appear with an inner diameter of about 32 nm and an outer diameter of about 54 nm and are estimated to contain 16 individual Dam1 complexes (Miranda et al., 2005; Westermann et al., 2005, 2006). Notably, the 16-fold symmetry of the rings complex is in striking contrast to the number of 13 protofilaments of the microtubule, which raises the possibility that the Dam1 ring complex does not recognize a distinct structural feature of the microtubule surface (Wang et al., 2007; Westermann et al., 2006). This is supported by the notion that Dam1c does not preferentially bind in a distinct orientation towards either end of microtubules (Ramey et al., 2011a). The microtubule binding ability of the complex is mainly conferred by the Dam1 and Duo1 subunits, especially by their C-terminal parts. End-on views of Dam1c rings assembled around microtubules reveal extensions of the Dam1 complex contacting the microtubule's surface which are absent in rings deleted of the Dam1 C-terminus (Wang et al., 2007). Furthermore, deletion of the Dam1 and Duo1 C-termini individually and in combination severely compromises microtubule binding *in*

vitro (Legal et al., 2016; Miranda et al., 2007; Westermann et al., 2005). Since both C-termini are rich in lysine and arginine residues and thus positively charged under physiological conditions it is tempting to speculate that these positively charged residues interact with the negatively charged C-terminal tails of the tubulin subunits. Indeed, removal of the acidic tubulin tails by limited proteolysis by Subtilisin weakens the interaction between Dam1c and microtubules (Ramey et al., 2011a; Westermann et al., 2005).

The discovery of the ring-forming Dam1 complex and its microtubule-tracking ability has thrilled the research community since a microtubule-embracing ring is considered as an ideal coupler to convert microtubule dynamics into chromosome movement while still allowing the exchange of tubulin subunits at the highly dynamic plus end. However, new questions concerning the mode of microtubule binding and tracking, cargo movement and the oligomeric state of the complex *in vitro* and *in vivo* were raised. Biophysical approaches helped answer most of these questions and shed light on the mechanism of microtubule binding and cargo transport. Optical trapping assays using either recombinant proteins or isolated kinetochore particles were employed to test for the requirement of Dam1c to establish robust attachments *in vitro*. Beads decorated with the respective proteins were attached to dynamic microtubule tips. The strength of attachments was assessed by application of a constant or increasing load. These biophysical assays, driven by the Biggins and Asbury labs, impressively demonstrated that Dam1c strengthens attachments between beads and dynamic microtubules (Akiyoshi et al., 2010; Asbury et al., 2006; Gutierrez et al., 2020; Sarangapani et al., 2013; Umbreit et al., 2014). Furthermore, theses assays proved to be a valuable tool to study the effect of various mutants of the Dam1 complex or of phosphorylation by kinases such as Ipl1 or Cdk1 (Grishchuk et al., 2008a; Gutierrez et al., 2020; Sarangapani et al., 2013).

Oligomerization of Dam1c into rings is apparently not essential for independent tracking of depolymerizing microtubules (Gestaut et al., 2008; Grishchuk et al., 2008b). However, the mechanism of microtubule tracking differs between Dam1c assemblies of different sizes (Grishchuk et al., 2008b). Two mechanistically distinct modes of plus end-tracking by the Dam1 complex have been proposed (Efremov et al., 2007). The first model, also called the biased diffusion model, suggests that Dam1c can freely and bidirectionally diffuse along the microtubule lattice. However, diffusion towards the plus end is limited by the curling protofilaments of the depolymerizing microtubule and thus biased towards the minus end (Gestaut et al., 2008). A prerequisite for this assumption is a relatively weak interaction between Dam1c and the microtubule surface which allows for rapid release and reformation of noncovalent binding (Efremov et al., 2007). Alternatively, the forced walk model proposes that the force generated by the flaring protofilaments during microtubule depolymerization (power stroke) pushes against the Dam1c ring moving it towards the minus end (Efremov et al., 2007; Koshland et al., 1988; Westermann et al., 2006). Irrespective of the mode of plus end-tracking by Dam1c, efficient conversion of microtubule depolymerization into chromosome

movement requires further components. A combination of a ring-shaped and a fibrillary component such as Dam1c and Ndc80c are considered as an ideal mechanistic device for optimal harnessing of the depolymerization force. While Dam1c moves along the depolymerizing microtubule as described above, Ndc80c helps align the cargo optimally in direction of the generated force, finally allowing for highly efficient conversion of the force generated by microtubule depolymerization into cargo movement (Volkov et al., 2013).

1.2.5.4. The Dam1c ring – one ring, two rings or no ring at all?

Observation of Dam1c rings *in vitro* raised the question in how far these assemblies represent the physiological properties of the complex and whether the experimental conditions, especially the protein concentrations of Dam1c, reflect the situation within the cell. As mentioned before, biophysical assays suggest the requirement for oligomerization of the Dam1 complex to establish load-bearing attachments (Umbreit et al., 2014). However, direct evidence for or against ring formation *in vivo* was missing for long time. Quantitative fluorescence microscopy was employed to estimate the copy number of Dam1c at kinetochores, yielding values of 16 – 20 (Joglekar et al., 2006) and about 12 copies (Dhatchinamoorthy et al., 2017). Notably, these copy numbers are in good agreement with the 16-fold symmetry of the ring complex visualized by electron microscopy *in vitro*, supporting the idea of a single Dam1c ring at each kinetochore (Jenni and Harrison, 2018; Wang et al., 2007; Westermann et al., 2006). Furthermore, electron cryotomography of yeast cells identified complete or partial Dam1c rings at the plus ends of kinetochore microtubules, but not elsewhere on the mitotic spindle. In agreement with the *in vitro* data, the Dam1c rings found *in vivo* comprised 17 Dam1c heterodecamers (Ng et al., 2019). However, the concept of a single Dam1c ring was challenged by a study suggesting the presence of two rings at each kinetochore which are bridged by the Ndc80 complex (Kim et al., 2017). The spacing between the two Dam1c rings depends on the distance between the interaction sites within Ndc80c and can be modulated *in vitro* by insertion of heptad repeats. Varying the distance between the Dam1c rings *in vivo* does not support cell viability suggesting a functional relevance of correct spacing between the complexes (Kim et al., 2017). It is worth mentioning that the concept presented in this study strongly contradicts the results of several other studies that support the idea of a single Dam1c ring employing a broad methodological spectrum. Furthermore, the idea of the double Dam1c ring was not further investigated in more detail until now.

1.2.5.5. The Ndc80 complex serves as kinetochore receptor of Dam1c

Kinetochores hierarchically assemble on centromeric DNA specified by the presence of a distinct histone protein with interdependency between different subcomplexes (Biggins, 2013; Musacchio and Desai, 2017). In contrast to most other kinetochore proteins, full recruitment of the Dam1 complex requires microtubules and an intact mitotic spindle since drug-induced

depolymerization impairs kinetochore localization of the complex (Janke et al., 2002; Jones et al., 1999; Li et al., 2002), suggesting that the complex is brought to the kinetochore during the establishment of kinetochore-microtubule attachments. The microtubule-binding activity of the complex implies that Dam1c is part of the outer kinetochore. However, the binding partner at the kinetochore remained unknown so far. Eventually, the Ndc80 complex was identified as potential kinetochore receptor for Dam1c by systematic and large-scale yeast two-hybrid screens (Shang et al., 2003; Tong et al., 2001; Wong et al., 2007) and microscopy analysis (Janke et al., 2002). Recombinant Dam1c and Ndc80c, expressed and purified from *E. coli*, only weakly bind to each other in solution (Lampert et al., 2010; Tien et al., 2010). Nevertheless, Dam1c allows Ndc80c to track dynamic microtubule plus end while Ndc80c itself fails in doing so (Lampert et al., 2010; Tien et al., 2010). Notably, the interaction is sensitive to phosphorylation of the Dam1 complex by Ipl1 (Lampert et al., 2010; Tien et al., 2010) and is thus considered as key regulatory step for the formation of bioriented kinetochore-microtubule attachments. Several studies attempted to map and identify the Dam1c-Ndc80c binding interface using different technical approaches. Lampert et al. (2013) identified Ndc80 residues 256 – 273 as critical for the interaction with Dam1c. These residues are part of a region between the CH domain and the coiled-coil region which probably protrude from the surface and thus offer interaction surfaces with polar residues. In addition, this region is close to the CH domain of Nuf2 and thus near the surface of the microtubule. Deletion of these residues does not compromise Ndc80 complex formation but disrupts interaction with the Dam1 complex *in vitro*. In contrast, deletion of the N-terminal tail of Ndc80 (amino acids 1 – 116) does not affect interaction with Dam1c but is lethal in combination with deletion of residues 256 - 273 (Lampert et al., 2013). Notably, kinetochore localization of Dam1c is severely compromised in cells expressing Ndc80$^{\Delta 256–273}$ demonstrating the relevance of these residues for Dam1c kinetochore recruitment by Ndc80c (Lampert et al., 2013).

Another study from the Tanaka lab proposes an interaction between Dam1c and the loop region of Ndc80 which interrupts protrudes from the coiled-coil region and is highly conserved among eukaryotes (Maure et al., 2011). Deletion of a large loop region (amino acids 480 – 520) is lethal, while deletion of a smaller region (Ndc80$^{\Delta 490\text{-}510}$) is viable, but temperature sensitive. Mutating seven conserved residues within the loop to alanine (Ndc80^{7A}) results in a milder phenotype than the deletion mutant. Cells carrying the Ndc80$^{\Delta 490\text{-}510}$ allele are proficient in forming initial lateral kinetochore-microtubule attachments, but fail in establishing biorientation (Maure et al., 2011). Furthermore, Dam1c recruitment to kinetochores is strongly impaired in cells expressing Ndc80$^{\Delta 490\text{-}510}$ apparent as localization away from and between kinetochore clusters. The possible function of the Ndc80 loop in Dam1c binding was further confirmed by a yeast two-hybrid assays showing that only wild type Ndc80, but not Ndc80$^{\Delta 490\ 510}$, interacts with Dam1 (Maure et al., 2011). However, biochemical data about the implication of the Ndc80 loop in Dam1c binding are missing so far.

A third study mapped the Ndc80c-Dam1c binding interface by crosslinking mass spectrometry analysis of the complexes in presence of Taxol-stabilized microtubules (Kim et al., 2017). Three potential interaction sites within Ndc80 were mapped, each of them in proximity to either the C-terminus of Dam1, Ask1 or Spc34. Notably, mutations of Ndc80 affecting the putative interaction sites are lethal (Tien et al., 2013). Furthermore, the binding regions of the three mentioned Dam1c subunits are phosphorylated by Ipl1 which disrupts binding of Ndc80c to Dam1c (Lampert et al., 2010; Tien et al., 2010). Manipulation of Dam1c-Ndc80c either by mimicking constitutive Ipl1 phosphorylation of Dam1c or by small insertions into Ndc80 weakens the interaction between the two complexes in the presence of microtubules. *In vivo*, these mutants negatively affect the formation of bioriented kinetochore-microtubule attachments (Kim et al., 2017).

All these studies identified different regions of the Ndc80 protein as essential for binding Dam1c, making it difficult to define a distinct binding interface. It is possible that Dam1c and Ndc80c contact each other at multiple sites or that binding sites change depending on tension applied to the complexes. It is worth mentioning that all three studies mainly used either deletion or insertion of several amino acids to manipulate Dam1c binding to Ndc80c. Thus, one cannot definitely exclude minor structural changes of Ndc80c that indirectly effect Dam1c binding.

Besides Ndc80c-dependent recruitment, microtubules are essential for Dam1c loading onto kinetochores (Janke et al., 2002; Jones et al., 1999; Li et al., 2002). Furthermore, there is evidence that Dam1c itself promotes its own recruitment to microtubules in a cooperative manner *in vitro* (Gestaut et al., 2008).

1.2.5.6. Dam1c is a substrate of the three major mitotic kinases Ipl1, Mps1 and Cdk1

Dynamic phosphorylation and dephosphorylation of kinetochore proteins has been described as crucial regulatory event during formation and correction of kinetochore-microtubule attachments and SAC signaling. Multiple kinases such as Ipl1/Aurora B, Mps1 and Cdk1 and counteracting protein phosphatases are implicated in a complex network with sophisticated crosstalk between the individual signaling cascades (reviewed in Saurin, 2018). Notably, several subunits of the Dam1 complex are substrates of the conserved kinases Ipl1, Mps1 and Cdk1 (Table 1).

Table 1: Overview of phosphorylation sites of the Dam1 complex
Phosphorylated residues of Dam1c subunits and the modifying kinase are listed. References refer to the studies that first identified the listed phosphorylation sites.

subunit	residues	modifying kinase	reference
Dam1	S20, S257 S265, S292	Ipl1	Cheeseman et al., 2002
Spc34	T199	Ipl1	Cheeseman et al., 2002
Ask1	S200	Ipl1	Cheeseman et al., 2002
Dam1	S13, S49, S217, S218, S221, S232	Mps1	Shimogawa et al., 2006
Ask1	S216, S250	Cdk1	Li and Elledge, 2003
Dam1	S31	PKA	Shah et al., 2019

Phosphorylation of Dam1c by Ipl1 is best studied so far and appears to play a key role in error correction and formation of bioriented kinetochore-microtubule attachments. Three studies independently reported phosphorylation of one or several Dam1c subunits, which is either cell cycle specific or depends on Ipl1 (Cheeseman et al., 2001a; Kang et al., 2001; Li et al., 2002). Ipl1-dependent phosphorylation of Dam1 achieves its maximum during S-phase when bioriented attachments are formed. Phosphorylation finally decreases in metaphase when tension is applied on bioriented sister chromatids (Keating et al., 2009). Cheeseman et al. (2002) finally mapped Ipl1-dependent phosphorylation sites within the Dam1 complex and described their physiological function *in vivo*. Furthermore, the authors proposed a consensus sequence for Ipl1 which is R/K-x-S/T-I/L/V. Six Ipl1-dependent phosphorylation sites within Dam1c were identified and are listed in Table 1. Mutating the phosphorylation sites in Spc34 or Ask1 to alanine or aspartic acid to prevent or mimic constitutive phosphorylation has little if any effect on cell proliferation (Cheeseman et al., 2002). In a similar manner, manipulation of individual Dam1 phosphorylation sites is well tolerated. However, preventing phosphorylation of Dam1 at all four sites ($Dam1^{4A}$) is lethal while the respective phospho-mimicking mutation ($Dam1^{4D}$) causes severe growth defects demonstrating the physiological relevance of Dam1c phosphorylation by Ipl1 (Cheeseman et al., 2002). Notably, the $Dam1^{4D}$ allele partially suppresses the growth defect of the temperature-sensitive *ipl1-2* allele at the restrictive temperature, suggesting that Dam1 is a key substrate of the Ipl1 kinase (Cheeseman et al., 2002). This conclusion is further supported by the observation that cells in which phosphorylation of Dam1c is partially prevented display a high frequency of chromosome segregation errors reminiscent of Ipl1 loss-of-function. Similarly, mimicking Ipl1-dependent phosphorylation causes lagging chromosomes presumably by the inability to establish stable kinetochore-microtubule attachments (Cheeseman et al., 2002). Binding of Ipl1-phosphorylated Dam1c to Ndc80c is severely compromised (Kim et al., 2017; Lampert et al., 2010; Sarangapani et al., 2013; Tien et al., 2010), fitting to Ipl1's role in releasing erroneous kinetochore-microtubule attachments. Notably, the three phosphorylation sites in the Dam1 C-terminus and in Ask1 and Spc34 are mapped close to potential interaction interfaces with

Ndc80c, explaining how Ipl1 phosphorylation may affect binding between the two complexes (Kim et al., 2017). In addition to disrupting the Dam1c-Ndc80c interaction, Ipl1 promotes microtubule catastrophe and detachment of kinetochore particles by phosphorylating Dam1c which further destabilizes the kinetochore-microtubule interface and favors detachment of kinetochores from dynamic microtubules (Sarangapani et al., 2013). Besides the phosphorylation sites within the C-terminus, phosphorylation of Dam1 S20 is attributed a key role in regulating oligomerization of Dam1c. Dam1c mimicking Ipl1 phosphorylation of all four sites in Dam1 has a decreased ability to form oligomers *in vitro* and displays reduced microtubule binding (Wang et al., 2007). Structural analyses suggest that Dam1 S20 is located within the conserved oligomerization interface of Dam1c and phosphorylation presumably negatively regulates assembly of higher oligomeric structures (Jenni and Harrison, 2018; Zelter et al., 2015). Both *in vitro* and *in vivo* data show that Ipl1 phosphorylation mainly weakens binding of kinetochores to microtubule ends, while lateral attachments are not affected. The selective sensitivity of end-on attachments might play an important role in error correction and reformation of new bioriented attachments (Doodhi et al., 2021; Kalantzaki et al., 2015). While the physiological function of Dam1c phosphorylation by Ipl1 is well characterized *in vivo* and *in vitro*, little is known about phosphorylation by Mps1, the effector kinase of the spindle assembly checkpoint. Shimogawa et al. (2006) identified six potential Mps1 phosphorylation sites within the Dam1 subunit (Table 1). Preventing phosphorylation of S218 and S221 individually or in combination clusters kinetochores closer to the spindle pole bodies while the cells show normal viability, cell cycle progression and chromosome segregation. However, the S218A and S221A alleles show genetic interactions with the *spc110-226* allele (Shimogawa et al., 2006). In this study, phosphorylation sites were mapped after *in vitro* phosphorylation of only the Dam1 subunit in absence of other subunits. Hence, it is conceivable that Dam1 is not the only Mps1 substrate within the complex (Shimogawa et al., 2006). Besides its role in spindle pole body duplication and SAC signaling, Mps1 is attributed to be involved in establishing biorientation and ensuring error-free chromosome segregation (Jones et al., 2005; Maure et al., 2007).

As implied by the name Dam1 (*Duo1 and Mps1 interacting factor*, Hofmann et al., 1998), early studies report genetic interactions between temperature-sensitive alleles of both Dam1 and Mps1, suggesting a functional connection between these proteins. For instance, the *dam1-1* and *mps1-1* alleles are synthetically lethal. However, the fact that *dam1-1* cells do not require a functional spindle assembly checkpoint suggests that Mps1 fulfills additional functions at the kinetochore besides SAC signaling (Jones et al., 1999). In agreement with these observations, other Dam1c alleles such as *dam1-11*, *dam1-24* and *dad1-1* are hypersensitive to mild inhibition of Mps1 (Dorer et al., 2005). So far, it remains an open question whether Dam1c and Mps1 physically interact at the kinetochore and Dam1c serves as additional kinetochore receptor for Mps1.

Besides Ipl1 and Mps1, Cdk1 (Cdc28-Clb2 in budding yeast) phosphorylates Dam1c in a cell cycle dependent manner (Li and Elledge, 2003). Cdk1 phosphorylates Ask1 residues S216 and S250 (Li and Elledge, 2003), however, other subunits were not tested for Cdk1-dependent phosphorylation so far. Preventing phosphorylation of Ask1 by alanine substitutions of the modified serine residues ($Ask1^{2A}$) causes no obvious growth defect in otherwise unperturbed cells. However, further compromising Ask1 function or Cdk1 activity is synthetically lethal with the $Ask1^{2A}$ allele (Li and Elledge, 2003). Ask1 is presumably dephosphorylated by Cdc14 during mitotic exit (Higuchi and Uhlmann, 2005; Li and Elledge, 2003) which is required for regulation of microtubule dynamics and correct execution of anaphase A spindle elongation (Higuchi and Uhlmann, 2005). Biophysical experiments measuring the binding strength between purified kinetochore particles and dynamic microtubules suggest that Cdk1 phosphorylation of Ask1 strengthens binding of kinetochores to microtubules and presumably promotes oligomerization of Dam1c (Gutierrez et al., 2020).

Ipl1, Mps1 and Cdk1 have well described mitotic functions. Thus, posttranslational modification of Dam1c by these kinases appears plausible. However, two studies report phosphorylation of Dam1c by protein kinase A (PKA) which may link kinetochore function to cellular glucose signaling (Li et al., 2005; Shah et al., 2019). Dam1 S31 was identified as the only PKA phosphorylation site within the Dam1 complex and, notably, preventing or mimicking phosphorylation of S31 negatively affects kinetochore localization of Dam1c, spindle integrity and chromosome segregation (Shah et al., 2019). Nevertheless, considering the highly similar consensus sequences of Ipl1 (R/K-x-S/T-I/L/V) and PKA (R-R-x-S/T-any hydrophobic), a role of Ipl1 in $Dam1^{S31}$ phosphorylation *in vivo* cannot be completely ruled out.

1.2.5.7. Identification of potential Dam1c binding proteins

The cellular function of Dam1c, its molecular architecture and phosphorylation by kinases has been extensively studied during the past years. However, relatively little is known about proteins that directly interact with Dam1c. To date, Ndc80c and microtubules are the only identified proteins that bind to Dam1c and *in vitro* binding of Ndc80c to Dam1c was only observed in the context of microtubules (Lampert et al., 2010; Tien et al., 2010).

Screens for genetic or yeast two-hybrid interactions were employed to untangle the network of protein-protein interactions at the kinetochore and the mitotic spindle and identified a large number of potential interactors of Dam1c (e.g. Ito et al., 2001; Uetz et al., 2000; Wong et al., 2007). However, studies verifying and characterizing these interactions in detail are missing so far. Comprehensive data on potential interactors are curated in the *Saccharomyces* Genome Database (SGD, www.yeastgenome.org). Proteins and alleles showing a physical or genetic interaction with Dam1c can be roughly classified into three different categories according to their physiological functions. First, various alleles of Dam1c subunits show genetic interactions with each other (Cheeseman et al., 2001a; Enquist-Newman et al., 2001)

suggesting that misfunction of Dam1c *in vivo* is tolerated to a certain degree but is fatal when function of the complex is further compromised. Second, many temperature-sensitive Dam1c alleles arrest in metaphase at the restrictive temperature in a cell cycle dependent manner. Thus, inactivation of the spindle assembly checkpoint, for instance by deletion of Mad2, Bub1 or compromising Mps1 kinase activity (*mps1-1*), is lethal in combination with some Dam1c alleles (Cheeseman et al., 2001b; Enquist-Newman et al., 2001; Jones et al., 1999). In addition, synthetic lethality was observed for two Dam1c alleles in combination with a deletion of the CPC component Bir1 (Cheeseman et al., 2001b; Jones et al., 1999). Lastly, the third group comprises microtubule-binding proteins such as the molecular motors Cin8 and Kar3 (Cheeseman et al., 2001b; Jones et al., 1999) and plus end-tracking proteins such as Stu1, Stu2, Bik1 and Bim1 (Cheeseman et al., 2001a, 2001b; Enquist-Newman et al., 2001; Jones et al., 1999). In case of Bim1 and Stu2, interactions with Dam1 or Duo1 were identified by yeast two-hybrid analyses (Ito et al., 2001; Kalantzaki et al., 2015; Uetz et al., 2000; Wong et al., 2007). Bik1, Bim1 and Stu2 as plus end-associated proteins (+TIPs) are potential interactors of particular interest due to their localization to and regulatory function at microtubule plus ends (revied in Akhmanova and Steinmetz, 2008, 2015). Thus, it is very likely that these proteins contribute to the functionality of Dam1c. A role for Stu2 and its human homolog chTOG in chromosome segregation was recently described (Herman et al., 2020; Miller et al., 2016, 2019).

1.2.5.8. Crosslinking mass spectrometry and cryo-EM analyses reveal insights into the topology of the Dam1 complex

Low resolution EM structures of Dam1c rings assembled around microtubules were published relatively soon after discovery of the complex (Miranda et al., 2005; Westermann et al., 2005). However, detailed structural analyses including mapping of the individual subunits within the complex were missing for a long time. Individual monomeric negatively stained Dam1c appears as T-shaped particles in electron microscopy consisting of an elongated crossbar with a so-called protrusion domain that projects roughly perpendicularly from the middle region of the crossbar (Figure 8A). The C-terminus of the Dam1 subunit partially contributes to this protrusion domain (Wang et al., 2007). Three-dimensional modelling of dimeric and trimeric particles revealed two distinct binding interfaces which mediate oligomerization of the complex (Figure 9A and B). First, the protrusion domain of the first monomer contacts the one end of the crossbar of the second monomer. Second, the other end of the crossbar of the first monomer interacts with the middle part of the crossbar of the second monomer (Ramey et al., 2011b; Wang et al., 2007).

However, obtaining high-resolution structural data on the Dam1 complex proved to be challenging (Ramey et al., 2011a; Wang et al., 2007). Nevertheless, different biochemical approaches helped elucidate the arrangement of the individual subunits within the complex. In

the absence of individual subunits, the remaining Dam1c subunits assemble into distinct subcomplexes which allow to draw conclusion about interactions between the subunits of the complex. In the absence of Hsk3, for instance, Ask1, Dad2 and Dad4 form a subcomplex, while Dad1, Dad3, Dam1, Duo1, Spc19 and Spc34 form another subcomplex which is capable of microtubule binding *in vitro* and kinetochore localization *in vivo* (Miranda et al., 2007; Umbreit et al., 2014). Removal of the Dam1 subunit results in a complex consisting of Ask1, Dad2, Dad4, Hsk3, Spc19 and Spc34, but lacking Duo1, Dad1 and Dad3 (Miranda et al., 2007). Similar complex disruption is achieved by truncation of individual subunits such as Dam1 and Duo1 or introduction of single amino acid substitutions (Legal et al., 2016; Westermann et al., 2005). The N-termini of four subunits were located by fusing them to MBP and visualizing the complex including the bulky tag by electron microscopy (Ramey et al., 2011b). These data are complemented by insights from crosslinking mass spectrometry analyses of the Dam1 complex in the absence and presence of microtubules (Legal et al., 2016; Zelter et al., 2015). In combination, these different approaches allowed to model the topology of the subunits within the complex with relatively high accuracy (Figure 8B).

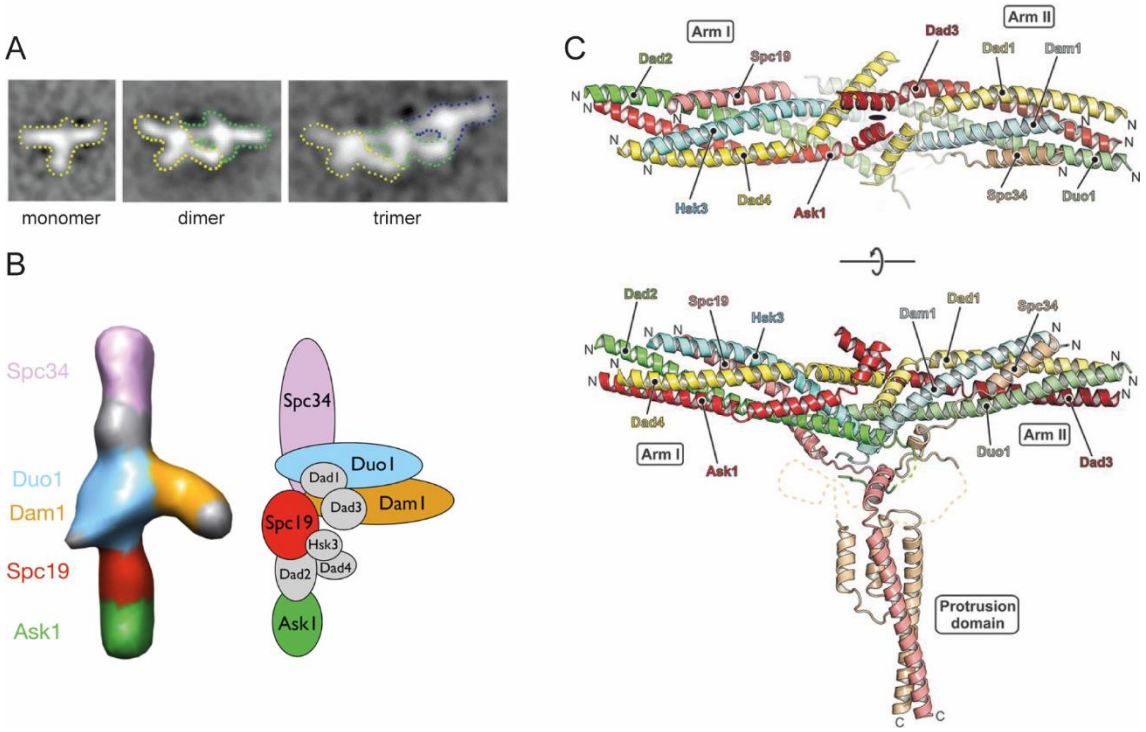

Figure 8: Molecular structure of the Dam1 complex
A: EM micrographs of monomeric, dimeric and trimeric Dam1 complex. The outline of individual monomers is marked by dashed lines. Images from Wang et al., 2007.
B: Subunit organization within the monomeric Dam1 complex according to Ramey et al., 2011b. The positions of Ask1, Duo1, Spc19 and Spc34 were determined by fusion of the respective protein to MBP and previous biochemical data. The position of Dam1 is derived from studies on C-terminally truncated Dam1.
C: Cryo-EM structure of *C. thermophilum* Dam1 complex published by Jenni and Harrison, 2018. View along the two-fold symmetry axis (top) and side view (bottom) of the complex are shown as ribbon diagram. Pairs of subunits that were identified as structural paralogs are depicted in matching colors.

Pioneering work to this field was contributed by Jenni and Harrison (2018) who solved a high-resolution cryo-EM structure of the *Chaetomium thermophilum* Dam1 complex. To allow detailed structural analysis, they engineered a complex lacking most flexible and unstructured regions, resulting in a complex of about 115 kDa. The recombinant complex forms tube-like structures consisting of stacks of Dam1c rings with 17 monomers that are oriented in alternating directions. Consistent with previous studies, Dam1c forms a T-shaped complex consisting of a crossbar and a protrusion domain (Figure 8C). The crossbar can be subdivided into arm I and arm II, each containing coiled-coil regions. Arm I consists of Ask1, Dad2, Dad4, Hsk3 and the N-terminal part of Spc19, arm II of Dad1, Dad3, Dam1, Duo1 and the N-terminal part of Spc34. The five subunits of each arm form a five-helix bundle with their N-termini at the distal ends of the arms and merge in the central region of the complex. From there, the protrusion domain, composed of Spc19 and Spc34, almost perpendicularly extends from the central region. (Jenni and Harrison, 2018). The complex displays a two-fold (pseudo-) symmetry regarding the two arms since each subunit within arm I can be assigned a corresponding counterpart in arm II which is similar in its conformation. The five pairs are Ask1-Dad3, Dad2-Duo1, Dad4-Dad1, Hsk3-Dam1 and Spc19-Spc34 (Jenni and Harrison, 2018). Sequence similarity between some Dam1c subunits had already been reported before suggesting that the subunits arose from genome duplication (van Hooff et al., 2017). Jenni and Harrison (2018) identified two interfaces at which Dam1c monomers interact during oligomerization, which match the contact sites identified previously (Figure 9; Ramey et al., 2011b; Wang et al., 2007). At interface I, the tip of arm II contacts the base of the protrusion domain of the second monomer. At interface II, arm I of the second complex engages with the central region and parts of arm I of the first monomer (Jenni and Harrison, 2018). The surface-exposed residues of the binding interfaces are highly conserved across various yeast species while most other regions of the complex are less conserved. Both hydrophobic and charged residues are found at the dimerization interfaces (Jenni and Harrison, 2018). Unfortunately, the published structure misses several functionally important regions of the complex, including the unstructured C-termini of Dam1 and Duo1 and the sites that are phosphorylated by Cdk1 or Ipl1. However, the structural information on the residual parts of the complex allow to make predictions about the localization of the aforementioned regions. For instance, the putative position of the Dam1 N-terminus with its Ipl1 phosphorylation site allows to speculate how phosphorylation of Dam1 S20 negatively affects oligomerization of Dam1c (Jenni and Harrison, 2018).

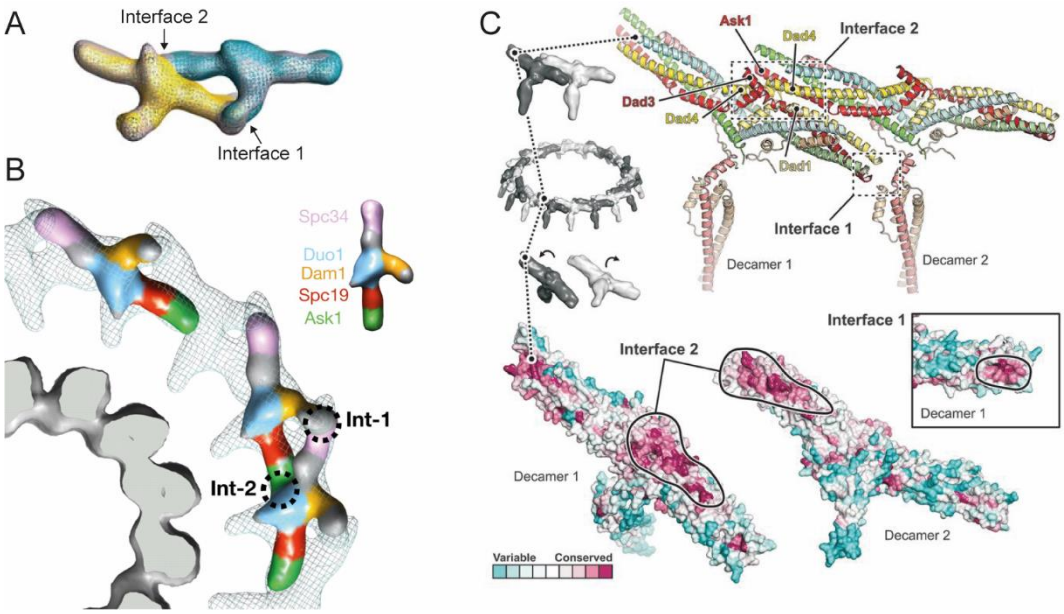

Figure 9: Structural details of the Dam1c oligomerization interfaces
A: Three-dimensional reconstruction of dimeric Dam1c from single-particle electron microscopy data. The two individual monomers are colored in yellow and blue, and the two dimerization interfaces are highlighted. Image from Wang et al., 2007.
B: Modelling of monomeric and dimeric Dam1c into the Dam1c ring structure (grey mashes) assembled around a microtubule (solid grey mass in lower left corner). Both monomeric and dimeric Dam1c fit snugly into the Dam1c ring structure without major conformational changes. Image from Ramey et al., 2011b.
C: Cryo-EM structure of a Dam1c dimer extracted from an assembled ring (top). Oligomerization interfaces are marked by dashed boxes. Surface-exposed amino acids at interface 2 are highly conserved across species, while more variability is allowed at other sites of the complex. Image from Jenni and Harrison, 2018.

1.2.5.9. Function of the Dam1 complex during meiosis

The physiological function of the Dam1c complex during mitosis has been extensively studied, but relatively little is known about its role in meiotic chromosome segregation. Since mitosis and meiosis II are very similar in respect of segregating sister chromatids it is reasonable to speculate that Dam1c functions in a similar manner in mitosis and meiosis II. In meiosis I, when homologous chromosomes each consisting of two sister chromatids are separated, Dam1c together with Ndc80 is removed from kinetochores in premeiotic S-phase and prophase I (Borek et al., 2021; Miller et al., 2012). Low gene expression of Hsk3 and Dad3 during these stages of meiosis might support removal of Dam1c from kinetochores (Miller et al., 2012). In the absence of Hsk3, Dam1c dissociates into two subcomplexes that are only partially if at all functional (Miranda et al., 2007; Umbreit et al., 2014). Reduction of functional Dam1c and also Ndc80c during early stages of meiosis I might prevent premature kinetochore assembly on meiotic chromosomes and thus allows formation of a meiosis-specific kinetochore configuration which is required for coorientation of sister kinetochores (Borek et al., 2021; Miller et al., 2012).

Phosphorylation of the Dam1 subunit at residues S218 and S221 by Mps1 is essential to maintain stable attachments of chromosomes to microtubules of the meiotic spindle (Meyer et

al., 2018), which resembles the effect of Mps1 phosphorylation during mitosis (Shimogawa et al., 2006).

1.3. Microtubule-associated proteins support the function of the outer kinetochore in chromosome segregation

1.3.1. EB proteins are key regulators of the microtubule network

A large number of diverse proteins localize to the mitotic spindle and influence microtubule dynamics. Similar to kinetochore proteins, many of the these microtubule-associated proteins (MAPs) are conserved across various eukaryotic species and fulfill conserved functions in different organisms (review in Akhmanova and Steinmetz, 2008, 2015). Members of the family of end-binding (EB) proteins are considered as master regulators of the microtubule network as they directly affect microtubule dynamics and recruit a large set of cargo proteins to microtubules. While there are three EB proteins in mammalian cells (EB1, EB2 and EB3), Bim1 (*binding to microtubules 1*) is the only member of this family found in budding yeast and considered as the homolog of EB1. Notably, EB proteins are autonomous plus end-tracking proteins (+TIPs) which specifically recognize and bind to the plus ends of polymerizing microtubules (Akhmanova and Steinmetz, 2008, 2015; Bieling et al., 2007). EB proteins share a conserved architecture comprising an N-terminal Calponin homology (CH) domain which is required and sufficient for microtubule binding (Hayashi and Ikura, 2003), followed by a flexible linker region and a coiled-coil domain which mediates homodimerization of two EB proteins (Honnappa et al., 2005). The C-terminal part comprises an end-binding protein homology (EBH) domain which is essential for binding of cargo proteins. To recruit proteins to microtubules, EB proteins specifically bind the linear tetrapeptide sequence SxIP (serine – any amino acid – isoleucine – proline) with their EBH domain (Honnappa et al., 2005, 2009). SxIP motifs are frequently flanked by basic amino acids which further support association with the negatively charged patches on the surface of the EBH domain. Furthermore, addition of a negative charge in proximity to the SxIP motif by phosphorylation in some cases negatively regulates binding to the EBH domain (Honnappa et al., 2009; Zimniak et al., 2012). Besides the EBH domain, the C-terminal EEY/F tail (EETF in Bim1) of EB proteins interacts with CAP-Gly (cytoskeleton-associated protein glycine-rich) domains which are present in proteins such as CLIP-170 (Bik1 in yeast) (Weisbrich et al., 2007). EBH domain and EEY/F motif of mammalian EB1 are in such close proximity to each other that simultaneous binding of two cargoes is sterically excluded (Honnappa et al., 2009; Stangier et al., 2018). However, structural analysis shows that budding yeast Bim1 is capable of simultaneous binding of two different cargoes via the EBH domain and its EETF tail since both binding sites are separated by a longer linker compared to the mammalian protein (Stangier et al., 2018).

1.3.2. Function of +TIPs in chromosome segregation

Screens for genetic and yeast two-hybrid interactions demonstrate that a diverse set of MAPs and especially +TIPs crucially contribute to chromosome segregation. The probably best studied example is chTOG (Stu2 in yeast) which contributes to error correction and chromosome biorientation both in human and yeast cells (Herman et al., 2020; Miller et al., 2016, 2019). An interaction between Stu2 and Dam1c was suggested by two independent studies using yeast two-hybrid screens (Kalantzaki et al., 2015; Wong et al., 2007). However, this interaction was never tested in more detail using biochemical approaches.

In contrast to chTOG/Stu2, the function of EB1/Bim1 in chromosome segregation is less well understood. Human EB1 localizes to the growing plus end of microtubules attached to kinetochores (Tirnauer et al., 2002). Furthermore, it is reported to support localization of the Ska complex to kinetochores and induces formation of distinct Ska complex structures on microtubules *in vitro* (Thomas et al., 2016). An interaction between their budding yeast counterparts, Dam1c and Bim1, respectively, has not been analyzed so far, even though several studies suggest physical and genetic interactions between these proteins (Enquist-Newman et al., 2001; Ito et al., 2001; Uetz et al., 2000; Wong et al., 2007).

1.4. Aims of this project

The function of the Dam1 complex in mitosis has been studied extensively during the last two decades. However, many aspects are still poorly understood and new findings raise new questions. Dam1c binds along the whole microtubule lattice *in vitro* without any apparent preference for certain structural features of the microtubule. In contrast, the complex predominantly localizes to kinetochores *in vivo* raising the question of how Dam1c is specifically recruited to and enriched at kinetochores. Especially the question of how assembly of the Dam1c ring is exclusively restricted to kinetochores requires detailed investigation. Autonomous plus end-tracking proteins (+TIPs) are known to contribute essentially to kinetochore function and chromosome segregation and physical and genetic interactions between kinetochore proteins and members of this diverse family of proteins have been reported. Due to their localization to the dynamic microtubule plus end, these proteins appear as ideal candidates to position Dam1c at the plus end close to the kinetochore. Notably, genetic and yeast two-hybrid studies suggest an interaction between Dam1c and the +TIP Bim1. Even though these results were published almost 20 years ago, detailed experimental data about the interaction between Dam1c and Bim1 is missing to date. Analysis of +TIP function at the kinetochore is complicated by the fact that these proteins are crucial for integrity of the mitotic spindle. Therefore, novel mutants are required to specifically investigate their function at the kinetochore without interfering with their role in regulation of microtubule dynamics.

In this study, the interplay between the Dam1 complex and Bim1 is analyzed using a combination of biochemical, genetic and cell biological approaches, complemented by

structural analyses. Furthermore, it is investigated how Bim1 additionally recruits Bik1 to Dam1c, how this relates to Dam1c ring assembly and how the interaction is regulated by the conserved kinase Mps1. These findings shed new light on the mechanisms leading to formation of bioriented kinetochore-microtubule attachments and their regulation in space and time.

2. Material and Methods

2.1. Purification of recombinant proteins

2.1.1. Purification of Dam1 complex from *E. coli*

BL21 Rosetta cells carrying the plasmid pSW1 (Dam1^{WT}c), pSW4 (Dam1-19c), pSW17 (Dam1^{4D}c) and pAD17 (Dam1$^{\Delta SxIP}$c) were used to purify Dam1c. The Hsk3 subunit C-terminally fused to a 6xHis tag allows purification of the whole complex by metal ion affinity chromatography. Cells were grown in LB medium with 100 µg/ml ampicillin and 34 µg/ml chloramphenicol at 37 °C, shaking at 220 rpm, until an OD_{600} = 0.7 was reached. IPTG was added to a final concentration of 1 mM and cells were further incubated at 37 °C for 4 hours. Cells were finally harvested by centrifugation (20 minutes, 6000 rpm, Avanti JXN-26 centrifuge (Beckman Coulter), JLA-8.1000 rotor), washed once with PBS and stored at -80 °C until further use.

For cell lysis, cells were resuspended in lysis buffer (20 mM Na_2HPO_4/NaH_2PO_4 (pH 6.6), 500 mM NaCl, 20 mM imidazole, 0.01 % (v/v) Triton X-100, 0.5 mM TCEP) with 1 mM PMSF and Pierce Protease Inhibitor (Thermo Scientific) and lysed by sonification. The lysate was cleared by centrifugation at 18000 rpm at 4 °C for 30 minutes (Sorvall RC6 Plus centrifuge, SS-34 rotor). Cleared lysate was loaded on two HisTrap 5 ml columns (GE Healthcare) connected in series and installed on an ÄKTA FPLC system (GE Healthcare). The columns were washed with lysis buffer and bound protein was eluted by a linear imidazole gradient from 20 mM to 510 mM. Elution fractions were collected and analyzed by SDS-PAGE. Appropriate elution fractions were pooled and subjected to a buffer exchange to cation exchange buffer A (20 mM Na_2HPO_4/NaH_2PO_4 (pH 6.6), 150 mM NaCl, 1 mM EDTA, 0.5 mM TCEP) using a HiPrep Desalting 26/10 column (GE Healthcare), followed by cation exchange chromatography (HiTrapS 5 ml column, GE Healthcare) using a linear NaCl gradient from 150 mM to 1 M. Elution fractions were analyzed by SDS-PAGE and appropriate fractions were pooled and subjected to size exclusion chromatography (HiLoad 16/600 Superdex 200 column, GE Healthcare). The buffer for size exclusion chromatography contained 25 mM HEPES (pH 7.4), 250 mM NaCl, 0.5 mM TCEP and 5 % (v/v) glycerol. Protein samples were aliquoted, snap-frozen in liquid N_2 and stored at -80 °C until further use.

2.1.2. Purification of recombinant GST-Bim1 and Bim1 variants from *E. coli*

BL21 cells carrying the plasmid pTZ12 (GST-Bim1^{WT}), pTZ15 (GST-Bim1$^{1-133}$), pTZ13 (GST-Bim1$^{120-344}$), pTZ39 (GST-Bim1$^{185-344}$) or pTZ40 (GST-Bim1$^{205-344}$) were used for expression and purification of GST-tagged Bim1 proteins. A TEV protease cleavage site is located between GST and Bim1 to enable removal of the GST tag from Bim1.

Cells were grown in LB medium with 100 µg/ml ampicillin at 37 °C, shaking at 220 rpm, until an OD = 0.7 was reached. Cultures were cooled down to 18 °C and 0.1 mM IPTG was added.

Cells were further incubated shaking at 18 °C overnight. The cells were harvested by centrifugation (20 minutes, 6000 rpm, Avanti JXN-26 centrifuge (Beckman Coulter), JLA-8.1000 rotor), washed once with PBS and stored at -80 °C.

Cells were resuspended in lysis buffer (25 mM NaH_2PO_4/Na_2HPO_4 (pH 6.8), 300 mM NaCl, 1 mM EDTA, 0.5 mM TCEP, 0.05 % (v/v) Triton X-100) with 1 mM PMSF and Pierce Complete Protease Inhibitor (Thermo Scientific) and lysed by sonification. The lysate was cleared by centrifugation at 18000 rpm at 4 °C for 30 minutes (Sorvall RC6 Plus centrifuge, SS-34 rotor) and loaded on a GSTrap 5 ml column (GE Healthcare) installed on an ÄKTA FPLC system (GE Healthcare). The column was washed with lysis buffer and GST-tagged proteins were eluted with elution buffer (50 mM Tris (pH 8.0), 150 mM NaCl, 10 mM reduced glutathione). Elution fractions were collected and analyzed by SDS-PAGE. Appropriate elution fractions were pooled and subjected to buffer exchange using a HiPrep 26/10 column (GE Healthcare) to ion exchange buffer A (25 mM NaH_2PO_4/Na_2HPO_4 (pH 6.6), 150 mM NaCl, 1 mM EDTA, 1 mM DTT). For removal of the GST tag, 0.1 % (v/v) Tween-20 was added and the protein was incubated with TEV protease (overnight at 4 °C) and subsequently applied to a GSTrap column again. GST and residual GST-Bim1 bound to the column while Bim1 passed through the column without binding. Bim1 was loaded for anion exchange chromatography on a HiTrapQ 1 ml column (GE Healthcare) and a linear NaCl gradient from 150 mM to 1 M was applied to elute the protein. Finally, the eluted protein was loaded on a Superdex200 10/300 GL column (GE Healthcare) for gel filtration (buffer with 25 mM HEPES (pH 7.4), 250 mM NaCl, 0.5 mM TCEP, 5 % (v/v) glycerol). To purify GST-tagged proteins, GST-Bim1 was directly subjected to gel filtration after elution from the GSTrap column. Protein aliquots were snap-frozen in liquid N_2 and stored at -80 °C.

2.1.3. Purification of recombinant Bik1 from *E. coli*

Bik1 was purified from BL21 Rosetta cells carrying the pET28a-Bik1-6xHis plasmid. The 6xHis tag fused to the C-terminus of Bik1 allows for purification by metal ion affinity chromatography. Cells were grown in LB medium with 100 µg/ml ampicillin and 34 µg/ml chloramphenicol at 37 °C, shaking at 220 rpm, until an OD_{600} = 0.7 was reached. The culture was cooled to 18 °C and further cultivated shaking at 18 °C overnight in the presence of 0.1 mM IPTG. The cells were harvested by centrifugation (20 minutes, 6000 rpm, Avanti JXN-26 centrifuge (Beckman Coulter), JLA-8.1000 rotor), washed once with PBS and stored at -80 °C.

Cells were resuspended in lysis buffer (20 mM Na_2HPO_4/NaH_2PO_4 (pH 7.4), 500 mM NaCl, 0.01 % (v/v) Triton X-100, 20 mM imidazole, 1 mM DTT) supplemented with 1 mM PMSF and Pierce Protease Inhibitor (Thermo Scientific) and lysed by sonification. The lysate was cleared by centrifugation (30 minutes, 18000 rpm, 4 °C, Sorvall RC6 Plus centrifuge, SS-34 rotor) and loaded on a HisTrap 5 ml column (GE Healthcare) installed on an ÄKTA FPLC system (GE Healthcare). The column was washed with lysis buffer and protein bound to the column was

eluted by a linear imidazole gradient from 20 mM to 510 mM. Elution fractions were analyzed by SDS-PAGE. Appropriate elution fractions were pooled and loaded on a HiLoad 16/600 Superdex 200 column (GE Healthcare) for gel filtration. The gel filtration buffer was composed of 25 mM HEPES (pH 7.4), 350 mM NaCl, 1 mM $MgCl_2$, 2.5 % (v/v) glycerol and 0.5 mM TCEP. Glycerol was added to a final concentration of 5 % (v/v) and protein aliquots were snap-frozen in liquid N_2 and stored at -80 °C.

2.1.4. Infection of Sf9 cells with baculoviruses for recombinant protein expression

Sf9 insect cells were diluted to 0.8 x 10^6 cells/ml in Spodopan serum-free medium (Pan Biotech) and incubated at 27 °C, shaking at 100 rpm. Next day, the cells were infected with a baculovirus carrying an expression construct for the protein of interest and a GFP reporter gene. The number of infected cells correlates with the number of GFP-positive cells. Cells were harvested two to three days after infection when the fraction of GFP-positive cells was around 70 – 95 %. Protein purification from Sf9 cells is described in the following sections.

2.1.5. Purification of Mps1 from Sf9 insect cells

Mps1 was fused to a C-terminal StrepII tag allowing purification via Strep-Tactin beads. Infected cells were resuspended in lysis buffer (20 mM Na_2HPO_4/NaH_2PO_4 (pH 7.4), 300 mM NaCl, 2.5 (v/v) % glycerol, 0.01 (v/v) % Tween-20) supplemented with 1 mM PMSF and Pierce Protease Inhibitor (Thermo Scientific) and lysed by sonification. The lysate was incubated at 4 °C for ten minutes and cleared twice by centrifugation (Eppendorf tabletop centrifuge, 15000 rpm, 4 °C, 15 minutes). Strep-Tactin beads (Qiagen) were washed with lysis buffer and incubated with the cleared lysate while rotating for four hours at 4 °C. Afterwards, the beads were separated from the lysate by centrifugation and washed three times with lysis buffer. Mps1-StrepII was eluted from the beads by addition of elution buffer (lysis buffer with 2.5 mM desthiobiotin). Glycerol was added to a final concentration of 5 % (v/v) and aliquots were snap-frozen in liquid N_2 and stored at -80 °C.

2.1.6. Purification of Ndc80 complex from Sf9 insect cells

For expression of Ndc80 complex in Sf9 cells, the cells were infected with a baculovirus carrying an expression construct for all four subunits of the Ndc80 complex (Ndc80, Nuf2, Spc24 and Spc25). The C-terminus of Ndc80 was fused to a Flag tag. Infected cells were resuspended in lysis buffer (20 mM Na_2HPO_4/NaH_2PO_4 (pH 6.8), 150 mM NaCl, 5 % (v/v) glycerol, 0.05 % (v/v) Tween-20, 0.5 mM TCEP) with 1 mM PMSF and Pierce Protease Inhibitor (Thermos Scientific) and lysed by sonification. The lysate was cleared twice by centrifugation (Eppendorf tabletop centrifuge, 15000 rpm, 4 °C, 15 minutes). Anti-Flag M2 agarose beads (Sigma-Aldrich) were equilibrated with lysis buffer and incubated with the cleared lysate rotating at 4 °C for three hours. The beads were collected by centrifugation and

washed three times with lysis buffer. Ndc80c-Flag was eluted from the beads by addition of elution buffer (lysis buffer with 0.5 µg/µl 3xFlag peptide). Protein aliquots were snap-frozen in liquid N_2 and stored at -80 °C.

2.1.7. Purification of Stu2 from Sf9 insect cells

Stu2 was expressed as a fusion protein with a C-terminal Flag tag. Infected cells were resuspended in lysis buffer (20 mM Na_2HPO_4/NaH_2PO_4 (pH 8.0), 300 mM NaCl, 2.5 % (v/v) glycerol, 0.05 % (v/v) Tween-20, 1 mM DTT) with 1 mM PMSF and Pierce Protease Inhibitor (Thermo Scientific) and lysed by Dounce homogenization. The lysate was cleared twice by centrifugation (Eppendorf tabletop centrifuge, 15000 rpm, 4 °C, 15 minutes). Anti-Flag M2 agarose beads (Sigma-Aldrich) were equilibrated with lysis buffer and incubated with the lysate rotating at 4 °C for three hours. The beads were separated from the lysate by centrifugation and washed three times with lysis buffer. Stu2-Flag was eluted from the beads with elution buffer (lysis buffer with 0.5 µg/µl 3xFlag peptide). Glycerol was added to a final concentration of 5 % (v/v) and protein aliquots were snap-frozen in liquid N_2 and stored at -80 °C.

2.2. Biochemical methods

2.2.1. SDS-PAGE

Protein samples were analyzed by discontinuous SDS-PAGE. The stacking gel was composed of 125 mM Tris (pH 6.8), 0.1 % (w/v) SDS and 5.1 % acrylamide, the separation gel of 0.375 mM Tris (pH 8.8), 0.1 % (w/v) SDS and 12.5 % acrylamide. Polymerization of acrylamide was initiated by addition of APS and TEMED.

Protein samples were loaded on gels in a gel electrophoresis chamber (Mini-PROTEAN Tetra Cell, Bio-Rad) filled with SDS-PAGE running buffer and proteins were separated by application of a voltage of 80 V (stacking gel) or up to 200 V (separation gel). PageRuler Unstained or PageRuler Plus Prestained Protein Ladder (Thermo Scientific) were used as reference for molecular weight of proteins.

2.2.2. Coomassie staining of proteins separated by SDS-PAGE

After separation of proteins by SDS-PAGE, proteins were fixed and stained by Coomassie staining according to Fairbanks (Fairbanks et al., 1971). Gels were immersed in solution A (25 % (v/v) isopropanol, 10 % (v/v) acetic acid, 0.05 % (w/v) Coomassie Brilliant Blue R), briefly heated in the microwave and incubated shaking for at least ten minutes. Solution A was exchanged for solution B (10 % (v/v) isopropanol, 10 % (v/v) acetic acid, 0.005 % (w/v) Coomassie Brilliant Blue R) heated in the microwave and again incubated shaking for at least ten minutes. Solution B was exchanged for solution D (10 % (v/v) acetic acid) and incubated

shaking until the gel was destained. After destaining, the gel was stored in distilled water.

2.2.3. Silver staining of proteins after SDS-PAGE

For silver staining after SDS-PAGE, the gel was incubated in fixation solution (10 % (v/v) acetic acid, 45 % (v/v) methanol) for 60 minutes, washed in H_2O for another 60 minutes and incubated with sensitizer solution (0.9 mM $Na_2S_2O_3$ in H_2O) for 60 seconds. Afterwards, the gel was washed three time for 20 seconds with H_2O, incubated with staining solution (0.1 % (v/v) formaldehyde, 2 g/l $AgNO_3$) for 20 minutes, washed three times for 20 seconds with H_2O and incubated with the developer solution (0.05 % (v/v) formaldehyde, 30 µM $Na_2S_2O_3$, 60 g/l Na_2CO_3). The reaction was stopped by addition of 10 % (v/v) acetic acid when staining of proteins became visible.

2.2.4. Western blot

For western blot analysis, protein samples were separated by SDS-PAGE. Proteins were transferred to a nitrocellulose membrane (Amershan Protran 0.45 µm NC, GE Health Life Sciences) in an electrophoresis chamber filled with transfer buffer by application of a constant voltage of 150 V (90 – 120 minutes) or 30 V (overnight) at 4 °C. Afterwards, the membrane was stained with Ponceau S to test for correct transfer of proteins, destained with distilled water and blocked with 5 % (w/v) milk in TBST for 1 hour at room temperature or overnight at 4 °C. For detection of proteins, the membrane was incubated with the respective antibodies. Detailed information about antibody usage is listed in Table 2. The membrane was washed three times with TBST for ten minutes and incubated with a suitable HRP-conjugated secondary antibody. After incubation with the antibody, the membrane was finally washed three times with TBST followed by detection of signals. The membrane was briefly incubated with Amersham ECL Western Blotting Detection Reagent (GE Life Sciences) and signals were detected with an Amersham Imager 600 (GE Healthcare).

Table 2: List of antibodies used in this study
Information about all antibodies, the manufacturers, dilutions and incubation conditions.

antibody	company and product number	preparation	incubation
anti-Flag, mouse, monoclonal M2 antibody, HRP-conjugated	Sigma-Aldrich F1804	1:10000 in TBST with 5 % (w/v) milk	1 hour at room temperature
anti-GFP, mouse, monoclonal	Roche 11814460001	1:1000 in TBST with 2.5 % (w/v) milk	overnight at 4 °C
anti-GST, goat, polyclonal	GE Healthcare 27457701	1:1000 in TBST with 5 % (w/v) milk	1 hour at room temperature
anti-Myc, mouse, monoclonal, 9E10	Covance MMS-150R	1:1000 in TBST with 2.5 % (w/v) milk	3 – 4 hours at room temperature or overnight at 4 °C

anti-penta-His, mouse, HRP-conjugated	Qiagen 1014992	1:2500 in TBST with 2.5 % (w/v) milk	3 – 4 hours at room temperature or overnight at 4 °C
anti-Pgk1, mouse, monoclonal	Invitrogen 22C5D8	1:5000 in TBST with 2.5 % (w/v) milk	3 - 4 hours at room temperature or overnight at 4 °C
anti-StrepII, mouse, monoclonal	Qiagen 34850	1:1000 TBST with 2.5 % (w/v) milk	3 - 4 hours at room temperature or overnight at 4 °C
anti-goat IgG, mouse, monoclonal, HRP-conjugated	Santa Cruz Biotech sc-2354	1:10000 in TBST with 5 % (w/v) milk	1 hour at room temperature
anti-mouse IgG, sheep, HRP-conjugated	GE Healthcare, NA931	1:10000 in TBST with 5 % (w/v) milk	1 hour at room temperature

2.2.5. Analytical size exclusion chromatography

Analytical size exclusion chromatography (SEC) was performed using a Superose 6 Increase 3.2/300 column (GE Healthcare) installed to an ETTAN FPLC system (GE Healthcare). Protein samples with a volume of 60 µl were prepared, incubated on ice for 20 minutes and centrifuged in a tabletop centrifuge (full speed, ten minutes, 4 °C) to remove any precipitated protein. 50 µl of the sample were loaded on the gel filtration column. SEC was performed at 4 °C with a flow rate of 40 µl/minute. The SEC buffer contained 20 mM HEPES (pH 7.4), 200 mM NaCl, 1 mM $MgCl_2$, 2.5 % (v/v) glycerol and 0.5 mM TCEP. Deviations from this composition are mentioned in the descriptions of the respective experiments. Elution fractions of 100 µl were collected and analyzed by SDS-PAGE.

2.2.6. GST-Bim1 pull down assays with recombinant proteins

15 µl of glutathione sepharose 4B beads (GE Healthcare), which were blocked with BSA, were loaded with equimolar amounts of GST or GST-tagged Bim1 proteins. GST was used as negative control to exclude unspecific binding of proteins. Beads were washed once with pull down buffer (25 mM HEPES (pH 7.4), 300 mM NaCl, 1 mM $MgCl_2$, 5 (v/v) % glycerol, 0.5 mM TCEP, 2 mM EDTA, 0.1 (v/v) % Triton X-100) and incubated with 120 µl 5 µM recombinant Dam1c for 15 minutes, rotating at 4 °C. Afterwards, the beads were collected by centrifugation, washed three times with pull down buffer (5 minutes, rotating at 4 °C) and boiled in 50 µl SDS loading buffer to elute proteins from beads. Input and pull down samples were analyzed by SDS-PAGE.

2.2.7. GST-Bim1 pull down assays with soluble yeast cell extracts

Glutathione sepharose 4B beads (GE Healthcare) were pre-blocked with BSA, loaded with up to 45 µg of GST-Bim1$^{185-344}$ for 15 minutes, rotating at 4 °C, and finally briefly washed with pull down buffer (25 mM HEPES (pH 7.4), 300 mM NaCl, 1 mM $MgCl_2$, 5 (v/v) % glycerol, 0.5 mM TCEP, 0.1 (v/v) % Triton X-100). Soluble yeast cell extracts were prepared according to 2.3.6.

300 – 400 µl cell lysate with a protein concentration of 2 µg/µl was added to the loaded beads and incubated at 4 °C, rotating for 15 – 60 minutes. Afterwards, the beads were collected by centrifugation and washed three times with pull down buffer (5 minutes, rotating at 4 °C). Finally, the beads were boiled in 50 µl 1x loading buffer for elution of proteins. Input and pull down samples were analyzed by SDS-PAGE and western blot.

2.2.8. Pull down with Ndc80c from Sf9 cells

Sf9 cells expressing Ndc80c-Flag were resuspended in lysis buffer (20 mM Na_2HPO_4/NaH_2PO_4 (pH 6.8), 150 mM NaCl, 5 % (v/v) glycerol, 0.05 % (v/v) Tween-20, 0.5 mM TCEP) and lysed by sonification. The lysate was cleared by centrifugation. Ndc80c-Flag was immobilized on anti-Flag M2 agarose beads (Sigma-Aldrich) by incubation with the cleared lysate for one hour at 4 °C. The beads were washed three times with pull down buffer (25 mM HEPES (pH 7.4), 200 mM NaCl, 1 mM $MgCl_2$, 2.5 % (v/v) glycerol, 0.5 mM TCEP, 0.01 % (v/v) Triton X-100) and afterwards incubated with Dam1c, Bim1 or Dam1c pre-incubated with increasing amounts of Bim1 for 15 minutes, rotating at 4 °C. The total volume of binding reactions was 100 µl. After incubation, the beads were briefly washed three times with pull down buffer. Proteins bound to the beads were eluted with elution buffer (pull down buffer with 0.5 µg/µl 3xFlag peptide) and input and pull down samples were analyzed by SDS-PAGE.

2.2.9. Pull down with Stu2 from Sf9 cells

Sf9 cells expressing Stu2-Flag were resuspended in lysis buffer (20 mM Na_2HPO_4/NaH_2PO_4 (pH 8.0), 300 mM NaCl, 2.5 % (v/v) glycerol, 0.05 % (v/v) Tween-20) and lysed by sonification. The lysate was cleared by centrifugation. Anti-Flag M2 agarose beads (Sigma-Aldrich) were loaded with Stu2-Flag by incubation with the cleared lysate for one hour and washed three times with interaction buffer (20 mM HEPES (pH 7.4), 200 mM NaCl, 1 mM $MgCl_2$, 0.5 mM TCEP, 2.5 % (v/v) glycerol, 0.01 % (v/v) Triton X-100). 15 µl of loaded beads were incubated with 100 µl 4 µM Dam1c, 4 µM Bik1 or buffer. Empty beads were incubated with the respective proteins to test for unspecific binding of Dam1c and Bik1. Assembled reactions were incubated at 4 °C for 15 minutes. Afterwards, beads were collected by centrifugation and washed three times with interaction buffer. Proteins were eluted from beads by incubation with elution buffer (interaction buffer supplemented with 0.5 µg/µl 3xFlag peptide) for 30 minutes at 4 °C. Input and elution samples were subsequently analyzed by SDS-PAGE.

2.2.10. *In vitro* kinase assay

In vitro kinase assays were performed in a total reaction volume of 20 µl. 6.75 µg recombinant Dam1c or 1.5 µg recombinant Bim1 were incubated with Mps1 kinase in kinase buffer (20 mM HEPES (pH 7.5), 100 mM KCl, 10 mM $MgCl_2$, 10 mM $MnCl_2$, 25 mM β-glycerolphosphate,

1 mM DTT) supplemented with 50 µM ATP and 0.5 µCi ^{32}P-γ-ATP for 30 minutes at 30 °C. Reactions were stopped by addition of 6x loading buffer. Samples were analyzed by SDS-PAGE and Coomassie staining. Gels were dried overnight and incorporation of ^{32}P into proteins was detected by autoradiography. A sheet of Amersham Hyperfilm ECL was placed on the dried gel and afterwards developed with a Cawomat 2000 IR (Cawo).

For *in vitro* phosphorylation by Mps1 prior to analytical size exclusion chromatography, reactions with a total volume of 60 µl were prepared. Dam1c and Bim1 were diluted in kinase buffer lacking $MnCl_2$. Recombinant Mps1 and 500 µM ATP were added and samples were incubated at 30 °C for 2 hours. ATP was omitted from control samples. Samples were subsequently subjected to analytical SEC (2.2.5).

2.2.11. Crosslinking and mass spectrometry analysis

For determination of the appropriate crosslinker concentration, BS3 (bis(sulfosuccinimidyl)suberate) was diluted to concentrations from 0 µM o 2500 µM. An equimolar mixture of BS3 consisting of light- and heavy-labelled crosslinker (BS3-H_{12} and BS3-D_{12}) was used, which is required for identification of crosslinked peptides by mass spectrometry. 1 µg Dam1c was incubated with BS3 in a total volume of 6 µl at 35 °C for 45 minutes. NH_4HCO_3 was added to a final concentration of 100 mM to stop the crosslinking reaction. Samples were mixed with loading buffer and analyzed by SDS-PAGE followed by silver staining.

Prior to mass spectrometric analysis, 60 µg Dam1c was crosslinked in the absence or presence of 7.4 µg Bim1. The crosslinker was used at a concentration of 600 µM. Further processing of samples and identification of crosslinked peptides was performed as described by Herzog et al. (2012). Distance restraints were visualized as proximity map using the free software xVis (Grimm et al., 2015).

Processing of crosslinked samples, mass spectrometric analysis and data analysis was performed by Pascaline Rombaut and Franz Herzog (Gene Center Munich, Ludwig Maximilian University Munich).

2.2.12. Negative stain electron microscopy of Dam1c, Bim1 and Bik1

Dam1c alone and in presence of Bim1 was prepared by size exclusion chromatography and crosslinked in the presence of 0.75 % (w/v) glutaraldehyde for 60 seconds. The reaction was stopped by addition of Tris. Further procession of the samples is described in the following section.

Dam1c, Dam1c-Bim1 and Dam1c-Bim1-Bik1 complexes were prepared by size exclusion chromatography (final concentrations ranging from 0.005 mg/ml to 0.05 mg/ml). For EM analysis of complexes assembled at low-salt conditions, samples were diluted in buffer to a final NaCl concentration of 10 mM. Samples were applied on freshly glow-discharged carbon-

coated copper grids (Agar Scientific, G400C) for two minutes, blotted with Whatman no. 4 filter paper, washed two times with ddH_2O and stained with 0.75 % (w/v) uranyl formate. Negatively stained proteins were imaged with a JEOLJEM-1400 transmission electron microscope equipped with a LaB_6 cathode operating at 120 kV. Digital electron micrographs were recorded with a 4k x 4k CMOS Camera F416 (TVIPS) under minimal dose conditions with a pixel size of 1.36 Å. A total of 28140 single particles for Dam1c and 36980 single particles for crosslinked Dam1c-Bim1 were boxed using crYOLO (Wagner et al., 2019) after training it with 10 manually boxed micrographs.

An iterative stable alignment and clustering approach (ISAC) was carried out for reference-free classification (Yang et al., 2012), implemented in the SPIRE software (Moriya et al., 2017). An initial 3D structure was calculated from the best 2D class averages, excluding monomeric Dam1c particles, with the validated *ab initio* 3D structure determination approach VIPER (Moriya et al., 2017) implemented in SPHIRE. Reconstructions were visualized by CHIMERA (Pettersen et al., 2004).

Samples were prepared and analyzed by Lena Engelhard, Cole Bourque, Björn Udo Klink and Christos Gatsogiannis (Department of Structural Biochemistry, Max Planck Institute of Molecular Physiology, Dortmund; Institute for Medical Physics and Biophysics and Center for Soft Nanoscience, Westfälische Wilhelms-Universität Münster).

2.2.13. Determination of protein concentrations

Protein concentrations of purified recombinant proteins were measured with a NanoDrop One (Thermo Scientific) based on the protein specific extinction coefficient at 280 nm (ε_{280}).

Protein concentration of cell lysates were measured in a Bradford assay (Bio-Rad) according to the manufacturer's instructions. To compare relative protein concentrations, the absorption at 280 nm was measured with NanoDrop One (Thermo Scientific).

2.3. Yeast methods

All yeast strains were based on the S288C strain background. As far as possible, all strains within one experimental setup were isogenic.

2.3.1. Transformation of yeast strains

50 ml YEPD medium were inoculated to OD_{600} = 0.2 from a saturated overnight culture of the respective yeast strain and incubated at 30 °C, 180 rpm until an OD_{600} = 0.6 – 0.8 was reached. The cells were harvested by centrifugation (2500 rpm, 2 minutes), washed once with 10 ml ddH_2O, transferred to a 1.5 ml tube and resuspended in 1.5 ml 1x TE +1x LiAc solution. 200 µl of the yeast cell suspension were mixed in a fresh tube with 1.2 ml PEG solution (40 % (w/v) PEG-3350, 1x TE, 1x LiAc), 200 µg of salmon sperm carrier DNA, and transforming DNA. As control, a sample without transforming DNA was prepared. The samples were incubated at

room temperature for 30 minutes with end-over-end rotation, followed by a heat shock at 42 °C for 12 minutes. Afterwards, the cells were collected by centrifugation, resuspended in 150 µl ddH_2O, plated on drop-out medium plates (selection for auxotrophic marker) or YEPD plates (selection for antibiotic resistance) and incubated at 30 °C. In the latter case, next day, the cells were transferred to a YEPD plate supplemented with the respective antibiotic using a sterile velvet cloth and incubated at 30 °C. Colonies appearing after two to three days were restreaked on the respective selective medium and incubated at 30 °C.
Integration of the DNA constructs at the correct locus was tested by PCR using genomic DNA or western blot analysis.

2.3.2. Preparation of DNA for yeast cell transformation

For transformation of yeast cells, either PCR products with approximately 40 bp of sequence homology with the integration locus or linearized integration plasmids were used. PCR products were based on the integration cassettes developed by Janke et al. (2004), Lee et al. (2013) and Longtine et al. (1998). Integration plasmids were designed in a way that allows either replacement of a gene of interest or integration into a marker locus.
Before transformation, the quality and size of PCR products was analyzed by agarose gel electrophoreses. Integration plasmids were linearized by restriction digest and linearization was confirmed by agarose gel electrophoresis. The linearized plasmids and PCR products were used for transformation without further purification.

2.3.3. Mating of yeast strains

Haploid yeast strains with opposing mating types were streaked across each other on a YEPD plate and incubated at 30 °C for five hours to overnight. Strains were taken either from a plate or form a saturated overnight culture. Afterwards, the parental strains and the new diploid strain were streaked on selective medium which only allows growth of the diploid strain, but not the two parental strains, and incubated at 30 °C for two to three days. Alternatively, individual zygotes were picked using a Singer MSM200 semi-automatic tetrad dissection microscope and incubated on a YEPD plate at 30 °C for two to three days.

2.3.4. Preparation of sporulation cultures, dissection of diploid yeast strains and genotyping

1 ml of a saturated overnight culture of a diploid yeast strain was centrifuged at 2500 rpm for two minutes. The cells were washed twice in 1 ml sterile ddH_2O, resuspended in 4 ml sporulation medium supplemented with SC and incubated at room temperature in a rotating wheel for several days. Appearance of tetrads was monitored by microscopy.
For tetrad dissection, 250 µl of a sporulation culture were centrifuged at 2500 rpm for two minutes and the cells were incubated in 37.5 µl of a zymolase solution (zymolase 100 T,

1 mg/ml in 1 M sorbitol) for 3.5 minutes at 37 °C. Afterwards, 200 µl of cold 0.1 M KH_2PO_4/K_2HPO_4 buffer (pH 7.0) was added and the cells were streaked on a YEPD plate using a platinum inoculation loop. Tetrads were dissected using a Singer MSM200 semi-automatic tetrad dissection microscope followed by incubation at 30 °C for two to three days.
For genotyping of spores, individual spores were taken up in minimal medium and transferred to YEPD, drop-out and mating type tester plates (minimal medium with DDY55 and DDY56) using a 48 well pinning tool. Drop-out and mating type tester plates were incubated at 30 °C, YEPD plates at 25 °C, 30 °C, 34 °C and 37 °C. Growth of spores on different plates was evaluated and spores with the desired genotype were selected for further experiments.

2.3.5. Serial dilution assay

Serial dilution assays were performed for analysis of growth phenotypes. Cells from a saturated overnight culture were diluted in minimal medium to OD_{600} = 0.4. The cell suspension was transferred to a 96 well plate and diluted 1:4 in minimal medium in five serial steps. Cells were transferred to YEPD plates using a 48 well pinning tool and incubated at different temperatures. If required, YEPD plates were supplemented with benomyl (20 µg/ml) or cincreasin (200 µM or 400 µM).

2.3.6. Preparation of soluble yeast cells extracts

For preparation of soluble yeast cell extracts, cells were grown in liquid culture (50 – 200 ml) to $OD_{600} \approx 0.8$ and harvested by centrifugation. Cells were resuspended in 700 µl lysis buffer (25 mM HEPES (pH 8.0), 150 mM NaCl, 2 mM EDTA, 1 mM DTT, 5 % (v/v) glycerol) supplemented with 1 mM PMSF and Pierce Protease Inhibitor (Thermo Scientific). 400 µl glass beads (0.25 – 0.5 mm diameter, Roth) were added to the cell suspension and cells were disrupted by bead beating (three times 30 seconds, Mini Bead Beater, Biospec Products). NP-40 was added to a final concentration of 0.1 % (v/v) and the lysate was incubated at 4 °C for 20 minutes. Samples were briefly centrifuged at 5000 rpm and the supernatant was transferred to a fresh tube. The lysate was cleared by centrifugation at 15000 rpm for 20 minutes at 4 °C. The supernatant was again transferred to a fresh tube and the protein concentration was determined.

2.3.7. Preparation of yeast cells extracts for western blot analysis

Yeast cell extracts for western blot analysis were prepared as described by Kushnirov (2000).An equivalent of 2.0 – 2.5 OD_{600} of yeast cells from a logarithmically growing culture was harvested by centrifugation, resuspended in 200 µl 0.1 mM NaOH and incubated at room temperature for five minutes. Afterwards, the cells were pelleted by centrifugation, resuspended in 50 µl 1x loading buffer and boiled at 95 °C for five minutes. Samples were centrifuged at 15000 rpm for one minute and 6 – 12 µl of the supernatant were loaded for SDS-

PAGE.

2.3.8. Live cell microscopy

All yeast strains used for live cell microscopy carried the *Ade2* wild type gene to reduce cellular fluorescent background.

5 ml YEP or doTrp medium supplemented with the appropriate carbon source (glucose or raffinose and galactose) were inoculated to OD_{600} = 0.2 – 0.3 from a saturated overnight culture and incubated at 30 °C, 180 rpm for four to five hours. 200 µl of the culture were centrifuged at 2500 rpm for two minutes, resuspended in 200 µl SD doTrp or SRG doTrp medium and briefly sonicated in a sonicating water bath. For immobilization of cells on glass bottom dishes (No 1.5, MatTek corporation), 70 µl of a concanavalin A solution (0.1 mg/ml in PBS, Sigma) were spread on the glass window of the dish and incubated at room temperature for 15 minutes. Afterwards, the concanavalin A solution was removed and the glass window briefly washed with medium. 70 µl of the prepared cell suspension were added to the glass window and incubated at 30 °C for 15 minutes. The excess liquid was removed and the glass window gently washed three times with medium. Finally, the dish was filled with 2.5 ml of SD doTrp or SRG doTrp.

For inhibition of Mps1 by cincreasin, cells were grown in the presence of the respective concentration of the inhibitor (0.5 mM, 1 mM or 2 mM) or 0.1 % (v/v) DMSO for 2 hours prior to immobilization as described above. Cincreasin or DMSO were also added to the imaging medium.

Live cell microscopy was performed with a DeltaVision Elite wide-field microscope (GE Healthcare Life Sciences) with a Plan Apo 60x/1.42 oil objective or a Super-Plan Apo 100x/1.4 oil objective, solid state light source (SSCI) and sCMOS camera at a temperature of 30 °C. Z-stacks with a spacing of 0.2 – 0.4 µm spanning a total distance of 6 µm were acquired and maximum projections were generated. If required, images were deconvolved afterwards. The software SoftWoRx (GE Healthcare Life Sciences) was used for control of the microscope system, generation of maximum projections and deconvolution.

During time lapse microscopy, images of pre-selected fields of view were acquired every 60 seconds.

2.3.9. Analysis of cell cycle progression

70 ml YEPD were inoculated from a saturated overnight culture to OD_{600} = 0.2 and incubated at 30 °C, 180 rpm for one hour. α factor was added to a final concentration of 10 µg/ml and the culture was further incubated for approximately 2 hours until more than 90 % of cells were arrested in a G1-like state as judged by microscopy. To release cells from α factor arrest, cells were harvested by centrifugation, washed twice with 50 ml pre-warmed YEPD with 100 µg/µl pronase (Roche) and once with YEPD without pronase, resuspended in 70 ml pre-warmed

YEPD and further incubated at 37 °C. Samples for western blot (2.3.7) and FACS analysis (2.3.13) were taken immediately before and every 15 minutes after release from α factor arrest over a total time of 120 minutes. Approximately 45 minutes after release, 10 µg/ml α factor was added to the cultures to arrest cells in the following G1-phase.

2.3.10. Depletion of Cdc20 by an auxin-inducible degron system

Endogenous Cdc20 was C-terminally fused to a 9xMyc-AID (auxin-inducible degron) tag in a pGal-OsTir strain background. In this strain background, expression of the E3 ubiquitin ligase OsTir is induced in the presence of galactose and repressed in the presence of glucose. In the presence of the auxin analog 1-naphthaleneacetic acid (NAA), OsTir mediates polyubiquitination of AID-tagged substrates leading to their rapid proteasomal degradation (Nishimura et al., 2009).

Cells from a saturated overnight culture were inoculated to OD_{600} = 0.2 in YEPRG medium and grown at 30 °C for 2 hours. Depletion of AID-tagged Cdc20 was induced by addition of 1 mM NAA. Cells were further cultivated for 2 – 2.5 hours and further prepared for live cell microscopy (2.3.8) or preparation of yeast cell extracts (2.3.7).

2.3.11. Isolation of genomic DNA (gDNA) from yeast cells

200 µl of a saturated overnight culture were harvested by centrifugation (2500 rpm, two minutes). The cells were resuspended in 0.5 ml lysis buffer (50 ml Tris (pH 7.5), 1 % (w/v) SDS, 20 mM EDTA), approximately 500 µl glass beads (0.25 – 0.5 mm diameter, Roth) were added and cells were disrupted by bead beating (Disruptor Genies, Scientific Industries) for two minutes. Samples were subsequently incubated at 75 °C for ten minutes. 150 µl 5 M NaCl and 200 µl 5 M potassium acetate were added and incubated on ice for ten minutes. The lysate was cleared by centrifugation at 15000 rpm for 10 minutes. 500 µl of the clear supernatant were mixed with 1 ml ethanol and centrifuged at 15000 rpm for 10 minutes to precipitate the gDNA. The supernatant was removed, the pellet briefly washed in 70 % (v/v) ethanol and gDNA was again precipitated by centrifugation (15000 rpm, 10 minutes). The supernatant was discarded, the pellet dried and finally resuspended in 50 µl TE with 0.2 µg/µl RNAse A (Roche).

2.3.12. Verification of genotypes by sequencing

To verify the genotype of yeast strains by sequencing, gDNA of the respective strains was isolated as described in 2.3.11. The genomic locus of interest was amplified by PCR using Q5 High-Fidelity DNA Polymerase (NEB) or SapphireAmp fast PCR-hot start Master Mix (TaKaRa) according to the manufacturer's instructions. Primers were designed in a way that a PCR product is only generated if the desired integration construct was integrated at the correct locus. To this end, the forward primer annealed to a region upstream of the integration locus

while the reverse primer annealed to a sequence which is specific to the integration construct. PCR products were analyzed by agarose gel electrophoresis, isolated by column purification and submitted for sequencing (Eurofins Genomics).

2.3.13. FACS analysis of the DNA content of fixed yeast cells

Cells from 0.5 ml yeast culture were harvested by centrifugation (2500 rpm, 2 minutes) and resuspended in 300 µl ddH_2O. 700 µl ethanol were added dropwise and samples were incubated overnight at 4 °C. Next day, cells were collected by centrifugation (2500 rpm, 2 minutes), resuspended in 1 ml 50 mM Tris (pH 7.5), sonicated for up to 30 seconds in a sonicating water bath, pelleted again and resuspended in 1 ml 50 mM Tris (pH 7.5) with 0.2 mg/ml RNAse A (Roche). Samples were incubated at 50 °C for 2 hours and 50 µl of 20 mg/ml Proteinase K (Roth) were added followed by further incubation at 50 °C for 2 hours. Cells were collected by centrifugation and resuspended in 300 µl 50 mM Tris (pH 7.5). 50 µl of the cell suspension were incubated with 450 µl of a SYTOX Green solution (Thermo Fisher Scientific, 1 µM in 10 mM Tris (pH 7.5)) at room temperature for 30 minutes protected from light. Samples were analyzed with a MACSQuant VYB flow cytometer (Miltenyi Biotec) and data were processed with the software FlowJo.
FACS samples were processed and analyzed by Karolin Jänen (Department of Molecular Genetics I, University of Duisburg-Essen).

2.4. General molecular biology methods

2.4.1. General PCR techniques

DNA fragments were amplified by PCR using specific oligonucleotide primers. Depending on the template and the complexity of the PCR product, PCRs were performed using Q5 High-Fidelity DNA Polymerase (NEB), Ranger DNA Polymerase (Meridian Bioscience) or SapphireAmp fast PCR-hot start Master Mix (TaKaRa) according to the manufacturer's instructions. PCR was performed in a C1000 Touch Thermal Cycler (Bio-Rad) with cycling conditions as described in Table 3.

Table 3: Overview of PCR cycling conditions used for different DNA polymerases

Q5 High-Fidelity DNA Polymerase			**Ranger DNA Polymerase**			**SapphireAmp fast PCR-hot start Master Mix**		
5 min.	95 °C		5 min.	95 °C		1 min.	98 °C	
30 sec.	95 °C	30 – 35 repeats	1 min.	95 °C	30 – 35 repeats	5 sec.	98 °C	30 – 35 repeats
30 sec.	54 °C		1 min.	54 °C		5 sec.	54 °C	
30 sec. per kb PCR product	72 °C		4 min.	68 °C		10 sec. per kb PCR product	72 °C	
up to 15 min.	72 °C		10 min.	68 °C		2 min.	72 °C	

2.4.2. General cloning methods

Plasmids were generated using standard cloning techniques. For integration of single DNA fragments into plasmid vectors, the desired fragment was amplified by PCR using primers which introduce specific cleavage sites for restriction enzymes. Both vector and fragments were digested with the respective restriction enzymes and ligated using the T4 DNA Ligase (NEB) according to the manufacturer's instructions. Chemically competent *E. coli* cells were transformed with the ligation product as described in 2.4.5.

Multiple fragments were integrated into a linearized vector using Gibson assembly. Desired fragments were amplified by PCR using oligonucleotide primers which introduce overlapping DNA sequences at both ends of the fragment. Vector and fragments were assembled using the Gibson Assembly Master Mix (NEB) according to the manufacturer's instructions. Chemically competent *E. coli* cells were transformed with 1 – 1.5 µl of the reaction as described in 2.4.5.

Point mutations were generated by site directed mutagenesis PCR. Primers were designed in a manner that the site of the point mutation is flanked by about 20 matching base pairs on each side. For generation of deletion mutants, primers were complementary to the sequence flanking the region to be deleted. Insertions were generated by amplification of the desired fragment by PCR using primers which introduce a region of at least 25 bases that are complementary to the region of insertion. The PCR product is then used as mega-primer in a subsequent PCR.

All mutations described above were generated by PCR using Q5 High-Fidelity DNA Polymerase (NEB) according to the manufacturer's instructions. After PCR, *Dpn*I (NEB) was added to the reaction and incubated at 37 °C for at least 2 hours for digestion of template DNA. Competent *E. coli* cells were transformed with 1 – 2 µl of the reaction as described in 2.4.5.

2.4.3. Restriction digests

All restriction digests were performed with enzymes produced by NEB according to the manufacturer's instructions. For restriction digest of PCR products amplified with Q5 High-Fidelity DNA Polymerase (NEB), the restriction enzymes were directly added to the PCR if the enzyme is active in PCR buffer. Alternatively, the PCR product was purified and subsequently used for restriction digest in an appropriate buffer.

2.4.4. Purification of nucleic acids

Plasmid DNA was purified using the NucleoSpin Plasmid Mini Kit (Machery-Nagel). Cultures of *E. coli* cells were grown overnight at 37 °C in LB medium supplemented with the appropriate antibiotic to select for cells carrying the desired plasmid. Plasmid purification was performed according to the manufacturer's instructions.

DNA from PCR or restriction digest was purified using the FastGene Gel/PCR Extraction Kit (Nippon Genetics). The same kit was used for extraction of DNA from agarose gels after gel electrophoresis.

2.4.5. Transformation of chemically competent *E. coli* cells

DH5α and XL10 Gold cells were used for propagation and amplification of plasmid DNA, BL21 and BL21 Rosetta cells for expression and purification of recombinant proteins.

Chemically competent cells were thawed on ice and 50 µl were transferred to a 1.5 ml tube. An appropriate amount of transforming DNA was added and cells were incubated on ice for 30 minutes. Afterwards, cells were heat-shocked at 42 °C for 30 seconds and incubated on ice for two minutes. 100 µl SOC medium was added and cells were incubated at 37 °C for one hour. Cells were finally plated on LB plates selecting for the respective antibiotic resistance and incubated overnight at 37 °C.

2.4.6. Agarose gel electrophoresis

DNA was analyzed by agarose gel electrophoresis. Gels were prepared by dissolving 1 % (w/v) agarose (Lonza) in TAE buffer by boiling. The solution was cooled down slightly, peqGREEN DNA/RNA Dye (peqlab, 1:10000 dilution) was added to stain DNA and the gel was casted in an agarose gel electrophoresis chamber (peqlab). After the gel was solidified, the chamber was filled with TAE buffer. Samples were mixed with an appropriate volume of 6x TriTrack Dye (Thermo Scientific) and loaded on the gel. In addition, a sample of GeneRuler 1 kb DNA Ladder (Thermo Scientific) was loaded as reference to estimate the size of DNA fragments. A constant voltage of 120 V was applied to separate DNA according to its size. DNA bound to the peqGREEN dye was visualized by excitation with UV light using a Gel Doc system (Bio-Rad).

2.4.7. *E. coli* colony PCR

After transformation, *E. coli* colonies were tested for presence of the desired plasmid construct by colony PCR. Primers were designed in a way that the integration site in the plasmid is flanked by both primers, resulting in a smaller PCR product in the absence of any integrated fragments. In case of successful integration, the PCR product shows an increased size. Colonies were picked from a plate and a small amount was transferred to a PCR tube with 10 µl of PCR mix (SapphireAmp fast PCR-hot start Master Mix, TaKaRa). PCR was performed as recommended by the manufacturer. 4 – 6 µl of the PCR were analyzed by agarose gel electrophoresis to identify colonies carrying the desired plasmid.

2.5. Bioinformatical methods

2.5.1. Multiple sequence alignment and secondary structure prediction

Sequences of homologous proteins from different yeast species were obtained from the Fungal Orthogroups Repository (Broad Institute). Multiple sequence alignments were generated using the MAFFT algorithm (Katoh et al., 2019) and further processed and visualized using Jalview (Waterhouse et al., 2009). Results are displayed using the Clustalx coloring scheme with a 50 % conservation threshold.

The secondary structure of *S. cerevisiae* Duo1 was predicted using JPred (Drozdetskiy et al., 2015) and visualized in Jalview (Waterhouse et al., 2009).

2.5.2. Quantification of fluorescence signals in live cell microscopy

Fluorescence signal intensities from live cell microscopy data was quantified using the software Fiji/ImageJ. All images of a dataset were adjusted to equal brightness and contrast. For signal quantification, a box of 6 x 6 pixel size was placed around the signal and the raw integrated densities were measured. The same measurement was repeated in an area with cellular background signal. The fluorescence signal was corrected by subtraction of the local background signal. Individual values were normalized to the mean value of a reference sample (for example a wild type strain) for easier comparison.

2.5.3. Quantification of signal intensities from western blots and Coomassie-stained gels

Signals from western blots and Coomassie-stained gels were quantified using the free software Fiji/ImageJ. Only samples from the same membrane or gel were compared with each other. A rectangular box was placed around the signal of interest and the raw integrated density was measured. Local background was measured by placing an equally sized box within the same lane. The initially measured signal was corrected for local background by subtraction of

the background signal.

2.5.4. Statistical analysis

Graphs were generated and statistical analyses performed with the software GraphPad Prism 9. Unless otherwise stated, the mean ± standard deviation (SD) is plotted. Number of experimental repeats and analyzed objects and statistical tests are listed in the respective figure legends.

2.6. General buffers, solutions, media, chemicals and machines

Table 4: List of buffers and solutions and their compositions

Buffer/Solution	Composition
4x stacking buffer	0.5 M Tris (pH 6.8) 0.4 % (w/v) SDS
4x separation buffer	1.5 M Tris (pH 8.8) 0.4 % (w/v) SDS
6x loading dye for SDS-PAGE	0.1 M Tris (pH 6.8) 30 % (v/v) β-mercaptoethanol 58 % (v/v) glycerol 12 %% (w/v) SDS bromophenol blue
10x LiAc	1 M lithium acetate (pH 7.5)
50 % PEG	50 % (w/v) PEG-3350
PBS	8 g/l NaCl 0.2 g/l KCl 1.44 g/l Na_2HPO_4 0.24 g/l KH_2PO_4 pH 7.4
Ponceau S	2.5 g/l Ponceau S 40 % (v/v) methanol 15 % (v/v) acetic acid
running buffer for SDS-PAGE	25 mM Tris 192 mM glycine 0.5 g/l SDS
solution A	25 % (v/v) isopropanol 10 % (v/v) acetic acid 0.05 % (w/v) Coomassie Brilliant Blue R
solution B	10 % (v/v) isopropanol 10 % (v/v) acetic acid 0.005 % (w/v) Coomassie Brilliant Blue R
solution D	10 % (v/v) acetic acid
TAE	40 mM Tris (pH 7.8) 1.27 mM EDTA 0.13 % (v/v) acetic acid
TBST	20 mM Tris (pH 7.5) 150 mM NaCl 0.01 % (v/v) Tween-20

10x TE	0.1 M Tris (pH 7.5) 0.01 M EDTA
western blot transfer buffer	31.3 mM Tris 240 mM glycine 0.25 g/l SDS 20 % (v/v) methanol

Table 5: List of media and additives and their compositions

Medium/Additive	Composition
100x doAde solution	5 g/l L-leucine 2 g/l L-tryptophan 2 g/l uracil 5 g/l L-lysine 2 g/l L-histidine
100x doHis solution	2 g/l adenine hemisulfate 5 g/l L-leucine 2 g/l L-tryptophan 2 g/l uracil 5 g/l L-lysine
100x doLeu solution	2 g/l adenine hemisulfate 2 g/l L-tryptophan 2 g/l uracil 5 g/l L-lysine 2 g/l L-histidine
100x doLys solution	2 g/l adenine hemisulfate 5 g/l L-leucine 2 g/l L-tryptophan 2 g/l uracil 2 g/l L-histidine
100x doTrp solution	2 g/l adenine hemisulfate 5 g/l L-leucine 2 g/l uracil 5 g/l L-lysine 2 g/l L-histidine
100x doUra solution	2 g/l adenine hemisulfate 5 g/l L-leucine 2 g/l L-tryptophan 5 g/l L-lysine 2 g/l L-histidine
do plates	minimal medium supplemented with do solution 22 g/l Bacto agar
LB medium	20 g/l LB broth for plates: 22 g/l Bacto agar
minimal medium	1.7 g/l yeast nitrogen base 5 g/l $(NH_4)_2SO_4$ for plates: 22 g/l Bacto agar and 2 % (w/v) glucose

300x SC	2 g/l adenine hemisulfate 5 g/l L-leucine 2 g/l L-tryptophan 2 g/l uracil 5 g/l L-lysine 2 g/l L-histidine
SD doTrp	minimal medium supplemented with 2 % (w/v) glucose 1x doTrp
SOC medium	20 g/l Bacto trypton 5 g/l Bacto yeast extract 10 mM NaCl 2.5 mM KCl 10 mM $MgCl_2$ x 6 H_2O 10 mM $MgSO_4$ x 7 H_2O 20 mM glucose pH 7.0
sporulation medium	1 % (w/v) potassium acetate 0.1 % (w/v) Bacto yeast extract 0.05 % (w/v) glucose
SRG doTrp	minimal medium supplemented with 2 % (w/v) raffinose 2 % (w/v) galactose 1x doTrp
YEP	11 g/l Bacto yeast extract 22 g/l Bacto peptone 0.05 g/l adenine hemisulfate
YEPD	YEP medium supplemented with 2 % (w/v) glucose for plates: 22 g/l Bacto agar
YEPRG	YEP medium supplemented with 2 % (w/v) raffinose 2 % (w/v) galactose for plates: 22 g/l Bacto agar

Table 6: List of chemicals used in this study

Chemical/reagent	Manufacturer
3x Flag peptide	Westermann lab
acetic acid	VWR Chemicals
adenine hemisulfate	Alfa Aesar
agarose (for gel electrophoresis)	Lonza
$AgNO_3$	Sigma-Aldrich
ammonium sulfate	Roth
ampicillin	Roth
anti-Flag M2 agarose beads	Sigma-Aldrich
APS	Merck
Bacto agar	BD
Bacto peptone	BD
Bacto yeast extract	Gibco
benomyl	Sigma-Aldrich
Bradford Assay Reagent	Bio-Rad
bromophenol blue	Merck

BS3 (bis(sulfosuccinimidyl)suberate)	Creative Molecules
BSA	Roth
chloramphenicol	Sigma
cincreasin	Maybridge
concanavalin A	Sigma
Coomassie Brilliant Blue R	Sigma-Aldrich
desthiobiotin	Sigma
DMSO	Sigma-Aldrich
DTT	Roth
D-galactose	Sigma-Aldrich
D-glucose	PanRead AppliChem
D-raffinose	Biosynth
EDTA	Westermann lab
α factor	AppliChem
formaldehyde	Roth
ethanol	Fisher Chemical
geneticin (G418)	VWR Life Science
glass beads (0.25 – 0.5 mm diameter)	Roth
glutathione sepharose beads 4B	GE Healthcare
glycerol	Roth
β-glycerolphosphate	Sigma Life Science
glycine	PanReac AppliChem
HCl	Bernd Kraft
HEPES	Roth
imidazole	PanReac AppliChem
IPTG	Thermo Scientific
isopropanol	Fisher Chemical
KCl	Sigma-Aldrich
K_2HPO_4	Merck
KH_2PO4	Fluka
LB	PanReac AppliChem
L-glutathione (reduced)	AppliChem
L-histidine	Sigma-Aldrich
L-leucin	Sigma-Aldrich
L-lysine	Sigma
lithium acetate	Alfa Aesar
β-mercaptoethanol	Roth
methanol	Fisher Chemical
$MgCl_2$	Fluka
$MgSO_4$	Merck
milk (powdered)	Roth
$MnCl_2$	Roth
NAA	Roth
NaCl	PanReac AppliChem
Na_2CO_3	Merck
Na_2HPO_4	Sigmar-Aldrich
NaH_2PO4	Sigmar-Aldrich
NaOH	PanReac AppliChem
$Na_2S_2O_3$	Sigma-Aldrich
nourseothricin	Jena Bioscience
NP-40 (alternative)	Calbiochem

^{32}P-γ-ATP	Hartmann Analytic
PEG-3350	Aldrich
peq GREEN	peqlab
PMSF	Sigma
Ponceau S	Serva
potassium acetate	Sigma-Aldrich
rapamycin	Diagonal
Rotiphorese Gel 30 (37.5:1 acrylamid-bisacrylamid solution)	Roth
salmon sperm DNA	PanReac AppliChem
SDS	Roth
sorbitol	Roth
Strep-Tactin Superflow beads	Qiagen
SYTOX Green	Thermo Fisher Scientific
TCEP	Roth
TEMED	Merck
Tris	PanReac AppliChem
Triton X-100	Sigma
Tween-20	Sigma
uracil	Sigma
yeast nitrogen base	BD

Table 7: List of enzymes used in this study

Enzyme	Manufacturer
Gibson Assembly Master Mix	NEB
pronase	Roche
Proteinase K	Roth
Q5 Hot Start High-Fidelity DNA Polymerase	NEB
Ranger DNA Polymerase	Meridian Bioscience
restriction enzymes	NEB
RNase A	Roche
SapphireAmp fast PCR-hot start master mix	TaKaRa
T4 DNA Ligase	NEB
TEV protease	Westermann lab
zymolase 100 T	Carl Roth

Table 8: List of machines and devices

Device/machine	Description	Manufacturer
5424R/5424	tabletop centrifuge	Eppendorf
5810R	centrifuge	Eppendorf
ÄKTA	FPLC system	GE Healthcare
Amersham Imager 600	chemiluminescence detector	GE Healthcare
Avanti JXN-26	centrifuge	Beckman Coulter
BioPhotometer D30	photometer	Eppendorf
Bio RS-24	end-over-end rotator	Biosan
C1000 Touch Thermal Cycler	PCR cycler	Bio-Rad
Cawomat 200 IR	development of ECL films	Cawo
DeltaVision Elite	widefiled microscope	GE Healthcare Life Sciences
Digital Sonifier 450	sonifier	Branson
Disruptor Genies	cell disruptor	Scientific Industries

ETTAN	FPLC system	GE Healthcare
Innova 44	shaking incubator	New Brunswick Scientific
Julabo 5A	water bath	Julabo
MACSQuant VYB	flow cytometer	Miltenyi Biotec
ME711K	microwave	Samsung
Mini Bead Beater	cell disruptor	Biospec Industires
Mini-PROTEAN Tetra Cell	gel electrophoresis chamber	Bio-Rad
MR3001	magnetic stirring and heating plate	Heidolph
MSM 200	semi-automatic tetrad dissection microscope	Singer
Multitron Standard	shaking incubator	Infors HT
NanoDrop One	spectrophotometer	Thermo Scientific
PMR-30	platform rocker	Grant-bio
PowerPac Basic/HC	power supply	Bio-Rad
PureLab Flex	ultrapure water supply	Elga Veolia
RC6 Plus	centrifuge	Sorvall
Revolver	end-over-end rotator	Labnet
SBH200D	heating block	Stuart
Seven Compact	pH meter	Mettler Toledo
TC-7	rotating wheel	New Brunswick Scientific
Thermo Mixer C	heating block	Eppendorf
Unimax 1010	shaking plate	Heidolph
Universal Hood II	UV imager	Bio-Rad
USC-TH	ultrasonic cleaner	VWR

Table 9: List of software

Name	Purpose	Provider
Adobe Illustrator 2020	preparation of figures	Adobe
Fiji	image processing	open source
FlowJo	processing of FACS data	Becton, Dickinson & Company
JalView	visualization of multiple sequence alignment and secondary structure prediction	open source
GraphPad Prism 9	statistical analysis, preparation of graphs	GraphPad Software
Microsoft Office	text editing, writing, basic data analysis	Microsoft
SeqBuilder	*in silico* cloning	DNA Star
SeqMan Pro	analysis of DNA sequencing results	DNA Star
SoftWoRx	control of DeltaVision microscope	GE Healthcare
Unicorn	control of FPLC systems	GE Healthcare

Table 10: Plasmid list

Name	Coding sequence	Purpose	Source
pSW1	Dam1^{WT}c with Hsk3-6xHis	protein purification	Westermann lab
pSW4	Dam1-19c with Hsk3-6xHis (Dam1 Q205 Stop)	protein purification	Westermann lab
pSW17	Dam1^{4D}c with Hsk3-6xHis (Dam1 S20D, S257D, S265D, S292D)	protein purification	Westermann lab
pAD21	Dam1$^{\Delta SxIP}$c with Hsk3-6xHis	protein purification	this study
pTZ12	GST-Bim1	protein purification	Zimniak et al., 2009
pTZ15	GST-Bim1$^{1-133}$	protein purification	Zimniak et al., 2009
pTZ13	GST-Bim1$^{120-344}$	protein purification	Zimniak et al., 2009
pTZ39	GST-Bim1$^{185-344}$	protein purification	Zimniak et al., 2009
pTZ40	GST-Bim1$^{205-344}$	protein purification	Zimniak et al., 2009
pET28a-Bik1-6xHis	Bik1-6xHis	protein purification	Westermann lab
	Stu2-Flag	protein purification	Westermann lab
	StrepII-Mps1	protein purification	Westermann lab
	Ndc80c-Flag	protein purification	Westermann lab
pAD4	Duo1^{WT}-6xFlag in pRS306	yeast transformation	this study
pAD5	Duo1$^{\Delta SxIP}$-6xFlag in pRS306	yeast transformation	this study
pDD526	Pds1-18xMyc	yeast transformation	Westermann lab
pAD19	*dam1-19* in pRS305	yeast transformation	this study
pAD24	Dam1^{WT} in pRS305	yeast transformation	this study
pAD25	Dam1^{4A} (S217A, S218A, S221A, S232A)	yeast transformation	this study
pAD47	Duo1^{WT}-6xFlag in pRS303	yeast transformation	this study
pAD48	Duo1$^{\Delta SxIP}$-6xFlag in pRS303	yeast transformation	this study
pAD53	Duo1^{WT} in pRS303	yeast transformation	this study
pAD54	Duo1$^{\Delta SxIP}$ in pRS303	yeast transformation	this study
pSW809	Ndc80^{WT} in pRS306	yeast transformation	Lampert et al., 2013
pAD67	Ndc80$^{\Delta 490–510}$ in pRS306	yeast transformation	this study
pAD56	Ask1^{WT} in pRS303	yeast transformation	this study
pAD72	Ask1^{2A} (S216A, S250A) in pRS303	yeast transformation	this study
pAD73	Ask1^{2D} (S216D, S250D) in pRS303	yeast transformation	this study
pAD76	Dam1^{S20D} in pRS305	yeast transformation	this study

Table 11: List of yeast strains

Name	Genotype	Source
DDY902	Mat a, *his3Δ200*, *ura3-52*, *ade2-1*, *leu2-3,112*	Westermann lab
DDY904	Mat α, *his3Δ200*, *ura3-52*, *leu2-3,112*, *lys2-801*	Westermann lab
DDY1502	Mat a, *mad1*Δ::His3, *his3Δ200*, *leu2-3,112*, *ura3-52*, *ade2-101*	Westermann lab
DDY1503	Mat a, *mad2*Δ::Ura3, *his3Δ200*, *leu2-3,112*, *ura3-52, ade2-101*	Westermann lab
SWY754	Mat a, *bim1*Δ::KanMx6, *his3Δ200*, *ura3-52*, *ade2-1*, *leu2-3,112*	Westermann lab
strain 3013	Mat a, *mps1*Δ::KanMx6, Trp1::10xMyc-*mps1-as1*	Jones et al., 2005
ADY5	Mat a, Duo1^{WT}-6xFlag::Leu2, *his3Δ200*, *ura3-52*, *ade2-1*	this study
ADY8	Mat a, Duo1$^{\Delta SxIP}$-6xFlag::Leu2, *his3Δ200*, *ura3-52*, *lys2-801*	this study
ADY14	Mat a, *duo1*Δ::His3, *leu2-3,112*::Duo1$^{\Delta SxIP}$-6xFlag::Leu2, *ura3-52*, *ade2-1*	this study
ADY17	Mat a, Duo1^{WT}-6xFlag::KanMx6, *his3Δ200*, *ura3-52*, *ade2-1*, *leu2-3,112*	this study
ADY20-2	Mat a, Duo1$^{\Delta C(R223Stop)}$-6xFlag::KanMx6, *his3Δ200*, *ura3-52*, *lys2-801*, *ade2-1*, *leu2-3,112*	this study
ADY99	Mat a, Duo1^{WT}-6xFlag::KanMx6, *mad2*Δ::Ura3, *his3Δ200*, *lys2-801*, *ade2-1*, *leu2-3,112*	this study
ADY101	Mat a, *duo1*Δ::His3, *leu2-3,112*::Duo1$^{\Delta SxIP}$-6xFlag::Leu2, *mad2*Δ::Ura3, *lys2-801*, *ade2-1*	this study
ADY103	Mat a, Duo1$^{\Delta C\ (R223Stop)}$-6xFlag::KanMx6, *mad2*Δ::Ura3, *his3Δ200*, *ade2-1*, *leu2-3,112*	this study
ADY29	Mat a, Pds1-18xMyc::Leu2, his3Δ200, ura3-52, ade2-1	this study
ADY226	Mat a, *duo1*Δ::His3; *leu2-3,112*::Duo1^{WT}-6xFlag::Leu2; Pds1-18xMyc::Leu2, *ura3-52*, *lys2-801*, *ade2-1*	this study
ADY227	Mat a, *duo1*Δ::His3; *leu2-3,112*::Duo1$^{\Delta SxIP}$-6xFlag::Leu2; Pds1-18xMyc::Leu2; *ura3-52*, *ade2-1*	this study
ADY240	Mat a, Pds1-18xMyc::Leu2, *his3Δ200*, *ura3-52*, *lys2-801*	this study
ADY231	Mat a, Dad1-GFP::KanMx6; Pds1-18xMyc::Leu2, *his3Δ200*, *ura3-52*, *lys2-801*	this study
ADY232	Mat a, Dad1-GFP::KanMx6; Pds1-18xMyc::Leu2; *duo1*Δ::His3; *leu2-3,112*::Duo1^{WT}-6xFlag::Leu2, *ura3-52*, *lys2-801*	this study
ADY233	Mat a, Dad1-GFP::KanMx6; Pds1-18xMyc::Leu2; duo1Δ::His3; *leu2-3,112*::Duo1$^{\Delta SxIP}$-6xFlag::Leu2, *ura3-52*, *lys2-801*	this study
ADY66	Mat a, *duo1*Δ::His3; *leu2-3,112*::Duo1$^{\Delta SxIP}$-6xFlag::Leu2; Dad1-GFP::KanMx6, *ura3-52*	this study
ADY68	Mat a, Dad1-GFP::His3, *ura3-52*, *leu2-3,112*	this study
ADY72	Mat a, Duo1-6xFlag::KanMx6; Dad1-GFP::His3, *ura3-52*, *lys2-801*, *leu2-3,112*	this study
ADY290	Mat a, Dad1-GFP::His3, *bim1*Δ::KanMx6, *ura3-52*, *leu2-3,112*	this study
ADY145.3	Mat α, Duo1-6xFlag::KanMx6, *ipl1-2*, *his3Δ200*, *ura3-52*, *lys2-801*, *leu2,3-112*	this study
ADY197	Mat α, *mps1*Δ::KanMx6, Trp1::10xMyc-*mps1-as1*, *ipl1-2*, Duo1^{WT}-6xFlag::KanMx6, *ura3-52*	this study
ADY330	Mat a, Duo1^{WT}-6xFlag::Leu2, Dam1^{WT}::Ura3, Dad1-GFP::His3, Spc42-mCherry::KanMx6, *lys2-801*	this study
ADY335	Mat α, Duo1^{WT}-6xFlag::Leu2, Dam1^{4A}::Ura3, Dad1-GFP::His3, Spc42-mCherry::KanMx6, *lys2-801*	this study

ADY288.1	Mat a, Duo1^{WT}-6xFlag::Leu2; *ura3-52*::pGal-1xMyc-Mps1::Ura3, *his3Δ200*, *ade2-1*, *trp1-1*	this study
ADY349	Mat α, Dad1-GFP::His3, Ndc80-mRuby2::KanMx6, *ura3-52*, *lys2-801*, *leu2-3,112*	this study
ADY351	Mat α, Dad1-GFP::His3, Ndc80-mRuby2::KanMx6, *ura3-52*::pGal-1xMyc-Mps1::Ura3, *lys2-801*, *leu2-3,112*	this study
ADY356	Mat a, Dad1-GFP::His3, Nup60-RedStar2::natNT2, *ura3-52*, *leu2-3,112*	this study
ADY357	Mat a, Dad1-GFP::His3, Nup60-RedStar2::natNT2, *ura3-52*::pGal-1xMyc-Mps1::Ura3, *lys2-801*, *leu2-3,112*	this study
ADY312	Mat α, *ura3-52*::pGal-osTir::Ura3, Dad1-GFP::His3, Cdc20-AID-9xMyc::KanMx6, *lys2-801*, *leu2-3,112*	this study
ADY532	Dad1-GFP::His3, Spc42-mCherry::KanMx6, *pdr5Δ*::KanMx6, *ura3-52*, *lys2-801*, *leu2,3-112*	this study
ADY352	Mat α, Duo1^{WT}::Leu2, *his3Δ200*, *ura3-52*, *lys2-801*	this study
ADY353	Mat α, Duo1$^{\Delta SxIP}$::Leu2, *his3Δ200*, *ura3-52*, *lys2-801*	this study
ADY382	Mat α, Duo1^{WT}::Leu2, *bik1*Δ::Ura3, *his3Δ200*, *lys2-801*	this study
ADY386.1	Mat α, Duo1 $^{\Delta SxIP}$::Leu2, *bik1*Δ::Ura3, *his3Δ200*, *lys2-801*	this study
ADY341	Mat α, Duo1^{WT}::Leu2, Dad1-GFP::His3, *ura3-52*, *lys2-801*	this study
ADY343	Mat α, Duo1 $^{\Delta SxIP}$::Leu2, Dad1-GFP, *ura3-52*	this study
ADY384	Mat α, Duo1^{WT}::Leu2, Dad1-GFP::His3, *bik1*Δ::Ura3, *lys2-801*	this study
ADY388	Mat α, Duo1$^{\Delta SxIP}$::Leu2, Dad1-GFP::His3, *bik1*Δ::Ura3, *lys2-801*	this study
ADY249	Mat α, *tor1-1*, *fpr1*Δ::natNT2, RPL13A-2xFKBP12::Trp1, Duo1^{WT}-6xFlag::His3, *ura3-52*, *ade2-1*, *leu2,3-112*	this study
ADY251	Mat α, *tor1-1*, *fpr1*Δ::natNT2, RPL13A-2xFKBP12::Trp1, Duo1^{WT}-6xFlag::His3, Ndc80-FRB-GFP::KanMx6, *ura3-52*, *ade2-1*, *leu2,3-112*	this study
ADY253	Mat α, *tor1-1*, *fpr1*Δ::natNT2, RPL13A-2xFKBP12::Trp1, Duo1^{WT}-6xFlag::His3, Ndc80-FRB-GFP::KanMx6, *leu2,3-112*::Ndc80^{WT}::Leu2, *ura3-52*, *ade2-1*	this study
ADY254	Mat α, *tor1-1*, *fpr1*Δ::natNT2, RPL13A-2xFKBP12::Trp1, Duo1$^{\Delta SxIP}$-6xFlag::His3, Ndc80-FRB-GFP::KanMx6, *leu2,3-112*::Ndc80^{WT}::Leu2, *ura3-52*, *ade2-1*	this study
ADY257	Mat α, *tor1-1*, *fpr1*Δ::natNT2, RPL13A-2xFKBP12::Trp1, Duo1^{WT}-6xFlag::His3, Ndc80-FRB-GFP::KanMx6, *leu2,3-112*::Ndc80$^{\Delta 1-116}$::Leu2, *ura3-52*, *ade2-1*	this study
ADY258	Mat α, *tor1-1*, *fpr1*Δ::natNT2, RPL13A-2xFKBP12::Trp1, Duo1$^{\Delta SxIP}$-6xFlag::His3, Ndc80-FRB-GFP::KanMx6, *leu2,3-112*::Ndc80$^{\Delta 1-116}$::Leu2, *ura3-52*, *ade2-1*	this study
ADY259	Mat α, *tor1-1*, *fpr1*Δ::natNT2, RPL13A-2xFKBP12::Trp1, Duo1^{WT}-6xFlag::His3, Ndc80-FRB-GFP::KanMx6, *leu2,3-112*::Ndc80$^{\Delta 256-273}$::Leu2, *ura3-52*, *ade2-1*	this study
ADY260	Mat α, *tor1-1*, *fpr1*Δ::natNT2, RPL13A-2xFKBP12::Trp1, Duo1$^{\Delta SxIP}$-6xFlag::His3, Ndc80-FRB-GFP::KanMx6, *leu2,3-112*::Ndc80$^{\Delta 256-273}$::Leu2, *ura3-52*, *ade2-1*	this study
ADY263	Mat α, *tor1-1*, *fpr1*Δ::natNT2, RPL13A-2xFKBP12::Trp1; Duo1^{WT}::His3; Ndc80-FRB-GFP::KanMx6, *ura3-52*, *ade2-1*, *leu2,3-112*	this study
ADY264	Mat α, *tor1-1*, *fpr1*Δ::natNT2, RPL13A-2xFKBP12::Trp1; Duo1$^{\Delta SxIP}$::His3; Ndc80-FRB-GFP::KanMx6, *ura3-52*, *ade2-1*, *leu2,3-112*	this study
ADY394	Mat α, *tor1-1*, *fpr1*Δ::natNT2, RPL13A-2xFKBP12::Trp1; Duo1^{WT}::His3; Ndc80-FRB-GFP::KanMx6, *leu2,3-112*::Ndc80^{WT}::Leu2, *ura3-52*, *ade2-1*	this study
ADY395	Mat α, tor1-1, *fpr1*Δ::natNT2, RPL13A-2xFKBP12::Trp1; Duo1^{WT}::His3; Ndc80-FRB-GFP::KanMx6, *leu2,3-112*::Ndc80$^{\Delta 490-510}$::Leu2, *ura3-52*, *ade2-1*	this study

ADY396	Mat α, *tor1-1*, *fpr1*Δ::natNT2, RPL13A-2xFKBP12::Trp1; Duo1$^{\Delta SxIP}$::His3; Ndc80-FRB-GFP::KanMx6, *leu2,3-112*::Ndc80^{WT}::Leu2, *ura3-52*, *ade2-1*	this study
ADY397	Mat α, *tor1-1*, *fpr1*Δ::natNT2, RPL13A-2xFKBP12::Trp1; Duo1$^{\Delta SxIP}$::His3; Ndc80-FRB-GFP::KanMx6, *leu2,3-112*::Ndc80$^{\Delta 490-510}$::Leu2, *ura3-52*, *ade2-1*	this study
ADY499	Mat a, Duo1^{WT}::His3, Ndc80^{WT}::Ura3, Dad1-GFP::KanMx6, Spc42-RedStar2::natNT2, *leu2,3-112*	this study
ADY501	Mat a, Duo1^{WT}::His3, Ndc80$^{\Delta 490-510}$::Ura3, Dad1-GFP::KanMx6, Spc42-RedStar2::natNT2, *lys2-801*, *leu2,3-112*	this study
ADY507	Mat a, Duo1$^{\Delta SxIP}$::His3, Ndc80^{WT}::Ura3, Dad1-GFP::KanMx6, Spc42-RedStar2::natNT2, *leu2,3-112*	this study
ADY509	Mat a, Duo1$^{\Delta SxIP}$::His3, Ndc80$^{\Delta 490-510}$::Ura3, Dad1-GFP::KanMx6, Spc42-RedStar2::natNT2, *leu2,3-112*	this study

3. Results

3.1. Biochemical and structural analysis of the Dam1c-Bim1 complex

3.1.1. Purification of recombinant Dam1c and Bim1 from *E. coli*

Both Dam1c and Bim1 were purified from *E. coli* as described in 2.1.1 and 2.1.2. In brief, Dam1c was purified by metal ion affinity chromatography exploiting the 6xHis tag at the C-terminus of the Hsk3 subunit, followed by cation exchange chromatography and a final buffer exchange or size exclusion chromatography (SEC) step. Bim1 and truncated Bim1 variants were expressed as N-terminal GST fusion proteins with a TEV cleavage site between the tag and Bim1. Proteins were purified by binding of the GST tag to glutathione sepharose and then subjected to SEC. For removal of the tag, the protein was incubated with TEV protease and Bim1 was further purified by anion exchange chromatography and SEC. Representative images of purified Dam1c and Bim1, respectively, are shown in Figure 10. Recombinant proteins were used for biochemical binding assays, crosslinking mass spectrometry and structural analyses.

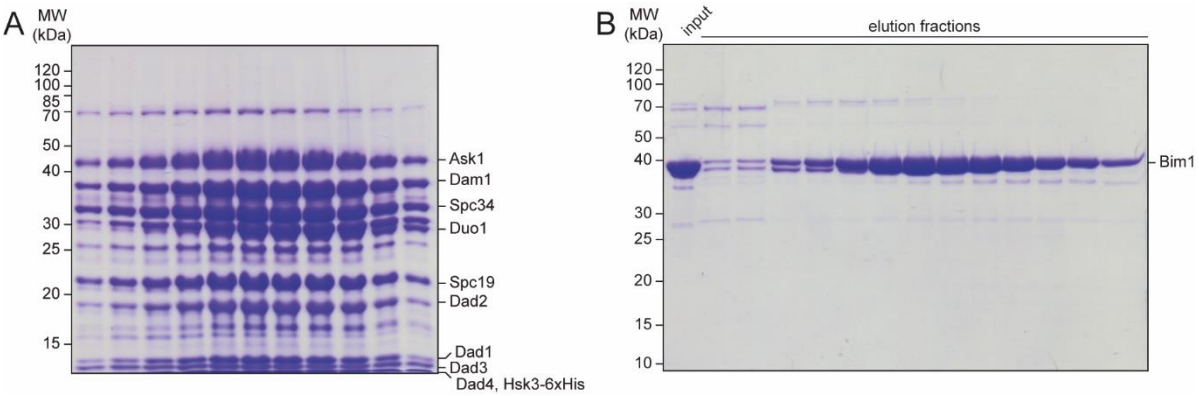

Figure 10: Representative images of purified Dam1c and Bim1
SDS-PAGE analysis of elution fractions of Dam1c after cation exchange chromatography (A) and Bim1 after gel filtration (B).

3.1.2. Dam1c and Bim1 form a stable complex in solution and solid phase binding assay

Previous publications suggested a physical interaction between Dam1c and Bim1 (Ito et al., 2001; Uetz et al., 2000; Wong et al., 2007). However, this observation is based on yeast two-hybrid screens and the interaction has never been analyzed biochemically. Using the purified recombinant proteins, binding of Bim1 to the Dam1 complex was probed by analytical SEC. During SEC, molecules are separated according to their Stokes radius, which is determined by their molecular weight and shape. Larger molecules elute early during SEC, while smaller molecules elute later. Binding between molecules is indicated by earlier elution of the complex compared to the individual components. Elution of proteins from the column is monitored by measuring the absorbance at 280 nm. SDS-PAGE analysis of elution fractions gives further insights into binding between the proteins.

Dam1c and Bim1 alone and in combination were subjected to analytical SEC. Dam1c and

Bim1 alone eluted after about 1.2 and 1.65 ml, respectively, reflecting the different molecular weights and shapes of the proteins (Figure 11A; Dudziak et al., 2021). Addition of Bim1 to Dam1c caused only, if at all, a minor shift of the elution profile under these conditions. Binding of Bim1 to Dam1c was indicated by the disappearance of the Bim1 peak in the chromatogram and an increase in the absorbance at 280 nm of the Dam1c peak. Furthermore, stoichiometric coelution of Bim1 with Dam1c was clearly visible by SDS-PAGE analysis of the elution fractions (Figure 11B). Binding between Bim1 and Dam1c was additionally confirmed by solid phase binding assays which will be described later (Figure 16B and C).

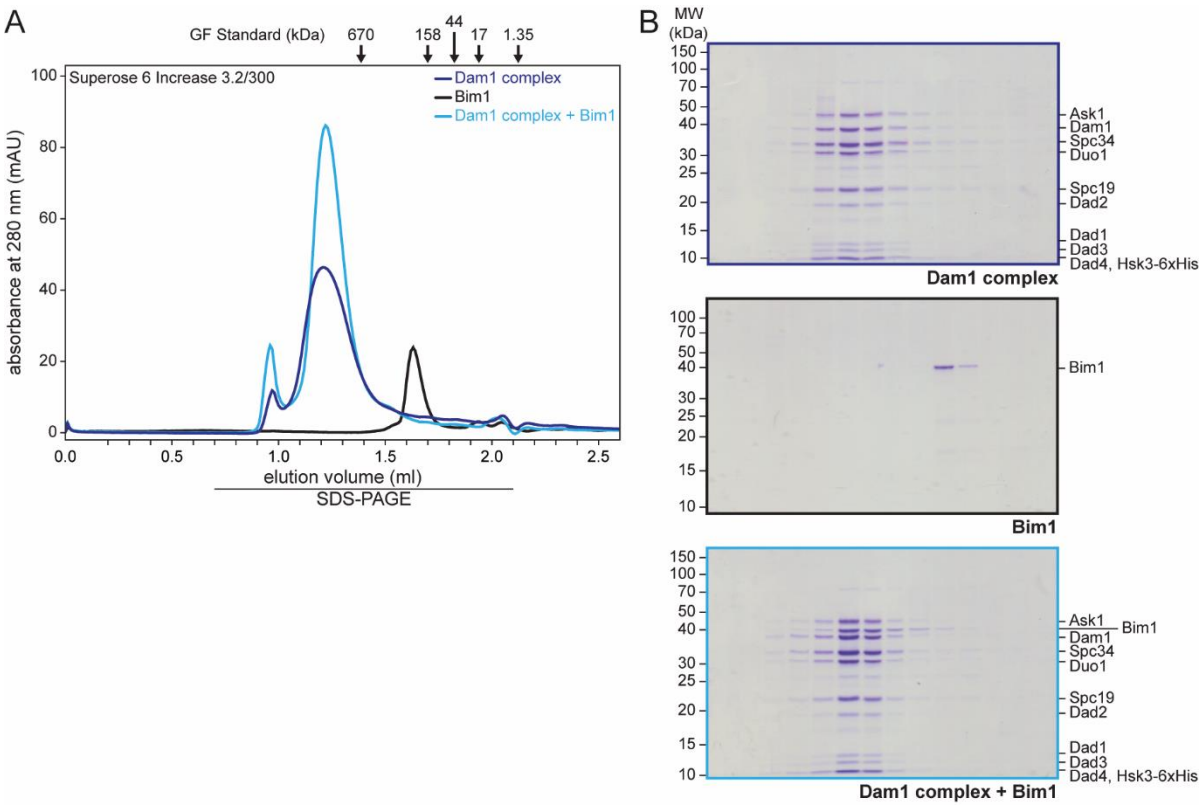

Figure 11: Analytical SEC of Dam1c and Bim1
A: Chromatograms of SEC runs of Dam1c and Bim1 alone and in combination. Elution positions of globular standard proteins and their molecular weight are indicated at the top.
B: SDS-PAGE analysis of elution fractions from SEC runs shown in A.

3.1.3. Crosslinking mass spectrometry analysis of the Dam1c-Bim1 complex

To get more detailed information on the topology of the Dam1c-Bim1 complex and potential binding sites for Bim1, the complex was analyzed by crosslinking followed by mass spectrometry. The crosslinker BS3 (bis(sulfosuccinimidyl)suberat), which is used in this experiment, covalently crosslinks lysine residues of proteins within a distance of about 12 Å. Crosslinked proteins were further processed as described in 2.2.11. In an initial experiment, the optimal crosslinker concentration that ensures efficient while preventing excessive crosslinking was determined by incubating Dam1c with increasing amounts of BS3. Samples were analyzed by SDS-PAGE followed by silver staining. Crosslinking is indicated by disappearance of the individual proteins and emergence of a high molecular weight

crosslinking product (Figure 12; Dudziak, 2016). A BS3 concentration of 600 µM allowed for efficient crosslinking of Dam1c.

Next, Dam1c alone or in presence of an equimolar amount of Bim1 was crosslinked by BS3 and further processed and analyzed by mass spectrometry as described in 2.2.11. The results were visualized using the free software xVis (Grimm et al., 2015) giving a graphical proximity map of the complex as output.

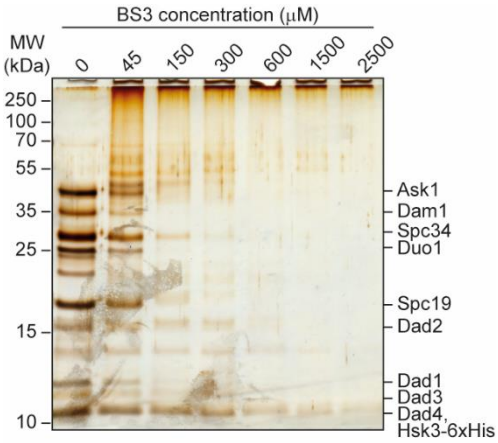

Figure 12: BS3 crosslinker titration
Dam1c was incubated with increasing concentrations of the crosslinker BS3 to optimize crosslinking conditions. Proteins were analyzed by SDS-PAGE followed by silver staining. Image from Dudziak, 2016.

Analysis of the Dam1 complex in absence of Bim1 revealed a large number of crosslinks between individual subunits (Figure 13A; Dudziak, 2016). A dense network of crosslinks was found between the subunits Dam1, Duo1, Spc19 and Spc34. Crosslinked lysine residues of Spc34 were mainly located in the N-terminal portion of the protein, while the C-terminal parts of Dam1 and Duo1 were multiply crosslinked. Crosslinked lysine residues of Spc19 are predominantly located in the middle region of the protein. Overall, the proximity map of crosslinked Dam1c is in agreement with previously published crosslinking data (Legal et al., 2016; Zelter et al., 2015). Furthermore, the extensive crosslinking network between Dam1, Duo1 and Spc34 fits to the cryo-EM structure of the complex with all these three subunits localized in arm II of the complex. Crosslinks between Spc19 and Spc34 reflect their proximity within the protrusion domain (Jenni and Harrison, 2018).

In the presence of Bim1, the overall pattern of crosslinks between Dam1c subunits was hardly changed, suggesting that Bim1 binding does not induce a major conformational change of the complex (Figure 13B). 18 crosslinks between Bim1 and the Dam1 subunits Spc34, Dam1, Spc19, Dad4 and Duo1 were identified (Appendix Table 1). Crosslinks to Dam1 involved lysine residues within the flexible C-terminal tail of the protein which additionally harbors three Ipl1 and four Mps1 phosphorylation sites. Thus, phosphorylation of the C-terminal part of Dam1 might serve as regulation hub for Bim1 binding to the complex. As already seen in the absence of Bim1, the C-termini of Dam1 and Duo1 were connected by multiple crosslinks, suggesting proximity of these protein regions. Notably, the C-terminus of Duo1 was also crosslinked to the EBH cargo binding domain of Bim1 ($Duo1^{K236}$ – $Bim1^{K223}$). Together with the Dam1-Bim1 crosslinks, Duo1, Dam1 and Spc34 appear to form a tripartite binding platform. Finally, the crosslinks of Bim1 with Spc19 and Spc34 indicate proximity of Bim1 to the protrusion domain of the Dam1 complex.

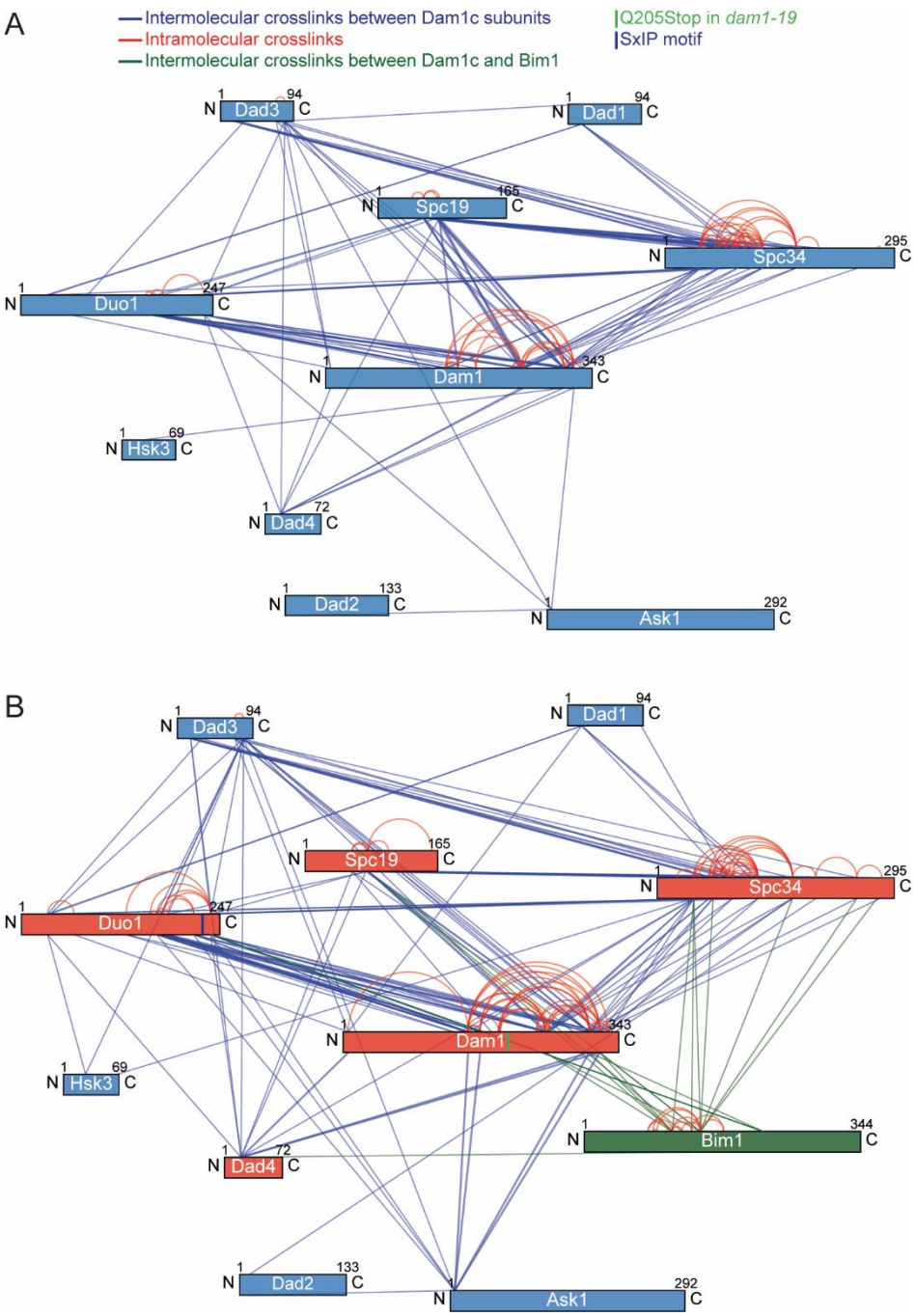

Figure 13: Crosslinking proximity map of Dam1c and Dam1c-Bim1 complex
Crosslinking mass spectrometry analysis of Dam1c in the absence (A) and presence (B) of Bim1. Each protein is represented as bar. Dam1c subunits crosslinked to Bim1 are shown in red, other subunits in blue and Bim1 in green. Intramolecular crosslinks are indicated by red lines. Blue and green lines indicate intermolecular crosslinks between Dam1c subunits and between Dam1c subunit and Bim1, respectively. The blue mark in Duo1 labels the position of a conserved SxIP motif, the green mark in Dam1 the position of a premature stop codon found in the *dam1-19* allele.
Crosslinking samples were processed and analyzed by Pascaline Rombaut and Franz Herzog (Gene Center Munich, Ludwig Maximilian University Munich, Munich). Crosslinking data were obtained in context of Alexander Dudziak's master thesis (Dudziak, 2016).

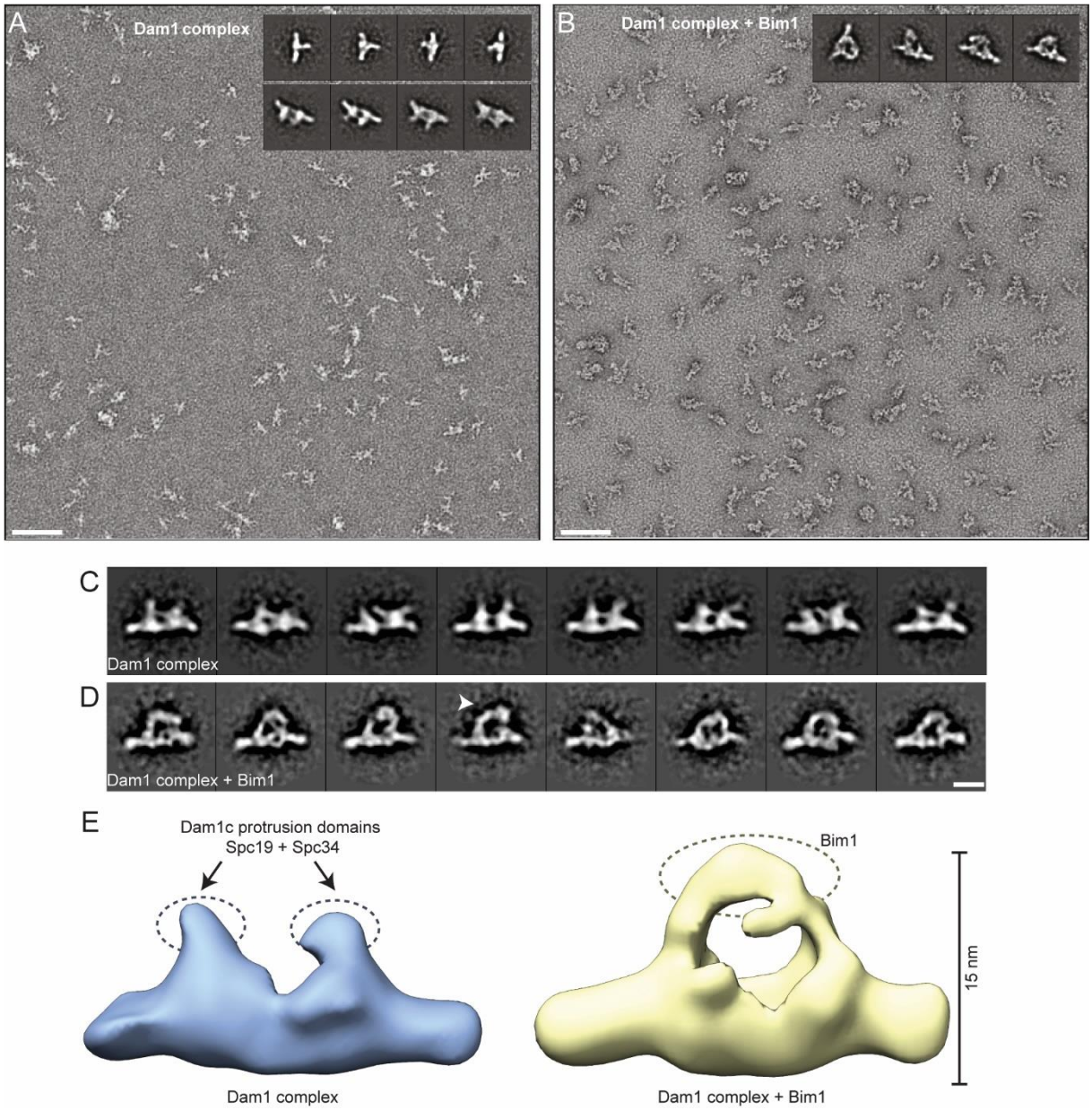

Figure 14: Negative stain EM of Dam1c and Bim1 and three-dimensional reconstruction of the complex

A, B: Representative EM micrographs of negatively stained Dam1c (A) and Dam1c-Bim1 complex (B). Inlays show magnified representative complex particles. Scale bar: 100 nm.

C, D: Representative 2D class averages of dimeric Dam1c (C) and Dam1c-Bim1 complex (D). The white arrowhead in D points at Bim1 bridging the protrusion domains of Dam1c.

E: Three-dimensional reconstruction of Dam1c in the absence (left) or presence (right) of Bim1. The protrusion domains consisting of Spc19 and Spc34 and Bim1 are marked by dashed ovals.

Electron microscopy data were collected, processed and analyzed by Lena Engelhard and Christos Gatsogiannis (Department of Structural Biochemistry, Max Planck Institute of Molecular Physiology, Dortmund and Institute for Medical Physics and Biophysics and Center for Soft Nanoscience, Westfälische Wilhelms-Universität Münster).

3.1.4. Negative stain electron microscopy reveals a distinct Bim1 binding site

Dam1c has been visualized by negative stain electron microscopy in previous studies which allows to draw conclusions about the shape and topology of the complex. In a similar approach, the Dam1c-Bim1 complex was analyzed by electron microscopy (EM) after negative staining. Consistent with previous publications, Dam1c alone appeared as T-shaped monomer or π-

shaped dimer. The protrusion domains of the complex were clearly visible and projected almost perpendicularly from the rest of the complex (Figure 14A and C). In the presence of Bim1, the complex was predominantly found as dimer. However, drawing a quantitative conclusion about the ratio between monomeric and dimeric species compared to the complex in absence of Bim1 is not possible, since Dam1c and Bim1 were crosslinked to prevent dissociation of the complex during sample preparation. Bim1 was visible as additional mass that localizes with the protrusion domains of a Dam1c dimer (Figure 14B and D). Three-dimensional structures of Dam1c and Dam1c-Bim1 complex were calculated based on 2D class averages (Figure 14E). The reconstruction reveals that Bim1 bridges the protrusion domains of two adjacent Dam1c monomers. This observation is consistent with the crosslinking data which reveal a proximity between the Dam1c protrusion domain consisting of Spc19 and Spc34 and Bim1 (Figure 13B).

For a more systematic analysis of the effect of Bim1 on the Dam1c oligomerization state, samples were prepared for negative stain EM without prior crosslinking. Under lower salt concentrations, Dam1c alone formed larger oligomers, as seen by EM (Figure 15A). In presence of Bim1, Dam1c formed even larger oligomers with well-defined curvatures which were reminiscent of partially assembled Dam1c rings (Figure 15B). This finding suggests that Bim1 is able to trigger Dam1c oligomerization or probably even ring formation by crosslinking the protrusion domains of adjacent Dam1 complexes.

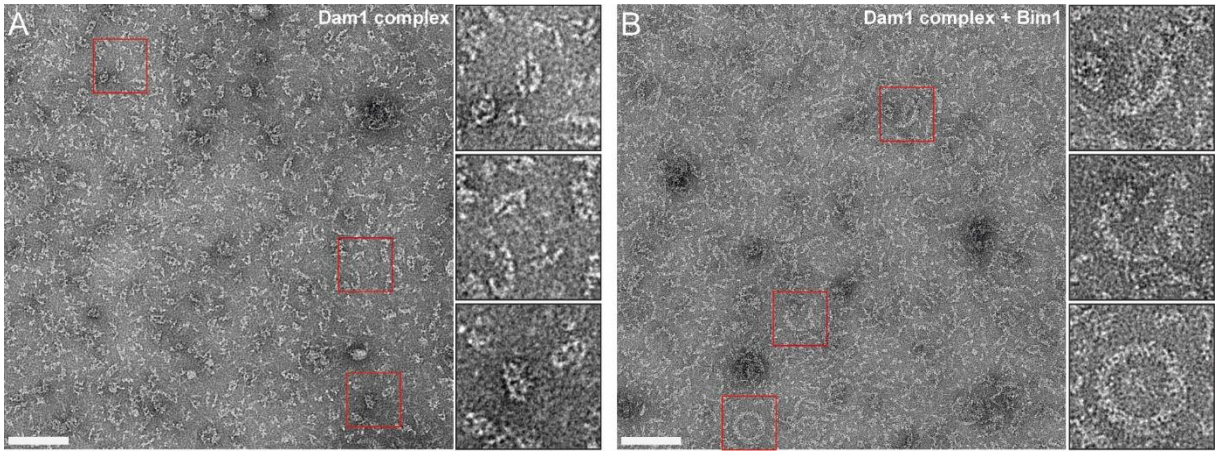

Figure 15: Negative stain EM images of oligomerized Dam1c-Bim1 complex
Dam1c alone (A) or in presence of Bim1 (B) was incubated in low salt buffer, negatively stained and visualized by EM. Under these conditions, Dam1c tends to form larger oligomers (A), which is further promoted by Bim1 (B). Areas within the red boxes are displayed as magnified images. Scale bar: 100 nm. Electron microscopy data were collected, processed and analyzed by Cole Bourque, Björn Udo Klink and Christos Gatsogiannis (Department of Structural Biochemistry, Max Planck Institute of Molecular Physiology, Dortmund and Institute for Medical Physics and Biophysics and Center for Soft Nanoscience, Westfälische Wilhelms-Universität Münster).

3.1.5. The EBH domain of Bim1 is required and sufficient for binding to Dam1c

Members of the family of EB proteins such as Bim1 comprise several functional domains. The N-terminal CH domain mediates microtubule binding and the EBH domain and C-terminal ETF motif are required for cargo binding. Both domains are separated by a flexible linker that

contributes to microtubule binding and also facilitates homodimerization of Bim1 (Figure 16A; Akhmanova and Steinmetz, 2008). To test for the contribution of the different domains to Dam1c binding, a pull down assay with truncated Bim1 proteins fused to GST was performed. GST-tagged Bim1 proteins were immobilized on glutathione sepharose beads and incubated with recombinant Dam1c. Bound Dam1c was detected by western blot analysis using an anti-penta-His antibody which recognizes the His-tagged Hsk3 subunit. GST-Bim1^{WT} stably bound Dam1c under these experimental conditions, confirming the results of the analytical SEC (Figure 16B). The Bim1 CH domain in combination with the flexible linker (GST-Bim1$^{1-133}$) was unable to bind Dam1c. In contrast, constructs containing the EBH cargo binding domain (amino acids 120-344 and 185-344) were both able to interact with Dam1c. A short N-terminal truncation of the EBH domain (GST-Bim1$^{205-344}$) was sufficient to prevent binding of Dam1c. These results strongly suggest that the interaction between Dam1c and Bim1 depends on Bim1's EBH domain.

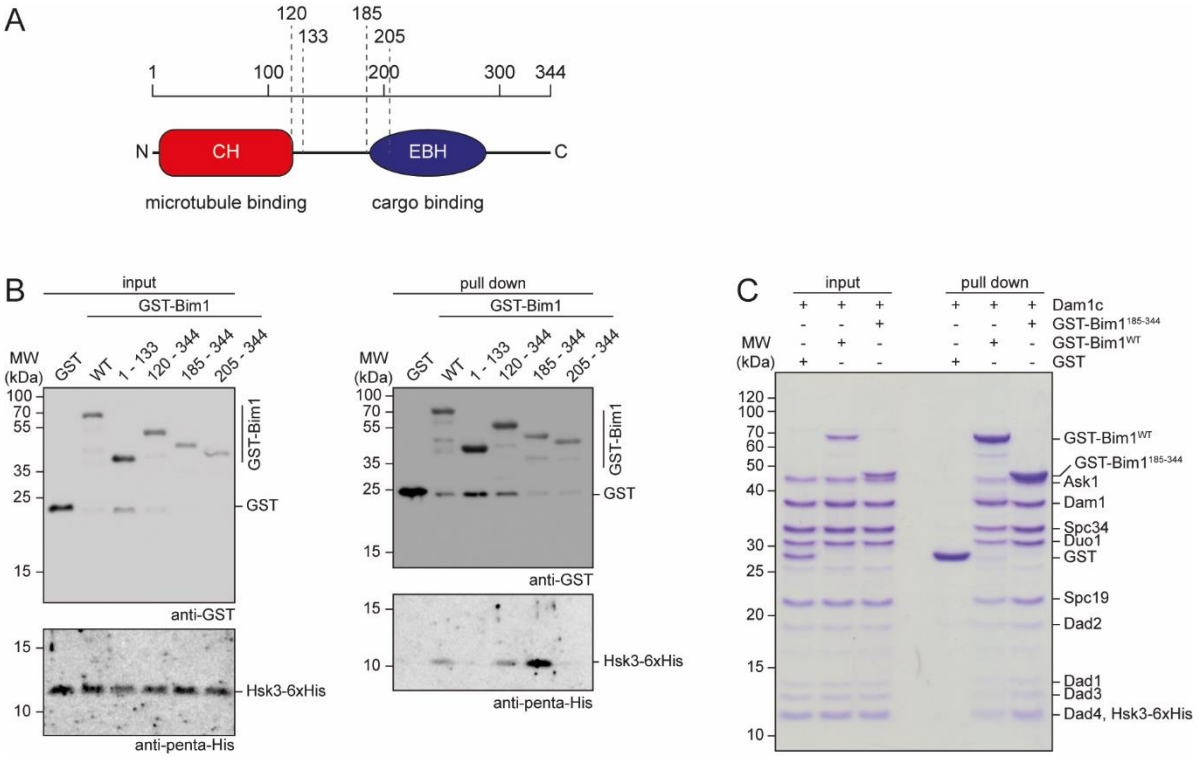

Figure 16: The EBH domain of Bim1 is required and sufficient to bind Dam1c
A: Schematic illustration of Bim1 and its functional domains. Dashed lines mark the boundaries of truncation proteins used in the following pull down assays. For reasons of simplicity, Bim1 is shown as monomer.
B: Pull down assays to test Dam1c binding to different Bim1 truncation proteins fused to GST. GST-Bim1 variants were immobilized on beads and incubated with recombinant Dam1c. Binding of the complex was analyzed by western blot by detecting the 6xHis-tagged subunit Hsk3. Data was obtained in context of Alexander Dudziak's master thesis (Dudziak, 2016).
C: Pull down assays comparing Dam1c binding to GST-Bim1^{WT} and GST-Bim1$^{185-344}$. Input and pull down samples were analyzed by SDS-PAGE followed by Coomassie staining. GST served as control to exclude unspecific binding of Dam1c to the GST tag.

Comparing binding of Dam1c to GST-Bim1$^{120-344}$ and GST-Bim1$^{185-344}$ showed a striking difference regarding binding efficiency. GST-Bim1$^{185-344}$ that lacks the flexible linker appears

to be a stronger Dam1c binder compared to the protein containing this segment (Figure 16B and C). Presumably, Bim1^{WT} adopts a conformation that partially prevents binding of Dam1c.

3.1.6. A conserved SxIP motif in the C-terminus of Duo1 is essential for Bim1 binding

Two different mechanisms of cargo binding by Bim1 are known. The EBH domain of Bim1 binds to the short tetrapeptide sequence SxIP of cargo proteins (Honnappa et al., 2009). Alternatively, the C-terminal ETF (EEY in other EB proteins) specifically recognizes CAP-Gly domains of other proteins (Weisbrich et al., 2007). The fact that an intact EBH domain is essential and sufficient to bind Dam1c (Figure 16) suggests that the interaction between Dam1c and Bim1 depends on binding of the EBH domain to a so far unknown SxIP motif of the Dam1 complex. The crosslinking data showed that Duo1^{K236} is in proximity to Bim1^{K223} which is located within the EBH domain.

The sequences of Duo1 proteins from various yeast species were compared in a multiple sequence alignment using the MAFFT algorithm (Katoh et al., 2019). Comparison of the sequences identified an SxIP motif in the C-terminus of Duo1 (amino acids 225 – 228; Figure 17) which is in proximity to K236 that was crosslinked to Bim1^{K223}. The motif is located within a predicted unstructured region of Duo1. Thus, our data link the EBH cargo binding domain of Bim1 to a predicted binding sequence in the Duo1 C-terminus.

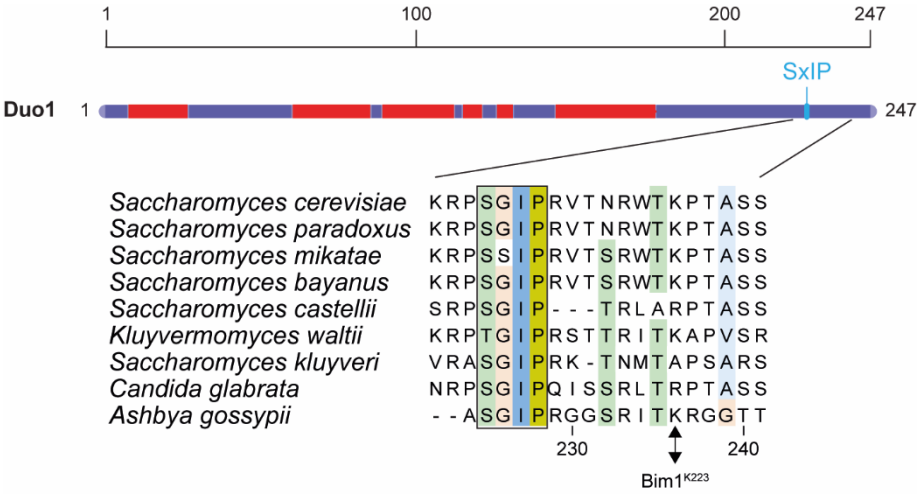

Figure 17: Multiple sequence alignment of Duo1 proteins identifies a conserved SxIP motif in the C-terminus

Secondary structure prediction of Duo1 (top) and multiple sequence alignment of Duo1 proteins from different yeast species. Duo1 is represented as bar with predicted α-helical regions shown in red and unstructured regions in blue. Multiple sequence alignment identifies a highly conserved SxIP motif within the C-terminus of Duo1. A conserved SxIP motif is labelled by a black box. The double-headed arrow marks K236 which was found to be crosslinked with Bim1^{K223}. Amino acids are colored according to the Clustal coloring scheme.

To explore whether the identified SxIP motif is required for Bim1 binding, recombinant Dam1c lacking this motif (Dam1$^{\Delta SxIP}$c) was purified from *E. coli* and used for biochemical binding assays. Binding of Bim1 to Dam1$^{\Delta SxIP}$c was tested by analytical SEC. Dam1$^{\Delta SxIP}$c eluted at a

similar position as the wild type complex, showing that deletion of the SxIP motif is compatible with formation of an intact Dam1 complex (Figure 18A). In the presence of Bim1, Dam1$^{\Delta SxIP}$c and Bim1 eluted independently from each other, demonstrating that Bim1 is not capable of binding the mutant Dam1c (Figure 18A and B). The result was confirmed by a pull down assay with immobilized GST-Bim1$^{185-344}$. While the wild type complex robustly bound to Bim1, Dam1$^{\Delta SxIP}$c failed in Bim1 binding (Figure 18C).

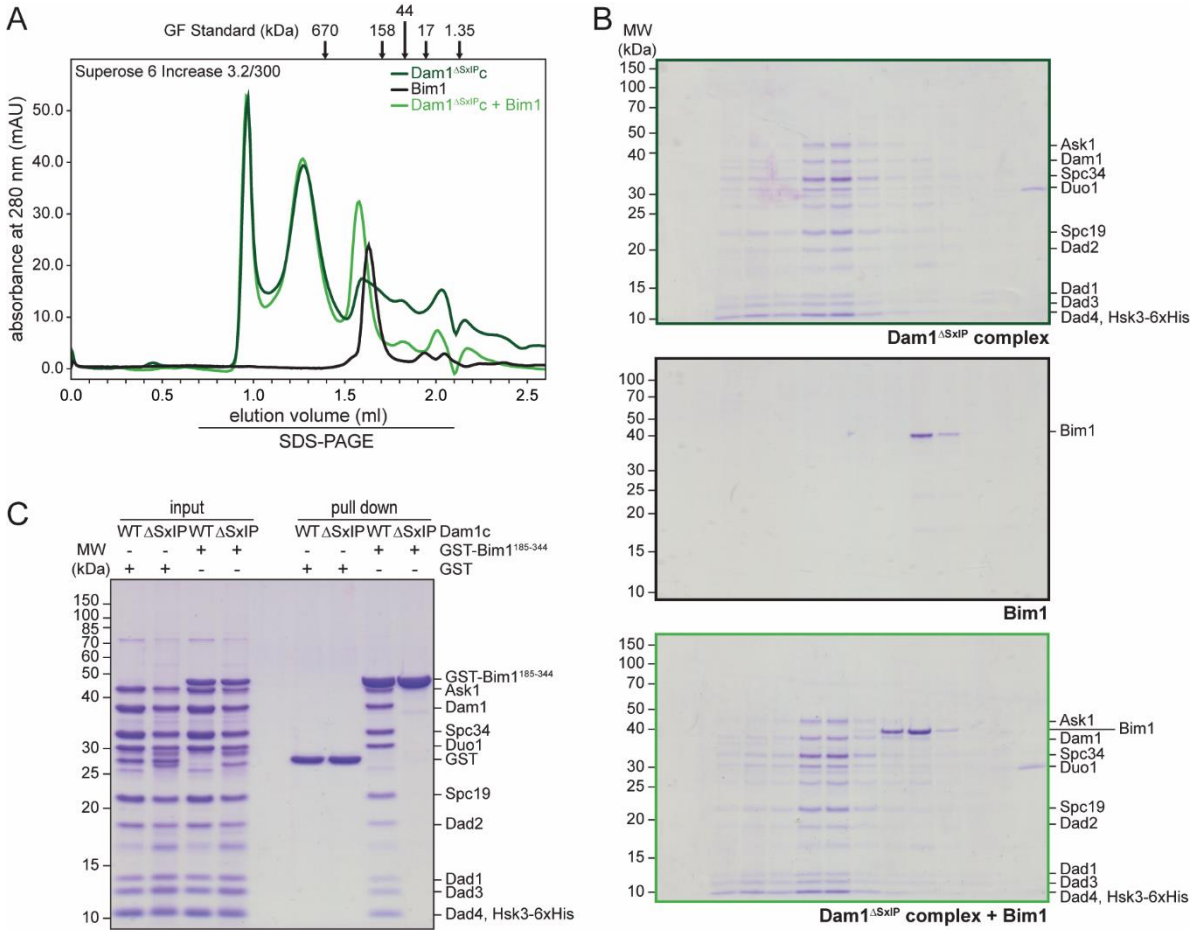

Figure 18: Deletion of the SxIP motif of Duo1 prevents binding of Bim1 to Dam1c
A, B: Analytical SEC of Dam1$^{\Delta SxIP}$c and Bim1 alone and in combination. Chromatograms are displayed in A, SDS-PAGE of elution fractions in B. The elution positions of gel filtration standard proteins are indicated at the top of the chromatograms.
C: Pull down assay to test for binding of Dam1$^{\Delta SxIP}$c to immobilized GST-tagged Bim1$^{185-344}$. Input and pull down samples were analyzed by SDS-PAGE.

3.2. *In vivo* analysis of the physiological function of the Dam1c-Bim1 complex

3.2.1. Deletion of the Duo1 SxIP motif prevents Bim1 binding of Dam1c from yeast cell extracts

With the knowledge that binding of Bim1 to Dam1c strictly depends on the SxIP motif of Duo1, it is possible to construct yeast strains that are deficient in Dam1c-Bim1 complex formation. To this end, the wild type Duo1 gene was replaced by Duo1^{WT} or Duo1$^{\Delta SxIP}$ fused to a 6xFlag tag. Alternatively, the respective Duo1 alleles were integrated at the exogenous Leu2 locus while Duo1 at the endogenous locus was deleted. Both strategies result in yeast strains which

solely express either Duo1^{WT}-6xFlag or Duo1$^{\Delta SxIP}$-6xFlag.

To test whether the deletion of Duo1's SxIP motif is also sufficient to disrupt Bim1 binding of Dam1c that was expressed in yeast cells, soluble cell extracts of Duo1^{WT} and Duo1$^{\Delta SxIP}$ yeast strains were prepared and used in pull down assays (Figure 19). GST-Bim1$^{185-344}$ was immobilized on beads and incubated with either of the two cell lysates. Binding of Dam1c was followed by western blot analysis of the pull down samples by detection 6xFlag-tagged Duo1. In agreement with the *in vitro* results using recombinant proteins, Dam1c lacking the Duo1 SxIP motif is deficient in Bim1 binding, while the wild type protein robustly bound to Bim1 (Figure 19). Bim1 binding was also prevented by deletion of the Duo1 C-terminus by introduction of a premature stop codon right in front of the SxIP motif (Duo1$^{\Delta C}$, R223Stop; Appendix Figure 1). These observations exclude the possibility that binding between these proteins might be mediated indirectly through an additional protein that was not included in the *in vitro* experiments.

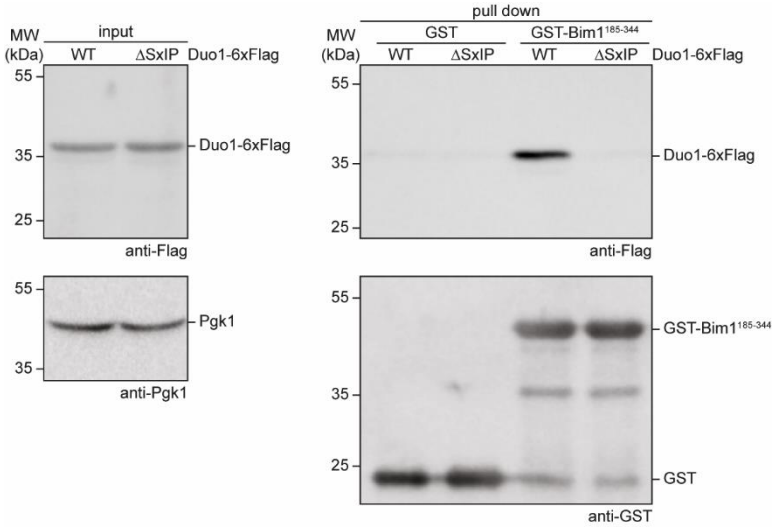

Figure 19: Endogenous Dam1c lacking the SxIP motif does not bind Bim1
Soluble cell extracts were prepared from yeast strains with 6xFlag-tagged Duo1^{WT} or Duo1$^{\Delta SxIP}$. Binding of Dam1c was tested by a pull down assay with GST-Bim1$^{185-344}$ immobilized on beads and followed by western blot analysis of input and pull down samples.

3.2.2. Viability of yeast cells is mildly compromised when Dam1c-Bim1 binding is disrupted

As an initial test in how far binding of Bim1 to Dam1c affects yeast cell viability, a serial dilution assay with yeast strains carrying different Duo1 alleles was performed. Cells of the respective strains were spotted on YEPD in a series of 1:4 dilutions and incubated at 30 °C and 37 °C. In addition, growth of the strains was also tested in presence of the microtubule-depolymerizing drug benomyl. A strain with 6xFlag-tagged Duo1^{WT} grew almost indistinguishably from a wild type strain with untagged Duo1, demonstrating that the C-terminal tag does not interfere with the cellular function of Duo1 (Figure 20A). Strains with the Duo1$^{\Delta SxIP}$ or Duo1$^{\Delta C}$ allele displayed no growth defect at 30 °C or 37 °C. Furthermore, the two strains grew comparable to a wild

type strain in the presence of benomyl. Inactivation of the spindle assembly checkpoint by deletion of *Mad2* only mildly affected growth of the Duo1$^{\Delta SxIP}$ strain at 37 °C. These results demonstrate that the interaction between Dam1c and Bim1 is not essential for cell proliferation. Surprisingly, deletion of the Duo1 C-terminus did not affect growth even though this part of Duo1 was proposed to be one of the major microtubule-binding regions of Dam1c (Legal et al., 2016; Miranda et al., 2007; Westermann et al., 2005).

For a more detailed characterization of the Duo1$^{\Delta SxIP}$ strain, the DNA content of cells from logarithmically growing cultures was measured by FACS analysis. The Duo1^{WT} strain showed an equal distribution of cells with 1C, 2C and intermediate DNA content, which is characteristic of cells in G1, mitosis and S-phase, respectively (Figure 20B). In contrast, the culture of the Duo1$^{\Delta SxIP}$ strain was enriched in cells with 2C DNA content suggesting that cells require more time to finish mitosis. This effect was not apparent in the serial dilution assay (Figure 20A) in which growth is analyzed over two days.

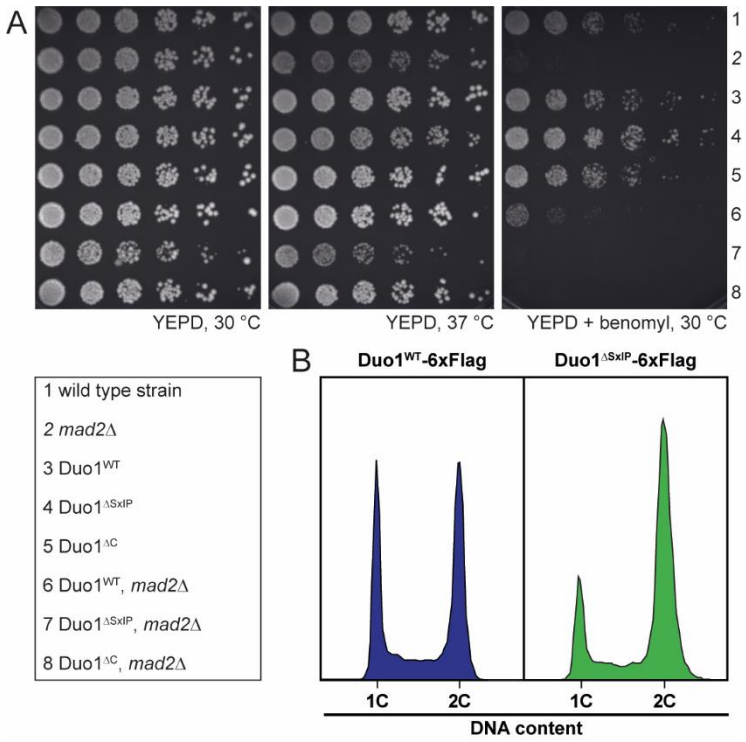

Figure 20: Growth analysis of yeast strains with different Duo1 alleles
A: 1:4 serial dilutions of yeast strains of the indicated genotype were spotted on YEPD or YEPD + benomyl and incubated at different temperatures.
B: FACS analysis of the DNA content of logarithmically growing Duo1^{WT} or Duo1$^{\Delta SxIP}$ cells. Cells with 1C and 2C DNA content are in G1 and mitosis, respectively. An intermediate DNA content is characteristic of S-phase cells.
FACS samples were processed and analyzed by Karolin Jänen (Department of Molecular Genetics I, University of Duisburg-Essen).

3.2.3. Binding of Bim1 to Dam1c is required for timely mitotic progression

The phenotype and effect of the Duo1$^{\Delta SxIP}$ allele was further analyzed by live cell microscopy. Dad1, a subunit of the Dam1 complex, was C-terminally fused to GFP to track the localization

of the complex by fluorescence microscopy. Tagging of Dad1 did not affect growth when cells were grown at 30 °C. However, growth was compromised at 37 °C, indicating that Dad1-GFP is a temperature-sensitive allele (Figure 21). This effect was even more pronounced in a strain additionally carrying the Duo1$^{\Delta SxIP}$ allele which grew very slowly at 37 °C. This result suggests that disruption of the Dam1c-Bim1 interaction is detrimental to cells under certain conditions.

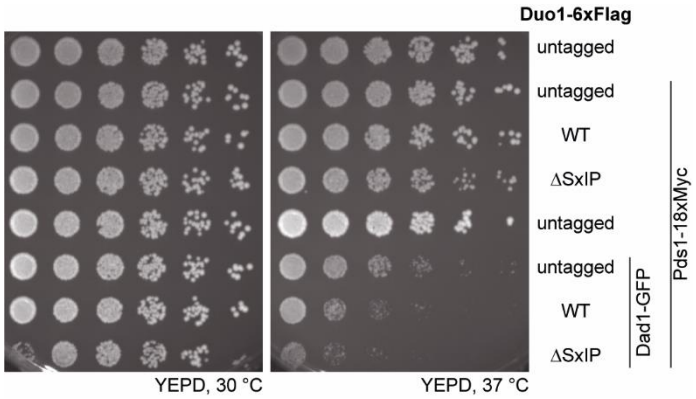

Figure 21. Serial dilution assays of different strains combining different Duo1 alleles with Dad1-GFP
Growth of strains with 6xFlag-tagged Duo1^{WT} or Duo1$^{\Delta SxIP}$ in combination with untagged or GFP-tagged Dad1-GFP was analyzed at 30 °C and 37 °C. Cells were spotted in a 1:4 serial dilution.

For live cell microscopy, cells were grown at 30 °C, a temperature at which no growth defect was observed. Cells from a log phase culture were immobilized in glass bottom dishes and live cell microscopy was performed as described in 2.3.8. Time lapse movies were acquired with a time resolution of one minute over 45 minutes total (Movie 1). Dad1-GFP signals appeared as a single dot in unbudded and as two dots in budded cells, representing the clustered kinetochores. In cells with rather small buds, the two Dad1-GFP signals were separated by less than 2 µm corresponding to a metaphase cell, while large budded cells frequently showed Dad1-GFP signals further apart, indicative of anaphase. Separation of Dad1-GFP clusters during anaphase was characterized by an initial rapid spindle elongation (anaphase A) followed by slower movement (anaphase B). Finally, the spindle disassembled and kinetochore clusters moved independently from each other. While Duo1^{WT} cells exhibited normal timing of Dad1-GFP cluster separation, Duo1$^{\Delta SxIP}$ cells were delayed in progression from metaphase to anaphase (Movie 1). A high percentage of large budded cells whose bud was almost equally sized as the mother cell (super large or XL budded) with short inter-kinetochore distance was present in the Duo1$^{\Delta SxIP}$ culture (Figure 22A). Time lapse microscopy showed that the kinetochore clusters tumbled within the cell with constant distance between the clusters for 45 minutes or even longer (Movie 1). Though most of these cells finally entered anaphase and finished mitosis, this observation clearly indicates delayed mitotic progression of the Duo1$^{\Delta SxIP}$ strain.

The mitotic delay of the Duo1$^{\Delta SxIP}$ strain observed by live cell microscopy was further assessed by analysis of cell cycle progression. Duo1^{WT} and Duo1$^{\Delta SxIP}$ strains with GFP-tagged Dad1 were synchronized in a G1-like state by exposure to α factor. Cells were released from the arrest and further cultivated at 37 °C. Accumulation and degradation kinetics of Pds1, the budding yeast Securin, was analyzed by western blot. Pds1 accumulates during S-phase and

mitosis and is degraded upon entry into anaphase (Cohen-Fix et al., 1996). Furthermore, cellular DNA content was measured by FACS analysis. Samples were taken every 15 minutes over 2 hours. Both Duo1^{WT} and Duo1$^{\Delta SxIP}$ displayed similar Pds1 accumulation kinetics, reaching its maximum about 45 minutes after release from α factor arrest (Figure 22B and C).

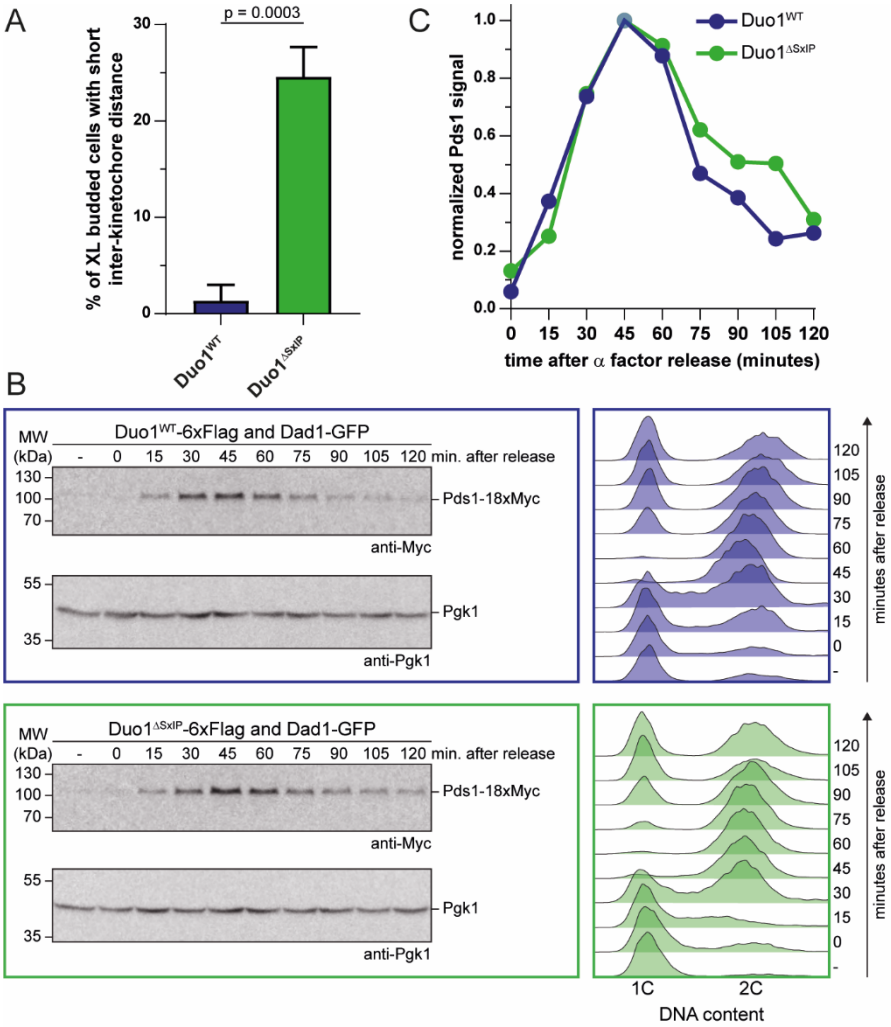

Figure 22: Analysis of cell cycle progression in Duo1^{WT} and Duo1$^{\Delta SxIP}$ strains
A: Quantification of extra large budded cells with short inter-kinetochore distances observed by live cell fluorescence microscopy. Mean ± standard deviation from three independent experiments is displayed. p-value was calculated with an unpaired t-test.
B: Western blot analysis of Pds1 accumulation and degradation kinetics and FACS analysis of DNA content after release from α factor arrest. Samples were collected every 15 minutes over 2 hours. Cells with a 1C and 2C DNA content are in G1 and mitosis, respectively, while cells with an intermediate DNA content are in S-phase.
C: Quantification of Pds1 signals in western blot shown in B. Background-corrected values were normalized to the 45 minutes sample of the respective strain.
FACS samples were processed and analyzed by Karolin Jänen (Department of Molecular Genetics I, University of Duisburg-Essen).

In wild type cells, Pds1 levels gradually decreased afterwards until almost no protein was detectable after 120 minutes. Though Duo1$^{\Delta SxIP}$ cells initiated Pds1 degradation simultaneously with the Duo1^{WT} strain, substantial amounts of Pds1 were still detectable 120 minutes after release from α factor. These observations were complemented by FACS

analysis of the cellular DNA content. Immediately before and after release from the arrest, the majority of cells had a 1C DNA content as expected for cells arrested in a G1-like state (Figure 22B). 45 minutes after release, cells of both Duo1^{WT} and Duo1$^{\Delta SxIP}$ strains had replicated their genome resulting in a 2C DNA content. In the wild type strain, the first cells with a 1C DNA content emerged after 75 minutes, indicating that these cells had finished mitosis. In contrast, this subpopulation was much smaller in the Duo1$^{\Delta SxIP}$ strain. Here, first cells had finished mitosis about 90 minutes after release. In conclusion, these data demonstrate that Duo1$^{\Delta SxIP}$ cells are delayed in cell cycle progression compared to wild type cells, presumably by prolonged metaphases.

3.2.4. Association with Bim1 is required for complete loading of Dam1c to metaphase kinetochores

The phenotype of the Duo1$^{\Delta SxIP}$ allele was further characterized by live cell fluorescence microscopy, now with emphasis on localization of Dam1c to kinetochore clusters. Again, localization of Dam1c was tracked by fusion of Dad1 to GFP. As described previously, metaphase cells are characterized by a short distance between the two Dad1-GFP clusters. The brightness of the Dad1-GFP signal appeared much weaker in Duo1$^{\Delta SxIP}$ cells compared to wild type cells (Movie 1, Figure 23A). Quantification of signal intensities of Dad1-GFP at metaphase kinetochore clusters indeed revealed a significant reduction of Dam1c in Duo1$^{\Delta SxIP}$ cells by about 20 % compared to wild type cells (Figure 23B). In contrast, signal intensities were undistinguishable in anaphase in both strain backgrounds. In the wild type strain, Dad1-GFP signals were comparable in metaphase and anaphase, suggesting constant amounts of the complex are loaded at metaphase and anaphase kinetochores. Noticeably, Duo1$^{\Delta SxIP}$ cells only showed reduced Dam1c at kinetochores in metaphase but not in anaphase, suggesting that loading of the complex to kinetochores is delayed in Duo1$^{\Delta SxIP}$ cells. However, cells might initiate anaphase when sufficient copies of Dam1c are loaded.

The reduced Dad1-GFP signal intensity was not a consequence of altered cellular Dad1-GFP amounts, since the overall protein levels were similar in both Duo1^{WT} and Duo1$^{\Delta SxIP}$ strains as determined by western blotting (Figure 23C).

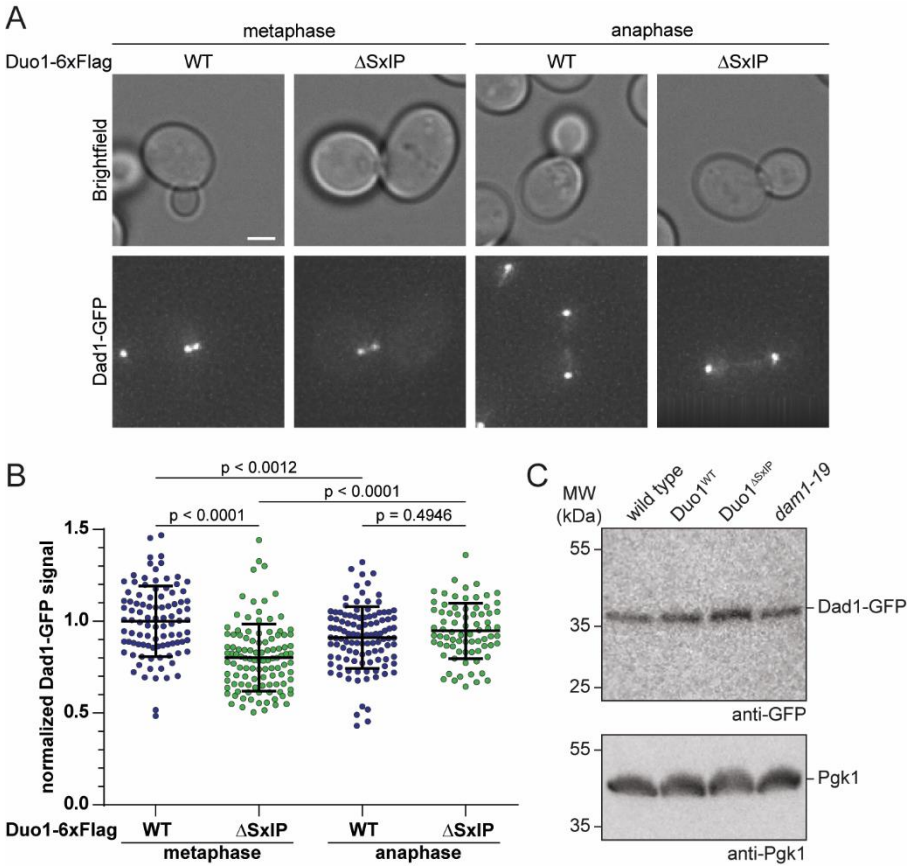

Figure 23 Live cell fluorescence microscopy of Duo1^{WT} and Duo1$^{\Delta SxIP}$ strains
A: Representative images of wild type and Duo1$^{\Delta SxIP}$ cells in metaphase and anaphase. Brightfield images are shown as reference for cell morphology. Dam1c was visualized by Dad1-GFP. Scale bar: 2 µm.
B: Quantification of Dad1-GFP signals at metaphase and anaphase kinetochore clusters in Duo1^{WT} and Duo1$^{\Delta SxIP}$ cells. Mean ± standard deviation is displayed. Each dot represents the value measured for an individual kinetochore cluster. p-values were calculated by a one-way ANOVA test with Sidak's multiple comparison test. n ≥ 76 kinetochore clusters were analyzed per condition.
C: Western blot analysis of different yeast strains expressing Dad1-GFP. Duo1^{WT} and Duo1$^{\Delta SxIP}$ had a C-terminal 6xFlag tag.

3.2.5. Deletion of Bim1 partially phenocopies the Duo1$^{\Delta SxIP}$ allele

An alternative way to prevent binding of Bim1 to Dam1c is deleting the Bim1 gene. A *bim1⊿* strain was viable, but displayed reduced growth at 37 °C. Notably, deletion of Bim1 is synthetically lethal in combination with Dad1-GFP when cells were grown at 37 °C (Figure 24). The effect is reminiscent of the Duo1$^{\Delta SxIP}$ allele which also impaired growth at 37 °C when combined with Dad1-GFP (Figure 21). The exacerbated phenotype of the Dad1-GFP *bim1*Δ strain presumably was a consequence of complete loss of Bim1 which serves various cellular functions.

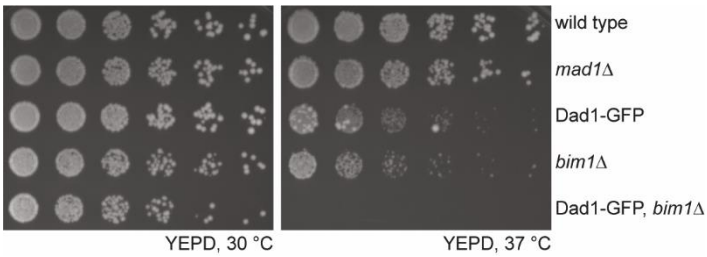

Figure 24: Growth analysis of Dad1-GFP and *bim1*Δ strains
Growth of yeast strains with the indicated genotypes was analyzed in a serial dilution assay. Cells were incubated at 30 °C or 37 °C.

Live cell microscopy of a Dad1-GFP *bim1*Δ strain at 30 °C showed that Dad1-GFP clusters were not properly separated from each other which made a quantification of signal intensities of individual kinetochore clusters impossible. However, similar to previous observations made in the Duo1$^{\Delta SxIP}$ strain, the Dad1-GFP signal tumbled within the cell for an extended period of time before cells eventually entered anaphase (Movie 2). This observation further supports the conclusion that binding of Bim1 to Dam1c is necessary for correct timing of mitotic progression.

3.3. Exploration of phosphorylation-based regulatory mechanisms of the Dam1c-Bim1 interaction

3.3.1. Truncation of the Dam1 C-terminus enables Bim1 binding under stringent binding conditions

The crosslinking data revealed spatial proximity of the Dam1 C-terminus to the Duo1 C-terminus and Bim1 (Figure 13). Even though the previous experiments showed that binding of Bim1 to Dam1c solely depends on the SxIP motif of Duo1, it is conceivable that the C-terminus of Dam1 participates in some way in this interaction. To test in how far Dam1's C-terminus contributes to Bim1 binding, a Dam1 complex with truncated C-terminal tail was purified. This complex is based on the temperature-sensitive *dam1-19* allele which encodes a truncated Dam1 protein due to a premature stop codon (Q205Stop). Binding of Bim1 to Dam1^{WT}c and Dam1-19c was tested by analytical SEC under high salt conditions (400 mM NaCl). Dam1^{WT}c bound Bim1 under these stringent conditions, however, to a lesser extent as seen in previous experiments under physiological salt concentrations. Here, the majority of Bim1 eluted independently from Dam1^{WT}c, indicating a reduction in binding (Figure 25A). In contrast, stoichiometric amounts of Bim1 coeluted with the Dam1-19 complex displaying robust binding under these conditions (Figure 25B). This result suggests that removal of the Dam1 C-terminus promotes binding of Bim1 to Dam1c. Furthermore, reduced binding to the wild type complex under high salt concentrations shows that the interaction is mainly mediated by electrostatic interactions.

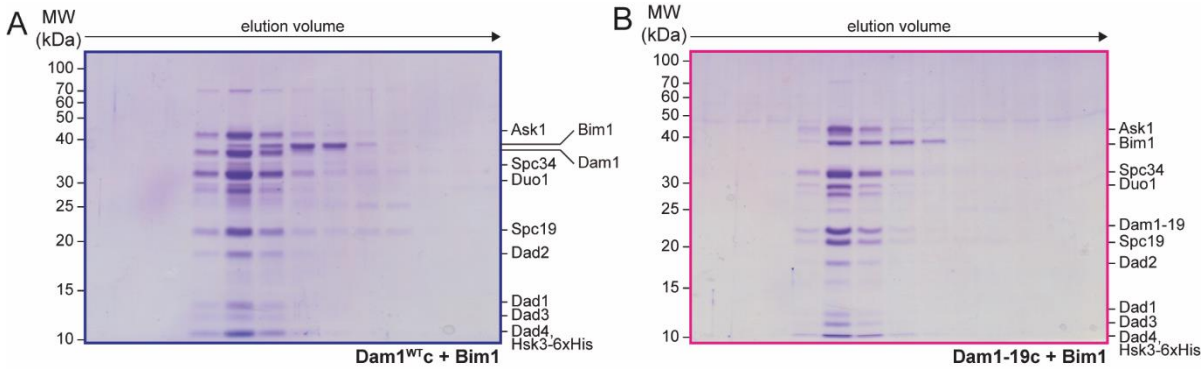

Figure 25: Comparison of Bim1 binding to Dam1^{WT}c and Dam1-19c
Binding of Bim1 to Dam1^{WT}c (A) and Dam1-19c (B) was probed by analytical SEC under stringent binding conditions (400 mM NaCl). Elution fractions were analyzed by SDS-PAGE.

3.3.2. Excessive Bim1 binding increases Dam1c at kinetochore clusters

To examine whether truncation of the Dam1 C-terminus affects Dam1c localization *in vivo*, Dam1^{WT} and *dam1-19* strains with GFP-tagged Dad1 were imaged by live cell fluorescence microscopy. In *dam1-19* cells, Dad1-GFP signals appeared as two separated clusters in budded cells and localization was indistinguishable from wild type cells both in metaphase and anaphase (Figure 26A). Dad1-GFP signal intensities at metaphase and anaphase kinetochore clusters were quantified as described before. Noticeably, localization of Dam1c to metaphase kinetochores was significantly increased by 20 % in *dam1-19* cells compared to Dam1^{WT} cells (Figure 26B). In anaphase, Dad1-GFP signals were reduced in *dam1-19* cells compared to metaphase. However, the value was still increased relative to anaphase signals in wild type cells. Increased kinetochore localization of *dam1-19* is not a consequence of altered protein levels since equal amounts of Dad1-GFP were present in Dam1^{WT} and *dam1-19* strains (Figure 23C).

The results of these experiments show that increased Bim1 binding promotes excessive accumulation of Dam1c at kinetochore clusters. This is in striking contrast du the Duo1$^{\Delta SxIP}$ allele which is reduced in kinetochore localization during metaphase. Considering the fact that the *dam1-19* allele causes slow growth over a broad range of temperatures (Cheeseman et al., 2001b), accumulation of increased levels of Dam1c at kinetochores might be detrimental for the function of the complex.

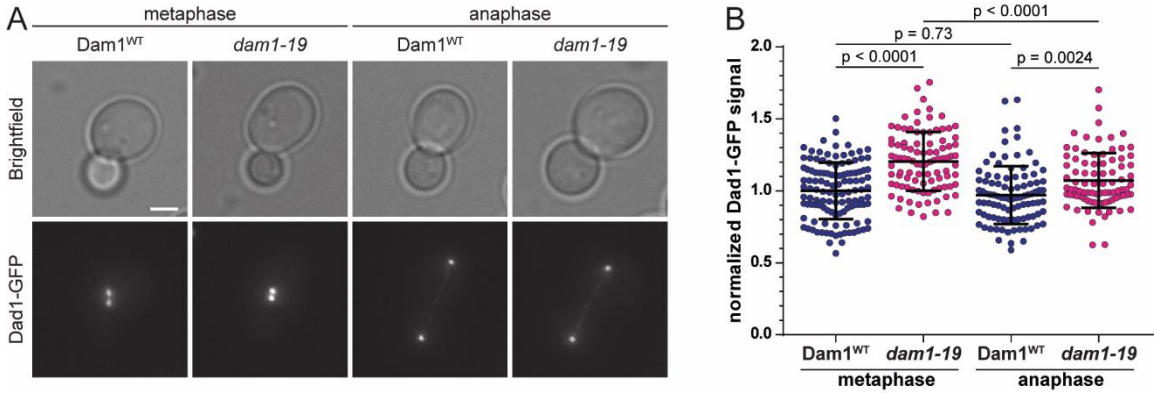

Figure 26: Live cell microscopy of *dam1-19* yeast cells
A: Live cell microscopy of Dam1^{WT} and *dam1-19* strains. Dad1 was C-terminally fused for visualization of Dam1c. Representative images show cells in metaphase and anaphase. Scale bar: 2 µm.
B: Quantification of Dad1-GFP signals at kinetochore clusters in metaphase and anaphase. Mean ± standard deviation is plotted. p-values were calculated by a one-way ANOVA with Sidak's test for multiple comparisons. n ≥ 86 kinetochore clusters were analyzed for each condition.

3.3.3. The Dam1 C-terminus is a potential regulatory hub for protein-protein interactions

Closer inspection of the Dam1 C-terminus, which is deleted in the *dam1-19* allele, uncovered functionally important features of this region. The Dam1 C-terminus was identified as crucial microtubule-binding element of Dam1c and appears to contribute to the domain that connects the Dam1c ring with the microtubule surface (Legal et al., 2016; Miranda et al., 2007; Wang et al., 2007; Westermann et al., 2005). Furthermore, this region of Dam1 is phosphorylated at

multiple residues by Ipl1/Aurora B and Mps1 (Figure 27A) which was previously described to modulate function of Dam1c (Lampert et al., 2010; Sarangapani et al., 2013; Tien et al., 2010; Wang et al., 2007).

The following model is proposed based on the results of this and other studies. The C-terminus of Dam1 is in spatial proximity to the SxIP motif within the C-terminus of Duo1 as shown by crosslinking mass spectrometry data (Figure 13). By this, Dam1 is able to partially mask the SxIP motif and block binding by Bim1 (Figure 27B). Removal of the C-terminus, either by truncation (*dam1-19* allele) or by phosphorylation, might relieve this intramolecular inhibition which finally unmasks the SxIP motif and allows unrestricted Bim1 binding. This model is tested in the next set of experiments.

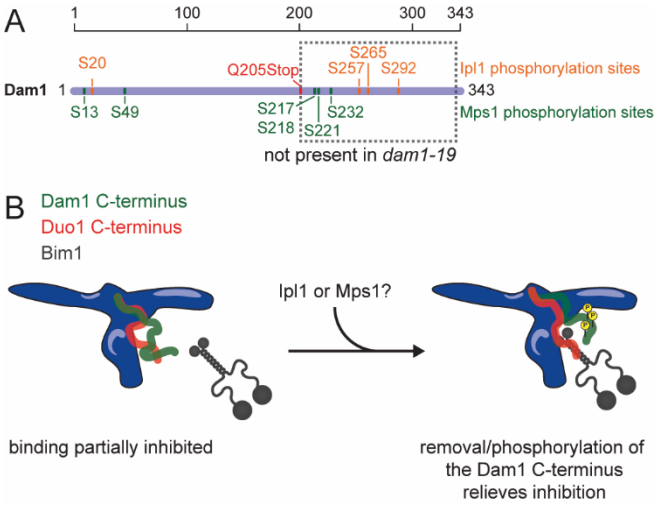

Figure 27: Model for phosphorylation-regulated Bim1 binding to Dam1c
A: Schematic of Dam1 with annotated Ipl1 and Mps1 phosphorylation sited. The C-terminal region deleted by the *dam1-19* Q205Stop mutation is framed by the grey dashed box.
B: The Dam1 C-terminus partially masks the Duo1 SxIP motif of Duo1. Removal of the C-terminus by truncation or phosphorylation-induced conformational change relieves the intramolecular inhibition and allows Bim1 binding.

3.3.4. Inhibition of Mps1, but not Ipl1 weakens the Dam1c-Bim1 interaction

To test whether Mps1 or Ipl1 kinase activity are involved in regulating the interaction between Dam1c and Bim1, a yeast strain with the temperature-sensitive *ipl1-2* and the analog-sensitive *mps1-as1* allele was constructed. In this strain, Ipl1 is inactive at the restrictive temperature of 37 °C and Mps1 can be selectively inhibited by the ATP analog 1NM-PP1 (Jones et al., 2005). Inhibition of each kinase resulted in lethality as demonstrated in a serial dilution assay (Figure 28A).

For preparation of soluble cell extracts, yeast cells were initially grown at 30 °C in the absence of 1NM-PP1. Afterwards, Ipl1 (37 °C, no 1NM-PP1), Mps1 (30 °C, with 1NM-PP1) or both kinases (37 °C, with 1NM-PP1) were inhibited. To demonstrate that both kinases are fully functional under permissive conditions, the same strain was also grown at 30 °C in the absence of 1NM-PP1. Furthermore, a strain with wild type alleles of both kinases was used in this experiment. Soluble cell lysates were prepared from the yeast strains grown under the mentioned conditions and used in a pull down assay. GST-Bim1$^{185-344}$ was immobilized on glutathione sepharose beads, incubated with the soluble cell extracts and binding of Dam1c to Bim1 was probed by western blot analysis of the input and pull down samples. Duo1 from a strain with both wild type kinases robustly bound to GST-Bim1$^{185-344}$ but not to GST, excluding any unspecific binding to the beads (Figure 28B). Dam1c from the *ipl1-2*, *mps1-as1* strain

bound GST-Bim1$^{185-344}$ to a comparable extend when cells were grown at 30 °C in the absence of 1NM-PP1. However, inhibition of Mps1 strongly reduced binding of Dam1c to Bim1, while reduction in Ipl1 kinase activity only mildly reduced binding to Bim1. Growing the cells at 37 °C in the presence of 1NM-PP1 and thus inhibiting both kinases reduced binding similarly to Mps1 inhibition alone. This experiment suggests that Mps1 rather than Ipl1 kinase activity positively regulates the interaction between Dam1c and Bim1.

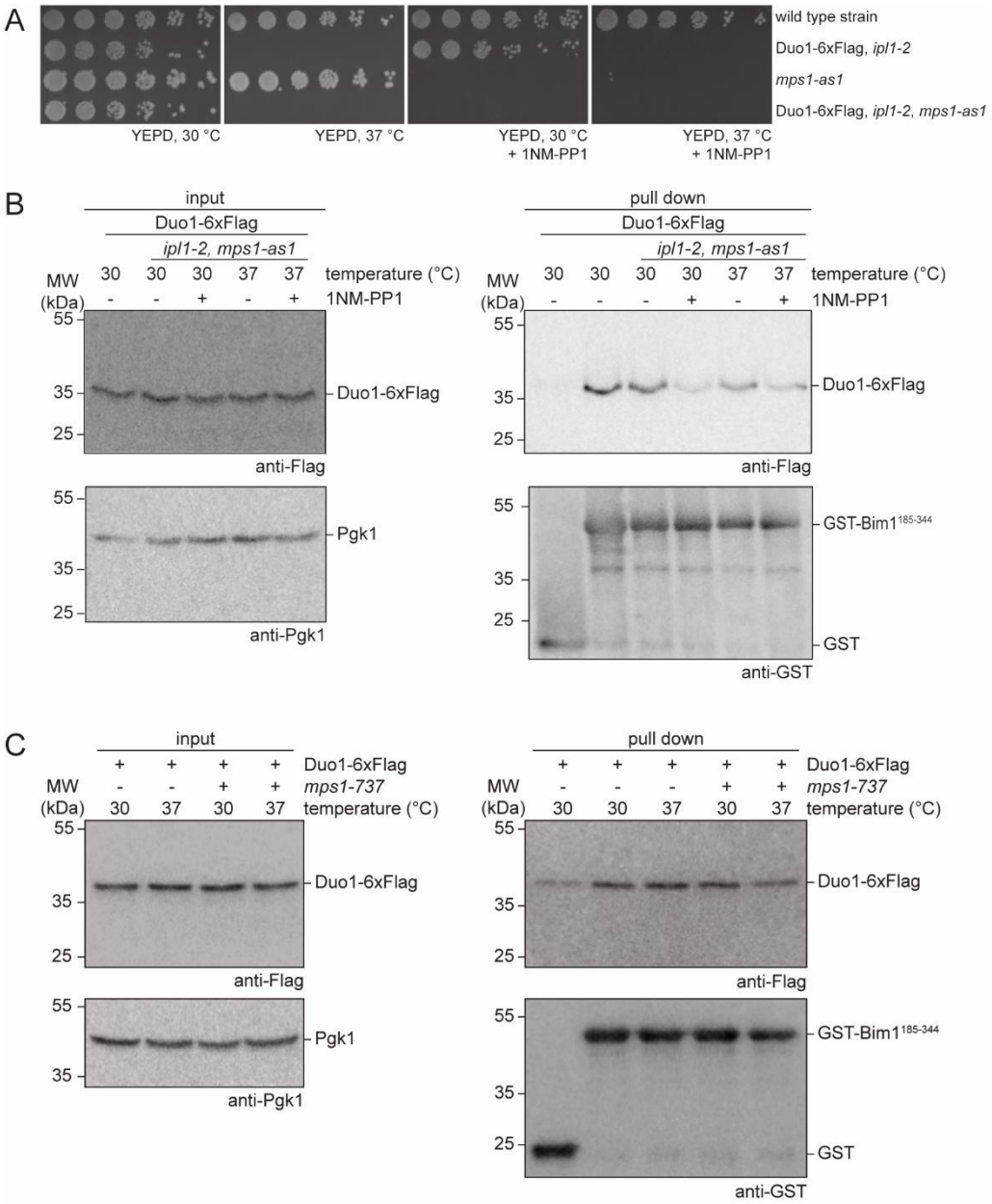

Figure 28: Mps1 kinase activity is required for efficient Bim1 binding by Dam1c
A: Serial dilution assay of various yeast strains with conditional Ipl1 and Mps1 alleles. Ipl1 and kinase activity is compromised when cells were grown at 37 °C (*ipl1-2*) or in the presence of the ATP analog 1NM-PP1 (*mps1-as1*).
B, C: Pull down assays to analyze binding of 6xFlag-tagged Duo1 to immobilized GST-Bim1$^{185-344}$. Yeast cell with the *ipl1-2* and *mps1-as1* alleles (B) were grown under conditions that inhibit either one or both kinases. In C, yeast strains with wild type Mps1 or *mps1-737* were used. Soluble cell lysates were prepared and binding of Duo1 to Bim1 was tested. Input and pull down samples were analyzed by western blot.

To further confirm the role of Mps1 as regulatory kinase for this interaction, the same experiment was repeated using the temperature-sensitive *mps1-737* allele. Similar to *ipl1-2*, kinase activity is compromised when cells were grown at 37 °C. In a pull down assay, Dam1c from an Mps1^{WT} strain robustly bound to immobilized GST-Bim1$^{185-344}$ irrespective of the temperature at which the cells were grown (Figure 28C). In contrast, Dam1c from the *mps1-737* strain showed diminished binding to GST-Bim1$^{185-344}$ after growth at 37 °C, but unaffected binding when grown at 30 °C. In this experiment, the effect of Mps1 inhibition appeared to be somewhat weaker compared to Figure 28B, presumably due to different degrees of stringency of the *mps1-as1* and *mps1-737* alleles under their respective restrictive conditions.

3.3.5. Inhibition of Mps1 by the small molecule cincreasin reduces Dam1c at kinetochores

If the C-terminus of Dam1 has an inhibitory function on Bim1 binding by partially masking the SxIP motif of Duo1 (Figure 27B), one can speculate that preventing phosphorylation of the Dam1 C-terminus by Mps1 would impair Bim1 binding and thus reduce Dam1c at kinetochore clusters as seen for the Duo1$^{\Delta SxIP}$ allele. To test this hypothesis, localization of Dam1c to metaphase kinetochore clusters was quantitatively analyzed by live cell fluorescence microscopy. Yeast strains either carried the Dam1^{WT} or Dam1^{4A} (S217A, S218A, S221A, S232A) allele in which four putative Mps1 phosphorylation sites were mutated to alanine to prevent their phosphorylation by Mps1. Again, Dad1 was fused to GFP to analyze Dam1c localization and spindle pole bodies (SPB) were labelled by Spc42-mCherry. Quantification of Dad1-GFP signals at metaphase kinetochore clusters showed no difference

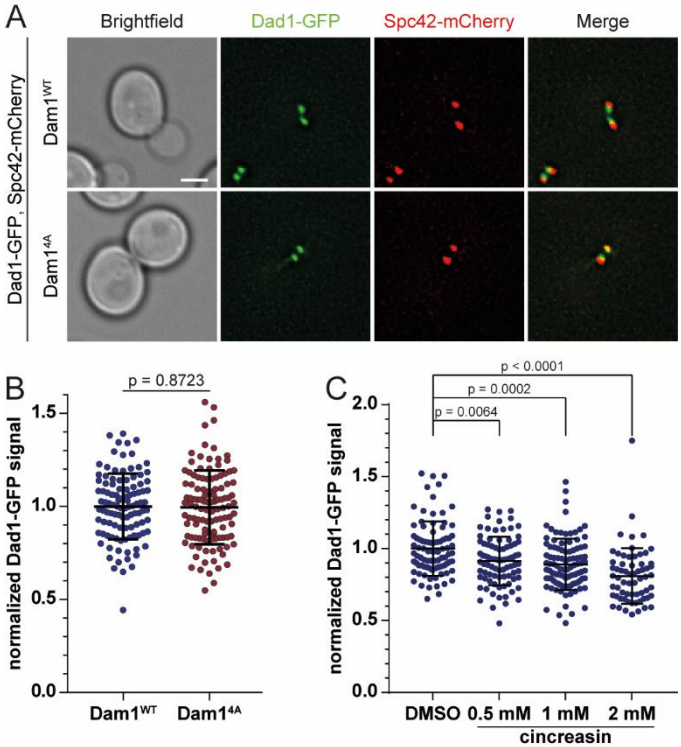

Figure 29: Inhibition of Mps1 affects kinetochore localization of Dam1c
A: Representative images of Dam1^{WT} and Dam1^{4A} metaphase cells expressing Dad1-GFP. Spindle pole bodies were labelled by Spc42-mCherry. Scale bar: 2 µm.
B: Quantification of Dad1-GFP signal intensities at metaphase kinetochore clusters of cells expressing Dam1^{WT} or Dam1^{4A}. Mean ± standard deviation is shown. An unpaired t-test was used to calculate the p-value. n ≥ 106 kinetochore clusters.
C: Quantification of Dad1-GFP signals at metaphase clusters after inhibition of Mps1 by cincreasin. Mean ± standard deviation is plotted. p-values were calculated by a one-way ANOVA with Dunnett correction for multiple comparisons. n ≥ 64 kinetochore clusters.

between Dam1^{WT} and Dam1^{4A} cells, suggesting that preventing phosphorylation of these residues by Mps1 is not sufficient to affect kinetochore loading of Dam1c. However, additional phosphorylation sites might be functionally relevant. For instance, Mps1 also phosphorylates Dam1 S13 and S49 which were excluded from this experiment. Furthermore, it cannot be excluded that Mps1 also phosphorylates other subunits than Dam1 which might be relevant in this context.

A more general analysis of the effect of Mps1 on Dam1c loading to kinetochores requires specific inhibition of the kinase. However, this is technically challenging in the context of live cell microscopy since Mps1 kinase activity is essential for SPB duplication (Winey et al., 1991). Thus, inhibition of Mps1 leads to formation of monopolar spindles which makes analysis of separated metaphase kinetochore clusters impossible. The small molecule cincreasin was described to selectively inhibit Mps1 function at the kinetochore without interfering with SPB duplication (Dorer et al., 2005). Cells were treated with 0.5, 1 or 2 mM cincreasin or DMSO as control for 2.5 h and analyzed by live cell fluorescence microscopy. To increase cellular concentrations of cincreasin, the Pdr5 gene, which encodes a multidrug transporter, was deleted. Separated spindle pole bodies, visualized by Spc42-mCherry, were considered as proof for formation of a bipolar spindle. Quantification of Dad1-GFP signal intensities at metaphase clusters showed that recruitment of Dam1c was mildly reduced in a dose-dependent manner compared to the DMSO control (Figure 29C). This data suggests that Mps1 kinase activity is indeed required for complete loading of Dam1c to kinetochores, presumably by promoting the interaction with Bim1. The effect of the treatment with relatively high doses of cincreasin appears to be rather weak, which might be owed to the experimental setup. Here, logarithmically growing cells were treated with the inhibitor, thus affecting cells during different stages of the cell cycle. However, Mps1 kinase activity is not required after establishing of kinetochore biorientation (Maure et al., 2007). Therefore, an unknown proportion of analyzed cells might be unaffected by cincreasin treatment, which dampens the observed effect.

In previous studies, cells were arrested after SPB duplication but before formation of a bipolar spindle using the temperature-sensitive *cdc34-2* allele (Jones et al., 2005; Maure et al., 2007). Cdc34 is a ubiquitin-conjugating enzyme involved in the regulation of the transition from G1- to S-phase. Inactivation of Cdc34 arrest cells with duplicated but unseparated SPBs (Goebl et al., 1988; Winey and Bloom, 2012). Inhibition of Mps1 immediately after release from the *cdc34-2* arrest allows to specifically investigate the function of Mps1 during formation of kinetochore-microtubule attachments. Unfortunately, it was not possible to reproduce this experimental setup so far, since *cdc34-2* cells arrested with a short bipolar spindle at the restrictive temperature. Thus, alternative experimental setups need to be developed in order to explore the role of Mps1 in kinetochore loading of Dam1c in more detail.

3.3.6. Overexpression of Mps1 promotes the interaction between Dam1c and Bim1 and affects kinetochore localization of Dam1c

The previous experiments showed that specific inhibition of Mps1 negatively affects Dam1c binding to Bim1 and kinetochore localization of the complex. In a complementary approach it was tested how overexpression of Mps1 and thus increased phosphorylation of its substrates changes Bim1 binding by Dam1c and kinetochore localization of the complex. For this purpose, yeast strains with an additional copy of the Mps1 gene under control of the inducible Gal promoter (pGal-Mps1) at the URA3 locus were constructed. The additional Mps1 gene also encoded for an N-terminal 1xMyc tag which allows detection of the overexpressed kinase by western blotting. In the presence of glucose, expression of the gene under control of the Gal promoter is repressed, while expression is induced in presence of galactose and absence of glucose.

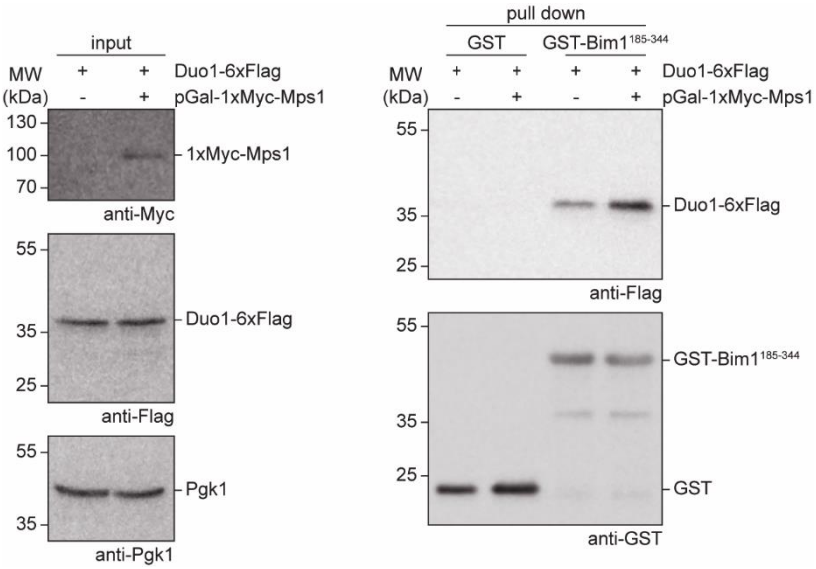

Figure 30: Bim1 binding of Dam1c is promoted by Mps1 overexpression
Binding of Duo1 to immobilized GST-Bim1$^{185-344}$ was tested in a pull down assay with soluble cell extracts from yeast strains with Mps1^{WT} or overexpressing Mps1 (pGal-Mps1). Input and pull down samples were analyzed by western blot. Dam1c bound to GST-Bim1$^{185-344}$ was detected by Duo1-6xFlag.

Binding of Dam1c to Bim1 after Mps1 overexpression was tested in a pull down assay. Mps1^{WT} and pGal-Mps1 cells were grown in medium with raffinose (YEPR) at 30 °C for 2 hours, then galactose was added to induce expression of Mps1 from the Gal promoter and cells were further cultivated for four hours. Soluble cell lysates were prepared and binding of Duo1-6xFlag to immobilized recombinant GST-Bim1$^{185-344}$ was analyzed by western blot analysis of input and pull down samples. As described before, Dam1c from the Mps1^{WT} strain robustly bound immobilized GST-Bim1$^{185-344}$ shown by the presence of Duo1 in pull down samples (Figure 30). Notably, the amount of Dam1c bound to Bim1 was strongly increased compared to the non-overexpression strain, suggesting that increased phosphorylation of Mps1 substrates indeed

promotes the interaction between Dam1c and Bim1.

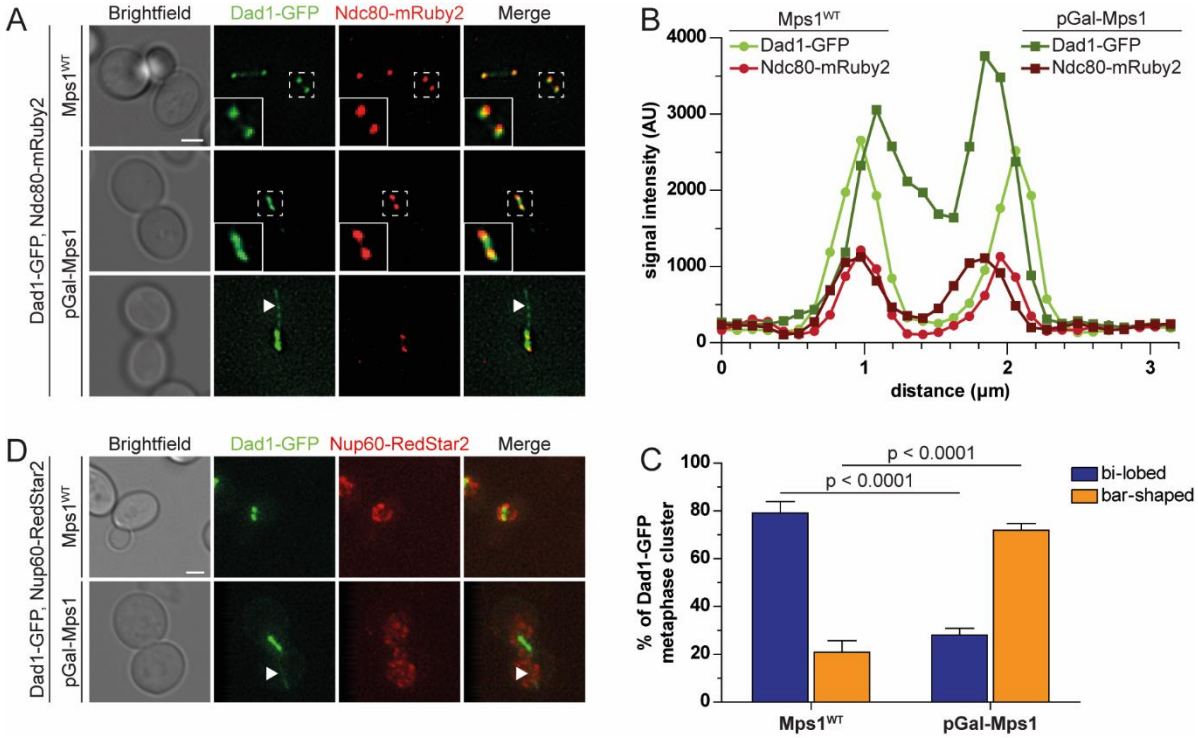

Figure 31: Dad1-GFP localization is affected by Mps1 overexpression
A: Representative images of Mps1^{WT} (top) and pGal-Mps1 (middle and bottom) metaphase cells expressing Dad1-GFP and Ndc80-mRuby2. Areas marked by white dashed boxes are shown as magnified inserts. The white arrowhead points on a random nuclear microtubule. Please note that brightness and contrast of the images in the bottom row were adjusted to make the highlighted structure clearly visible. Scale bar: 2 µm.
B: Line scans across metaphase kinetochore clusters of cells shown in A (marked by white dashed boxes). Signal intensities of Dad1-GFP and Ndc80-mRuby2 are plotted.
C: Quantification of Dad1-GFP cluster shape distinguishing between bi-lobed and bar-shaped forms. Mean ± standard deviation from three independent experiments is plotted. p-values were calculated by a two-way ANOVA with Sidak's test for multiple comparisons.
D: Representative images of Mps1^{WT} (top) and pGal-Mps1 (bottom) metaphase cells. Cells expressed Dad1-GFP and Nup60-RedStar2 to label the nuclear envelope. A random nuclear microtubule is labelled by the white arrowhead. Scale bar: 2 µm.

Next, it was investigated in how far overexpression of Mps1 impacts localization of Dam1c. In an Mps1^{WT} or pGal-Mps1 strain background, localization of Dam1c was visualized by Dad1-GFP and Ndc80 was C-terminally fused to mRuby2 (Ndc80-mRuby2) as a reference point for localization of kinetochores. In Mps1^{WT} metaphase cells, kinetochore clusters were clearly separated as shown by both Dad1-GFP and Ndc80-mRuby2 signals (Figure 31A, upper panel). As expected, cells overexpressing Mps1 arrested in metaphase due to constitutive activation of the spindle assembly checkpoint even in the absence of unattached kinetochores (Hardwick et al., 1996). Under Mps1 overexpression, Ndc80-mRuby2 clusters appeared as two separated clusters as seen in Mps1^{WT} strains (Figure 31A, middle and lower panel). In contrast, Dad1-GFP in Mps1 overexpressing cells frequently appeared as bar-shaped signal (Figure 31A, middle and lower panel). Line scans of Ndc80-mRuby2 and Dad1-GFP signals across the metaphase kinetochore clusters showed a clear separation of both signals in

Mps1^{WT} cells (Figure 31B). In pGal-Mps1 cells, distribution of Ndc80-mRuby2 was unaffected, but Dad1-GFP displayed increased accumulation between the two kinetochore clusters. Bar-shaped Dad1-GFP signals were found in about 72 % of Mps1-overexpressing cells, but only in 21 % of Mps1^{WT} cells (Figure 31C). In addition to the altered appearance of Dad1-GFP signals, elongated structures emanating from the kinetochore clusters and decorated by Dad1-GFP, but not Ndc80-mRuby2, were present in cells overexpressing Mps1 (Figure 31A, lower panel, and D). Staining of the nuclear envelope by Nup60-RedStar2 confirmed that these structures were located within the nucleus. Since Dam1c also localizes to microtubules, these structures presumably represent random nuclear microtubules.

Altered Dad1-GFP distribution under Mps1 overexpression might rather be a consequence of prolonged metaphase arrest than a specific effect of Dam1c phosphorylation by the kinase. This possibility was tested by arresting cells in metaphase by depletion of Cdc20. AID-tagged Cdc20 was rapidly degraded after addition of the auxin analog NAA in a strain expressing the ubiquitin ligase OsTIR (Figure 32A; Nishimura et al., 2009). Again, metaphase arrested cells displayed both bi-lobed and bar-shaped kinetochore clusters (Figure 32B). However, the majority of arrested cells still had clearly separated and bi-lobed Dad1-GFP signals (Figure 32C), contrasting the results of Mps1 overexpression. Thus, overexpression of Mps1 and concomitant phosphorylation of its substrates rather than a general metaphase arrest affects localization of Dad1-GFP.

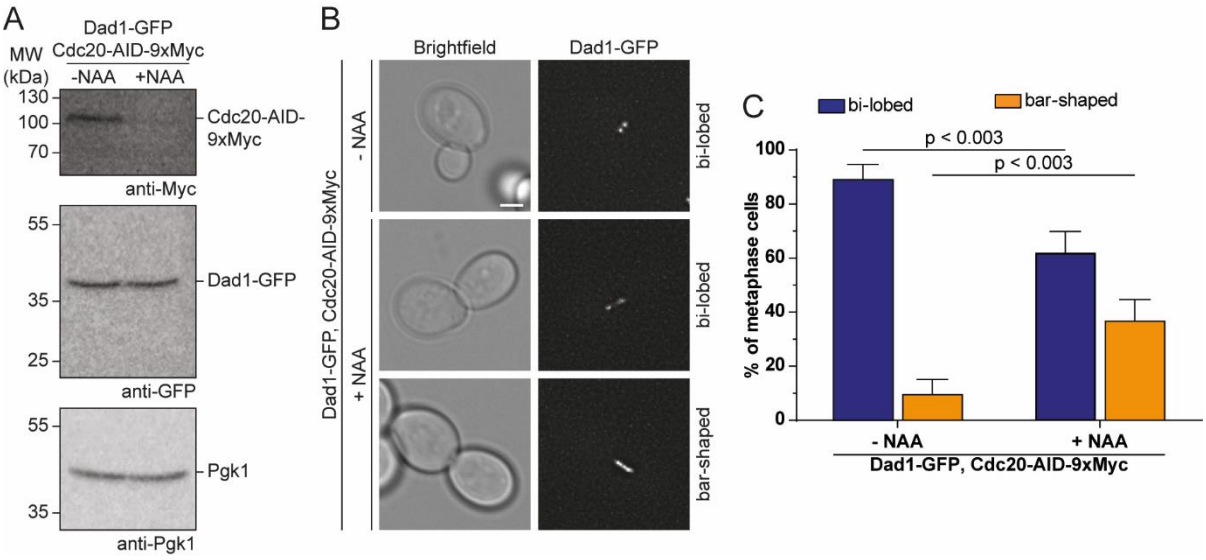

Figure 32: A metaphase arrest by Cdc20 depletion mildly affects Dad1-GFP localization
A: Western blot showing specific degradation of AID-tagged Cdc20 upon addition of the auxin analog NAA without affecting Dad1-GFP.
B: Representative images from live cell microscopy of metaphase cells from a log phase culture (top) or by Cdc20 depletion arrested culture (middle and bottom). Dad1-GFP appeared in two different configurations. Scale bar: 2 µm.
C: Quantification of bi-lobed and bar-shaped Dad1-GFP cluster shapes. Mean ± standard deviation from three independent experiments is shown. p-values were calculated by a two-way ANOVA with Sidak's test for multiple comparisons.

3.3.7. Mps1 phosphorylates several subunits of Dam1c and Bim1 *in vitro*

The *in vivo* data described so far give an insight into the regulation of Dam1c localization and binding to Bim1 in a cellular context. However, side effects of constitutive Mps1 kinase activity such as phosphorylation of further kinetochore components or altered localization and activity of other kinases and phosphatases might contribute to the observed effects. Biochemical assays using recombinant proteins were employed to further analyze the role of Mps1-dependent phosphorylation of Dam1c in a well-defined system.

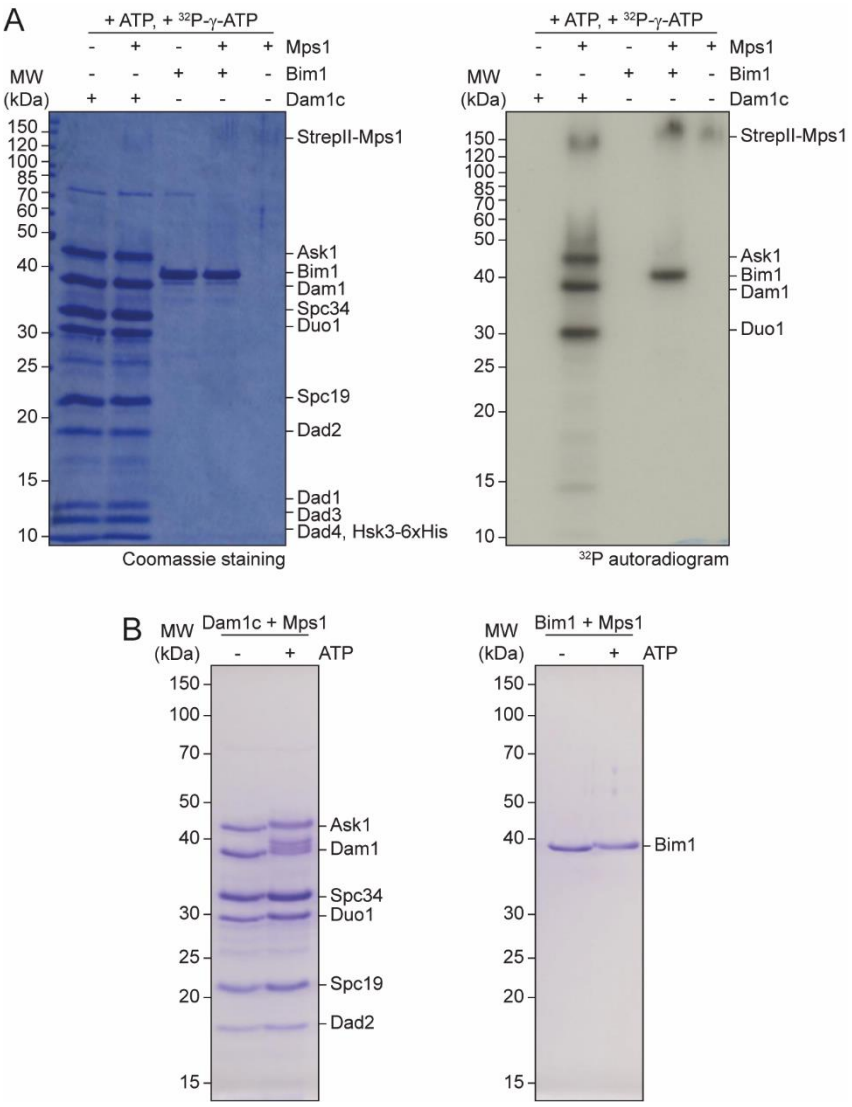

Figure 33: Mps1 phosphorylates multiple subunits of Dam1c and Bim1 *in vitro*
A: Dam1c and Bim1 were subjected to *in vitro* phosphorylation by Mps1. Samples were analyzed by SDS-PAGE (left) and incorporation of ^{32}P was detected by autoradiography (right). No phosphorylation occurred in samples lacking Mps1.
B: Dam1c and Bim1 were phosphorylated under more permissive conditions (500 µM ATP, 2 h incubation). Samples were analyzed by SDS-PAGE. Phosphorylation was indicated by appearance of slower migrating forms of Ask1, Dam1, Duo1 and Bim1 compared to samples lacking ATP.

Phosphorylation of both Dam1c and Bim1 was first tested in an *in vitro* kinase assay. Dam1c and Bim1 were incubated with ATP and recombinant budding yeast Mps1 purified from Sf9 insect cells. In addition, samples contained radioactively labelled ^{32}P-γ-ATP. During

phosphorylation, the γ-phosphate group of ATP carrying ^{32}P was transferred to substrate proteins enabling detection of phosphorylation by autoradiography. Samples lacking Mps1 served as negative controls. A previous study showed that Mps1 phosphorylates Dam1. However, only GST-Dam1 was used as substrate in these assays omitting the other subunits of the complex (Shimogawa et al., 2006). In contrast, the assay used here allows analysis of Mps1 phosphorylation in context of the entire complex. Autoradiography of samples after SDS-PAGE confirmed phosphorylation of Dam1, as described before. In addition, the Dam1c subunits Ask1 and Duo1, as well as Bim1, were phosphorylated in an Mps1-dependent manner (Figure 33A). As described before, Mps1 also exhibited autophosphorylation (Kemmler et al., 2009). Increasing the ATP concentration and extending the incubation time of the kinase reactions allowed to follow phosphorylation by SDS-PAGE without the use of radioactively labelled ATP. Phosphorylation of the proteins is indicated by slower migration during SDS-PAGE as shown in Figure 33B. This was especially apparent for Dam1 which showed at least two distinct bands, presumably reflecting different degrees of phosphorylation.

These data demonstrate that not only the Dam1 subunit but also Ask1, Duo1 and Bim1 are substrates of Mps1. Mapping of the so far unknown phosphorylation sites by mass spectrometry will crucially contribute to dissect the physiological function of Dam1c and Bim1 phosphorylation by Mps1 *in vivo*.

3.3.8. Phosphorylation by Mps1 inhibits Dam1c oligomerization

The effect of Dam1c phosphorylation by Mps1 was analyzed by size exclusion chromatography. Prior to SEC, Dam1c was phosphorylated by Mps1 in the presence of 500 µM ATP and samples were incubated at 30 °C for 2 hours. As control for unphosphorylated Dam1c, a reaction mix lacking ATP was prepared and treated in the same way. Unphosphorylated Dam1c showed a similar behavior in SEC as seen in previous experiments and eluted with a single peak. In contrast, phosphorylated Dam1c eluted later than the unphosphorylated complex as seen in the chromatograms of the SEC runs (Figure 34A). SDS-PAGE analysis of the elution fractions confirmed the shifted elution position of the phosphorylated complex. In addition, the chromatogram of the SEC run of unphosphorylated Dam1c showed a small peak between 0.9 and 1.0 ml. Even though no protein was detectable by SDS-PAGE followed by Coomassie staining, this peak presumably contains small amounts of highly oligomeric Dam1c. Strikingly, this peak was absent in the sample of Mps1-phosphorylated Dam1c (Figure 34). These results indicate that Mps1 negatively regulates Dam1c oligomerization in solution by phosphorylating several subunits of the complex.

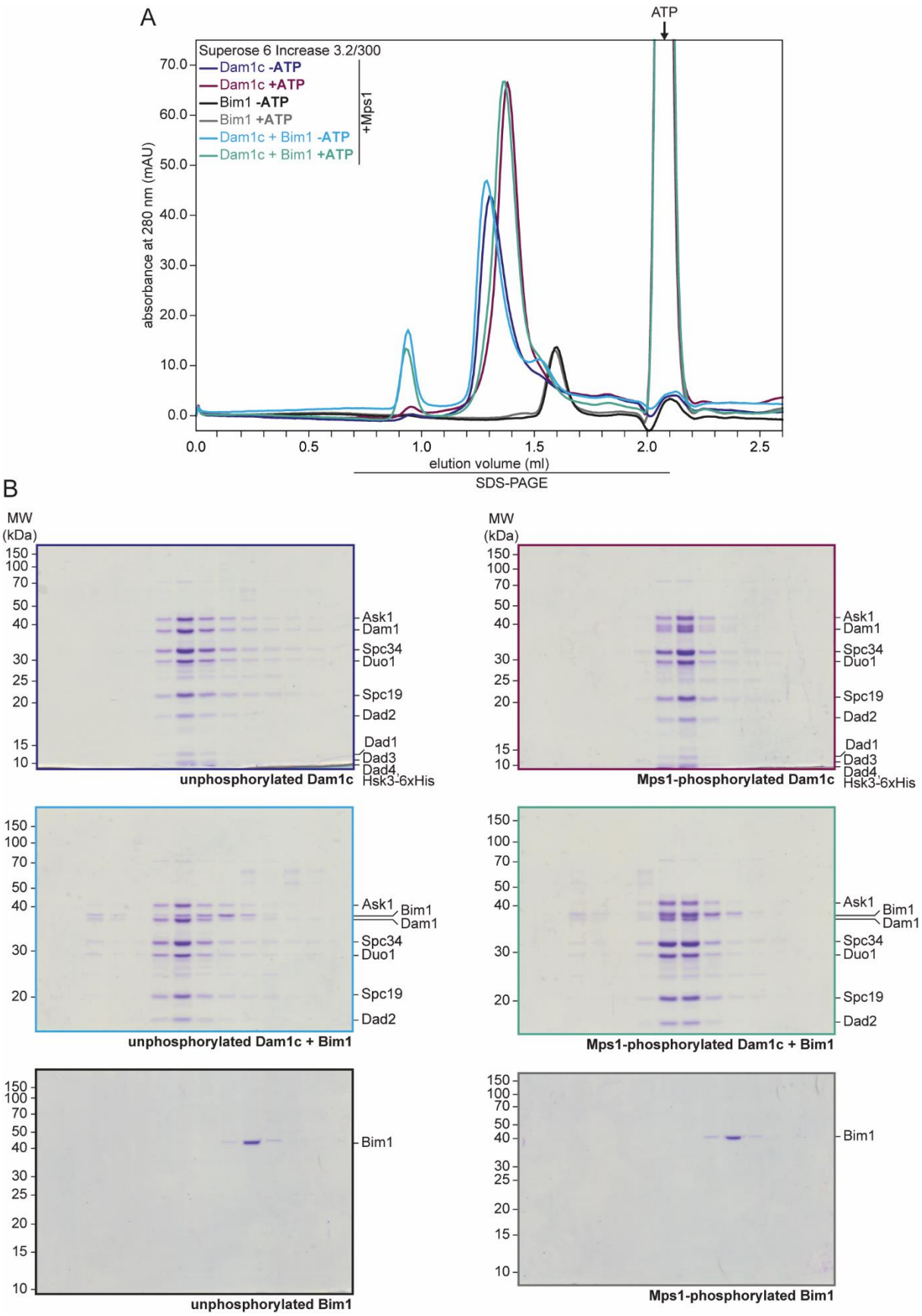

Figure 34 Legend on next page.

Figure 34: Phosphorylation by Mps1 regulates both Dam1c oligomerization and Bim1 binding
A: Chromatogram of analytical SEC runs. Dam1c and Bim1 individually or in combination were phosphorylated by Mps1 and subsequently analyzed by SEC. To show that the observed effects are specific to phosphorylation, the samples were also prepared lacking ATP under otherwise identical conditions. The SEC running buffer contained 400 mM NaCl. The peak after about 2.1 ml was caused by residual ATP.
B: Elution fractions from SEC runs shown in A were analyzed by SDS-PAGE followed by Coomassie staining. Please not that gels of samples combining Dam1c and Bim1 were run longer for better separation of phosphorylated Dam1 and Bim1. However, this led to loss of small Dam1c subunits from the gel.

3.3.9. Mps1-dependent phosphorylation promotes the interaction between Dam1c and Bim1

As described in the previous section, Dam1c oligomerization appeared to be compromised after phosphorylation by Mps1. As a next step, the impact of this phosphorylation on Bim1 binding was analyzed in more detail. Bim1 is an Mps1 substrate as well, but in contrast to Dam1c, phosphorylation did not affect the elution position of Bim1 in analytic SEC (Figure 34). In a previous experiment, the NaCl concentration in the SEC running buffer was increased to 400 mM in order to reveal differences between Dam1^{WT}c and Dam1-19c with respect to Bim1 binding (Figure 25). As seen before, the majority of Bim1 was eluted independently from unphosphorylated Dam1c and only a small fraction coeluted with the complex. Thus, Bim1 binding by unphosphorylated Dam1c was severely compromised by the elevated salt concentration (Figure 34). In contrast, the elution profile of phosphorylated Dam1c was slightly shifted to an earlier elution volume in the presence of Bim1 and almost stoichiometric amounts of Bim1 coeluted with phosphorylated Dam1c (Figure 34) resembling the effect observed for Bim1 binding to Dam1-19c (Figure 25). This data confirms the previous results that Mps1 kinase activity promotes binding between Dam1c and Bim1. The *in vitro* data additionally demonstrate that Mps1 directly promotes this interaction without requirement for additional proteins.

3.4. Analysis of Dam1c binding to further microtubule-associated proteins

In addition to Bim1, various other proteins localize to dynamic microtubule tips and are thus in spatial proximity to Dam1c. Thus, it is conceivable that further microtubule-associated proteins (MAPs) also interact with Dam1c and make crucial contributions to its function at the kinetochore. For instance, genetic and two-hybrid interactions between Dam1c and the MAPs Stu2 (Kalantzaki et al., 2015; Wong et al., 2007) and Bik1 (Cheeseman et al., 2001a) are described in literature. In the following sections, the potential interactions between Dam1c and these two MAPs will be characterized in detail by a combination of biochemical, structural and genetic analyses.

3.4.1. Stu2 does not bind to the Dam1 complex

Stu2, the budding yeast homolog of human chTOG, was suggested to physically interact with Dam1c based on yeast two-hybrid screens (Kalantzaki et al., 2015; Wong et al., 2007). However, biochemical data investigating this interaction are missing so far.

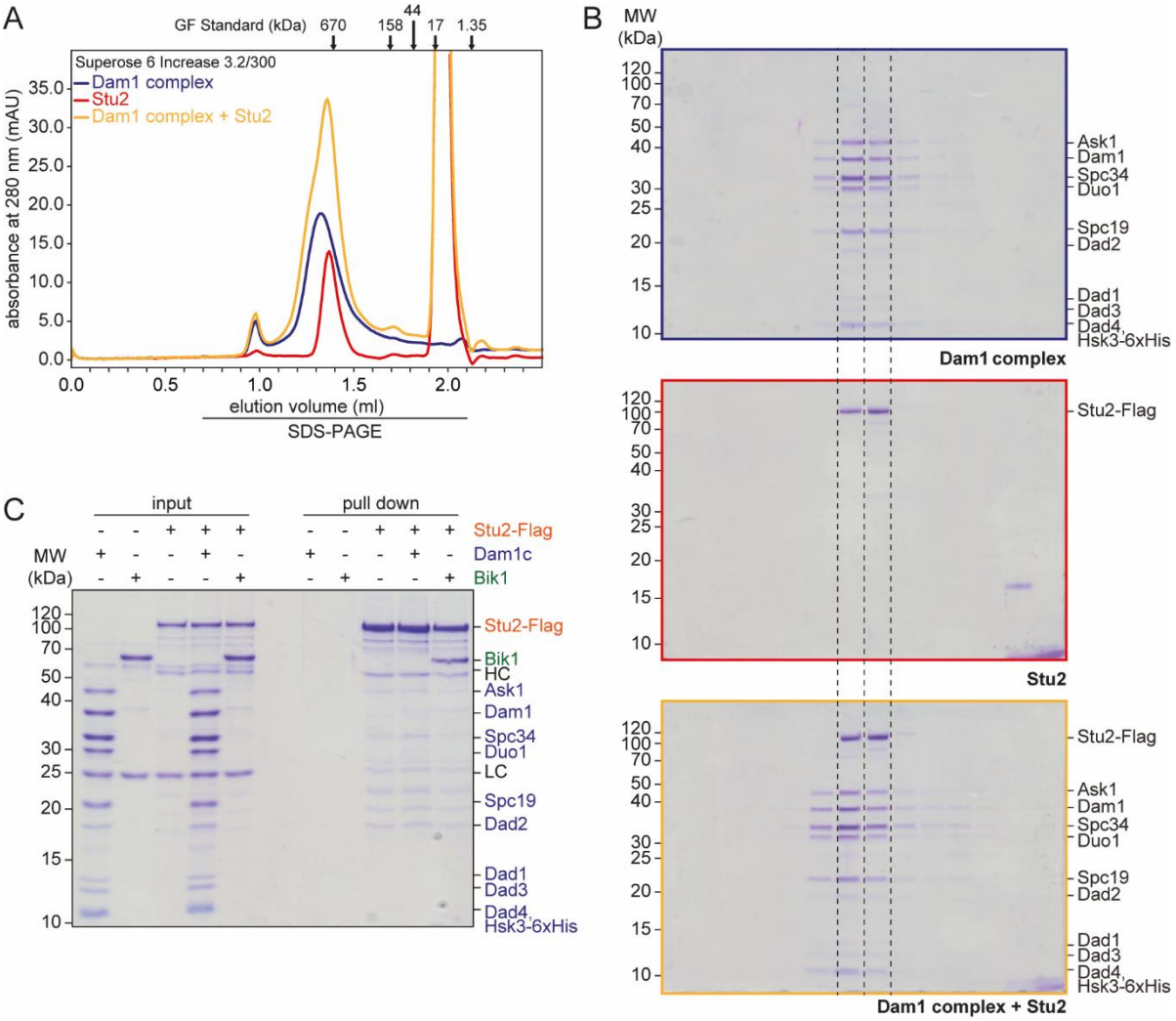

Figure 35: Dam1c does not bind Stu2
A, B: Chromatograms (A) and SDS-PAGE analysis and Coomassie staining of elution fractions (B) from analytical SEC of Dam1c and Stu2 alone or in combination.
C: Pull down assay analyzing binding of Dam1c and Bik1 to Stu2. Stu2-Flag was immobilized on anti-Flag M2 agarose beads and incubated with buffer, Dam1c or Bik1. Bik1 served as control that Stu2 indeed binds a known interacting protein under these experimental conditions. HC and LC denote the heavy and light chains of the anti-Flag antibody. Subunits of Dam1c are labelled in blue, Stu2-Flag in orange and Bik1 in green.

Stu2-Flag was purified from Sf9 insect cells and binding to Dam1c was tested by analytical SEC. Stu2 eluted only slightly later than Dam1c during SEC (Figure 35A and B). Combining Dam1c and Stu2 did not result in a shift of the peak in the chromatogram, but instead the curve exhibited an asymmetric shape (Figure 35A). SDS-PAGE analysis of the elution fractions showed no shift of the Dam1c elution position, implying that Stu2 does not bind Dam1c (Figure 35B). To further confirm this result, a pull down assay with immobilized Stu2-Flag was performed. Dam1c and Bik1 as positive control were added to Stu2. While Bik1 bound to Stu2,

showing that Stu2 is functional under these experimental conditions, Dam1c did not (Figure 35C). These results demonstrate that Bim1, but not Stu2, is a specific binding partner for Dam1c at microtubule plus ends.

3.4.2. Bik1 weakly binds Dam1c, but is recruited to Dam1c by Bim1

Another potential interaction partner for Dam1c is Bik1, the yeast homolog of CLIP-170. 6x-His-tagged Bik1 was purified from *E. coli*. As described before, Bik1 robustly bound Bim1 in solution as shown by size exclusion chromatography (Figure 36A and B), demonstrating functionality of the protein. Next, binding of Bik1 to Dam1c was tested. Bik1 eluted slightly later during analytical SEC than Dam1c, but both elution profiles were still clearly separated (Figure 36A). Analysis of a sample containing both Dam1c and Bik1 showed only small amounts of Bik1 coeluting with Dam1c. The elution profile in the chromatogram showed two separated peaks resembling the curves of the samples with the two individual components. However, an additional peak that was characterized by a steep slope and high absorbance at 280 nm was detected after an elution volume of about 1 ml. The respective elution fractions were analyzed by SDS-PAGE followed by Coomassie staining. In addition, samples containing Bik1 were also probed by western blot to detect even small amounts of Bik1 that were not visible in Coomassie staining. The bulk of Bik1 eluted independently from Dam1c with little if any protein associated with Dam1c as shown by analysis of the elution fractions (Figure 36B). However, Coomassie staining revealed small amounts of Dam1c eluting after about 1 ml, matching the position of the early peak seen in the chromatogram. Notably, the corresponding fraction also contained some Bik1 as seen by western blot: Bik1 was not eluted at this position when analyzed by SEC in the absence of Dam1c. These data suggest that Bik1 weakly associates with Dam1c. Furthermore, presence of Bik1 induces early elution of Dam1c from SEC the column, indicative of formation of larger assemblies of the complex.

Bim1 interacts with both Dam1c and Bik1 employing two different mechanisms. Binding to Dam1c requires the interaction between the EBH domain and Dam1c's SxIP motif, as shown in this study, while the C-terminal ETF sequence binds to the CAP-Gly domain of Bik1 (Blake-Hodek et al., 2010; Weisbrich et al., 2007). Based on this, it was tested whether Bim1 is able to bind Dam1c and Bik1 simultaneously and thus to recruit Bik1 to Dam1c. A mixture of Dam1c, Bim1 and Bik1 was subjected to analytic SEC. Two well-separated and distinct peaks appeared in the chromatogram. Again, the first peak appeared after an elution volume of 1.0 ml and was characterized by a steep slope and high absorbance at 280 nm (> 50 mAU). The second peak was found after 1.2 – 1.3 ml and was thus slightly shifted compared to Dam1c alone. In contrast to the sample lacking Bim1, no additional peak at the elution position of Bik1 was detected. Analysis of the corresponding elution fractions clearly revealed that the early eluting fractions indeed contained Dam1c, Bim1 and Bik1, indicating the formation of a ternary complex. Furthermore, all three components were also found in the elution fractions

corresponding to the second elution peak, which further confirms formation of a Dam1c-Bim1-Bik1 complex. These experiments show that Bik1 itself only weakly associates with Dam1c but can be recruited by Bim1 which simultaneously binds both Dam1c and Bik1. Notably, presence of Bik1 dramatically changed the elution position of Dam1c leading to early elution of a small fraction of the complex close to the void volume of the column. This can be either considered as unspecific aggregation of proteins or formation of large oligomeric structures that cannot be separated by the used SEC column. The Dam1c-Bim1-Bik1 complex was further analyzed in the following experiments.

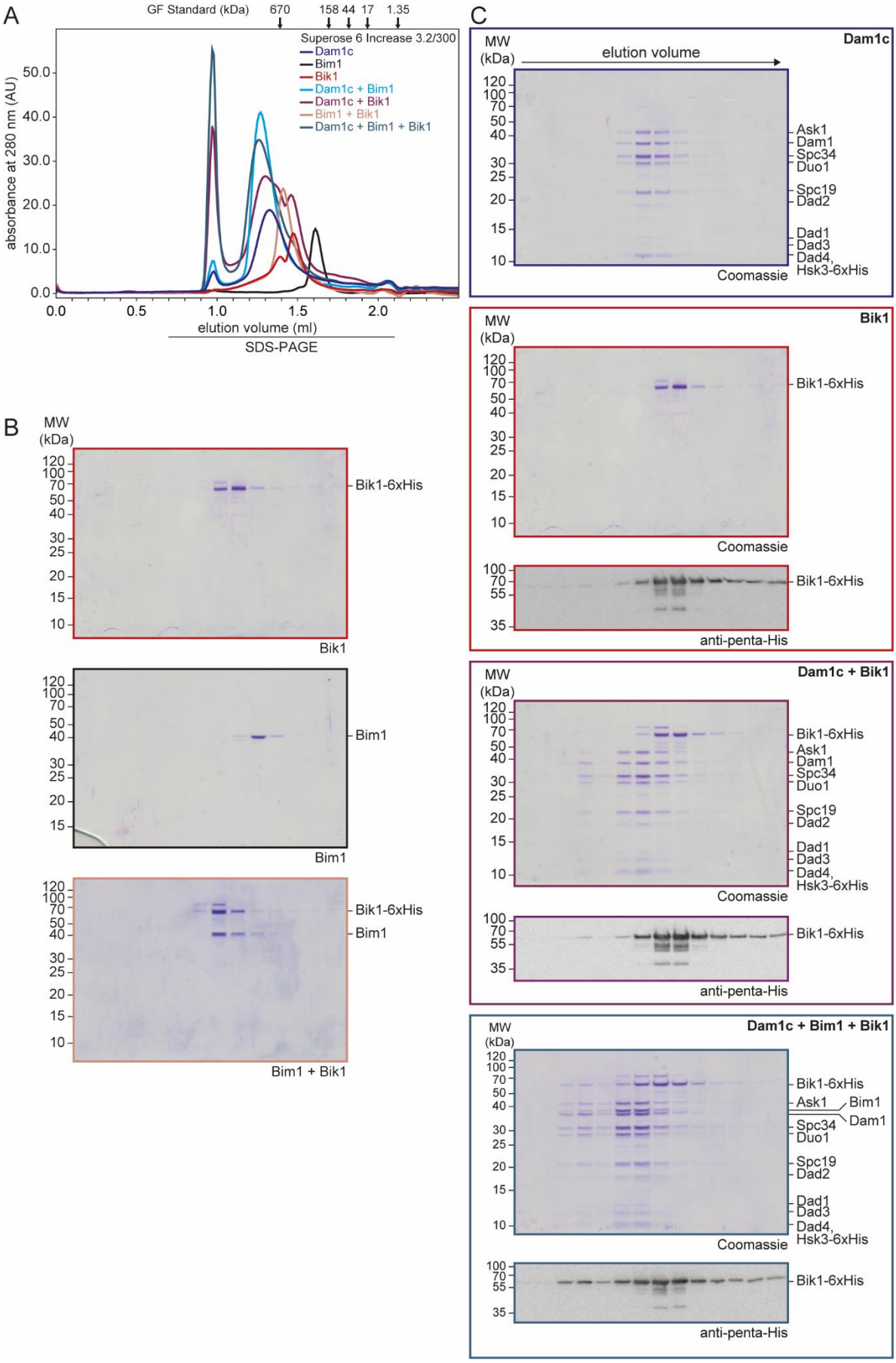

Figure 36 Legend on next page

Figure 36: Bik1 binds to Dam1c in a Bim1-dependent manner
Binding between Dam1c, Bim1 and Bik1 was tested by analytic SEC. Chromatograms are shown in A. Elution fractions were analyzed by SDS-PAGE and, if appropriate, by western blot to detect small amounts of Bik1 which were not visible in Coomassie staining. Gels of SEC runs analyzing the interaction between Bim1 and Bik1 are shown in B. SDS-PAGE and western blot analysis of runs with Dam1c, Bim1 and Bik1 are displayed in C. For the Dam1c-Bim1 sample, only the chromatogram but not analysis of elution fractions is shown. Please note that the SDS-PAGE analysis of Bik1 elution fractions (red box) is used twice in this figure.

3.4.3. Binding of Bim1-Bik1 triggers oligomerization of Dam1c

Oligomerization and ring formation of Dam1c is critical for functionality of the complex. Thus, the formation of large protein species consisting of Dam1c, Bim1 and Bik1, which elute early during SEC, might represent an important step of Dam1c ring assembly. In the following set of experiments, formation of large Dam1c assemblies was analyzed by systematically varying Dam1c concentrations and by addition of Bim1-Bik1.

Dam1c at input concentrations of 5 µM, 7.5 µM and 10 µM was analyzed by SEC. Chromatograms and SDS-PAGE analyses of elution fractions are shown in Figure 37A and B. The elution volume of Dam1c depended on the input concentration of the complex. An increase in input concentration resulted in earlier elution from the column (Figure 37A). For all three concentrations tested here, the elution profiles peaked between 1.2 and 1.3 ml. SDS-PAGE analysis of the elution fractions confirmed the shift in Dam1c elution position (Figure 37B). In this context, earlier elution of the complex can be considered as formation of larger protein assemblies. Thus, this experiment showed that Dam1c oligomerization in solution depends on the input concentration of the complex with high concentrations slightly shifting the equilibrium to higher oligomeric states such as trimers or tetramers.

Next, it was tested in how far binding of Bim1 and Bik1 to Dam1c supports formation of early eluting complex species. Again, Dam1c was used at input concentrations of 5 µM, 7.5 µM and 10 µM together with correspondingly adjusted concentrations of Bim1 and Bik1 (Figure 37A and C). Under all tested concentrations, Bim1 and Bik1 displayed robust binding to Dam1c. At the lowest tested concentration, the bulk of the complex was eluted slightly earlier than Dam1c alone due to binding of Bim1 and Bik1 and the concomitant increase in molecular weight. In addition, small amounts of the complex were eluted between 0.9 and 1.0 ml, as seen in the previous experiment, which were barely detectable by Coomassie staining of the elution fractions. Increasing the Dam1c concentration to 7.5 µM and 10 µM resulted in even earlier elution of the complex and the signal of the first peak (0.9 to 1.0 ml) rose above 100 mAU (Figure 37A). The shift of the elution position was even more apparent after SDS-PAGE analysis of the elution fractions. At 10 µM Dam1c, a large fraction of the complex was shifted toward an earlier elution volume, suggesting increased formation of large protein assemblies (Figure 37C). It is noteworthy that the first peak reached an absorbance at 280 nm of more than 100 mAU, even though the corresponding elution fractions contained relatively little protein as judged by SDS-PAGE. This effect might be caused by a change of the extinction

coefficient of the higher oligomeric complex compared to smaller oligomers.

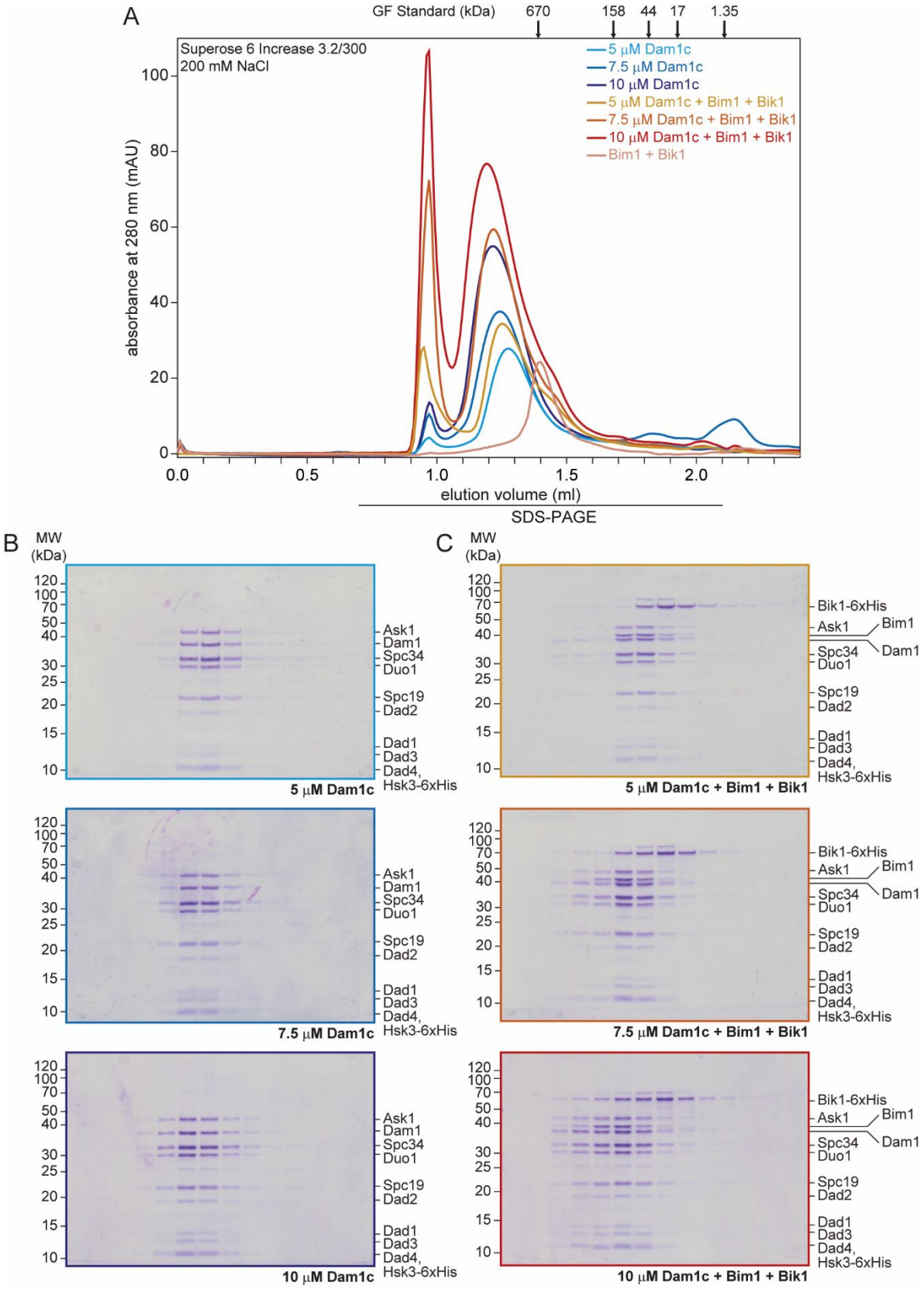

Figure **37** Legend on next page

Figure 37: Assembly of large Dam1c oligomers is induced by high protein concentrations and binding of Bim1-Bik1
Dam1c at input concentrations of 5 µM, 7.5 µM and 10 µM was subjected to analytical SEC either in the absence or presence of corresponding amounts of Bim1 and Bik1. Chromatograms are shown in A. The chromatogram of a sample analyzing Bim1 and Bik1 is shown, but not the corresponding SDS-PAGE analysis. SDS-PAGE analyses of elution fractions of Dam1c alone or in combination with Bim1 and Bik1 are shown in B and C. The SEC buffer contained 200 mM NaCl.

This experiment demonstrates that oligomerization of Dam1c in solution is regulated by at least two different factors. First, increasing concentrations of Dam1c favor assembly of the complex. Second, simultaneous binding of Bim1 and Bik1 to Dam1c support its oligomerization. Notably, both factors act in a concerted manner and appear to enhance each other.

3.4.4. Binding of Bim1 and Bik1 does not enhance oligomerization of a Dam1 complex mimicking Ipl1 phosphorylation

Early elution of Dam1c in combination with Bim1 and Bik1 might have two different reasons. First, Bim1 and Bik1 specifically trigger Dam1c oligomerization as seen in the presence of microtubules. Second, binding of the two proteins induces unspecific aggregation of the complex. If the first option is true, one would not expect to observe formation of large Dam1c assemblies when repeating the previous experiment with a Dam1 complex that is deficient in forming oligomers. Phosphorylation of Dam1 by Ipl1 was previously shown to suppress oligomerization of the complex (Wang et al., 2007). To test if Dam1c's intrinsic ability to oligomerize is required for the Bim1-Bik1-induced effect seen in previous experiments, Dam1^{4D}c which mimics Ipl1-dependent phosphorylation of Dam1 at four sites was analyzed by SEC in the absence and presence of Bim1 and Bik1.

Dam1^{4D}c alone was eluted later than the wild type complex as judged by position of the peaks of the chromatogram (Figure 38A). Bim1 was able to bind and recruit Bik1 to the Dam1^{4D}c indicated by a shift of the elution position and coelution of Bim1 and Bik1 with the Dam1^{4D} complex. Notably, no additional peak between 0.9 and 1.0 ml was observed for Dam1^{4D}c in the presence of Bim1 and Bik1 and no protein was detectable in the corresponding elution fractions (Figure 38B). The absence of early eluting Dam1c-Bim1-Bik1 complex in this experiment suggests that binding of Bim1 and Bik1 indeed induces specific oligomerization of Dam1c in solution. Furthermore, binding of Bim1 to Dam1c is not affected by mimicking phosphorylation of Dam1 by Ipl1. The finding that phosphorylation of Dam1 by Ipl1 prevents Bim1-Bik1-induced oligomerization of Dam1c but still allows binding of these proteins might play an important role during error correction. The oligomerization-suppressing effect of Ipl1 appears to override the effect of Bim1-Bik1 binding, thus preventing oligomerization as long as Ipl1 activity at the kinetochore is high. However, binding of Bim1-Bik1 keeps Dam1c in a primed state and can rapidly trigger Dam1c oligomerization as soon as Ipl1 activity decreases.

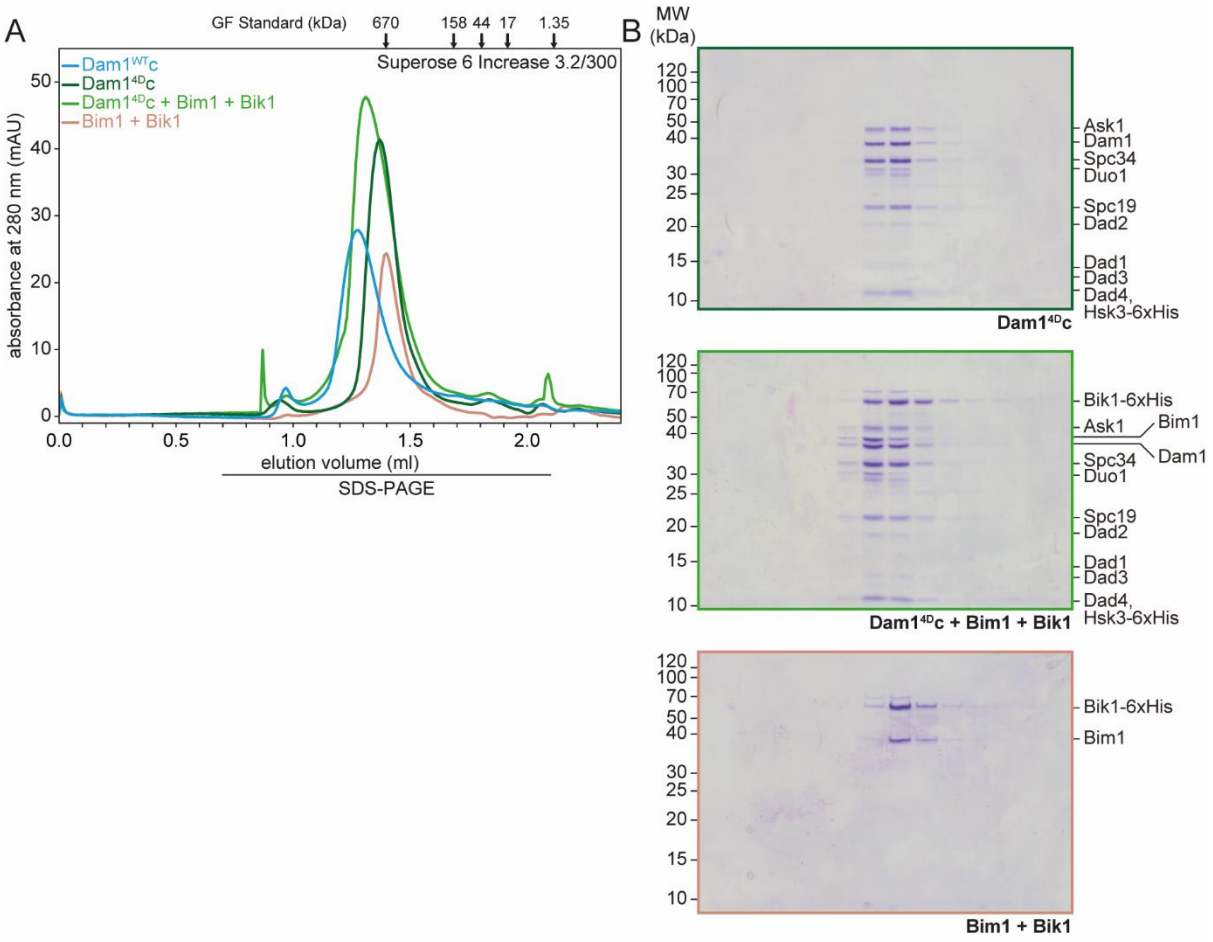

Figure 38: Bim1 and Bik1 cannot induce oligomerization of the Dam1^{4D} complex
Dam1^{4D} complex mimicking Ipl1-dependent phosphorylation of Dam1 was analyzed was SEC in the absence and presence of Bim1 and Bik1. Chromatograms of individual runs are shown in A and SDS-PAGE analyses of elution fractions in B. The chromatogram of a run of Dam1^{WT}c is displayed in A to demonstrate differences in retention volume between the two Dam1 complexes.

3.4.5. Binding of Bim1 and Bik1 induces Dam1c ring formation in solution

Both Dam1c concentration and binding of Bim1-Bik1 to Dam1c affect the formation of larger Dam1c assemblies. In addition, previous experiments showed that binding of Bim1 to Dam1c is sensitive to increased salt concentrations in the interaction buffer (Figure 25 and Figure 34). Thus, it was tested whether low salt concentrations additionally support Dam1c assembly and protect it against dissociation. To do so, 7.5 µM Dam1c was subjected to analytical SEC in the presence of Bim1 and Bik1 using an interaction buffer containing 100 mM NaCl compared to 200 mM in previous experiments (Figure 37). Under these conditions, the bulk majority of the Dam1c-Bim1-Bik1 complex eluted after 0.9 – 1.0 ml indicated by a sharply sloping peak that reaches a value of more than 300 mAU. Only small amounts were left at the original elution position of the complex at 1.3 – 1.4 ml (Figure 38). SDS-PAGE of the elution fractions confirmed that the complex was predominantly found in the early eluting fractions. This shows that the equilibrium between low and high oligomeric species can be modulated by the salt concentration of the interaction buffer.

For detailed characterization of the high oligomeric Dam1c, the complex consisting of Dam1c,

Bim1 and Bik1 was analyzed by electron microscopy after negative staining. Dam1c, Bim1 and Bik1 were diluted into buffer with only 10 mM NaCl to prevent disassembly of the complex. EM analysis of this sample revealed the presence of different Dam1c species displaying various degrees of oligomerization (Figure 39B). Most notably, some particles resembled completely assembled Dam1c rings while others presumably represented partially assembled rings with defined curvature. Purification of the samples by SEC allowed for separation of small oligomers from larger ones and completely assembled rings. EM analysis of the early eluting fractions revealed that Dam1c was mainly present as fully assembled rings in the presence of Bim1 and Bik1 (Figure 39C). Full Dam1c rings had an outer diameter of approximately 50 nm and a relatively thick circumference. In addition, the lumen of the ring sometimes appeared crowded, presumably by Bim1 and Bik1 that collapsed and flattened during EM sample preparation.

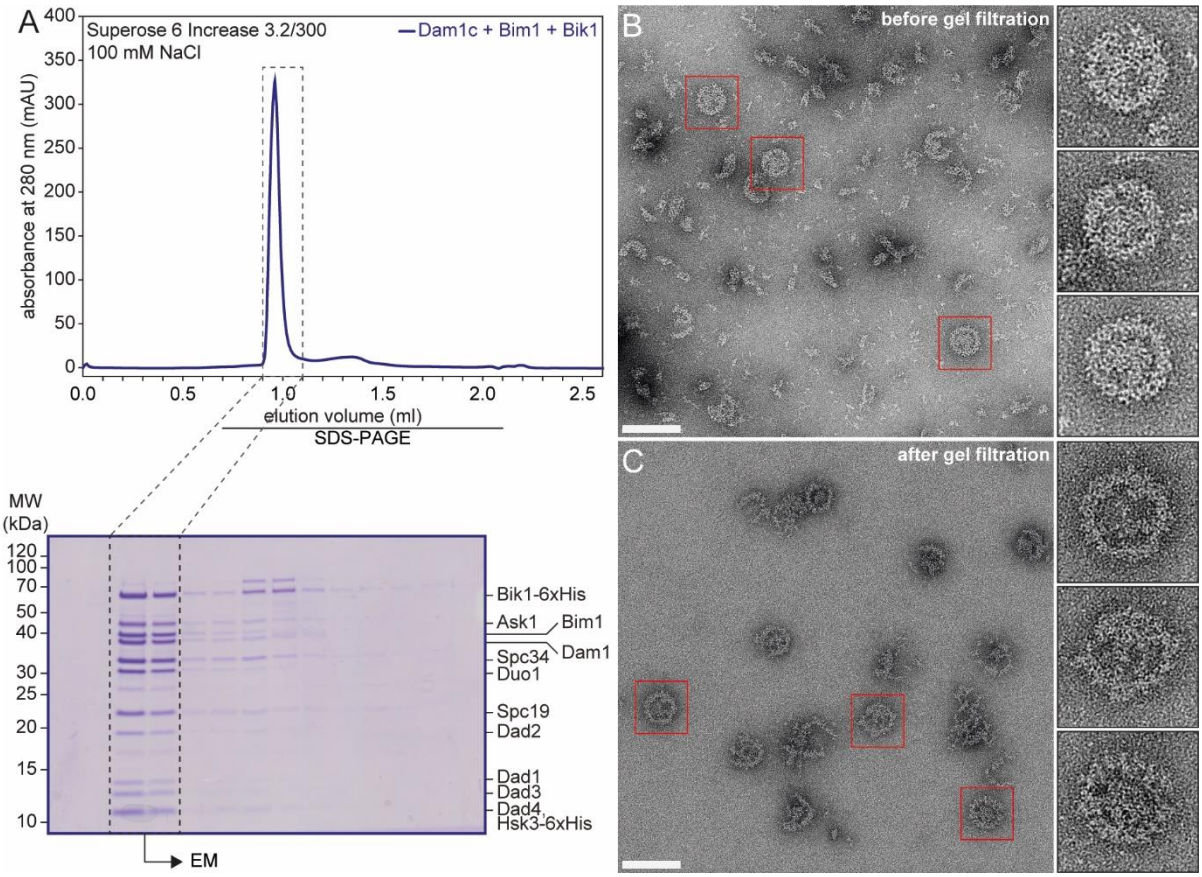

Figure 39: Dam1c forms rings in solution after binding of Bim1 and Bik1
A: Analytical SEC of 7.5 µM Dam1c in combination with Bim1 and Bik1. Chromatogram (top) and SDS-PAGE analysis of elution fractions (bottom) is shown. The interaction buffer contained 100 mM NaCl to promote assembly of high oligomeric structures. The black dashed box marks elution fractions analyzed by electron microscopy.
B, C: EM micrographs of Dam1c-Bim1-Bik1 complex before (B) and after (C) gel filtration. Proteins were diluted into buffer containing 10 mM NaCl. Particles framed by red boxes are shown as magnification on the right side. Scale bar: 100 nm.
Electron microscopy data were collected, processed and analyzed by Cole Bourque, Björn Udo Klink and Christos Gatsogiannis (Department of Structural Biochemistry, Max Planck Institute of Molecular Physiology, Dortmund and Institute for Medical Physics and Biophysics and Center for Soft Nanoscience, Westfälische Wilhelms-Universität Münster).

These finding clearly demonstrate that Bim1 and Bik1 do not only support oligomerization of Dam1c, but even trigger formation of full rings in the absence of microtubules. Since it is assumed that the ring form of Dam1c is essential for its physiological function, binding of Bim1 and Bik1 might crucially contribute to regulate Dam1c assembly *in vivo*.

3.4.6. Dam1c shows dispersed localization after Bik1 deletion *in vivo*

The biochemical and structural assays provided an insight into how Bim1 and Bik1 concertedly trigger Dam1c ring assembly in solution. To get a deeper understanding into the physiological relevance of this process, yeast strains were constructed which combine the Duo1^{WT} or Duo1$^{\Delta SxIP}$ allele with a deletion of Bik1 (*bik1*Δ). The combination of *bik1*Δ with either Duo1^{WT} or Duo1$^{\Delta SxIP}$ was viable at 30 °C. *bik1*Δ strains were mildly impaired in growth at 30 °C and were almost inviable at 16 °C irrespective of the Duo1 allele (Figure 40A). However, growth of the Duo1$^{\Delta SxIP}$ *bik1*Δ strain at 25 °C was more impaired than in a corresponding Duo1^{WT} strain. Growth phenotypes were further analyzed in the presence of the Mps1 inhibitor cincreasin (Dorer et al., 2005). Cells were spotted on YEPD containing either DMSO as solvent control or 200 µM or 400 µM cincreasin and were incubated at 25 °C (Figure 40B). Cincreasin did not affect growth of wild type strains but abolished growth of a *bim1*Δ strain as described before (Dorer et al., 2005). 200 µM of the inhibitor severely compromised growth of a Duo1^{WT} *bik1*Δ strain while a Duo1$^{\Delta SxIP}$ *bik1*Δ strain did not grow at all under these conditions. Increasing the inhibitor concentration to 400 µM prevented growth of both strains. Noticeably, cincreasin reduced growth of a Duo1$^{\Delta SxIP}$ strain compared to a Duo1^{WT} strain in a Bik1^{WT} background. Thus, preventing Bim1 binding to Dam1c is detrimental to cells in combination with mild inhibition of Mps1.

Localization of Dad1-GFP in Duo1^{WT} or Duo1$^{\Delta SxIP}$ strains combined with Bik1^{WT} or *bik1*Δ was analyzed by live cell fluorescence microscopy. In all four strains, Dad1-GFP appeared as two separated clusters in metaphase cells (Figure 40C). However, the buds of some Duo1$^{\Delta SxIP}$ and *bik1*Δ appeared to be abnormally large. Furthermore, Dad1-GFP signals were dispersed and showed several less well-defined clusters in *bik1*Δ strains irrespective of the Duo1 allele (Figure 40C and D).Quantification of Dad1-GFP signal intensities showed a significant reduction at metaphase kinetochore clusters in Duo1$^{\Delta SxIP}$ cells compared to Duo1^{WT} in a Bik1^{WT} strain background (Figure 40E). Deletion of Bik1 did not affect localization of Dad1-GFP in Duo1^{WT} cells but mildly reduced the mean signal intensity in a Duo1$^{\Delta SxIP}$ strain. These results suggest that preventing binding to Bim1 has a greater impact on kinetochore localization of Dam1c than the deletion of Bik1.

The microscopy data suggest that deletion of Bik1 has a less severe effect on Dam1c kinetochore recruitment than impaired Bim1 binding in context of the Duo1$^{\Delta SxIP}$ allele. Impaired

clustering of Dad1-GFP in *bik1*Δ cells, irrespective of the Duo1 allele, might be an indirect consequence of defects in spindle assembly and requires further investigation.

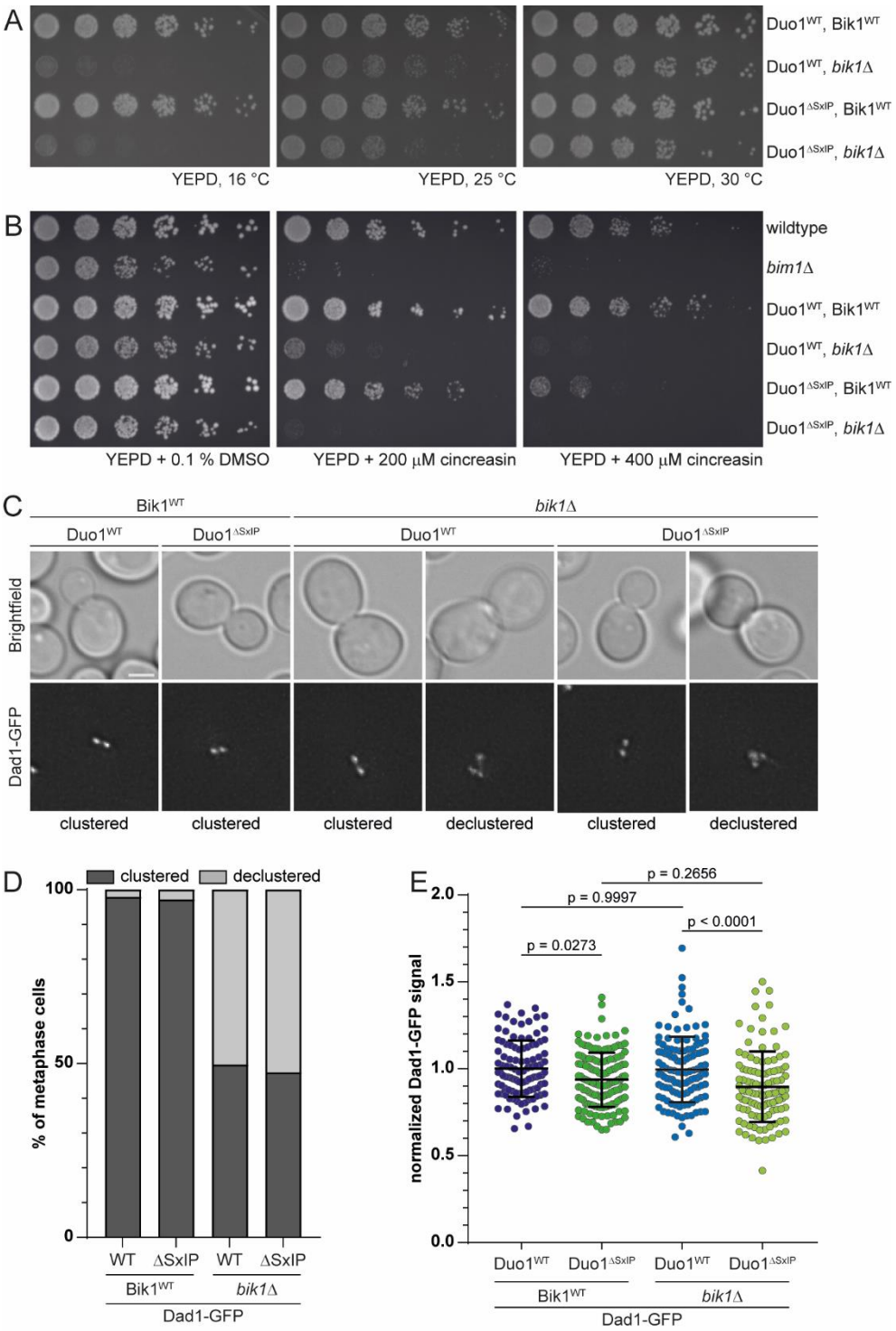

Figure 40: Deletion of Bik1 mildly aggravates phenotypes of the Duo1$^{\Delta SxIP}$ allele

A, B: Serial dilution assays of yeast strains combining Duo1^{WT} and Duo1$^{\Delta SxIP}$ with Bik1^{WT} or *bik1*Δ.Plates were incubated at the indicated temperatures. In B, Mps1 was inhibited by cincreasin. A *bim1*Δ strain served as control since it was reported to be inviable in the presence of the inhibitor. Plates were incubated at 25 °C.

C, D: Representative images from live cell microscopy. In metaphase cells, Dad1-GFP appeared as either two well-separated clusters or declustered. Scale bar: 2 µm. A quantification of Dad1-GFP shape is shown in D. Data from a single experiment are shown. n ≥ 181 cells per strain were analyzed.

E: Quantification of Dad1-GFP signal intensities in metaphase cells with the indicated genotypes. Mean ± standard deviation is plotted. Values were normalized to the mean of the Duo1^{WT} Bik1^{WT} strain. p-values were calculated by a one-way ANOVA with Sidak's multiple comparisons test. n ≥ 104 cells were analyzed.

3.4.7. Regulation of Dam1c oligomerization by multiple pathways is essential for cell viability

Different mechanisms have been proposed in literature which trigger or regulate Dam1c oligomerization (Figure 41A). For instance, phosphorylation of Dam1 by Ipl1 reduces oligomerization of the complex (Wang et al., 2007). On the contrary, phosphorylation of Ask1 by Cdc28/Cdk1 was suggested to promote oligomerization which strengthens kinetochore-microtubule attachments (Gutierrez et al., 2020). In this study, a third mechanism that controls Dam1c oligomerization was described which requires binding of Bim1 and Bik1 to Dam1c and is regulated by Mps1. The next experiments aimed to explore the effect when two or three of these pathways are deficient *in vivo*.

Similar to previous experiments, binding of Bim1 to Dam1c was disrupted by deletion of the SxIP motif of Duo1. Phosphorylation of Ask1 by Cdc28/Cdk1 was prevented by mutating S216 and S250 to alanine ($Ask1^{2A}$). Alternatively, constitutive phosphorylation was mimicked by substitution of the two serine residues by aspartic acid ($Ask1^{2D}$). $Ask1^{WT}$, $Ask1^{2A}$ and $Ask1^{2D}$ alleles were introduced into strains with either $Duo1^{WT}$ or $Duo1^{\Delta SxIP}$ background and screened for synthetic growth defects in serial dilution assay (Figure 41B). In a $Duo1^{WT}$ background, $Ask1^{2A}$ and $Ask1^{2D}$ strains grew indistinguishably from a $Ask1^{WT}$ strain at all tested temperatures. In contrast, growth of cells with both $Duo1^{\Delta SxIP}$ and $Ask1^{2A}$ alleles was severely compromised when grown at 16 °C and 25 °C but displayed normal growth at 30 °C and 37 °C. No growth defect was observed for strains with $Duo1^{\Delta SxIP}$ and $Ask1^{2D}$ allele indicating that constitutive phosphorylation of Ask1 by Cdc28/Cdk1 is not detrimental in a $Duo1^{\Delta SxIP}$ strain background. However, interfering with both Bim1- and Cdc28/Cdk1-induced Dam1c oligomerization severely compromised growth of yeast cells, especially when grown at low temperatures.

The effect of Ipl1-dependent phosphorylation, which prevents Dam1c oligomerization, was mimicked by substitution of Dam1 S20 with aspartic acid ($Dam1^{S20D}$). Again, yeast strains were generated with different combinations of the described Duo1, Ask1 and Dam1 alleles and analyzed in a serial dilution assay (Figure 41C). The $Dam1^{S20D}$ allele in combination with wild type alleles of Duo1 and Ask1 showed no growth defect at 25 °C, 30 °C and 37 °C, but was almost inviable at 16 °C. A combination of $Dam1^{S20D}$ and $Duo1^{\Delta SxIP}$ with $Ask1^{WT}$ did not change the growth phenotype of $Dam1^{S20D}$. However, interfering with all three oligomerization pathways by combining the $Duo1^{\Delta SxIP}$; $Ask1^{2A}$ and $Dam1^{S20D}$ alleles additionally compromised growth at 25 °C. This growth defect was mildly increased compared to a $Duo1^{\Delta SxIP}$ $Ask1^{2A}$ strain with $Dam1^{WT}$.

Taken together, multiple regulatory mechanisms control Dam1c oligomerization *in vivo* and interference with one or several pathways can severely compromise growth under certain conditions. However, it is noteworthy that these alleles still allow robust growth at higher

temperatures such as 30 °C and 37 °C. These results suggest that well-regulated Dam1c oligomerization is important for cell viability, especially at low temperatures when microtubule dynamics are affected (Li and Moore, 2020).

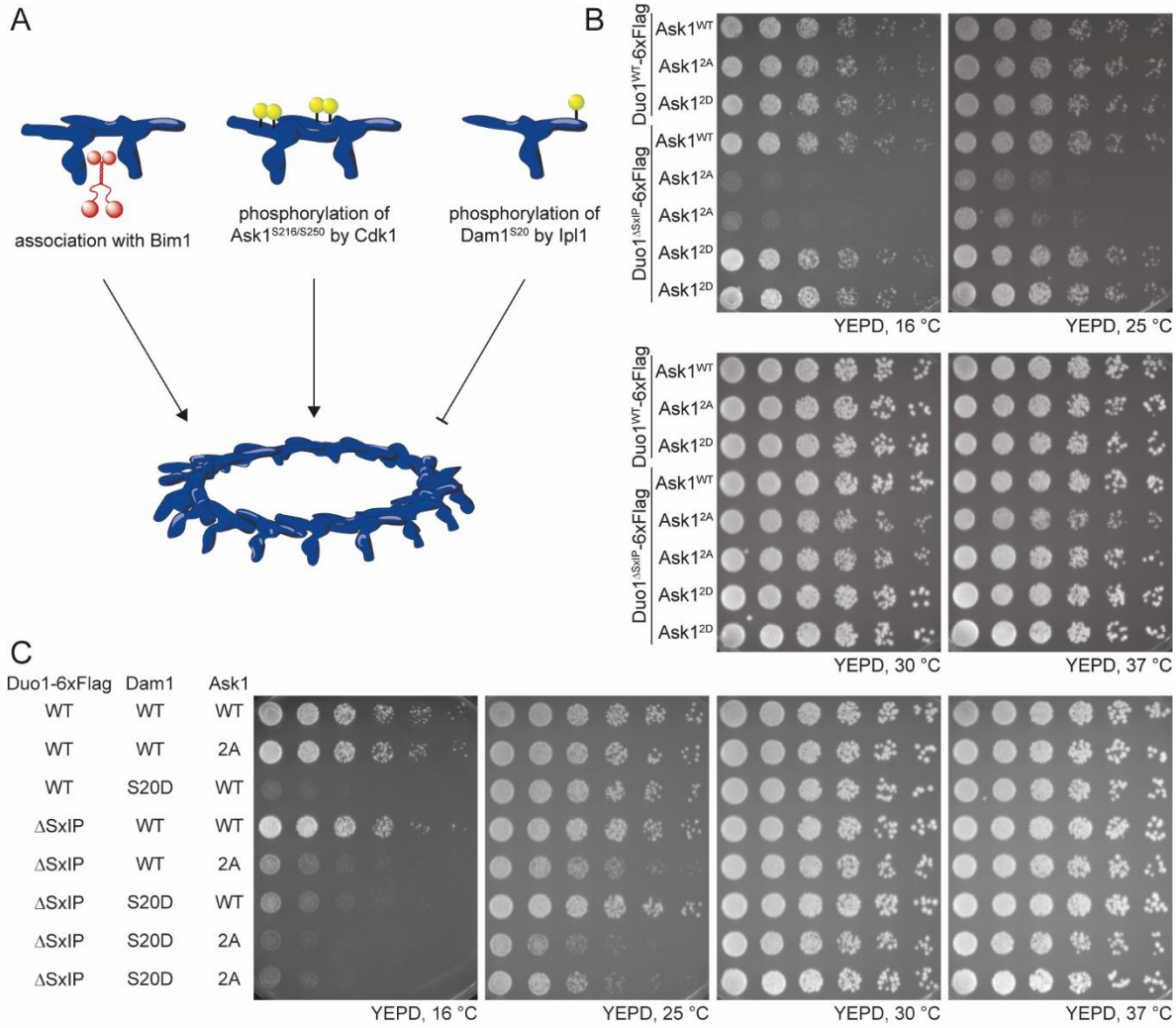

Figure 41: Multiple parallel pathways of Dam1c oligomerization are essential for viability
A: Illustration of different mechanisms that regulate Dam1c ring assembly. Oligomerization is induced by binding of Bim1 and Bik1 (this study) or Cdc28/Cdk1-dependent phosphorylation of Ask1 (Gutierrez et al., 2020) and is suppressed by phosphorylation of Dam1 by Ipl1 (Wang et al., 2007).
B, C: Serial dilution assays of yeast strains with different combinations of Duo1, Dam1 and Ask1 alleles that affect Dam1c oligomerization. Cells were serially diluted, spotted on YEPD plates and incubated at the indicated temperatures.

3.5. Characterization of the interplay between Dam1c, Bim1 and Ndc80c

Kinetochore localization of the Dam1 complex depends on its interaction with the Ndc80 complex (Janke et al., 2002; Kalantzaki et al., 2015; Lampert et al., 2010, 2013; Maure et al., 2011; Tien et al., 2010). This study so far described how Bim1 additionally supports kinetochore localization of Dam1c. Notably, Bim1 and the two Ndc80c subunits Ndc80 and Nuf2 share a highly conserved structural feature, the microtubule-binding calponin homology (CH) domain (Ciferri et al., 2008; Hayashi and Ikura, 2003). Considering that both Bim1 and Ndc80c bind Dam1c, two different scenarios how these interactions are interconnected in time and space can be envisioned. First, simultaneous binding of both Bim1 and Ndc80c to Dam1c

is possible, leading to the formation of a ternary complex. Possibly, Bim1 might even positively affect binding of Dam1c to Ndc80c. Second, Ndc80c binding is incompatible with Bim1 binding and Ndc80c eventually replaces Bim1. In the latter scenario, the Dam1c-Bim1 and Dam1c-Ndc80c complexes may represent two consecutive configurations of Dam1c at the kinetochore (Figure 42A). The following experiments aim to dissect the interplay between Dam1c, Ndc80c and Bim1 employing biochemical assays and yeast genetics.

3.5.1. Bim1 bound to Dam1c impairs its interaction with Ndc80c

Binding of Dam1c to Ndc80c in the presence of Bim1 was tested in a pull down assay. Flag-tagged Ndc80c expressed in Sf9 insect cells was immobilized on M2 anti-Flag agarose beads and incubated with constant amounts of recombinant Dam1c. In addition, Bim1 was added to a final concentration of 0 – 16 µM. Dam1c robustly bound to immobilized Ndc80c in the absence of Bim1 (Figure 42B, lane 3) and showed no unspecific interaction with empty beads (lane 1). Though binding of Dam1c to Ndc80c did not appear to be stoichiometric it was easily detectable by Coomassie staining. Addition of Bim1 reduced binding of Dam1c to Ndc80c in a concentration-dependent manner by up to 30 % (Figure 42B, lanes 5 – 9, and Figure 42C). Only minor amounts of Bim1 bound immobilized Ndc80c which might be favored by the relatively high Bim1 concentration of 16 µM (lane 4). Ndc80c and Bim1 did not form a complex during analytical SEC (Appendix Figure 2) suggesting that Bim1 does not bind Ndc80c.

Under the conditions of the pull down assay, Dam1c presumably formed dimeric or low-oligomeric structures. To gain a deeper insight in how Ndc80c interacts with large Dam1c assemblies, analytical SEC of Ndc80c with Dam1c preassembled in the presence of Bim1 and Bik1 was performed (Figure 43). Elution positions of Dam1c and Ndc80c partially overlapped with Ndc80c eluting slightly later than Dam1c (Figure 43A and B). Confirming the results of the pull down assays, Ndc80c and Dam1c formed a stable complex in solution. Notably, the Dam1c-Ndc80c complex eluted at two different positions. First, elution peaked in fraction 3 presumably representing complexes of high molecular weight. The second elution peak was found in fraction 6 which is relatively close to the elution positions of the individual complexes. An excess of Ndc80c over Dam1c was found at this position, while substoichiometric amounts of Ndc80c were present in the first peak. As seen in previous experiments, elution of Dam1c was shifted in the presence of Bim1 and Bik1 (Figure 43C, fractions 3 and 4) with minor amounts of the complex eluting in fractions 6 and 7. Addition of Ndc80c partially shifted the elution position of preassembled Dam1c-Bim1-Bik1 complex. A large fraction of Dam1c again eluted in fractions 3 and 4. Smaller amounts of the complex were eluted in fractions 5 and 6. Notably, the peak fractions differed in their compositions. Fractions 3 and 4 contained large amounts of Dam1c, Bim1 and Bik1, similar to the sample lacking Ndc80c. In addition, only minor amounts of Ndc80c were present in these fractions. Fractions 5 and 6 were characterized by the presence of both Dam1c and high amounts of Ndc80c. However, Bim1

and Bik1 were decreased in these fractions compared to the early elution fractions. Taken together, the data from analytical SEC is most consistent with the formation of two biochemically distinct complexes composed of Dam1c, Bim1, Bik1 and Ndc80c. First, a complex consisting of Dam1c, Bim1 and Bik1 with little Ndc80c formed, which eluted early during SEC. Second, a smaller complex consisting of Dam1c and Ndc80c, but reduced Bim1 and Bik1 content, that eluted slightly later from the column. This suggests that simultaneous binding of Bim1-Bik1 and Ndc80c to Dam1c is mutually exclusive and supports the idea that Bim1-Bik1 binding followed by Ndc80c binding might represent two consecutive steps during formation of kinetochore microtubule attachments.

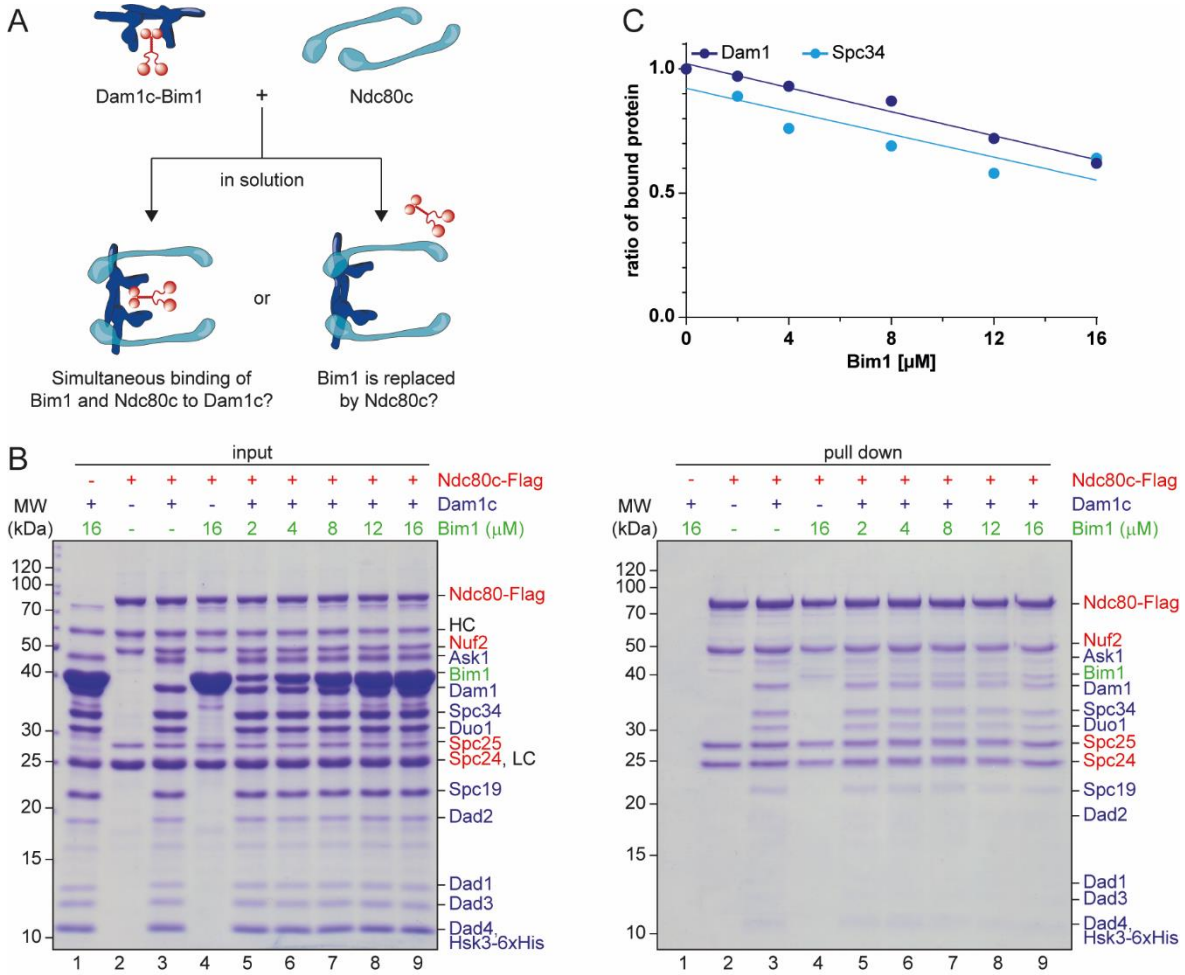

Figure 42: Bim1 and Ndc80c compete for Dam1c binding
A: Model of two different scenarios of complex formation involving Dam1c, Ndc80c and Bim1. Upon addition of Ndc80c to preformed Dam1c-Bim1 complex either a ternary complex is formed (lower left) or Ndc80c replaces Bim1 leading to dissociation of Bim1 from Dam1c (lower right).
B: Pull down assays to analyzed binding of Dam1c to immobilized Ndc80c in the presence of increasing concentrations of Bim1. Input and pull down samples were analyzed by SDS-PAGE. HC and LC mark the heavy and light chains of the M2 anti-Flag antibody. Subunits of Dam1c are labelled in blue, Ndc80c in red and Bim1 in green.
C: Quantification of signal intensities of Dam1 and Spc34 in pull down samples depending on the Bim1 concentration. A linear regression was calculated and plotted based on the data points.

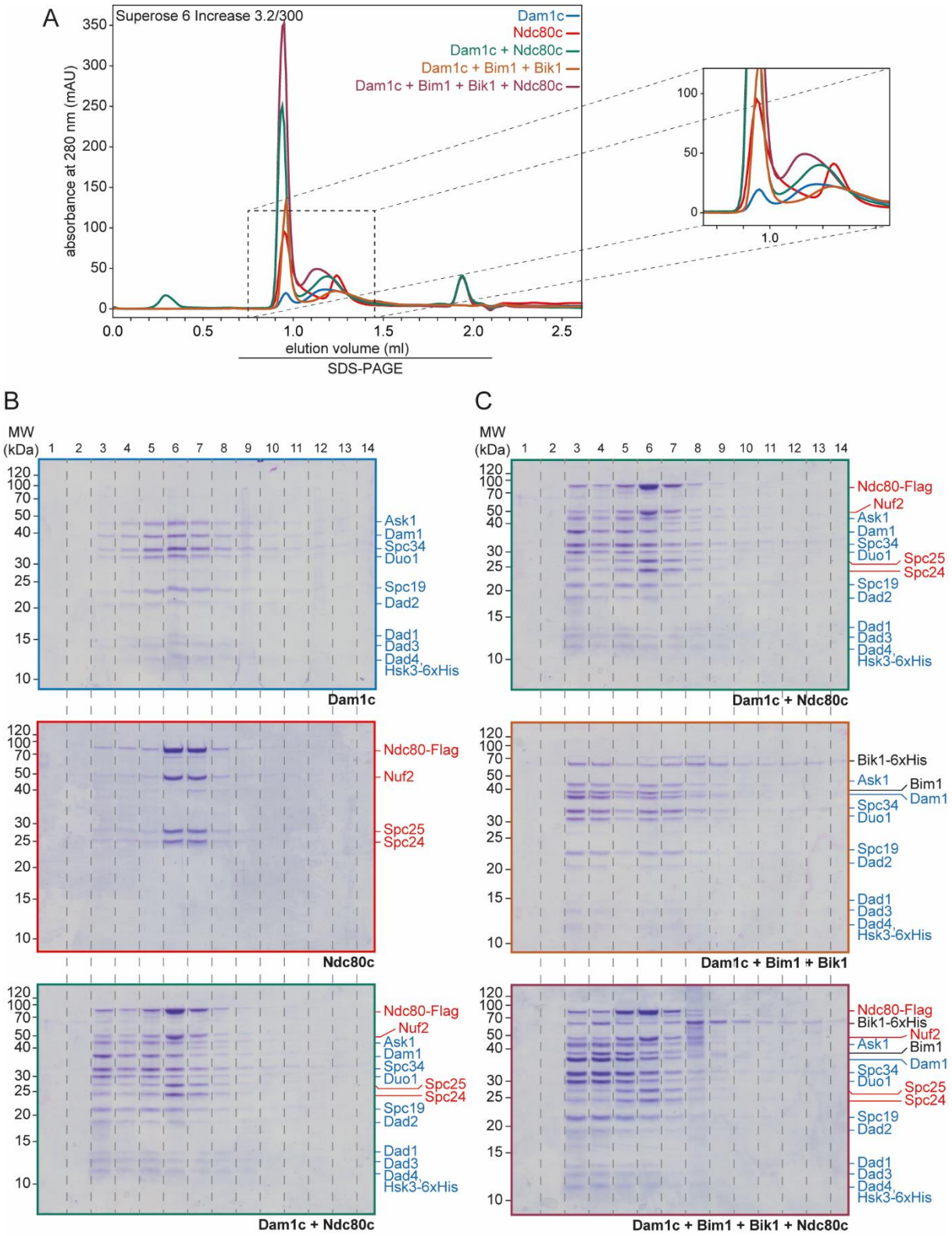

Figure 43: Binding of Ndc80c to Dam1c is impaired in the presence of Bim1 and Bik1
Binding of Ndc80c to preassembled Dam1c-Bim1-Bik1 complex was analyzed by analytical SEC.
A: Chromatograms of SEC runs. The area within the dashed box is shown as magnification on the right side. 3xFlag peptide that was used during Ndc80c purification was eluted between 1.9 and 2.0 ml.
B, C: SDS-PAGE analysis of elution fractions from SEC runs. Numbers of elution fractions are labelled on top of the gels. Please note that the gel for the Dam1c + Ndc80c sample is displayed twice for convenient comparison of elution positions of the different complexes. SEC buffer contained 150 mM NaCl.

3.5.2. Disrupting Bim1 binding to Dam1c restores growth of Ndc80 loop deletion strains

Binding of Dam1c to kinetochore-resident Ndc80c is required for formation of stable and load-bearing kinetochore-microtubule attachments. So far, this study demonstrates how Bim1 and Bik1 act in recruiting Dam1c to kinetochores. However, how this relates to Ndc80c binding *in vivo* is unclear so far. In the following experiments it was investigated how cell viability and Dam1c localization are affected if binding of both Bim1 and Ndc80c to Dam1c is impaired. This was tested *in vivo* by using the FRB system (Haruki et al., 2008). Yeast strains were constructed in which endogenous Ndc80 was C-terminally fused to FRB. In addition, the strains expressed FKBP12 fused to the large ribosomal subunit RPL13A. In the presence of rapamycin, FKBP12 and FRB dimerize and, due to the shuttling of the ribosomal subunit between nucleoplasm and cytoplasm, the FRB-tagged protein is efficiently removed from the nucleus. To test for the phenotypes of different Ndc80 alleles in this system, the corresponding alleles were integrated at the LEU2 locus under control of their native promotor. Growth of yeast strains was finally tested in a serial dilution assay.

Different mutations within Ndc80 have been described which disrupt its interaction with Dam1, for instance deletion of amino acids 256-273 ($Ndc80^{\Delta 256-273}$, Lampert et al., 2013) or 490-510 ($Ndc80^{\Delta 490-510}$, Kalantzaki et al., 2015). In addition, deletion of the N-terminal tail of Ndc80 might share redundant functions with the sequence covered by amino acids 256-273, though the tail is not essential for viability in yeast (Kemmler et al., 2009; Lampert et al., 2013). Combinations of these Ndc80 alleles with either $Duo1^{WT}$ or $Duo1^{\Delta SxIP}$ alleles integrated at the DUO1 locus were analyzed in a serial dilution assay.

In the absence of rapamycin, strains with different combinations of Ndc80 and Duo1 alleles grew indistinguishably from each other when grown at 30 °C (Figure 44). However, strains with the $Ndc80^{\Delta 256-273}$ allele were compromised in growth at 37 °C in the absence of rapamycin, suggesting that $Ndc80^{\Delta 256-273}$ exerts a dominant negative effect over wild type Ndc80. The growth defect was even more pronounced in a $Duo1^{\Delta SxIP}$ strain background compared to a $Duo1^{WT}$ strain. In the presence of rapamycin, growth was not affected when Ndc80 was not fused to FRB. As expected, expression of Ndc80-FRB without additional copy of wild type Ndc80 was lethal since Ndc80 is an essential kinetochore component. Deletion of the N-terminal tail of Ndc80 ($Ndc80^{\Delta 1-116}$) did not affect growth neither in combination with $Duo1^{WT}$ nor $Duo1^{\Delta SxIP}$. In contrast, deletion of amino acids 256-273 did not support growth in a $Duo1^{WT}$ background and the growth defect was not rescued by expression of $Duo1^{\Delta SxIP}$.

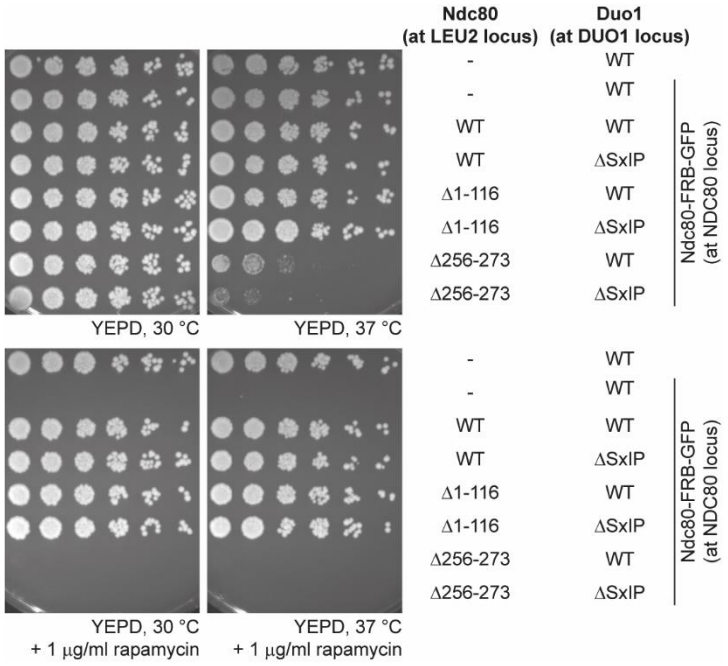

Figure 44: The Duo1$^{\Delta SxIP}$ allele does not rescue the growth defect caused by Ndc80$^{\Delta 256-273}$
Serial dilution assay to test for genetic interactions between Duo1^{WT} or Duo1$^{\Delta SxIP}$ and different Ndc80 alleles which were integrated at the LEU2 locus. The FRB system allows conditional removal of endogenous FRB-tagged Ndc80 upon treatment with rapamycin.

Similar to Ndc80$^{\Delta 256-273}$, deletion of amino acids 490-510 of Ndc80, which are located within the Ndc80 loop, was suggested to disrupt the interaction between Ndc80c and Dam1c. Yeast strains carrying the Ndc80$^{\Delta 490-510}$ allele are temperature-sensitive and exhibit impaired localization of Dam1c to kinetochores (Kalantzaki et al., 2015). The phenotypes of yeast strains combining Ndc80^{WT} or Ndc80$^{\Delta 490-510}$ with Duo1^{WT} or Duo1$^{\Delta SxIP}$ were analyzed using the Ndc80-FRB system as described above. In the absence of rapamycin, strains with any combination of the two Ndc80 and Duo1 alleles displayed no growth defect at 25 °C and 30 °C (Figure 45A). However, cells expressing Ndc80$^{\Delta 490-510}$ in combination with Duo1^{WT} were mildly compromised in growth at 37 °C, while the Duo1$^{\Delta SxIP}$ allele in combination with Ndc80$^{\Delta 490-510}$ was lethal at this temperature. At 37 °C, Ndc80$^{\Delta 490-510}$ appeared to exert a dominant-negative effect over the Ndc80 wild type protein which resulted in lethality in combination with the Duo1$^{\Delta SxIP}$ allele (Figure 45A). Strains with Ndc80-FRB but lacking any Ndc80 transgene integrated at the LEU2 locus were inviable in the presence of rapamycin, as expected. Consistent with previous results (Kalantzaki et al., 2015), the Ndc80$^{\Delta 490-510}$ strain was characterized by poor if any growth at 30 °C and 37 °C in a Duo1^{WT} background. In contrast, the Duo1$^{\Delta SxIP}$ allele partially suppressed this growth defect at 30 °C, but not at 37 °C. This result suggests that in this situation preventing Bim1 from binding to Dam1c is beneficial for cells when the interaction between Dam1c and Ndc80c is compromised. The fact that Duo1^{DSxIP} partially suppresses the growth phenotype of Ndc80$^{D490-510}$, but not of Ndc80$^{256-273}$, might indicated significant differences between both Ndc80 alleles regarding Dam1c binding.

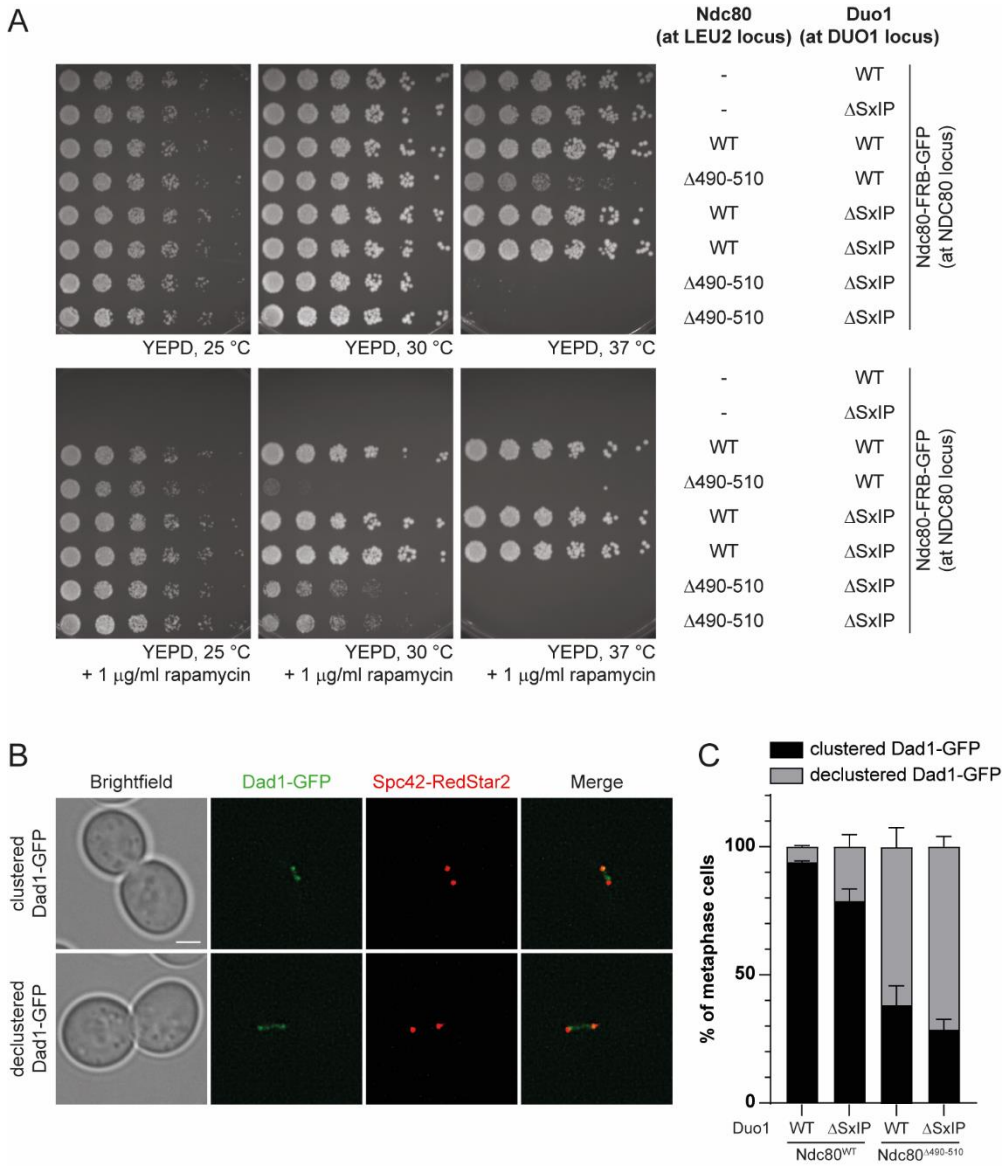

Figure 45: The Duo1$^{\Delta SxIP}$ allele partially rescues the phenotype of the Ndc80$^{\Delta 490-510}$ allele
A: Serial dilution assays of Ndc80-FRB strains with Ndc80^{WT} or Ndc80$^{\Delta 490-510}$ alleles, integrated at the LEU2 locus, in combination with Duo1^{WT} or Duo1$^{\Delta SxIP}$. Cells were serially diluted, spotted on YEPD plates without or with rapamycin to remove FRB-tagged Ndc80 from the nucleus and incubated at the indicated temperatures.
B: Representative images of live cell fluorescence microscopy. Cells combining Ndc80^{WT} or Ndc80$^{\Delta 490-510}$ with Duo1^{WT} or Duo1$^{\Delta SxIP}$ were grown at 34 °C for three hours. Localization of Dam1c was visualized by Dad1-GFP. Spc42-RedStar2 labelled spindle pole bodies. In metaphase cells, Dad1-GFP appeared either as two well-separated dots (upper panel) or as less distinct foci with stronger decoration of the mitotic spindle (lower panel). Scale bar: 2 µm.
C. Quantification of Dad1-GFP appearance in different yeast strains. Mean ± standard deviation from two independent experiments were plotted.

To analyze to which extent Dam1c recruitment to kinetochores is affected, live cell fluorescence microscopy was used to follow the localization of the complex. Dam1c was visualized by Dad1-GFP in cells combining Ndc80^{WT} or Ndc80$^{\Delta 490-510}$ with either Duo1^{WT} or Duo1$^{\Delta SxIP}$. In addition, spindle pole bodies were labelled with Spc42-RedStar2. Cells were first incubated at the permissive temperature of 25 °C and then shifted to 34 °C, the restrictive temperature of the Ndc80$^{\Delta 490-510}$ allele, for three hours. Ndc80$^{\Delta 490-510}$ strains arrested as large

budded cells with short spindles, indicative of a metaphase arrest (Figure 45B). In more than 90 % of wild type metaphase cells, Dad1-GFP appeared as two well separated dots, as seen in previous experiments (Figure 45C). This number was slightly decreased in a Duo1$^{\Delta SxIP}$ Ndc80^{WT} strain. In Ndc80$^{\Delta 490\text{-}510}$ strains, Dad1-GFP frequently appeared declustered with little if any enrichment at kinetochores but stronger decoration of the mitotic spindle (Figure 45B). This phenotype was observed more frequently in Duo1$^{\Delta SxIP}$ compared to Duo1^{WT} cells in a Ndc80$^{\Delta 490\text{-}510}$ strain background.

In summary, even though the Duo1$^{\Delta SxIP}$ allele partially rescues the temperature sensitivity of the Ndc80$^{\Delta 490\text{-}510}$ allele at 30 °C, it does not promote correct loading of Dam1c to metaphase kinetochores. Presumably, other mechanisms that cannot be unraveled by this microscopy assay significantly contribute to the observed growth phenotypes.

4. Discussion

The aim of this project was to characterize the interaction between the Dam1c complex and the plus end-tracking protein Bim1 using yeast genetics and biochemical reconstitution assays. These approaches were complemented by structural analyses of the Dam1c-Bim1 complex by electron microscopy and crosslinking mass spectrometry. Furthermore, a regulatory mechanism involving the conserved kinase Mps1 and the interplay between binding of Dam1c to either Bim1 or the Ndc80 complex were explored. These findings help understand the molecular mechanisms of kinetochore microtubule attachment formation in general and how Dam1c is specifically recruited to kinetochores in particular.

4.1. Bim1 binds to the SxIP motif of the Duo1 subunit and closely associates with the protrusion domain of the Dam1 complex

A large set of proteins that potentially interact with Dam1c was identified based on genetic interactions and yeast two-hybrid screens (Cheeseman et al., 2001a, 2001b; Ito et al., 2001; Jones et al., 1999; Uetz et al., 2000; Wong et al., 2007). However, only binding of Dam1c to microtubules and Ndc80c has been shown using biochemical approaches so far, and binding of Dam1c to Ndc80c was up to now only observed in presence of microtubules, indicating a relatively weak affinity between these components in solution (Lampert et al., 2010; Miranda et al., 2005; Tien et al., 2010; Westermann et al., 2005). Here, a direct interaction between Dam1c and the microtubule plus end-tracking protein Bim1 is demonstrated and characterized for the first time. Dam1c and Bim1 form a stable complex in solution (Figure 11). This interaction requires an intact EBH cargo binding domain of Bim1 as well as a conserved SxIP motif located in the unstructured C-terminal part of the Duo1 subunit (Figure 16 and Figure 18). Thus, this interaction follows the canonical mechanism by which EB proteins target a large set of cargo proteins to microtubule plus ends (Honnappa et al., 2005, 2009). Dam1c provides only a single SxIP motif and binding affinities between the EBH domain and peptides with an SxIP motif were described to be relatively low (Honnappa et al., 2005). High affinity binding of other cargo proteins to Bim1/EB1 is achieved either by using tandem SxIP motifs or by combining different short linear peptide motifs such as SxIP and KLTF (Kornakov et al., 2020). Considering these aspects, it is quite surprising that a single SxIP motif in Duo1 is sufficient for Bim1 binding and that a simple deletion of these amino acids disrupts the interaction (Figure 18 and Figure 19). *In vivo*, Dam1c most likely competes with a large variety of other proteins for Bim1 binding. The intrinsic propensity of Dam1c to oligomerize might compensate for the low affinity by combining several SxIP motifs within an oligomeric Dam1 complex.

It was observed that binding of Dam1c to immobilized Bim1 lacking its CH domain and linker region was increased compared to a full length protein (Figure 16). This allows to speculate that Bim1 might adopt a compact conformation in which cargo binding by the EBH domain is

impaired. A conformational change of Bim1 after phosphorylation by Ipl1 was previously suggested by Zimniak et al. (2009). Interestingly, structure prediction of monomeric Bim1 by AlphaFold suggests that the CH domain is localized closely to the coiled-coil region of the protein, giving the protein a rather compact than elongated structure (Jumper et al., 2021). Hence, it is conceivable that structural changes might be induced by phosphorylation of Bim1. In this context, it will be interesting to analyze the function of Bim1 phosphorylation by Mps1 in the future.

The C-terminus of Duo1, which contains the SxIP motif, is not resolved in the cryo-EM structure published by Jenni and Harrison (2018) due to its highly unstructured nature. Nevertheless, the results of the presented study give detailed insights into where Bim1 localizes in relation to Dam1c.

Chemical crosslinking and mass spectrometry analysis reveal proximity between Bim1 and the Dam1, Duo1, Spc34 and Spc19 subunits (Figure 13). Furthermore, Dam1, Duo1 and Spc34 are connected by a dense network of crosslinks. The proximity of Bim1 to Spc19 and Spc34 suggests that the protein closely associates with the protrusion domain of Dam1c which is composed of Spc19 and Spc34 (Jenni and Harrison, 2018). Electron microscopy analysis of the negatively stained Dam1c-Bim1 complex confirms these results (Figure 14). Bim1 appears to bridge the two protrusion domains of a dimeric Dam1 complex. Careful estimations of the molecular weight, based on the extra mass visible by EM, suggest that a single Bim1 homodimer (76.7 kDa) might associate with dimeric Dam1c. However, further investigation is required to confirm the stoichiometry of the Dam1c-Bim1 complex. At a first glance, proximity of Bim1 with the Dam1c protrusion domain appears to contradict to the finding that the Dam1c-Bim1 interaction depends on the SxIP motif of Duo1. However, the crosslinking map suggests proximity of Duo1 to Spc34 and Spc19. Furthermore, the published cryo-EM structure of Dam1c (Jenni and Harrison, 2018) allows to speculate that the flexible Duo1 C-terminus protrudes from the central part of the complex which is in agreement with its proximity to the protrusion domain.

The protrusion domains of Dam1c are thought to be oriented in parallel to the microtubule surface and presumably point towards the kinetochore (Jenni and Harrison, 2018). However, intrinsically Dam1c does not prefer any orientation in regard to the microtubule polarity (Ramey et al., 2011a). Binding of Bim1 to the protrusion domain might help to position Dam1c in the correct orientation. Bim1 specifically recognizes and binds the plus ends of growing microtubules. Binding of Bim1 helps target Dam1c specifically to the plus end and not to the microtubule lattice. Furthermore, Bim1 might align several Dam1 complexes with their protrusion domains pointing towards the kinetochore which could facilitate oligomerization and eventual interaction with the Ndc80 complex. Thus, Bim1 can be considered as reader for microtubule polarity which positions Dam1c to allow efficient binding to its kinetochore receptor Ndc80c. In addition, Bim1 supports Dam1c oligomerization *in vitro* by bridging individual Dam1

complexes.

4.2. Bim1 is a Dam1c kinetochore loading factor and required for proper mitotic timing

Disruption of the Dam1c-Bim1 interaction *in vivo* by the Duo1$^{\Delta SxIP}$ allele only mildly reduces cell viability when assayed in bulk growth assays (Figure 20 and Figure 21). This observation is less surprising considering that Bim1 itself is not essential for viability and only affects growth under extreme temperatures or in presence of benomyl (Schwartz et al., 1997). However, analysis of cell cycle progression and live cell fluorescence microscopy give a more detailed insight into the physiological relevance of Bim1 binding to Dam1c. Cell cycle progression of Duo1$^{\Delta SxIP}$ cells under unperturbed conditions is delayed by about 15 minutes compared to wild type cells presumably due to retarded kinetochore loading of Dam1c (Figure 22). Moreover, Dad1-GFP signals are reduced at metaphase kinetochores of Duo1$^{\Delta SxIP}$ cells (Figure 23). However, there is no difference at anaphase kinetochore clusters between Duo1$^{\Delta SxIP}$ and Duo1^{WT} cells suggesting that Duo1$^{\Delta SxIP}$ cells enter anaphase once Dam1c is loaded properly. Unaffected Dam1c levels at anaphase kinetochores might suggest that Bim1 is a transient interaction partner of Dam1c that might later be replaced by Ndc80c. In agreement with previous studies (Dhatchinamoorthy et al., 2017; Joglekar et al., 2006), the amount of Dam1c at kinetochores of wild types cells does not increase as cells progress from metaphase to anaphase, confirming that no additional copies of Dam1c are recruited at anaphase entry in contrast to other kinetochore complexes.

GFP-tagging of Dad1 exacerbates the growth defect of Duo1$^{\Delta SxIP}$ strains, especially at 37 °C, suggesting that Dam1c function is additionally compromised by tagging with the fluorophore (Figure 21). This effect is reminiscent of the synthetically lethal effect of *bim1*Δ in combination with the *dad1-1* allele (Enquist-Newman et al., 2001).

4.3. Mps1 phosphorylates the Dam1 C-terminus to regulate Bim1 binding

The C-terminus of the Dam1 subunit was attributed to crucially contribute to *in vitro* microtubule binding of the complex (Miranda et al., 2007; Ramey et al., 2011a; Wang et al., 2007; Westermann et al., 2005; Zelter et al., 2015). C-terminal truncation of Dam1, for example by the *dam1-19* allele (Q205Stop), reduces microtubule binding of the complex (Westermann et al., 2005). *In vivo*, *dam1-19* strains arrest with short, but intact spindles at the restrictive temperature and overall display slow growth at 25 °C and 30 °C (Cheeseman et al., 2001b). Furthermore, the Dam1 C-terminus is required for maintaining end-on kinetochore-microtubule attachments by interacting with Ndc80c while being dispensable for forming initial lateral attachments (Kalantzaki et al., 2015). Importantly, microtubule and Ndc80c binding by Dam1c are strictly regulated by Ipl1 phosphorylation (Cheeseman et al., 2002; Lampert et al., 2010; Legal et al., 2016; Tien et al., 2010).

Here, the C-terminus of Dam1 is shown to be an important regulator of Bim1 binding. Both the crosslinking data described in this study (Figure 13) and the published cryo-EM structure (Jenni and Harrison, 2018) prove steric proximity of the Dam1 and Duo1 C-termini allowing their physical interaction. However, rather than positively affecting Bim1 binding, the C-terminus of Dam1 seems to be a negative regulator of this interaction. This conclusion is based on two experimental observations: First, removal of the C-terminus seems to enhance binding of Dam1c to Bim1 *in vitro* (Figure 25). This effect is revealed under more stringent binding conditions by increasing the NaCl concentration of the interaction buffer. Second, deletion of the C-terminus *in vivo* increases, rather than decreases, loading of Dam1c to metaphase kinetochores (Figure 26). The latter observation is of particular interest since the reduced microtubule binding of the complex *in vitro* might suggest that kinetochore localization of the complex is impaired *in vivo*. However, *dam1-19* strains are generally impaired in growth even at permissive temperatures (Cheeseman et al., 2001b). This suggests that excessive binding of Bim1 to Dam1c and increased kinetochore loading of the complex is detrimental for mitotic progression. Probably, Dam1c is kept in a prolonged state of Bim1 binding that is not compatible with the molecular configuration of correctly end-on attached kinetochores and thus impairs errorfree mitotic progression.

The steric proximity between the C-termini of Dam1 and Duo1, as shown by crosslinking data (Figure 13) and suggested by the cryo-EM structure of the complex (Jenni and Harrison, 2018), explains how the Dam1 C-terminus negatively affects Bim1 binding to Dam1c. The Dam1 C-terminus probably partially masks the SxIP motif located in the C-terminus of Duo1 and thus sterically prevents binding of Bim1 (Figure 27). However, this inhibition of Bim1 binding must be regulated during the cell cycle. Notably, both Mps1 and Ipl1/Aurora B phosphorylate the Dam1 C-terminus at multiple sites (Figure 27; Cheeseman et al., 2002; Shimogawa et al., 2006) thus implicating these two conserved kinases as potential candidates for regulation of the interaction between Dam1c and Bim1.

Based on binding of Dam1c prepared from cell extracts of various kinase mutant strains (*mps1 737*, *mps1-as1*, *ipl1-2*), only inhibition of Mps1 but not of Ipl1 weakened binding of Bim1 demonstrating a requirement of Mps1 kinase activity for efficient interaction (Figure 28). Moreover, phosphorylation by Mps1 enhances binding of Bim1 to Dam1c under stringent conditions *in vitro*, resembling the effect of truncation of the Dam1 C-terminus (Figure 34). Preventing phosphorylation of the Dam1 C-terminus by Mps1 did not reduce kinetochore localization of the complex (Figure 29) suggesting that additional Mps1 substrates must exist that affect Dam1c recruitment to kinetochores. Phosphorylation of Ask1, Duo1 or Bim1, which are here identified as novel Mps1 substrates (Figure 33), might significantly contribute to kinetochore recruitment of Dam1c. Mapping and specific mutagenesis of Mps1 phosphorylation sites within these proteins will be critical to fully investigate the function of Mps1 in the process of Dam1c kinetochore loading.

Overexpression of Mps1 additionally directs Dam1c to the mitotic spindle without affecting localization of Ndc80 (Figure 31). The fact that Dam1c but not Ndc80c localization is affected by excessive Mps1 kinase activity suggests that this kinase plays an important role in regulating Dam1c localization. Due to the bar-shaped appearance of the Dad1-GFP clusters upon Mps1 overexpression, it was not possible to analyze whether increased amounts of Dam1c are present at kinetochores under these conditions. The altered localization of Dad1-GFP is only partially a consequence of the metaphase arrest induced by Mps1 overexpression. Whether Bim1 binding to Dam1c is required for formation of the bar-shaped Dad1-GFP clusters is unclear so far.

Mimicking Ipl1 phosphorylation of Dam1 (Dam1^{4D} complex) does not impair Bim1 binding *in vitro* (Figure 38). This result is rather noteworthy since Ipl1/Aurora B activity in most cases weakens protein-protein interactions at the kinetochore including binding of Dam1c to Ndc80c or microtubules (Kalantzaki et al., 2015; Lampert et al., 2010; Legal et al., 2016; Sarangapani et al., 2013; Tien et al., 2010). In contrast, the interaction with Bim1 appears to be refractory against Ipl1 phosphorylation. Presumably, the Dam1c-Bim1 complex persists at kinetochores even in the presence of high Ipl1 activity which might be an important initial step during the formation of kinetochore microtubule attachments. While microtubule binding of the kinetochore is weakened, association of Bim1 with Dam1c is required to recruit the complex to microtubule plus ends allowing the formation of new attachments. Furthermore, while Ipl1 activity suppresses Dam1c oligomerization, binding of Bim1-Bik1 keeps Dam1c in a primed state which allows rapid oligomerization of Dam1c when Ipl1 kinase activity decreases.

4.4. Binding of Bim1-Bik1 and phosphorylation by mitotic kinases regulate Dam1c oligomerization

Electron microscopy shows that Bim1 bridges the protrusion domains of two Dam1c heterodecamers (Figure 14) which probably stabilizes the dimer against disassembly and shifts the equilibrium towards the dimeric or higher oligomeric state. Interestingly, Bim1 even promotes further assembly of larger complexes with curvatures that resemble the shape of completely assembled Dam1c rings (Figure 15). Previous studies investigating oligomerization of Dam1c only focused on the intrinsic ability of the complex to assemble into rings in the presence of microtubules without any further binding proteins (Miranda et al., 2005; Westermann et al., 2005, 2006) or in the context of Ipl1- or Cdk1-dependent phosphorylation (Gutierrez et al., 2020; Sarangapani et al., 2013; Wang et al., 2007). Here, it is demonstrated for the first time that binding of an additional protein, Bim1, actively stabilizes and supports Dam1c oligomerization (Dudziak et al., 2021). Notably, Bim1 confers a new feature to the Dam1 complex which might be relevant for optimal kinetochore loading of Dam1c. While Dam1c itself does not read microtubule polarity (Ramey et al., 2011a) and thus randomly orients its protrusion domains either to the plus or minus end of the microtubule, Bim1

recognizes and specifically binds to the microtubule plus end (Bieling et al., 2007). By this, Bim1 might help align Dam1c in the correct orientation toward the microtubule plus end. Furthermore, Bim1 recruits Bik1, the yeast homolog of mammalian CLIP-170, to Dam1c as shown in this study (Figure 36). While Bik1 itself only weakly binds to Dam1c, a stoichiometric complex forms in presence of Bim1. In this situation, the EBH domain of Bim1 binds the SxIP motif of Duo1 and the C-terminal ETF sequence presumably binds the CAP-Gly domain of Bik1. In contrast to mammalian EB1, budding yeast Bim1 is capable of simultaneously binding two different cargo proteins both via their EBH domain and their ETF motif due to an increased spacing between the two binding sites (Stangier et al., 2018).

Binding of substoichiometric amounts of Bik1 in the absence of Bim1 already induces Dam1c oligomerization to a minor degree (Figure 36). The molecular requirements for this interaction are, however, unclear so far. However, the *in vivo* data suggest that the impact of Bik1 on Dam1c oligomerization and localization to kinetochores depends on Bim1. Deletion of Bik1 only mildly affects growth of yeast cells with a Duo1$^{\Delta SxIP}$ background compared to cells expressing Duo1^{WT} (Figure 40). In agreement with that, Dam1c localization to metaphase kinetochores of wild type cells is not affected at all when Bik1 is deleted and only slightly reduced in a Duo1$^{\Delta SxIP}$ strain background (Figure 40). Minor differences in growth and Dam1c kinetochore localization might be an indirect consequence of deleting Bik1 which is involved in regulation of microtubule dynamics (Blake-Hodek et al., 2010; Wolyniak et al., 2006). Altogether, Bim1 is required for recruitment of Bik1 to Dam1c and to induce oligomerization of the complex.

Binding of both Bim1 and Bik1 induces Dam1c ring formation *in vitro*, to the extent that these rings are even stable during size exclusion chromatography (Figure 39). So far, class averaging of the negatively stained Dam1c-Bim1-Bik1 complex has revealed a 16-fold symmetry of the rings (personal communication with Christos Gatsogiannis) which is in agreement with previous publications (Jenni and Harrison, 2018; Westermann et al., 2005). Bim1 and Bik1 appeared to be flattened during preparation of negatively stained samples. Therefore, high-resolution structural analyses using cryo-EM and tomography should allow a more detailed characterization of the molecular arrangement of the individual components of the assembled rings. Assuming a 1:1:1 stoichiometry of the Dam1c-Bim1-Bik1 complex, the fully assembled ring has a predicted molecular weight of more than 6 MDa.

The mechanism for Bim1-Bik1 induced oligomerization of Dam1c remains unclear so far. In case of Bim1, bridging two Dam1c heterodecamers appears as a straightforward mechanism for assembly of large Dam1c oligomers. Bik1 probably further enhances this effect by crosslinking different Bim1 homodimers or by stabilizing Bim1 bound to Dam1c. So far, it was assumed that +TIPs such as Bim1/EB1 merely direct further proteins to microtubule plus ends and affect their dynamics (Akhmanova and Steinmetz, 2008). In the present study, Bim1 is shown to be an integral part of a highly organized oligomeric complex and crucially contributes

to the functionality of the complex.

In contrast to Bim1, different mitotic kinases such as Ipl1/Aurora B and Cdk1 phosphorylate Dam1c and by this regulate the intrinsic ability of the complex to oligomerize. Ipl1 prevents assembly of larger oligomers by phosphorylation of Dam1 at residue S20 as shown by electron microscopy of recombinant Dam1c and *in vitro* single molecule studies (Wang et al., 2007; Zelter et al., 2015). In contrast, TIRF microscopy and optical trapping assays of recombinant Dam1c or kinetochore particles bound to microtubules suggests that Cdk1 promotes Dam1c assembly by phosphorylating Ask1 at residues S216 and S250 (Gutierrez et al., 2020). Even though the contribution of these phosphorylations to kinetochore function is not completely explored *in vivo*, it is suggested that dynamic phosphorylation and dephosphorylation are essential for correct kinetochore assembly (Cheeseman et al., 2002; Gutierrez et al., 2020). In the present study, binding of Bim1-Bik1 to Dam1c is identified as a novel mechanism that regulates oligomerization of the complex (Figure 41A). In contrast to the phosphorylation-dependent mechanisms, it is shown here that physical interaction of Dam1c with Bim1 and Bik1 contributes to assembly of Dam1c rings. Notably, disruption of individual oligomerization pathways is more or less well tolerated *in vivo*, but simultaneously interference with two or all three pathways causes severe growth defects especially when cells were grown at low temperatures such as 16 °C or 25 °C (Figure 41). The fact that the growth defects are milder at higher temperatures might be explained by compensatory or partially redundant unknown mechanisms that additionally regulate oligomerization of the Dam1 complex. Furthermore, growth defects are most likely more pronounced at low temperatures since microtubule dynamics are reduced under these conditions (Li and Moore, 2020) which might impair binding of microtubules to kinetochores and results in reduced growth upon dysregulation of Dam1c oligomerization.

In vitro data collected in this study also suggest both an indirect and direct role for Mps1 in regulating Dam1c assembly. Phosphorylation by Mps1 actively promotes binding of Bim1 to Dam1c and finally induces oligomerization (Figure 28, Figure 30 and Figure 34). In contrast, Mps1 suppresses oligomerization of Dam1c in the absence of any further proteins, as seen by analytical size exclusion chromatography, which rather resembles the effect of Ipl1-dependent phosphorylation (Figure 34). At a first glance, these two observations appear contradictory. However, these *in vitro* data may only incompletely represent the situation *in vivo* where additional factors such as Cdk1-dependent phosphorylation and so far unidentified factors may make crucial contributions to Dam1c oligomerization as well.

Regulation of Dam1c oligomerization by at least three different mechanisms appears redundant. However, closer inspection reveals important spatiotemporal differences between the different mechanisms (Figure 46). Global Cdk1 activity is high during M phase and decreases as cells enter anaphase due to destruction of Cyclin B and activity of counteracting phosphatases that dephosphorylate Cdk1 substrates (Holder et al., 2019; Örd and Loog,

2019). Ask1 phosphorylation by Cdk1 persists throughout M phase until anaphase onset (Li and Elledge, 2003) thus providing a basal stimulus for Dam1c oligomerization that is not restricted to a certain cellular localization. In contrast, Ipl1-dependent phosphorylation prevents Dam1c oligomerization (Wang et al., 2007) and is, due to the localization of Ipl1 during metaphase, restricted to kinetochores (Biggins and Murray, 2001). Hence, phosphorylation by Ipl1 can be considered as a locally restricted regulatory mechanism preventing Dam1c oligomerization in the context of error correction that is only active at kinetochores lacking correct microtubule attachments. In a similar manner, Mps1 localizes to unattached kinetochores (Hiruma et al., 2015; Ji et al., 2015; Kemmler et al., 2009; Saurin et al., 2011) and stimulates Bim1 binding which finally triggers Dam1c oligomerization. Taking these three regulatory pathways into account, it becomes obvious that regulation of Dam1c oligomerization is not a binary yes-or-no response. In contrast, integration of multiple pathways allows fine-tuned regulation of Dam1c assembly, which is additionally supported by the oligomeric nature of the fully assembled Dam1c ring. For instance, it is conceivable that individual Dam1 complexes within one ring differ regarding their phosphorylation status or associated proteins. Moreover, the described mechanisms might have different potency to induce Dam1c oligomerization. The *in vitro* data described in this study show that the Dam1^{4D} complex, which mimics Ipl1-dependent phosphorylation and is hence reduced in oligomerization, does not oligomerize upon binding of Bim1-Bik1 suggesting that phosphorylation by Ipl1 overrides Bim1-Bik1 binding (Figure 38). In addition, the impact of Bim1-Bik1 binding to Dam1c can be modulated by increasing protein concentrations which support oligomerization (Figure 37).

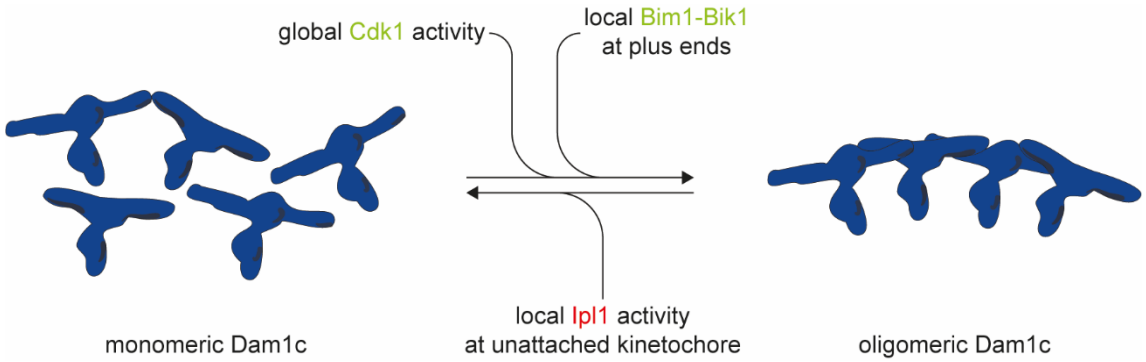

Figure 46: Dam1c oligomerization is regulated by different stimuli
Schematic depiction of different mechanisms that stimulate (phosphorylation by Cdk1, Bim1 binding) or inhibit (Ipl1) oligomerization of Dam1c. Cdk1, Ipl1 and Bim1 differ regarding their cellular localization and thus might allow spatiotemporal control of Dam1c oligomerization.

4.5. Binding of Dam1c to Bim1 and Ndc80c may represent two consecutive steps during establishing kinetochore-microtubule attachments

The biochemical experiments in this study demonstrate a physical interaction of recombinant Dam1c and Ndc80c in pull down assays and in solution (Figure 42 and Figure 43). Previous approaches to analyze binding of Dam1c and Ndc80c purified form *E. coli* in solution were not

successful, instead, the interaction depended on the presence of microtubules (Lampert et al., 2010; Tien et al., 2010). In the present study, Ndc80c was purified from eukaryotic Sf9 insect cells which, in contrast to *E. coli*, provide posttranslational modifications such as phosphorylation. The fact that recombinant Ndc80c purified from insect cells binds Dam1c in solution suggests that this interaction depends on phosphorylation of Ndc80c by one or multiple so far unknown kinases. This means that the interaction is not only negatively regulated by Ipl1 phosphorylation (Lampert et al., 2010; Tien et al., 2010), but might be also promoted by a different kinase in a cell cycle dependent manner. Identifying these kinases and elucidating the mechanism how they regulate Dam1c binding to Ndc80c will be addressed in future experiments.

Ndc80c and Bim1 are the only proteins, besides microtubules, that directly bind Dam1c (Dudziak et al., 2021; Lampert et al., 2010; Tien et al., 2010). Notably, both Ndc80c and Bim1 share a common structural feature, the CH domain, which confers microtubule binding activity to the proteins (Ciferri et al., 2008; Hayashi and Ikura, 2003). Considering the localization of Bim1 and Ndc80c at microtubule plus ends and kinetochores, respectively, both might represent two distinct receptors for Dam1c that are functionally relevant during different stages of microtubule binding by the kinetochore. First, Dam1c associates with Bim1 at the plus end of microtubules which can be thought of as an initial step that positions Dam1c at the plus end. In this context, Bim1 is a mobile receptor for Dam1c that specifically recognizes the microtubule plus end. In contrast, Ndc80c resides at the kinetochore and binding to Dam1c is considered as a final configuration for tension-bearing end-on attachments. Two possible scenarios can be envisioned how Dam1c is finally transferred to Ndc80c. Either, Dam1c binds Ndc80c in the presence of Bim1, meaning that Dam1c simultaneously interacts with both Ndc80c and Bim1, or, as the second option, Bim1 is displaced by Ndc80c. The *in vitro* data provided by this study rather support the latter option, hereafter called the hand-over model (Figure 48). In solid phase binding assays, increasing amounts of Bim1 reduce binding of Dam1c to immobilized Ndc80c rather than additionally promoting the interaction (Figure 42). Even though the inhibitory effect is relatively modest considering the high concentrations of Bim1 used in this assay, the results rather suggest that binding of Bim1 and Ndc80c to the Dam1c complex are mutually exclusive. This conclusion is further supported by binding studies in solution employing analytical size exclusion chromatography. Dam1c and Ndc80c form a stoichiometric complex in solution. However, when oligomeric Dam1c was assembled in the presence of Bim1 and Bik1, binding of Ndc80c was impaired (Figure 43). In this case, two distinct species of Dam1c were identified. On the one hand, Dam1c associates with stoichiometric amounts of Bim1 and Bik1, but little Ndc80c; on the other hand, Dam1c predominantly binds to Ndc80c while lacking Bim1 and Bik1. This suggests that Dam1c-Bim1-Bik1 and Dam1c-Ndc80c complexes are two distinct species of Dam1c that might exist at different time points during formation of kinetochore microtubule attachments. This conclusion is further supported by the *in vivo* data of the present

study. Different Ndc80 alleles such as Ndc80$^{\Delta 256-273}$ (Lampert et al., 2013) and Ndc80$^{\Delta 490-510}$ (Maure et al., 2011) were reported to impair Dam1c binding. Duo1$^{\Delta SxIP}$ partially suppresses the growth defect of Ndc80$^{\Delta 490-510}$, but not of Ndc80$^{\Delta 256-273}$ (Figure 44 and Figure 45). Both Ndc80 alleles strongly differ in their effect on cell viability. Cells expressing Ndc80$^{\Delta 256-273}$ are inviable (this study) or impaired in growth (Lampert et al., 2013). In contrast, cells carrying the Ndc80$^{\Delta 490-510}$ allele are viable at low temperatures but display severe growth defects when grown at 30 °C or higher temperatures (Maure et al., 2011; this study). This suggests that Ndc80$^{\Delta 490-510}$ retains partial functionality regarding its interaction with Dam1c in contrast to Ndc80$^{\Delta 256-273}$. Deletion of amino acids 256-273 of Ndc80 preserves the integrity of Ndc80c since the corresponding recombinant complex can be purified (Lampert et al., 2013).

The *in vitro* data shown in the present study suggest that Bim1 and Ndc80c compete for binding to Dam1c. Preventing Bim1 binding to Dam1c by deletion of the SxIP motif abolishes this competitive scenario enabling direct binding of Dam1c to Ndc80c and compensates for the impaired functionality of Ndc80$^{\Delta 490-510}$. By this mechanism, deletion of the Duo1 SxIP motif suppresses the growth defect caused by the Ndc80$^{\Delta 490-510}$ allele.

In summary, the combination of *in vitro* and *in vivo* data demonstrates that the general +TIP Bim1 is used specifically as kinetochore loading factor for Dam1c which is finally handed over to kinetochore-bound Ndc80c. This conclusion is in line with increasing evidence that different microtubule-associated proteins (MAPs) crucially contribute to various aspects of kinetochore function (Figure 47). The best characterized example is the association of Stu2/chTOG with Ndc80c in both yeast and mammalian cells, demonstrating the conservation of this mechanism across eukaryotes (Herman et al., 2020; Miller et al., 2016, 2019). Stu2 interacts with Ndc80c (Miller et al., 2016, 2019) by binding near the tetramerization region of the complex (Zahm et al., 2021). Stu2/chTOG strengthens kinetochore microtubule attachments *in vitro* and is required for error-free chromosome segregation (Herman et al., 2020; Miller et al., 2016, 2019). Furthermore, Stu2 apparently contributes to correction of erroneous kinetochore microtubule attachments and thus complements the function of Ipl1/Aurora B (Miller et al., 2019; Zahm et al., 2021). In addition, Stu2 supports formation of kinetochore microtubule attachments by rescuing microtubules from depolymerization and thus prevents laterally attached kinetochores to detach from microtubules (Kalantzaki et al., 2015).

In agreement with the results presented in this study, EB1 is required for kinetochore localization of the metazoan Ska complex, the functional homolog of Dam1c (Thomas et al., 2016).

Finally, unattached kinetochores sequester Stu1 in an Mps1-dependent manner and by this induce the formation of new dynamic microtubules which eventually capture the unattached kinetochore (Kolenda et al., 2018; Ortiz et al., 2009).

Collectively, these data demonstrate that different classes of MAPs complement the function

of the outer kinetochore and contribute to various aspects of chromosome segregation.

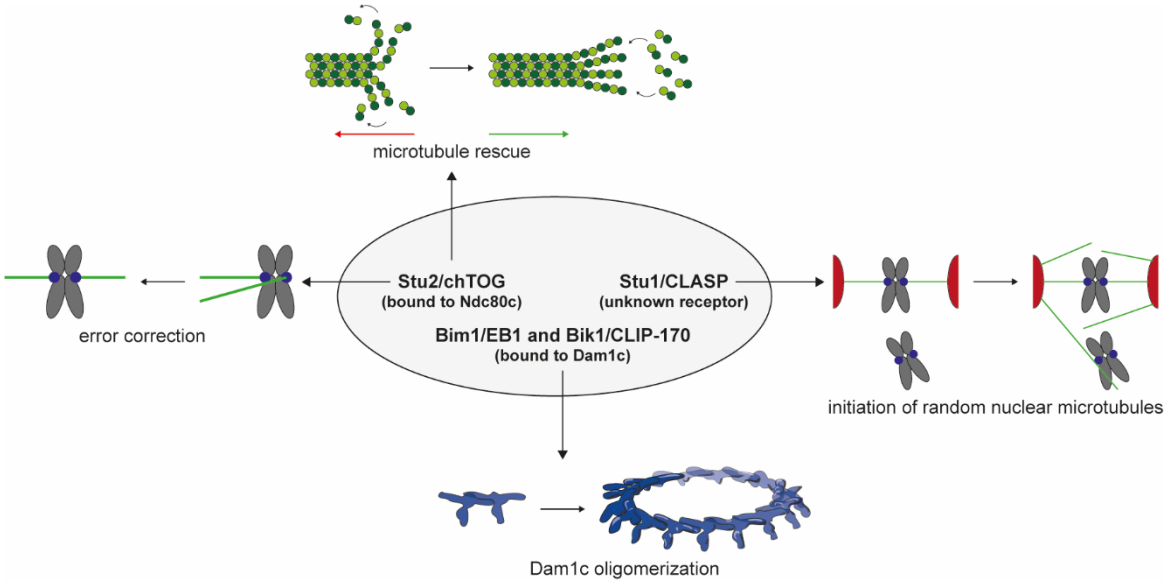

Figure 47: Functions of microtubule-associated proteins (MAPs) at the kinetochore
The MAPs Bim1/EB1, Stu1/CLASP and Stu2/chTOG modulate kinetochore function in various ways and contribute to error-free chromosome segregation. Stu2 is involved in error correction and rescue of microtubules to prevent detachment of laterally attached kinetochores. In the presence of unattached kinetochores, Stu1 is removed from the mitotic spindle and sequestered at unattached kinetochores. By this, the microtubules of the mitotic spindle are destabilized and new random nuclear microtubules are nucleated to capture unattached kinetochores. Bim1, together with Bik1, binds to Dam1c and induces oligomerization of the complex.

4.6. Phosphorylation by Mps1 triggers Dam1c ring assembly by promoting its interaction with Bim1

The results presented in this study strongly support the idea that Bim1 is required for loading of Dam1c to kinetochores and that this interaction is positively regulated by Mps1-dependent phosphorylation. Figure 48 graphically illustrates how kinetochore loading of Dam1c is supported by Bim1 and local Mps1 kinase activity and how the complex is finally transferred to Ndc80c.

Mps1 localizes to unattached kinetochores by binding to the Ndc80 complex, positioning the kinase to the microtubule-proximal region of the kinetochore (Hiruma et al., 2015; Ji et al., 2015; Kemmler et al., 2009). Both Dam1c and Bim1 localize to dynamic microtubules of the mitotic spindle. In case that this microtubule comes into proximity of an unattached kinetochore (Figure 48, lower panel), Mps1 phosphorylates Dam1c and Bim1 triggering the following events that eventually lead to Dam1c ring assembly and binding to Ndc80c (Dudziak et al., 2021): 1. Mps1 phosphorylates Bim1 and Dam1c and thus promotes their interaction. 2. Binding to Bim1 supports enrichment of Dam1c at the microtubule plus end since Bim1 specifically recognizes and binds to this part of the microtubule. Accumulation of Dam1c increases the local concentration of the complex at the microtubule tip which additionally favors Dam1c oligomerization, probably by cooperative microtubule binding of the complex (Gestaut et al., 2008). 3. Bim1 assists in positioning of Dam1c in the correct orientation relative to the

kinetochore with its protrusion domains pointing towards the kinetochore. This configuration is finally required for binding to the Ndc80 complex and formation of stable end-on attachments. 4. In biochemical reconstitution assays, Bim1 additionally recruits Bik1 to Dam1c and (5.) the ternary Dam1c-Bim1-Bik1 complex readily forms complete rings in solution in the absence of microtubules. Hence, Bim1 triggers formation of Dam1c rings at microtubule plus ends by recruiting Bik1 to the complex. It is conceivable that Bim1 also directs other proteins to the Dam1 complex which might affect its properties either in a similar or different manner.

Binding of Bim1 to Dam1c in an Mps1-regulated fashion can be considered as a priming step that prepares kinetochores for the formation of mature end-on microtubule attachments. Since the biochemical data presented in this study suggest that binding of Bim1 to Dam1c is refractory to Ipl1/Aurora B phosphorylation, Bim1 supports Dam1c loading to kinetochores during error correction in the presence of high Ipl1/Aurora B kinase activity. Association of Dam1c with Bim1 probably brings the complex into a primed state and allows rapid ring assembly as soon as kinase activity decreases.

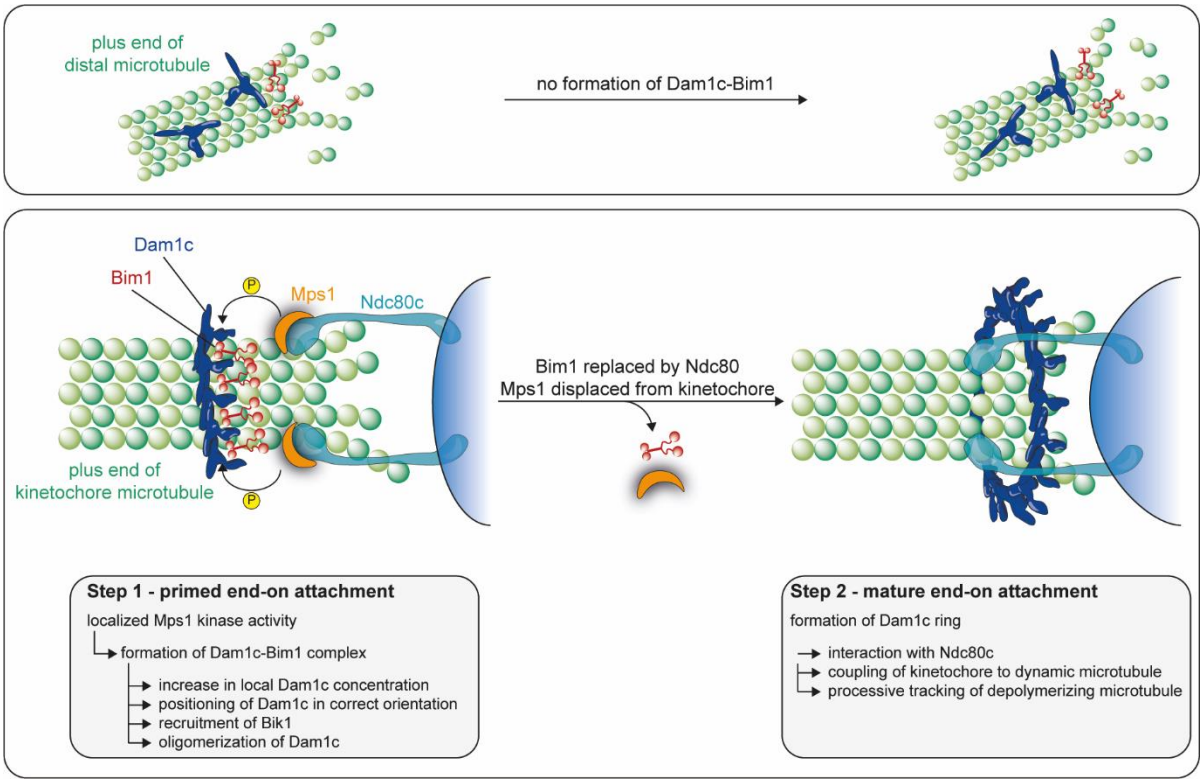

Figure 48: Model of Mps1-regulated assembly and oligomerization of the Dam1c-Bim1 complex at kinetochores

Upper panel: Dam1c and Bim1 localize to the plus end of a microtubule distal from an unattached kinetochore. Interaction of Dam1c with Bim1 is not promoted due to lack of Mps1 kinase activity, thus preventing assembly of oligomeric Dam1c.

Lower panel: Dam1c and Bim1 bound to the microtubule plus end in proximity of an unattached kinetochore are phosphorylated by Mps1. Mps1-mediated phosphorylation enhances binding of Bim1 to Dam1c. In addition, Bim1 recruits Bik1 to the Dam1 complex. These events trigger formation of Dam1c oligomers. Finally, Dam1c oligomerizes into a microtubule-encircling ring and physically interacts with Ndc80c. By this, Bim1 is displaced from Dam1c.

Dam1c eventually engages with kinetochore-resident Ndc80c, and the biochemical data presented in this study suggest that Bim1 might be replaced by Ndc80c to form mature end-on attachments (hand-over model). Coupling of Dam1c with Ndc80c is a crucial step to form load-bearing kinetochore-microtubule attachments and is required for processive tracking of depolymerizing microtubules by the kinetochore during anaphase. The requirement for functional Dam1c for chromosome segregation was demonstrated by several studies employing optical-trapping assays of purified or reconstituted kinetochore particles bound to dynamic microtubules. Dam1c is required to stabilize kinetochore microtubule attachments against applied forces and prevents disruption under increasing forces. Depletion or manipulation of Dam1c severely compromises microtubule binding under high forces (Asbury et al., 2006; Gutierrez et al., 2020; Powers et al., 2009; Sarangapani et al., 2013; Tien et al., 2010; Umbreit et al., 2014).

The exact molecular mechanism how Bim1 is replaced by Ndc80c is unclear so far. One possibility is that microtubule depolymerization leads to a loss of Bim1 from microtubule plus ends since its local concentration should be responsive to the polymerization state of the plus end. Alternatively, decreasing Mps1 kinase activity may gradually weaken binding of Bim1 to Dam1c. At unattached kinetochores, Mps1 binds to the CH domain of Ndc80 but is thought to be displaced upon microtubule binding (Hiruma et al., 2015; Ji et al., 2015). Therefore, Mps1 kinase activity at kinetochores is strongly reduced after microtubule binding leading to decreased phosphorylation of Dam1c and Bim1. In consequence, the interaction between Dam1c and Bim1 is weakened, which may enable Ndc80c to compete away Bim1 from Dam1c. Dam1c and Bim1 are also present at microtubules distal from kinetochores (Figure 48, upper panel). In this case, neither Dam1c nor Bim1 are phosphorylated by kinetochore-bound Mps1 and hence, their interaction is not promoted. In addition, accumulation of Dam1c at these sites might be prevented by loss of the low-oligomeric complex from depolymerizing microtubules. This mechanism explains why Dam1c is not generally enriched at the plus ends of all microtubules of the mitotic spindle such as the midzone, but exclusively localizes to a subset of kinetochore microtubules.

4.7. Outlook and future directions

The Dam1 complex is a central component of the kinetochore that is responsible for processive tracking of depolymerizing microtubules during chromosome segregation. Many of its molecular features have been investigated in detail over the past two decades. However, this study raises new questions regarding regulation of Dam1c localization, oligomerization and interaction with other proteins.

Association of Dam1c with Bim1 and Bik1 induces ring assembly of the complex which is considered as the functionally essential configuration of the complex *in vivo*. Future experiments need to address how Bim1 and Bik1 affect binding and tracking of dynamic

microtubules by the oligomerized complex. Ideally, these experiments are performed by total internal reflection (TIRF) microscopy with yeast tubulin instead of the commonly used porcine brain tubulin. Even though tubulin proteins belong to the most highly conserved proteins among eukaryotes there are significant differences between yeast and mammalian tubulin. Furthermore, yeast Bim1 and human EB1, for instance, differ regarding their molecular mechanisms of species-specific microtubule binding (Howes et al., 2017, 2018). Similar to previous experiments, biophysical optical-trapping assays can help to examine how Bim1 and Bik1 contribute to stabilize kinetochore microtubule attachments against applied forces. Furthermore, these types of experiments might allow a more direct analysis of the proposed hand-over model.

In addition to Bik1, Bim1 might recruit additional proteins to the Dam1 complex. Systematic screens to test whether known Bim1-binding proteins can simultaneously interact with Dam1c and Bim1 might help identify new proteins that additionally contribute to the function of the complex. A candidate for such a protein is Stu2 which functions at the kinetochore and potentially indirectly interacts with Dam1c (Kalantzaki et al., 2015; Miller et al., 2016, 2019). In the present study, a first low-resolution EM structure of the Dam1c-Bim1 complex derived from class averages of negatively stained samples is described. Future structural analyses will focus on different aspects. Cryo-EM and tomography are required to obtain high-resolution structural information on the Dam1c-Bim1 complex. This will provide more detailed insights into the exact topology of the binding interface and how Bim1 contacts and bridges the protrusion domains of different Dam1 complexes. Stabilization of the oligomeric complex might also enable analysis of the oligomerization interface and probably gives important insights into how phosphorylation by different kinases affects and regulates Dam1c oligomerization. Binding of Bim1 and Bik1 might additionally stabilize unstructured and flexible regions of Dam1c which makes it possible to resolve these parts of the complex by cryo-EM. By this, the already described cryo-EM structure of a heavily truncated Dam1 complex (Jenni and Harrison, 2018) can be complemented by structural information about functionally important regions of the complex.

In addition, structural analysis of the Dam1c-Ndc80c complex by cryo-EM will help to extend the knowledge about the configuration of an end-on attached kinetochore. However, this might be technically challenging due to the intricacy of the complex. Furthermore, Dam1c and Ndc80c are assumed to be assembled in a certain geometry at the kinetochore and microtubule binding might affect the configuration of the complex. Therefore, assembly of the Dam1c-Ndc80c complex in the presence of microtubules might generate a configuration closely resembling the arrangement at the outer kinetochore *in vivo*.

The physiological function of Ipl1-dependent phosphorylation of Dam1c is quite well understood. In contrast, the role of Mps1-dependent phosphorylation remains enigmatic so far. This study provides new insights into how Mps1 promotes loading of Dam1c to kinetochores.

The Dam1 subunit is a known Mps1 substrate (Shimogawa et al., 2006). In addition, the Duo1 and Ask1 subunits and Bim1 are identified as novel Mps1 substrates in this study. Mapping by mass spectrometry and selective mutagenesis of Mps1 phosphorylation sites in these proteins is crucial to investigate the physiological relevance of Dam1c and Bim1 phosphorylation by Mps1. Biochemical approaches need to be employed to further analyze the effect on Dam1c oligomerization and microtubule binding. Cell biological assays are required to test for the physiological consequences of mutations preventing or mimicking phosphorylation by Mps1 *in vivo*. Phenotypical analyses of Mps1 phosphorylation mutants will be performed by e.g. bulk growth assays, tracing of cell cycle progression and chromosome segregation and quantification of Dam1c kinetochore localization.

Several subunits of Dam1c are substrates of the conserved mitotic kinases Mps1, Cdk1 and Ipl1/Aurora B and the localization and function of the complex are regulated by these kinases. During mitosis, these kinases actually do not act on their own but are integrated into a complex signaling network consisting of various kinases and counteracting phosphatases (Saurin, 2018). An important issue that needs to be addressed in the future is how these different phosphorylation events are combined with each other and converge at the Dam1 complex. Combination of several stimuli that either promote or prevent Dam1c oligomerization might allow fine-tuning of the oligomeric state of the complex. Biochemical reconstitution assays specifically allowing or preventing phosphorylation by a distinct set of kinases will help elucidate how the function of the Dam1 complex is regulated by multiple kinases.

5. References

Abad, M.A., Medina, B., Santamaria, A., Zou, J., Plasberg-Hill, C., Madhumalar, A., Jayachandran, U., Redli, P.M., Rappsilber, J., Nigg, E.A., et al. (2014). Structural basis for microtubule recognition by the human kinetochore Ska complex. Nature Communications *5*, 2964.

Abad, M.A., Zou, J., Medina-Pritchard, B., Nigg, E.A., Rappsilber, J., Santamaria, A., and Jeyaprakash, A.A. (2016). Ska3 Ensures Timely Mitotic Progression by Interacting Directly With Microtubules and Ska1 Microtubule Binding Domain. Sci Rep *6*, 34042.

Akhmanova, A., and Steinmetz, M.O. (2008). Tracking the ends: a dynamic protein network controls the fate of microtubule tips. Nat. Rev. Mol. Cell Biol. *9*, 309–322.

Akhmanova, A., and Steinmetz, M.O. (2015). Control of microtubule organization and dynamics: two ends in the limelight. Nat. Rev. Mol. Cell Biol. *16*, 711–726.

Akiyoshi, B., and Gull, K. (2014). Discovery of Unconventional Kinetochores in Kinetoplastids. Cell *156*, 1247–1258.

Akiyoshi, B., Sarangapani, K.K., Powers, A.F., Nelson, C.R., Reichow, S.L., Arellano-Santoyo, H., Gonen, T., Ranish, J.A., Asbury, C.L., and Biggins, S. (2010). Tension directly stabilizes reconstituted kinetochore-microtubule attachments. Nature *468*, 576–579.

Alushin, G.M., Ramey, V.H., Pasqualato, S., Ball, D.A., Grigorieff, N., Musacchio, A., and Nogales, E. (2010). The Ndc80 kinetochore complex forms oligomeric arrays along microtubules. Nature *467*, 805–810.

Aravamudhan, P., Goldfarb, A.A., and Joglekar, A.P. (2015). The kinetochore encodes a mechanical switch to disrupt spindle assembly checkpoint signalling. Nature Cell Biology *17*, 868–879.

Asbury, C.L., Gestaut, D.R., Powers, A.F., Franck, A.D., and Davis, T.N. (2006). The Dam1 kinetochore complex harnesses microtubule dynamics to produce force and movement. PNAS *103*, 9873–9878.

Bieling, P., Laan, L., Schek, H., Munteanu, E.L., Sandblad, L., Dogterom, M., Brunner, D., and Surrey, T. (2007). Reconstitution of a microtubule plus-end tracking system in vitro. Nature *450*, 1100–1105.

Biggins, S. (2013). The composition, functions, and regulation of the budding yeast kinetochore. Genetics *194*, 817–846.

Biggins, S., and Murray, A.W. (2001). The budding yeast protein kinase Ipl1/Aurora allows the absence of tension to activate the spindle checkpoint. Genes Dev. *15*, 3118–3129.

Blake-Hodek, K.A., Cassimeris, L., and Huffaker, T.C. (2010). Regulation of microtubule dynamics by Bim1 and Bik1, the budding yeast members of the EB1 and CLIP-170 families of plus-end tracking proteins. Mol. Biol. Cell *21*, 2013–2023.

Borek, W.E., Vincenten, N., Duro, E., Makrantoni, V., Spanos, C., Sarangapani, K.K., de Lima Alves, F., Kelly, D.A., Asbury, C.L., Rappsilber, J., et al. (2021). The Proteomic Landscape of Centromeric Chromatin Reveals an Essential Role for the Ctf19CCAN Complex in Meiotic Kinetochore Assembly. Current Biology *31*, 283-296.e7.

Broad, A.J., DeLuca, K.F., and DeLuca, J.G. (2020). Aurora B kinase is recruited to multiple discrete kinetochore and centromere regions in human cells. Journal of Cell Biology *219*.

Camahort, R., Li, B., Florens, L., Swanson, S.K., Washburn, M.P., and Gerton, J.L. (2007). Scm3 Is Essential to Recruit the Histone H3 Variant Cse4 to Centromeres and to Maintain a Functional Kinetochore. Molecular Cell *26*, 853–865.

Carroll, C.W., Milks, K.J., and Straight, A.F. (2010). Dual recognition of CENP-A nucleosomes is required for centromere assembly. Journal of Cell Biology *189*, 1143–1155.

Chan, Y.W., Jeyaprakash, A.A., Nigg, E.A., and Santamaria, A. (2012). Aurora B controls kinetochore–microtubule attachments by inhibiting Ska complex–KMN network interaction. Journal of Cell Biology *196*, 563–571.

Cheerambathur, D.K., Gassmann, R., Cook, B., Oegema, K., and Desai, A. (2013). Crosstalk Between Microtubule Attachment Complexes Ensures Accurate Chromosome Segregation. Science *342*, 1239–1242.

Cheerambathur, D.K., Prevo, B., Hattersley, N., Lewellyn, L., Corbett, K.D., Oegema, K., and Desai, A. (2017). Dephosphorylation of the Ndc80 Tail Stabilizes Kinetochore-Microtubule Attachments via the Ska Complex. Developmental Cell *41*, 424-437.e4.

Cheeseman, I.M., Brew, C., Wolyniak, M., Desai, A., Anderson, S., Muster, N., Yates, J.R., Huffaker, T.C., Drubin, D.G., and Barnes, G. (2001a). Implication of a novel multiprotein Dam1p complex in outer kinetochore function. Journal of Cell Biology *155*, 1137–1146.

Cheeseman, I.M., Enquist-Newman, M., Müller-Reichert, T., Drubin, D.G., and Barnes, G. (2001b). Mitotic spindle integrity and kinetochore function linked by the Duo1p/Dam1p complex. J. Cell Biol. *152*, 197–212.

Cheeseman, I.M., Anderson, S., Jwa, M., Green, E.M., Kang, J. seog, Yates, J.R., Chan, C.S.M., Drubin, D.G., and Barnes, G. (2002). Phospho-regulation of kinetochore-microtubule attachments by the Aurora kinase Ipl1p. Cell *111*, 163–172.

Ciferri, C., Pasqualato, S., Screpanti, E., Varetti, G., Santaguida, S., Dos Reis, G., Maiolica, A., Polka, J., De Luca, J.G., De Wulf, P., et al. (2008). Implications for Kinetochore-Microtubule Attachment from the Structure of an Engineered Ndc80 Complex. Cell *133*, 427–439.

Cohen-Fix, O., Peters, J.M., Kirschner, M.W., and Koshland, D. (1996). Anaphase initiation in Saccharomyces cerevisiae is controlled by the APC-dependent degradation of the anaphase inhibitor Pds1p. Genes Dev. *10*, 3081–3093.

Daum, J.R., Wren, J.D., Daniel, J.J., Sivakumar, S., McAvoy, J.N., Potapova, T.A., and Gorbsky, G.J. (2009). Ska3 Is Required for Spindle Checkpoint Silencing and the Maintenance of Chromosome Cohesion in Mitosis. Current Biology *19*, 1467–1472.

Dhatchinamoorthy, K., Shivaraju, M., Lange, J.J., Rubinstein, B., Unruh, J.R., Slaughter, B.D., and Gerton, J.L. (2017). Structural plasticity of the living kinetochore. J. Cell Biol. *216*, 3551–3570.

Dimitrova, Y.N., Jenni, S., Valverde, R., Khin, Y., and Harrison, S.C. (2016). Structure of the MIND Complex Defines a Regulatory Focus for Yeast Kinetochore Assembly. Cell *167*, 1014-1027.e12.

Doodhi, H., Kasciukovic, T., Clayton, L., and Tanaka, T.U. (2021). Aurora B switches relative strength of kinetochore–microtubule attachment modes for error correction. Journal of Cell Biology *220*.

Dorer, R.K., Zhong, S., Tallarico, J.A., Wong, W.H., Mitchison, T.J., and Murray, A.W. (2005). A Small-Molecule Inhibitor of Mps1 Blocks the Spindle-Checkpoint Response to a Lack of Tension on Mitotic Chromosomes. Current Biology *15*, 1070–1076.

Drinnenberg, I.A., deYoung, D., Henikoff, S., and Malik, H.S. (2014). Recurrent loss of CenH3 is associated with independent transitions to holocentricity in insects. ELife *3*, e03676.

Drozdetskiy, A., Cole, C., Procter, J., and Barton, G.J. (2015). JPred4: a protein secondary structure prediction server. Nucleic Acids Research *43*, W389–W394.

Dudziak, A. (2016). Molecular analysis of outer kinetochore assembly in budding yeast (Master Thesis, University of Duisburg-Essen).

Dudziak, A., Engelhard, L., Bourque, C., Klink, B.U., Rombaut, P., Kornakov, N., Jänen, K., Herzog, F., Gatsogiannis, C., and Westermann, S. (2021). Phospho-regulated Bim1/EB1 interactions trigger Dam1c ring assembly at the budding yeast outer kinetochore. EMBO J *40*, e108004.

Dunsch, A.K., Linnane, E., Barr, F.A., and Gruneberg, U. (2011). The astrin–kinastrin/SKAP complex localizes to microtubule plus ends and facilitates chromosome alignment. Journal of Cell Biology *192*, 959–968.

Earnshaw, W.C., and Rothfield, N. (1985). Identification of a family of human centromere proteins using autoimmune sera from patients with scleroderma. Chromosoma *91*, 313–321.

Efremov, A., Grishchuk, E.L., McIntosh, J.R., and Ataullakhanov, F.I. (2007). In search of an optimal ring to couple microtubule depolymerization to processive chromosome motions. PNAS *104*, 19017–19022.

Enquist-Newman, M., Cheeseman, I.M., Van Goor, D., Drubin, D.G., Meluh, P.B., and Barnes, G. (2001). Dad1p, Third Component of the Duo1p/Dam1p Complex Involved in Kinetochore Function and Mitotic Spindle Integrity. MBoC *12*, 2601–2613.

Fairbanks, G., Steck, T.L., and Wallach, D.F.H. (1971). Electrophoretic analysis of the major polypeptides of the human erythrocyte membrane. Biochemistry *10*, 2606–2617.

Fischböck-Halwachs, J., Singh, S., Potocnjak, M., Hagemann, G., Solis-Mezarino, V., Woike, S., Ghodgaonkar-Steger, M., Weissmann, F., Gallego, L.D., Rojas, J., et al. (2019). The COMA complex interacts with Cse4 and positions Sli15/Ipl1 at the budding yeast inner kinetochore. Elife *8*.

Furuyama, S., and Biggins, S. (2007). Centromere identity is specified by a single centromeric nucleosome in budding yeast. PNAS *104*, 14706–14711.

Gaitanos, T.N., Santamaria, A., Jeyaprakash, A.A., Wang, B., Conti, E., and Nigg, E.A. (2009). Stable kinetochore–microtubule interactions depend on the Ska complex and its new component Ska3/C13Orf3. The EMBO Journal *28*, 1442–1452.

García-Rodríguez, L.J., Kasciukovic, T., Denninger, V., and Tanaka, T.U. (2019). Aurora B-INCENP Localization at Centromeres/Inner Kinetochores Is Required for Chromosome Bi-orientation in Budding Yeast. Current Biology *29*, 1536-1544.e4.

Gestaut, D.R., Graczyk, B., Cooper, J., Widlund, P.O., Zelter, A., Wordeman, L., Asbury, C.L., and Davis, T.N. (2008). Phosphoregulation and depolymerization-driven movement of the Dam1 complex do not require ring formation. Nat Cell Biol *10*, 407–414.

Ghodgaonkar-Steger, M., Potocnjak, M., Zimniak, T., Fischböck-Halwachs, J., Solis-Mezarino, V., Singh, S., Speljko, T., Hagemann, G., Drexler, D.J., Witte, G., et al. (2020). C-Terminal Motifs of the MTW1 Complex Cooperatively Stabilize Outer Kinetochore Assembly in Budding Yeast. Cell Reports *32*, 108190.

Goebl, M.G., Yochem, J., Jentsch, S., McGrath, J.P., Varshavsky, A., and Byers, B. (1988). The yeast cell cycle gene CDC34 encodes a ubiquitin-conjugating enzyme. Science *241*, 1331–1335.

Gordon, D.J., Resio, B., and Pellman, D. (2012). Causes and consequences of aneuploidy in cancer. Nat. Rev. Genet. *13*, 189–203.

Grimm, M., Zimniak, T., Kahraman, A., and Herzog, F. (2015). xVis: a web server for the schematic visualization and interpretation of crosslink-derived spatial restraints. Nucleic Acids Res. *43*, W362-369.

Grishchuk, E.L., Efremov, A.K., Volkov, V.A., Spiridonov, I.S., Gudimchuk, N., Westermann, S., Drubin, D., Barnes, G., McIntosh, J.R., and Ataullakhanov, F.I. (2008a). The Dam1 ring binds microtubules strongly enough to be a processive as well as energy-efficient coupler for chromosome motion. PNAS *105*, 15423–15428.

Grishchuk, E.L., Spiridonov, I.S., Volkov, V.A., Efremov, A., Westermann, S., Drubin, D., Barnes, G., Ataullakhanov, F.I., and McIntosh, J.R. (2008b). Different assemblies of the DAM1 complex follow shortening microtubules by distinct mechanisms. Proc Natl Acad Sci U S A *105*, 6918–6923.

Guimaraes, G.J., Dong, Y., McEwen, B.F., and DeLuca, J.G. (2008). Kinetochore-Microtubule Attachment Relies on the Disordered N-Terminal Tail Domain of Hec1. Current Biology *18*, 1778–1784.

Gutierrez, A., Kim, J. ook, Umbreit, N.T., Asbury, C.L., Davis, T.N., Miller, M.P., and Biggins, S. (2020). Cdk1 Phosphorylation of the Dam1 Complex Strengthens Kinetochore-Microtubule Attachments. Current Biology.

Hadders, M.A., Hindriksen, S., Truong, M.A., Mhaskar, A.N., Wopken, J.P., Vromans, M.J.M., and Lens, S.M.A. (2020). Untangling the contribution of Haspin and Bub1 to Aurora B function during mitosis. Journal of Cell Biology *219*.

Hanisch, A., Silljé, H.H., and Nigg, E.A. (2006). Timely anaphase onset requires a novel spindle and kinetochore complex comprising Ska1 and Ska2. The EMBO Journal *25*, 5504–5515.

Hardwick, K.G., Weiss, E., Luca, F.C., Winey, M., and Murray, A.W. (1996). Activation of the budding yeast spindle assembly checkpoint without mitotic spindle disruption. Science *273*, 953–956.

Haruki, H., Nishikawa, J., and Laemmli, U.K. (2008). The Anchor-Away Technique: Rapid, Conditional Establishment of Yeast Mutant Phenotypes. Molecular Cell *31*, 925–932.

Hauf, S., Cole, R.W., LaTerra, S., Zimmer, C., Schnapp, G., Walter, R., Heckel, A., van Meel, J., Rieder, C.L., and Peters, J.-M. (2003). The small molecule Hesperadin reveals a role for Aurora B in correcting kinetochore-microtubule attachment and in maintaining the spindle assembly checkpoint. J. Cell Biol. *161*, 281–294.

Hayashi, I., and Ikura, M. (2003). Crystal structure of the amino-terminal microtubule-binding domain of end-binding protein 1 (EB1). J. Biol. Chem. *278*, 36430–36434.

Herman, J.A., Miller, M.P., and Biggins, S. (2020). chTOG is a conserved mitotic error correction factor. ELife *9*, e61773.

Herskowitz, I. (1988). Life cycle of the budding yeast Saccharomyces cerevisiae. Microbiology and Molecular Biology Reviews *52*, 536–553.

Herzog, F., Kahraman, A., Boehringer, D., Mak, R., Bracher, A., Walzthoeni, T., Leitner, A., Beck, M., Hartl, F.-U., Ban, N., et al. (2012). Structural probing of a protein phosphatase 2A network by chemical cross-linking and mass spectrometry. Science *337*, 1348–1352.

Higuchi, T., and Uhlmann, F. (2005). Stabilization of microtubule dynamics at anaphase onset promotes chromosome segregation. Nature *433*, 171–176.

Hiruma, Y., Sacristan, C., Pachis, S.T., Adamopoulos, A., Kuijt, T., Ubbink, M., Castelmur, E. von, Perrakis, A., and Kops, G.J.P.L. (2015). Competition between MPS1 and microtubules at kinetochores regulates spindle checkpoint signaling. Science *348*, 1264–1267.

Hofmann, C., Cheeseman, I.M., Goode, B.L., McDonald, K.L., Barnes, G., and Drubin, D.G. (1998). Saccharomyces cerevisiae Duo1p and Dam1p, Novel Proteins Involved in Mitotic Spindle Function. Journal of Cell Biology *143*, 1029–1040.

Holder, J., Poser, E., and Barr, F.A. (2019). Getting out of mitosis: spatial and temporal control of mitotic exit and cytokinesis by PP1 and PP2A. FEBS Letters *593*, 2908–2924.

Honnappa, S., John, C.M., Kostrewa, D., Winkler, F.K., and Steinmetz, M.O. (2005). Structural insights into the EB1–APC interaction. The EMBO Journal *24*, 261–269.

Honnappa, S., Gouveia, S.M., Weisbrich, A., Damberger, F.F., Bhavesh, N.S., Jawhari, H., Grigoriev, I., van Rijssel, F.J.A., Buey, R.M., Lawera, A., et al. (2009). An EB1-binding motif acts as a microtubule tip localization signal. Cell *138*, 366–376.

van Hooff, J.J.E., Snel, B., and Kops, G.J.P.L. (2017). Unique Phylogenetic Distributions of the Ska and Dam1 Complexes Support Functional Analogy and Suggest Multiple Parallel Displacements of Ska by Dam1. Genome Biol Evol *9*, 1295–1303.

Hornung, P., Troc, P., Malvezzi, F., Maier, M., Demianova, Z., Zimniak, T., Litos, G., Lampert, F., Schleiffer, A., Brunner, M., et al. (2014). A cooperative mechanism drives budding yeast kinetochore assembly downstream of CENP-A. Journal of Cell Biology *206*, 509–524.

Howell, B.J., McEwen, B.F., Canman, J.C., Hoffman, D.B., Farrar, E.M., Rieder, C.L., and Salmon, E.D. (2001). Cytoplasmic dynein/dynactin drives kinetochore protein transport to the spindle poles and has a role in mitotic spindle checkpoint inactivation. Journal of Cell Biology *155*, 1159–1172.

Howes, S.C., Geyer, E.A., LaFrance, B., Zhang, R., Kellogg, E.H., Westermann, S., Rice, L.M., and Nogales, E. (2017). Structural differences between yeast and mammalian microtubules revealed by cryo-EM. J. Cell Biol. *216*, 2669–2677.

Howes, S.C., Geyer, E.A., LaFrance, B., Zhang, R., Kellogg, E.H., Westermann, S., Rice, L.M., and Nogales, E. (2018). Structural and functional differences between porcine brain and budding yeast microtubules. Cell Cycle *17*, 278–287.

Huis in 't Veld, P.J., Volkov, V.A., Stender, I.D., Musacchio, A., and Dogterom, M. (2019). Molecular determinants of the Ska-Ndc80 interaction and their influence on microtubule tracking and force-coupling. ELife *8*, e49539.

Ito, T., Chiba, T., Ozawa, R., Yoshida, M., Hattori, M., and Sakaki, Y. (2001). A comprehensive two-hybrid analysis to explore the yeast protein interactome. Proc. Natl. Acad. Sci. U.S.A. *98*, 4569–4574.

Janczyk, P.Ł., Skorupka, K.A., Tooley, J.G., Matson, D.R., Kestner, C.A., West, T., Pornillos, O., and Stukenberg, P.T. (2017). Mechanism of Ska Recruitment by Ndc80 Complexes to Kinetochores. Developmental Cell *41*, 438-449.e4.

Janke, C., Ortíz, J., Tanaka, T.U., Lechner, J., and Schiebel, E. (2002). Four new subunits of the Dam1–Duo1 complex reveal novel functions in sister kinetochore biorientation. The EMBO Journal *21*, 181–193.

Janke, C., Magiera, M.M., Rathfelder, N., Taxis, C., Reber, S., Maekawa, H., Moreno-Borchart, A., Doenges, G., Schwob, E., Schiebel, E., et al. (2004). A versatile toolbox for PCR-based tagging of yeast genes: new fluorescent proteins, more markers and promoter substitution cassettes. Yeast *21*, 947–962.

Jansen, L.E.T., Black, B.E., Foltz, D.R., and Cleveland, D.W. (2007). Propagation of centromeric chromatin requires exit from mitosis. Journal of Cell Biology *176*, 795–805.

Jenni, S., and Harrison, S.C. (2018). Structure of the DASH/Dam1 complex shows its role at the yeast kinetochore-microtubule interface. Science *360*, 552–558.

Jeyaprakash, A.A., Santamaria, A., Jayachandran, U., Chan, Y.W., Benda, C., Nigg, E.A., and Conti, E. (2012). Structural and Functional Organization of the Ska Complex, a Key Component of the Kinetochore-Microtubule Interface. Molecular Cell *46*, 274–286.

Ji, Z., Gao, H., and Yu, H. (2015). Kinetochore attachment sensed by competitive Mps1 and microtubule binding to Ndc80C. Science *348*, 1260–1264.

Joglekar, A.P., Bouck, D.C., Molk, J.N., Bloom, K.S., and Salmon, E.D. (2006). Molecular architecture of a kinetochore–microtubule attachment site. Nat Cell Biol *8*, 581–585.

Jones, M.H., Bachant, J.B., Castillo, A.R., Giddings, T.H., and Winey, M. (1999). Yeast Dam1p Is Required to Maintain Spindle Integrity during Mitosis and Interacts with the Mps1p Kinase. MBoC *10*, 2377–2391.

Jones, M.H., He, X., Giddings, T.H., and Winey, M. (2001). Yeast Dam1p has a role at the kinetochore in assembly of the mitotic spindle. PNAS *98*, 13675–13680.

Jones, M.H., Huneycutt, B.J., Pearson, C.G., Zhang, C., Morgan, G., Shokat, K., Bloom, K., and Winey, M. (2005). Chemical genetics reveals a role for Mps1 kinase in kinetochore attachment during mitosis. Curr. Biol. *15*, 160–165.

Jumper, J., Evans, R., Pritzel, A., Green, T., Figurnov, M., Ronneberger, O., Tunyasuvunakool, K., Bates, R., Žídek, A., Potapenko, A., et al. (2021). Highly accurate protein structure prediction with AlphaFold. Nature *596*, 583–589.

Kalantzaki, M., Kitamura, E., Zhang, T., Mino, A., Novák, B., and Tanaka, T.U. (2015). Kinetochore-microtubule error correction is driven by differentially regulated interaction modes. Nat. Cell Biol. *17*, 421–433.

Kang, J., Cheeseman, I.M., Kallstrom, G., Velmurugan, S., Barnes, G., and Chan, C.S.M. (2001). Functional cooperation of Dam1, Ipl1, and the inner centromere protein (INCENP)–related protein Sli15 during chromosome segregation. Journal of Cell Biology *155*, 763–774.

Katoh, K., Rozewicki, J., and Yamada, K.D. (2019). MAFFT online service: multiple sequence alignment, interactive sequence choice and visualization. Briefings in Bioinformatics *20*, 1160–1166.

Keating, P., Rachidi, N., Tanaka, T.U., and Stark, M.J.R. (2009). Ipl1-dependent phosphorylation of Dam1 is reduced by tension applied on kinetochores. J Cell Sci *122*, 4375–4382.

Kemmler, S., Stach, M., Knapp, M., Ortiz, J., Pfannstiel, J., Ruppert, T., and Lechner, J. (2009). Mimicking Ndc80 phosphorylation triggers spindle assembly checkpoint signalling. The EMBO Journal *28*, 1099–1110.

Kiermaier, E., Woehrer, S., Peng, Y., Mechtler, K., and Westermann, S. (2009). A Dam1-based artificial kinetochore is sufficient to promote chromosome segregation in budding yeast. Nat. Cell Biol. *11*, 1109–1115.

Kim, J. ook, Zelter, A., Umbreit, N.T., Bollozos, A., Riffle, M., Johnson, R., MacCoss, M.J., Asbury, C.L., and Davis, T.N. (2017). The Ndc80 complex bridges two Dam1 complex rings. ELife *6*, e21069.

Klare, K., Weir, J.R., Basilico, F., Zimniak, T., Massimiliano, L., Ludwigs, N., Herzog, F., and Musacchio, A. (2015). CENP-C is a blueprint for constitutive centromere–associated network assembly within human kinetochores. Journal of Cell Biology *210*, 11–22.

Kolenda, C., Ortiz, J., Pelzl, M., Norell, S., Schmeiser, V., and Lechner, J. (2018). Unattached kinetochores drive their own capturing by sequestering a CLASP. Nat Commun *9*, 886.

Kornakov, N., Möllers, B., and Westermann, S. (2020). The EB1–Kinesin-14 complex is required for efficient metaphase spindle assembly and kinetochore bi-orientation. Journal of Cell Biology *219*.

Koshland, D.E., Mitchison, T.J., and Kirschner, M.W. (1988). Polewards chromosome movement driven by microtubule depolymerization in vitro. Nature *331*, 499–504.

Kushnirov, V.V. (2000). Rapid and reliable protein extraction from yeast. Yeast *16*, 857–860.

Lacefield, S., Lau, D.T.C., and Murray, A.W. (2009). Recruiting a microtubule-binding complex to DNA directs chromosome segregation in budding yeast. Nat Cell Biol *11*, 1116–1120.

Lampert, F., Hornung, P., and Westermann, S. (2010). The Dam1 complex confers microtubule plus end–tracking activity to the Ndc80 kinetochore complex. The Journal of Cell Biology *189*, 641–649.

Lampert, F., Mieck, C., Alushin, G.M., Nogales, E., and Westermann, S. (2013). Molecular requirements for the formation of a kinetochore-microtubule interface by Dam1 and Ndc80 complexes. J. Cell Biol. *200*, 21–30.

Lechner, J., and Carbon, J. (1991). A 240 kd multisubunit protein complex, CBF3, is a major component of the budding yeast centromere. Cell *64*, 717–725.

Lee, S., Lim, W.A., and Thorn, K.S. (2013). Improved blue, green, and red fluorescent protein tagging vectors for S. cerevisiae. PLoS ONE *8*, e67902.

Legal, T., Zou, J., Sochaj, A., Rappsilber, J., and Welburn, J.P.I. (2016). Molecular architecture of the Dam1 complex-microtubule interaction. Open Biol *6*.

Li, G., and Moore, J.K. (2020). Microtubule dynamics at low temperature: evidence that tubulin recycling limits assembly. MBoC *31*, 1154–1166.

Li, Y., and Elledge, S.J. (2003). The DASH Complex Component Ask1 Is a Cell Cycle-Regulated Cdk Substrate in Saccharomyces cerevisiae. Cell Cycle *2*, 144–149.

Li, J., Li, Y., and Elledge, S.J. (2005). Genetic analysis of the kinetochore DASH complex reveals an antagonistic relationship with the ras/protein kinase A pathway and a novel subunit required for Ask1 association. Mol Cell Biol *25*, 767–778.

Li, Y., Bachant, J., Alcasabas, A.A., Wang, Y., Qin, J., and Elledge, S.J. (2002). The mitotic spindle is required for loading of the DASH complex onto the kinetochore. Genes Dev. *16*, 183–197.

London, N., Ceto, S., Ranish, J.A., and Biggins, S. (2012). Phosphoregulation of Spc105 by Mps1 and PP1 regulates Bub1 localization to kinetochores. Curr. Biol. *22*, 900–906.

Longtine, M.S., McKenzie, A., Demarini, D.J., Shah, N.G., Wach, A., Brachat, A., Philippsen, P., and Pringle, J.R. (1998). Additional modules for versatile and economical PCR-based gene deletion and modification in Saccharomyces cerevisiae. Yeast *14*, 953–961.

Malvezzi, F., Litos, G., Schleiffer, A., Heuck, A., Mechtler, K., Clausen, T., and Westermann, S. (2013). A structural basis for kinetochore recruitment of the Ndc80 complex via two distinct centromere receptors. The EMBO Journal *32*, 409–423.

Manning, A.L., Bakhoum, S.F., Maffini, S., Correia-Melo, C., Maiato, H., and Compton, D.A. (2010). CLASP1, astrin and Kif2b form a molecular switch that regulates kinetochore-microtubule dynamics to promote mitotic progression and fidelity. EMBO J *29*, 3531–3543.

Maure, J.-F., Kitamura, E., and Tanaka, T.U. (2007). Mps1 kinase promotes sister-kinetochore bi-orientation by a tension-dependent mechanism. Curr. Biol. *17*, 2175–2182.

Maure, J.-F., Komoto, S., Oku, Y., Mino, A., Pasqualato, S., Natsume, K., Clayton, L., Musacchio, A., and Tanaka, T.U. (2011). The Ndc80 Loop Region Facilitates Formation of Kinetochore Attachment to the Dynamic Microtubule Plus End. Current Biology *21*, 207–213.

Meluh, P.B., Yang, P., Glowczewski, L., Koshland, D., and Smith, M.M. (1998). Cse4p is a component of the core centromere of Saccharomyces cerevisiae. Cell *94*, 607–613.

Meyer, R.E., Brown, J., Beck, L., and Dawson, D.S. (2018). Mps1 promotes chromosome meiotic chromosome biorientation through Dam1. MBoC *29*, 479–489.

Miller, M.P., Ünal, E., Brar, G.A., and Amon, A. (2012). Meiosis I chromosome segregation is established through regulation of microtubule–kinetochore interactions. ELife *1*, e00117.

Miller, M.P., Asbury, C.L., and Biggins, S. (2016). A TOG Protein Confers Tension Sensitivity to Kinetochore-Microtubule Attachments. Cell *165*, 1428–1439.

Miller, M.P., Evans, R.K., Zelter, A., Geyer, E.A., MacCoss, M.J., Rice, L.M., Davis, T.N., Asbury, C.L., and Biggins, S. (2019). Kinetochore-associated Stu2 promotes chromosome biorientation in vivo. PLOS Genetics *15*, e1008423.

Miller, S.A., Johnson, M.L., and Stukenberg, P.T. (2008). Kinetochore Attachments Require an Interaction between Unstructured Tails on Microtubules and Ndc80Hec1. Current Biology *18*, 1785–1791.

Miranda, J.J.L., De Wulf, P., Sorger, P.K., and Harrison, S.C. (2005). The yeast DASH complex forms closed rings on microtubules. Nat. Struct. Mol. Biol. *12*, 138–143.

Miranda, J.L., King, D.S., and Harrison, S.C. (2007). Protein Arms in the Kinetochore-Microtubule Interface of the Yeast DASH Complex. MBoC *18*, 2503–2510.

Monda, J.K., Whitney, I.P., Tarasovetc, E.V., Wilson-Kubalek, E., Milligan, R.A., Grishchuk, E.L., and Cheeseman, I.M. (2017). Microtubule Tip Tracking by the Spindle and Kinetochore Protein Ska1 Requires Diverse Tubulin-Interacting Surfaces. Current Biology *27*, 3666-3675.e6.

Morgan, D.O. (2006). The Cell Cycle: Principles of control (London: New Science Press Ltd).

Moriya, T., Saur, M., Stabrin, M., Merino, F., Voicu, H., Huang, Z., Penczek, P.A., Raunser, S., and Gatsogiannis, C. (2017). High-resolution Single Particle Analysis from Electron Cryo-microscopy Images Using SPHIRE. J Vis Exp.

Musacchio, A. (2015). The Molecular Biology of Spindle Assembly Checkpoint Signaling Dynamics. Curr. Biol. *25*, R1002-1018.

Musacchio, A., and Desai, A. (2017). A Molecular View of Kinetochore Assembly and Function. Biology *6*, 5.

Ng, C.T., Deng, L., Chen, C., Lim, H.H., Shi, J., Surana, U., and Gan, L. (2019). Electron cryotomography analysis of Dam1C/DASH at the kinetochore-spindle interface in situ. J. Cell Biol. *218*, 455–473.

Nijenhuis, W., Vallardi, G., Teixeira, A., Kops, G.J.P.L., and Saurin, A.T. (2014). Negative feedback at kinetochores underlies a responsive spindle checkpoint signal. Nature Cell Biology *16*, 1257–1264.

Nishimura, K., Fukagawa, T., Takisawa, H., Kakimoto, T., and Kanemaki, M. (2009). An auxin-based degron system for the rapid depletion of proteins in nonplant cells. Nat. Methods *6*, 917–922.

Nishino, T., Rago, F., Hori, T., Tomii, K., Cheeseman, I.M., and Fukagawa, T. (2013). CENP-T provides a structural platform for outer kinetochore assembly. The EMBO Journal *32*, 424–436.

Nobel Prize Committee (2001). The Nobel Prize in Physiology or Medicine 2001. NobelPrize.Org.

Örd, M., and Loog, M. (2019). How the cell cycle clock ticks. MBoC *30*, 169–172.

Ortiz, J., Funk, C., Schäfer, A., and Lechner, J. (2009). Stu1 inversely regulates kinetochore capture and spindle stability. Genes Dev. *23*, 2778–2791.

Pekgöz Altunkaya, G., Malvezzi, F., Demianova, Z., Zimniak, T., Litos, G., Weissmann, F., Mechtler, K., Herzog, F., and Westermann, S. (2016). CCAN Assembly Configures Composite Binding Interfaces to Promote Cross-Linking of Ndc80 Complexes at the Kinetochore. Current Biology *26*, 2370–2378.

Perez-Riverol, Y., Csordas, A., Bai, J., Bernal-Llinares, M., Hewapathirana, S., Kundu, D.J., Inuganti, A., Griss, J., Mayer, G., Eisenacher, M., et al. (2019). The PRIDE database and related tools and resources in 2019: improving support for quantification data. Nucleic Acids Research *47*, D442–D450.

Pesenti, M.E., Weir, J.R., and Musacchio, A. (2016). Progress in the structural and functional characterization of kinetochores. Current Opinion in Structural Biology *37*, 152–163.

Peters, J.-M. (2006). The anaphase promoting complex/cyclosome: a machine designed to destroy. Nat Rev Mol Cell Biol *7*, 644–656.

Petrovic, A., Pasqualato, S., Dube, P., Krenn, V., Santaguida, S., Cittaro, D., Monzani, S., Massimiliano, L., Keller, J., Tarricone, A., et al. (2010). The MIS12 complex is a protein interaction hub for outer kinetochore assembly. Journal of Cell Biology *190*, 835–852.

Petrovic, A., Mosalaganti, S., Keller, J., Mattiuzzo, M., Overlack, K., Krenn, V., De Antoni, A., Wohlgemuth, S., Cecatiello, V., Pasqualato, S., et al. (2014). Modular Assembly of RWD Domains on the Mis12 Complex Underlies Outer Kinetochore Organization. Molecular Cell *53*, 591–605.

Petrovic, A., Keller, J., Liu, Y., Overlack, K., John, J., Dimitrova, Y.N., Jenni, S., van Gerwen, S., Stege, P., Wohlgemuth, S., et al. (2016). Structure of the MIS12 Complex and Molecular Basis of Its Interaction with CENP-C at Human Kinetochores. Cell *167*, 1028-1040.e15.

Pettersen, E.F., Goddard, T.D., Huang, C.C., Couch, G.S., Greenblatt, D.M., Meng, E.C., and Ferrin, T.E. (2004). UCSF Chimera--a visualization system for exploratory research and analysis. J Comput Chem *25*, 1605–1612.

Powers, A.F., Franck, A.D., Gestaut, D.R., Cooper, J., Gracyzk, B., Wei, R.R., Wordeman, L., Davis, T.N., and Asbury, C.L. (2009). The Ndc80 Kinetochore Complex Forms Load-Bearing Attachments to Dynamic Microtubule Tips via Biased Diffusion. Cell *136*, 865–875.

Primorac, I., Weir, J.R., Chiroli, E., Gross, F., Hoffmann, I., van Gerwen, S., Ciliberto, A., and Musacchio, A. (2013). Bub3 reads phosphorylated MELT repeats to promote spindle assembly checkpoint signaling. ELife *2*, e01030.

Raaijmakers, J.A., Tanenbaum, M.E., Maia, A.F., and Medema, R.H. (2009). RAMA1 is a novel kinetochore protein involved in kinetochore-microtubule attachment. J Cell Sci *122*, 2436–2445.

Ramey, V.H., Wang, H.-W., Nakajima, Y., Wong, A., Liu, J., Drubin, D., Barnes, G., and Nogales, E. (2011a). The Dam1 ring binds to the E-hook of tubulin and diffuses along the microtubule. Mol. Biol. Cell *22*, 457–466.

Ramey, V.H., Wong, A., Fang, J., Howes, S., Barnes, G., and Nogales, E. (2011b). Subunit organization in the Dam1 kinetochore complex and its ring around microtubules. Mol. Biol. Cell *22*, 4335–4342.

Redli, P.M., Gasic, I., Meraldi, P., Nigg, E.A., and Santamaria, A. (2016). The Ska complex promotes Aurora B activity to ensure chromosome biorientation. Journal of Cell Biology *215*, 77–93.

Rieder, C.L., Cole, R.W., Khodjakov, A., and Sluder, G. (1995). The checkpoint delaying anaphase in response to chromosome monoorientation is mediated by an inhibitory signal produced by unattached kinetochores. Journal of Cell Biology *130*, 941–948.

Santaguida, S., and Amon, A. (2015). Short- and long-term effects of chromosome mis-segregation and aneuploidy. Nature Reviews Molecular Cell Biology *16*, 473–485.

Sarangapani, K.K., Akiyoshi, B., Duggan, N.M., Biggins, S., and Asbury, C.L. (2013). Phosphoregulation promotes release of kinetochores from dynamic microtubules via multiple mechanisms. Proc. Natl. Acad. Sci. U.S.A. *110*, 7282–7287.

Saurin, A.T. (2018). Kinase and Phosphatase Cross-Talk at the Kinetochore. Front. Cell Dev. Biol. *6*.

Saurin, A.T., van der Waal, M.S., Medema, R.H., Lens, S.M.A., and Kops, G.J.P.L. (2011). Aurora B potentiates Mps1 activation to ensure rapid checkpoint establishment at the onset of mitosis. Nat Commun *2*, 316.

Schleiffer, A., Maier, M., Litos, G., Lampert, F., Hornung, P., Mechtler, K., and Westermann, S. (2012). CENP-T proteins are conserved centromere receptors of the Ndc80 complex. Nature Cell Biology *14*, 604–613.

Schmidt, J.C., Kiyomitsu, T., Hori, T., Backer, C.B., Fukagawa, T., and Cheeseman, I.M. (2010). Aurora B kinase controls the targeting of the Astrin–SKAP complex to bioriented kinetochores. Journal of Cell Biology *191*, 269–280.

Schmidt, J.C., Arthanari, H., Boeszoermenyi, A., Dashkevich, N.M., Wilson-Kubalek, E.M., Monnier, N., Markus, M., Oberer, M., Milligan, R.A., Bathe, M., et al. (2012). The Kinetochore-Bound Ska1 Complex Tracks Depolymerizing Microtubules and Binds to Curved Protofilaments. Developmental Cell *23*, 968–980.

Schneiter, R. (2004). Genetics, Molecular and Cell Biology of Yeast (Fribourg).

Schwartz, K., Richards, K., and Botstein, D. (1997). BIM1 Encodes a Microtubule-binding Protein in Yeast. MBoC *8*, 2677–2691.

Screpanti, E., De Antoni, A., Alushin, G.M., Petrovic, A., Melis, T., Nogales, E., and Musacchio, A. (2011). Direct Binding of Cenp-C to the Mis12 Complex Joins the Inner and Outer Kinetochore. Current Biology *21*, 391–398.

Shah, S.B., Parmiter, D., Constantine, C., Elizalde, P., Naldrett, M., Karpova, T.S., and Choy, J.S. (2019). Glucose Signaling Is Connected to Chromosome Segregation Through Protein Kinase A Phosphorylation of the Dam1 Kinetochore Subunit in Saccharomycescerevisiae. Genetics *211*, 531–547.

Shang, C., Hazbun, T.R., Cheeseman, I.M., Aranda, J., Fields, S., Drubin, D.G., and Barnes, G. (2003). Kinetochore Protein Interactions and their Regulation by the Aurora Kinase Ipl1p. MBoC *14*, 3342–3355.

Shepperd, L.A., Meadows, J.C., Sochaj, A.M., Lancaster, T.C., Zou, J., Buttrick, G.J., Rappsilber, J., Hardwick, K.G., and Millar, J.B.A. (2012). Phosphodependent Recruitment of Bub1 and Bub3 to Spc7/KNL1 by Mph1 Kinase Maintains the Spindle Checkpoint. Current Biology *22*, 891–899.

Sherman, F. (2002). Getting started with yeast. Methods Enzymol *350*, 3–41.

Shimogawa, M.M., Graczyk, B., Gardner, M.K., Francis, S.E., White, E.A., Ess, M., Molk, J.N., Ruse, C., Niessen, S., Yates, J.R., et al. (2006). Mps1 phosphorylation of Dam1 couples kinetochores to microtubule plus ends at metaphase. Curr. Biol. *16*, 1489–1501.

Sivakumar, S., Janczyk, P.Ł., Qu, Q., Brautigam, C.A., Stukenberg, P.T., Yu, H., and Gorbsky, G.J. (2016). The human SKA complex drives the metaphase-anaphase cell cycle transition by recruiting protein phosphatase 1 to kinetochores. ELife *5*, e12902.

Stangier, M.M., Kumar, A., Chen, X., Farcas, A.-M., Barral, Y., and Steinmetz, M.O. (2018). Structure-Function Relationship of the Bik1-Bim1 Complex. Structure *26*, 607-618.e4.

Stoler, S., Keith, K.C., Curnick, K.E., and Fitzgerald-Hayes, M. (1995). A mutation in CSE4, an essential gene encoding a novel chromatin-associated protein in yeast, causes chromosome nondisjunction and cell cycle arrest at mitosis. Genes Dev. *9*, 573–586.

Stoler, S., Rogers, K., Weitze, S., Morey, L., Fitzgerald-Hayes, M., and Baker, R.E. (2007). Scm3, an essential Saccharomyces cerevisiae centromere protein required for G2/M progression and Cse4 localization. PNAS *104*, 10571–10576.

Sullivan, K.F., Hechenberger, M., and Masri, K. (1994). Human CENP-A contains a histone H3 related histone fold domain that is required for targeting to the centromere. Journal of Cell Biology *127*, 581–592.

Tanaka, T.U., Rachidi, N., Janke, C., Pereira, G., Galova, M., Schiebel, E., Stark, M.J.R., and Nasmyth, K. (2002). Evidence that the Ipl1-Sli15 (Aurora kinase-INCENP) complex promotes chromosome bi-orientation by altering kinetochore-spindle pole connections. Cell *108*, 317–329.

Theis, M., Slabicki, M., Junqueira, M., Paszkowski-Rogacz, M., Sontheimer, J., Kittler, R., Heninger, A.-K., Glatter, T., Kruusmaa, K., Poser, I., et al. (2009). Comparative profiling identifies C13orf3 as a component of the Ska complex required for mammalian cell division. The EMBO Journal *28*, 1453–1465.

Thomas, G.E., Bandopadhyay, K., Sutradhar, S., Renjith, M.R., Singh, P., Gireesh, K.K., Simon, S., Badarudeen, B., Gupta, H., Banerjee, M., et al. (2016). EB1 regulates attachment of Ska1 with microtubules by forming extended structures on the microtubule lattice. Nat Commun *7*, 11665.

Tien, J.F., Umbreit, N.T., Gestaut, D.R., Franck, A.D., Cooper, J., Wordeman, L., Gonen, T., Asbury, C.L., and Davis, T.N. (2010). Cooperation of the Dam1 and Ndc80 kinetochore complexes enhances microtubule coupling and is regulated by aurora B. J. Cell Biol. *189*, 713–723.

Tien, J.F., Fong, K.K., Umbreit, N.T., Payen, C., Zelter, A., Asbury, C.L., Dunham, M.J., and Davis, T.N. (2013). Coupling Unbiased Mutagenesis to High-throughput DNA Sequencing Uncovers Functional Domains in the Ndc80 Kinetochore Protein of Saccharomyces cerevisiae. Genetics *195*, 159–170.

Tirnauer, J.S., Canman, J.C., Salmon, E. d., and Mitchison, T.J. (2002). EB1 Targets to Kinetochores with Attached, Polymerizing Microtubules. MBoC *13*, 4308–4316.

Tong, A.H.Y., Evangelista, M., Parsons, A.B., Xu, H., Bader, G.D., Pagé, N., Robinson, M., Raghibizadeh, S., Hogue, C.W.V., Bussey, H., et al. (2001). Systematic Genetic Analysis with Ordered Arrays of Yeast Deletion Mutants. Science *294*, 2364–2368.

Uetz, P., Giot, L., Cagney, G., Mansfield, T.A., Judson, R.S., Knight, J.R., Lockshon, D., Narayan, V., Srinivasan, M., Pochart, P., et al. (2000). A comprehensive analysis of protein–protein interactions in Saccharomyces cerevisiae. Nature *403*, 623–627.

Umbreit, N.T., Miller, M.P., Tien, J.F., Ortolá, J.C., Gui, L., Lee, K.K., Biggins, S., Asbury, C.L., and Davis, T.N. (2014). Kinetochores require oligomerization of Dam1 complex to maintain microtubule attachments against tension and promote biorientation. Nat Commun *5*, 4951.

Valverde, R., Ingram, J., and Harrison, S.C. (2016). Conserved Tetramer Junction in the Kinetochore Ndc80 Complex. Cell Reports *17*, 1915–1922.

Volkov, V.A., Zaytsev, A.V., Gudimchuk, N., Grissom, P.M., Gintsburg, A.L., Ataullakhanov, F.I., McIntosh, J.R., and Grishchuk, E.L. (2013). Long tethers provide high-force coupling of the Dam1 ring to shortening microtubules. Proc. Natl. Acad. Sci. U.S.A. *110*, 7708–7713.

Volkov, V.A., Huis in 't Veld, P.J., Dogterom, M., and Musacchio, A. (2018). Multivalency of NDC80 in the outer kinetochore is essential to track shortening microtubules and generate forces. ELife *7*, e36764.

Wagner, T., Merino, F., Stabrin, M., Moriya, T., Antoni, C., Apelbaum, A., Hagel, P., Sitsel, O., Raisch, T., Prumbaum, D., et al. (2019). SPHIRE-crYOLO is a fast and accurate fully automated particle picker for cryo-EM. Commun Biol *2*.

Wang, H.-W., Ramey, V.H., Westermann, S., Leschziner, A.E., Welburn, J.P.I., Nakajima, Y., Drubin, D.G., Barnes, G., and Nogales, E. (2007). Architecture of the Dam1 kinetochore ring complex and implications for microtubule-driven assembly and force-coupling mechanisms. Nat. Struct. Mol. Biol. *14*, 721–726.

Waterhouse, A.M., Procter, J.B., Martin, D.M.A., Clamp, M., and Barton, G.J. (2009). Jalview Version 2—a multiple sequence alignment editor and analysis workbench. Bioinformatics *25*, 1189–1191.

Wei, R.R., Schnell, J.R., Larsen, N.A., Sorger, P.K., Chou, J.J., and Harrison, S.C. (2006). Structure of a Central Component of the Yeast Kinetochore: The Spc24p/Spc25p Globular Domain. Structure *14*, 1003–1009.

Wei, R.R., Al-Bassam, J., and Harrison, S.C. (2007). The Ndc80/HEC1 complex is a contact point for kinetochore-microtubule attachment. Nature Structural & Molecular Biology *14*, 54–59.

Weir, J.R., Faesen, A.C., Klare, K., Petrovic, A., Basilico, F., Fischböck, J., Pentakota, S., Keller, J., Pesenti, M.E., Pan, D., et al. (2016). Insights from biochemical reconstitution into the architecture of human kinetochores. Nature *537*, 249–253.

Weisbrich, A., Honnappa, S., Jaussi, R., Okhrimenko, O., Frey, D., Jelesarov, I., Akhmanova, A., and Steinmetz, M.O. (2007). Structure-function relationship of CAP-Gly domains. Nat. Struct. Mol. Biol. *14*, 959–967.

Welburn, J.P.I., Grishchuk, E.L., Backer, C.B., Wilson-Kubalek, E.M., Yates, J.R., and Cheeseman, I.M. (2009). The Human Kinetochore Ska1 Complex Facilitates Microtubule Depolymerization-Coupled Motility. Developmental Cell *16*, 374–385.

Westermann, S., and Schleiffer, A. (2013). Family matters: structural and functional conservation of centromere-associated proteins from yeast to humans. Trends in Cell Biology *23*, 260–269.

Westermann, S., Avila-Sakar, A., Wang, H.-W., Niederstrasser, H., Wong, J., Drubin, D.G., Nogales, E., and Barnes, G. (2005). Formation of a dynamic kinetochore- microtubule interface through assembly of the Dam1 ring complex. Mol. Cell *17*, 277–290.

Westermann, S., Wang, H.-W., Avila-Sakar, A., Drubin, D.G., Nogales, E., and Barnes, G. (2006). The Dam1 kinetochore ring complex moves processively on depolymerizing microtubule ends. Nature *440*, 565–569.

Wilson-Kubalek, E.M., Cheeseman, I.M., Yoshioka, C., Desai, A., and Milligan, R.A. (2008). Orientation and structure of the Ndc80 complex on the microtubule lattice. J. Cell Biol. *182*, 1055–1061.

Wimbish, R.T., and DeLuca, J.G. (2020). Hec1/Ndc80 Tail Domain Function at the Kinetochore-Microtubule Interface. Front. Cell Dev. Biol. *8*.

Wimbish, R.T., DeLuca, K.F., Mick, J.E., Himes, J., Jiménez-Sánchez, I., Jeyaprakash, A.A., and DeLuca, J.G. (2020). The Hec1/Ndc80 tail domain is required for force generation at kinetochores, but is dispensable for kinetochore–microtubule attachment formation and Ska complex recruitment. MBoC *31*, 1453–1473.

Winey, M., and Bloom, K. (2012). Mitotic Spindle Form and Function. Genetics *190*, 1197–1224.

Winey, M., Goetsch, L., Baum, P., and Byers, B. (1991). MPS1 and MPS2: novel yeast genes defining distinct steps of spindle pole body duplication. Journal of Cell Biology *114*, 745–754.

Wojcik, E., Basto, R., Serr, M., Scaërou, F., Karess, R., and Hays, T. (2001). Kinetochore dynein: its dynamics and role in the transport of the Rough deal checkpoint protein. Nature Cell Biology *3*, 1001–1007.

Wolyniak, M.J., Blake-Hodek, K., Kosco, K., Hwang, E., You, L., and Huffaker, T.C. (2006). The Regulation of Microtubule Dynamics in Saccharomyces cerevisiae by Three Interacting Plus-End Tracking Proteins. MBoC *17*, 2789–2798.

Wong, J., Nakajima, Y., Westermann, S., Shang, C., Kang, J.-S., Goodner, C., Houshmand, P., Fields, S., Chan, C.S.M., Drubin, D., et al. (2007). A protein interaction map of the mitotic spindle. Mol. Biol. Cell *18*, 3800–3809.

Yamagishi, Y., Yang, C.-H., Tanno, Y., and Watanabe, Y. (2012). MPS1/Mph1 phosphorylates the kinetochore protein KNL1/Spc7 to recruit SAC components. Nature Cell Biology *14*, 746–752.

Yang, Z., Fang, J., Chittuluru, J., Asturias, F.J., and Penczek, P.A. (2012). Iterative Stable Alignment and Clustering of 2D Transmission Electron Microscope Images. Structure *20*, 237–247.

Zahm, J.A., Stewart, M.G., Carrier, J.S., Harrison, S.C., and Miller, M.P. (2021). Structural basis of Stu2 recruitment to yeast kinetochores. ELife *10*, e65389.

Zasadzińska, E., Huang, J., Bailey, A.O., Guo, L.Y., Lee, N.S., Srivastava, S., Wong, K.A., French, B.T., Black, B.E., and Foltz, D.R. (2018). Inheritance of CENP-A Nucleosomes during DNA Replication Requires HJURP. Developmental Cell *47*, 348-362.e7.

Zelter, A., Bonomi, M., Kim, J. ook, Umbreit, N.T., Hoopmann, M.R., Johnson, R., Riffle, M., Jaschob, D., MacCoss, M.J., Moritz, R.L., et al. (2015). The molecular architecture of the Dam1 kinetochore complex is defined by cross-linking based structural modelling. Nat Commun *6*, 8673.

Zhang, G., Kelstrup, C.D., Hu, X.-W., Kaas Hansen, M.J., Singleton, M.R., Olsen, J.V., and Nilsson, J. (2012). The Ndc80 internal loop is required for recruitment of the Ska complex to establish end-on microtubule attachment to kinetochores. Journal of Cell Science *125*, 3243–3253.

Zhang, Q., Sivakumar, S., Chen, Y., Gao, H., Yang, L., Yuan, Z., Yu, H., and Liu, H. (2017). Ska3 Phosphorylated by Cdk1 Binds Ndc80 and Recruits Ska to Kinetochores to Promote Mitotic Progression. Current Biology *27*, 1477-1484.e4.

Zimniak, T., Stengl, K., Mechtler, K., and Westermann, S. (2009). Phosphoregulation of the budding yeast EB1 homologue Bim1p by Aurora/Ipl1p. J. Cell Biol. *186*, 379–391.

Zimniak, T., Fitz, V., Zhou, H., Lampert, F., Opravil, S., Mechtler, K., Stolt-Bergner, P., and Westermann, S. (2012). Spatiotemporal regulation of Ipl1/Aurora activity by direct Cdk1 phosphorylation. Curr. Biol. *22*, 787–793.

6. Appendix

6.1. Appendix Figures

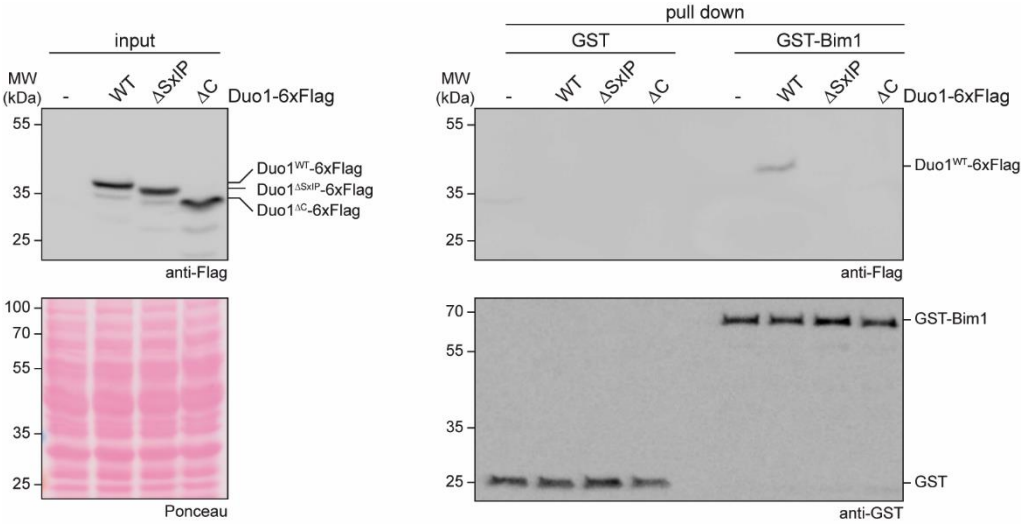

Appendix Figure 1: Deletion of the C-terminus of Duo1 abolishes Bim1 binding
Soluble cell extracts from yeast strains with 6xFlag-tagged Duo1^{WT}, Duo1$^{\Delta SxIP}$ and Duo1$^{\Delta C}$ were prepared and incubated with immobilized GST-Bim1. Binding of Duo1 to Bim1 was detected by western blot analysis of input and pull down samples. A strain with untagged Duo1 was used as control for unspecific binding of the anti-Flag antibody.

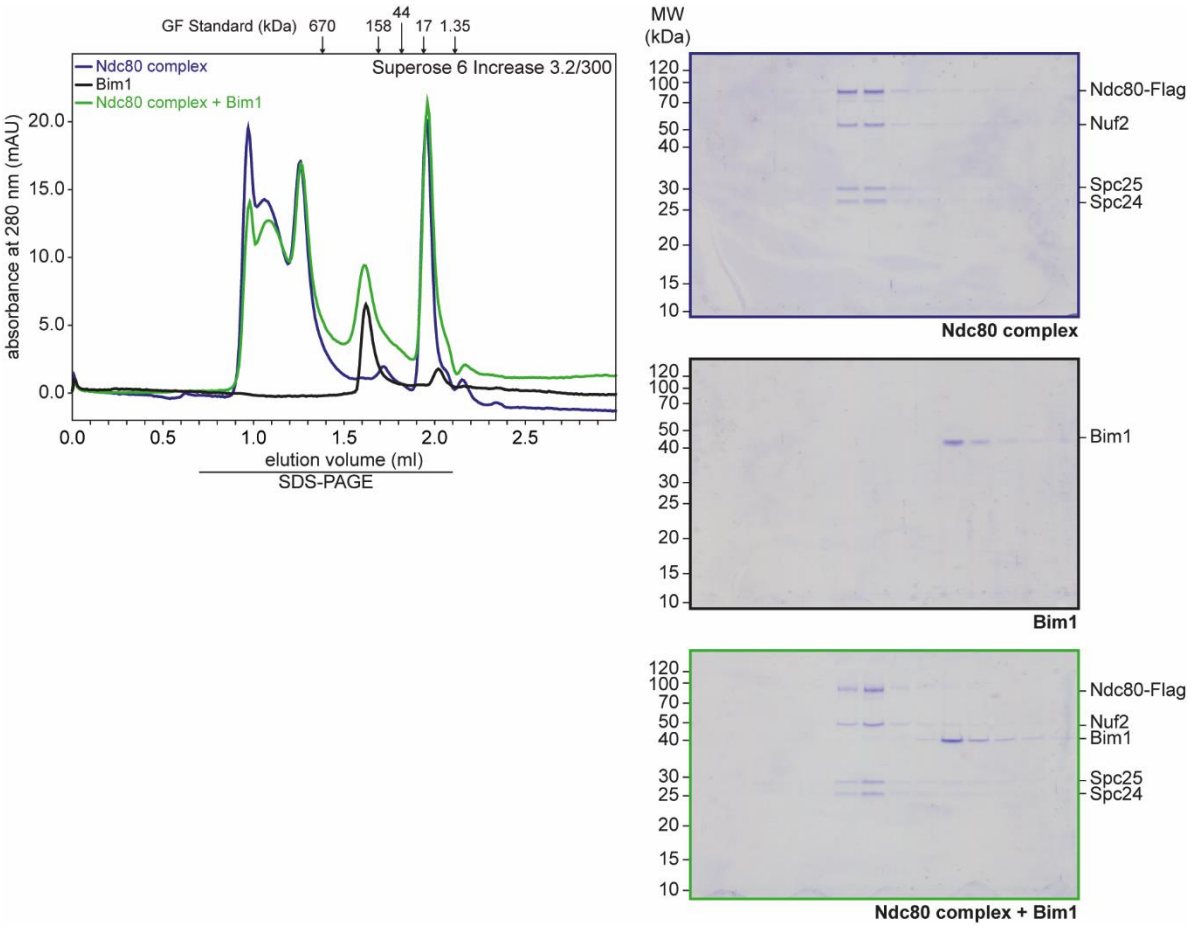

Appendix Figure 2: Bim1 does not bind Ndc80c in solution
Binding of Bim1 to Ndc80c was probed by analytical SEC. Chromatograms of individual SEC runs are shown on the left. Elution fractions were analyzed by SDS-PAGE which is shown on the right.

6.2. Appendix Tables

Appendix Table 1: List of crosslinks between Dam1c and Bim1

Protein	Position	Position in Bim1
Spc34	K46	K110
Spc34	K46	K134
Spc34	K46	K145
Spc34	K70	K145
Spc34	K169	K145
Spc34	K249	K145
Spc34	K274	K145
Dam1	K252	K110
Dam1	K252	K145
Dam1	K307	K110
Dam1	K307	K223
Dam1	K320	K110
Dam1	K320	K145
Spc19	K79	K110
Spc19	K79	K122
Spc19	K79	K145
Dad4	K21	K145
Duo1	K236	K223

Appendix Table 2: List of crosslinks between Duo1 and Spc19 or Spc34 in the presence of Bim1

Protein	Position	Position in Duo1
Spc34	K70	K33
Spc34	K94	K33
Spc34	K70	K36
Spc34	K46	K215
Spc34	K46	K236
Spc34	K65	K236
Spc34	K70	K236
Spc34	K126	K236
Spc19	K79	K183
Spc19	K76	K236

Appendix Table 3: List of crosslinks between the Dam1 C-terminus and Duo1

Position in Dam1	Position in Duo1
K252	K169
K252	K177
K252	K183
K252	K215
K252	K236
K256	K131
K256	K169
K256	K236
K307	K169
K307	K183
K307	K215
K307	K236
K320	K169
K320	K174
K320	K215
K320	K236

6.3. Movie legends

Movies from live cell fluorescence microscopy were submitted as AVI files.

Movie 1: Live cell fluorescence microscopy of Duo1^{WT} (upper panel) and Duo1$^{\Delta SxIP}$ (lower panel) cells during mitosis. Dam1c was visualized by C-terminal fusion of the Dad1 subunit to GFP. Brightfield images are shown on the left side, Dad1-GFP on the right side. Images were taken every minute over a total time of 45 minutes. Scale bar: 2 µm.

Movie 2: Live cell fluorescence microscopy of Bim1^{WT} (upper panel) and *bim1*Δ (lower panel) cells during mitosis. C-terminal fusion of Dad1-GFP allowed to visualize the localization of Dam1c. Brightfield images are depicted on the left side, Dad1-GFP on the right side. Images were taken every minute over a total time of 30 minutes. Please note that Dad1-GFP clusters are not separated in the *bim1*Δ strain due to a short mitotic spindle. Scale bar: 2 µm.

7. Data availability

Mass spectrometry data of crosslinked Dam1c and Dam1c-Bim1 complex have been deposited to the ProteomeXchange Consortium via the PRIDE (Perez-Riverol et al., 2019) partner repository with the dataset identifier PXD026935 (https://www.ebi.ac.uk/pride/archive/projects/PXD026935).

The electron microscopy data have been deposited to the Electron Microscopy Data Bank (EMDB, https://www.ebi.ac.uk/emdb/) with the identifier EMD-13152 for Dam1c and EMD-13151 for Dam1c-Bim1 complex.

Movies were submitted together with an electronic version of the thesis.

Acknowledgements

Many people accompanied me on my way to finishing this project and writing this thesis. All of these persons deserve my gratitude.

I thank Prof. Dr. Stefan Westermann, my supervisor and mentor over the past years, for the opportunity to work on the fascinating topic of the Dam1 complex, never-ending technical and scientific support and teaching me how to make good science. Whenever my project was stuck at some point, Stefan's input helped me to find a solution and develop my project in a successful direction.

I sincerely thank Prof. Dr. Andrea Musacchio and Prof. Dr. Thomas U. Mayer for reviewing my thesis.

Dr. Kerstin Killinger and Dr. Miriam Böhm for the warm welcome when I joined the lab as master student, endless supply with cake (I will never forget the three-tier cake that Kerstin made for my birthday two weeks after I had joined the lab), scientific and non-scientific advice in any situation, lots of fun and a positive lab atmosphere. Further thank goes to Miriam for our successful attendance at the Dynamic Kinetochore Workshop 2019 and being a good chief-supervisor during practical courses.

I thank Karolin Jänen for technical support, especially for preparation and analysis of FACS samples, but even more for being a great office mate, finding solutions to any problem and conversations beyond science. Together with Miriam, she keeps the lab running.

Dr. Nikolay Kornakov, a good colleague from the very beginning, Mensa companion and always keen to debate, for important technical support and sharing reagents.

Furthermore, I thank Simone Hohoff and my younger PhD siblings Sharvari Tendulkar, Jonas Neblik, Jennifer Harris and Christian Cozma for scientific discussion and diversion between the lab work.

Stephanie Rabe and Rita Nadorf do and did an excellent job in the administration of our lab.

Dr. Gerben Vader and Prof. Dr. Michael Ehrmann as members of my thesis advisory committee for their valuable advice and support for my project from the very beginning. Furthermore, I am very thankful to Michael Ehrmann for mentoring during my early master studies.

Prof. Dr. Christos Gatsogiannis, Lena Engelhard, Dr. Björn Udo Klink and Cole Bourque for electron microscopy of Dam1c, Bim1 and Bik1 and Dr. Franz Herzog and Pascaline Rombaut for analysis of crosslinked Dam1c-Bim1 complex.

Prof. Dr. Dominik Boos for scientific support and mentoring, and all members of the Boos lab for their input to further develop my project.

Christa Hornemann and Dr. Lucia Sironi from the IMPRS-LM coordination office who do a fantastic job in organizing the graduate school, care about the issues of the students and never lose the overview over the growing IMPRS community.

Dr. Lydia Didt for the organization of the CRC1093 graduate school.

My diligent bachelor students Richard Pleuger and Jasmin Petschulat.

Bastian Möllers for countless epic Tipp-Kick matches with incredible goals and sensational comebacks.

Ich danke meiner ganzen Familie für die nie endende Unterstützung während der letzten Jahre. Ihr habt mich durch sämtliche Höhen und Tiefen begleitet, standet immer an meiner Seite und habt nie den Glauben an mich verloren, weil ihr wusstet, dass ich meinen Weg finden werde. Dafür bin ich euch auf ewig dankbar. Bessere Eltern und Geschwister kann man sich nicht wünschen!

Zu guter Letzt bedanke ich mich bei meiner Verlobten Theresa. Seit Jahren stehst du treu an meiner Seite und begleitest mich, was immer auch kommt. Bei dir konnte ich sowohl meinen Frust und Ärger als auch meine Begeisterung über die Laborarbeit loswerden und du hattest immer ein offenes Ohr, wenn ich von Bim, Bam, Bum und Ähnlichem gesprochen habe.

Curriculum vitae

Der Lebenslauf ist in der Online-Version aus Gründen des Datenschutzes nicht enthalten.

Der Lebenslauf ist in der Online-Version aus Gründen des Datenschutzes nicht enthalten.

Der Lebenslauf ist in der Online-Version aus Gründen des Datenschutzes nicht enthalten.

Declarations

Hiermit erkläre ich, gem. § 7 Abs. (2) d) + f) der Promotionsordnung der Fakultät für Biologie zur Erlangung des Dr. rer. nat., dass ich die vorliegende Dissertation selbständig verfasst und mich keiner anderen als der angegebenen Hilfsmittel bedient, bei der Abfassung der Dissertation nur die angegebenen Hilfsmittel benutzt und alle wörtlich oder inhaltlich übernommenen Stellen als solche gekennzeichnet habe.

Essen, _____ _____
Unterschrift des Doktoranden

Hiermit erkläre ich, gem. § 7 Abs. (2) e) + g) der Promotionsordnung der Fakultät für Biologie zur Erlangung des Dr. rer. nat., dass ich keine anderen Promotionen bzw. Promotionsversuche in der Vergangenheit durchgeführt habe und dass diese Arbeit von keiner anderen Fakultät/Fachbereich abgelehnt worden ist.

Essen, _____ _____
Unterschrift des Doktoranden

Hiermit erkläre ich, gem. § 6 Abs. (2) g) der Promotionsordnung der Fakultät für Biologie zur Erlangung des Dr. rer. nat., dass ich das Arbeitsgebiet, dem das Thema „Biochemical and genetic analysis of Dam1c ring assembly at the budding yeast kinetochore“ zuzuordnen ist, in Forschung und Lehre vertrete und den Antrag von Alexander Dudziak befürworte und die Betreuung auch im Falle eines Weggangs, wenn nicht wichtige Gründe dem entgegenstehen, weiterführen werde.

_____
Name des Mitglieds der Universität
Duisburg-Essen in Druckbuchstaben

Essen, _____ _____
Unterschrift des Mitglieds der Universität Duisburg-Essen